UNIVERSITY OF OKLAHOMA

GRADUATE COLLEGE

INTEGRATED PROTONIC CERAMIC ELECTROCHEMICAL CELL FOR SUSTAINABLE ENERGY ECONOMY USING WATER-ENERGY NEXUS FRAMEWORK

A DISSERTATION

SUBMITTED TO THE GRADUATE FACULTY

in partial fulfillment of the requirements for the

Degree of

DOCTOR OF PHILOSOPHY

By

LATEEF AKOREDE JOLAOSO

Norman, Oklahoma

2023

INTEGRATED PROTONIC CERAMIC ELECTROCHEMICAL CELL FOR SUSTAINABLE ENERGY ECONOMY USING WATER-ENERGY NEXUS FRAMEWORK

A DISSERTATION APPROVED FOR THE

SCHOOL OF AEROSPACE AND MECHANICAL ENGINEERING

BY THE COMMITTEE CONSISTING OF

Dr. Pejman Kazempoor, Chair

Dr. Janet Allen

Dr. Steven Crossley

Dr. Ramkumar Parthasarathy

Dr. Hamidreza Shabgard

Acknowledgement

All praises are due to the Creator of all that exist, Allah, the one with whose mercy all goodness is perfected. Glory to Him in the beginning and the end, His peace and blessing on the one sent to be mercy to the universe. While the journey is tough, with supports and determination the end is sweet.

Firstly, I would like to express my deepest gratitude to my advisor, Dr. Pejman Kazempoor for taking chance on me. His unwavering support, patience, guidance, and invaluable mentorship throughout the journey of completing my PhD dissertation. His expertise and encouragement have been instrumental to my transition as an independent researcher and motivated me to strive for excellence.

I extend my sincere appreciation to my committee members, Dr. Janet Allen, Dr. Steven Crossley, Dr. Ramkumar Parthasarathy, and Dr. Hamidreza Shabgard for their insightful feedback, constructive criticism, and commitment to excellence. Their collective expertise has enriched the quality of my work and contributed significantly to its overall refinement.

I am profoundly thankful to my family for their enduring love, encouragement, and understanding. Their unwavering support provided the foundation for my academic pursuits, and I am truly grateful for the sacrifices they made to see me through this educational endeavor. I am indebted to my mum and all my siblings for your physical, emotional, and spiritual support, I hope to pay it forward. I wanted to take a moment to express my deepest appreciation to my friends from all parts of the world, you are all invaluable.

Furthermore, I am extremely grateful to my wife Kareemah Oyeleye, for your support throughout this journey, you are highly reliable and dependable. Also, I appreciate my children Abdullah,

AbdurRahman, AbdulBarr and the little princess in the house Rumaysah for their love, hugs, and smiles they throw at me after having a rough day in the lab, we did this together.

This accomplishment is not just mine but a result of the collaborative efforts and support from each of you. Thank you for being an integral part of this significant chapter in my academic journey.

May Allaah have mercy on my father

Table of Contents

List of Figures

List of Tables

Abbreviations

AEC	Alkaline electrolytic cell
AECs	Alkaline electrochemical cells
BOP	Balance of plant
CCS	Carbon capture system
CAES	Compressed air energy storage
CO_2RR	Carbon dioxide reduction reaction
CPP	Coal power plant
DALY	Disability adjusted life year
DOE	Department of Energy
EA	Economic analysis
EES	Electrical energy storage
ESP	Electrostatic precipitator
EES	Engineering equation solver
EIA	Energy information administration
ESS	Energy storage system
EST	Energy storage technologies
FE	Faradaic efficiency
FES	Flywheel energy storage
FOB	Free on board
FU	Fuel utilization
GE	General Electric
GES	Gravity energy storage

GWP	Global warming potential
HEN	Heat exchange network
HER	Hydrogen evolution reaction
HPS	High pressurized steam
ISO	International Organization for Standardization
IEA	International energy agency
LCOH	Levelized cost of hydrogen
LCOM	Levelized cost of methane
LCA	Life cycle analysis
LCIA	Life cycle impact assessment
LMTD	Log mean temperature difference
MACRS	Modified accelerated cost recovery system
MEA	Membrane electrode assembly
MIEC	Mixed ionic-electronic conductors
NEA	Net energy analysis
NG	Natural gas
Ng	Negatrode
N_2RR	Nitrogen reduction reaction
OCV	Open-circuit voltage
O&M	Operational and maintenance
ORR	Oxygen reduction reaction
OER	Oxygen evolution reactions
PCEC	Protonic ceramic electrochemical cell

PCER	Protonic ceramic electrochemical reactor
PCFC	Protonic ceramic fuel cell
PCO	Protonic ceramic oxides
PEM	Proton exchange membrane/ polymer electrolyte membrane
PEMEC	Polymer electrolyte membrane (PEM) electrolytic cell
PEN	Positrode, electrolyte membrane, and negatrode
PHS	Pumped hydro storage
PP	Power plant
Ps	Positrode
PtX	Power to chemical
PV	Photovoltaic
REC	Reversible electrochemical cells
RePCEC	Reversible protonic ceramic electrochemical cell
rSOC	Regenerative/reversible SOC
RT	Roundtrip
RWGS	Reverse water gas shift
SEM	Scanning electron microscopy
SOC	Solid oxide cell
SOEC	Solid oxide electrolysis cell
SOFC	Solid oxide fuel cell
SSRS	Solid-state reactive sintering
TCC	Total capital cost

TDC	Total direct cost
TEA	Techno-economic analysis
TRACI	Tool for the Reduction and Assessment of Chemical and Other Environmental Impacts
TRL	Technological readiness level
TSMB CCS	Two-stage membrane-based carbon capture system
WoS	Web of science
WTRU	Wastewater treatment and recovery unit
XtP	Chemical to power

Abstract

Reliance on fossil fuels will continue for the next decades even though there are global pushes away from it to mitigate the overarching climate challenge, most especially by its highest consumers and availability. While there is a hastening global shift away from fossil fuel, integrating its assets into this technology helps limit the risk and future losses of stranded assets and reduce the cost of investment in the new technologies. Moreover, the generation of electricity from intermittent renewable sources like solar and wind has witnessed a significant surge in recent years, leading to a pressing demand for practical energy storage systems. Electrical energy storage is anticipated to play a pivotal role in the future global energy system, facilitating load-leveling operations to support the greater integration of renewable and distributed generation. Reversible electrochemical cells (RECs) offer a promising option for addressing the fossil fuel assets integration and energy storage challenges through the interconversion between electrical and chemical energy and concurrent utilizing carbon emission. In their electrolysis mode, the RECs convert electricity into durable, storable, and portable valuable chemical fuels such as syngas and methane. Conversely, the produced chemical fuels can be used as reactants in the fuel cell mode to generate electricity on demand with minimal (hydrocarbons) or zero when H_2 or NH_3 is used emissions. However, a challenging goal for this type of technology remains to achieve optimal operation and high roundtrip efficiencies, which has hindered the deployment of previous electrochemical cells. This dissertation demonstrates how reversible protonic ceramic electrochemical cells (RePCECs) can be integrated with fossil fuel power plants and renewable energy sources as a potential energy storage system. In this work, integrated RePCEC systems are designed and examined using computational modeling at scales to determine appropriate system configurations and operating conditions that achieve high roundtrip efficiencies. Cell level design of the PCEC is the first approach, several cells are assembled for the stack level model that is integrated into combined cycle powerplant and solar photovoltaic for the system level model. After critical literature review, this answered the operational and integration research questions proposed to address these challenges. The designed systems perform two functions, utilizing captured CO_2 and storing renewable energy through co-electrolysis of steam and CO_2.

The co-electrolysis reaction involves endothermic water electrolysis and exothermic methanation reaction. To enhance high roundtrip efficiency, there is a need for thermal balance and management in the electrolysis mode. This involves operating the RePCEC stack under conditions

that favor methane production to balance out heat needed by water electrolysis, it crucial for the RePCEC system operation. Methanation is enhanced by low temperatures. Leveraging on fabricated BCZYYb-electrolyte RePCEC, the cell model designed revealed that the optimum temperature for methane production is 450℃ at atmospheric pressure. Thus, to achieve optimum system performance, operating in the temperature range 450-525℃ is recommended at the given configuration, combining between the optimum temperature for methane production and temperature for the optimum stack roundtrip efficiency. Configuration with carbon capture system and purge stream is the optimum configuration from the seven conceptualized and evaluated.

The modeling outcomes include a thermodynamic examination of integrated RePCEC systems, calibration of cell and stack level models, and steady-state simulation and integration into a 600MW combined cycle power plant retrofitted with two two-stage membrane-based carbon capture system and a wastewater treatment and recovery unit. At 100% powerplant loading, the stack and system roundtrip efficiencies are 72% and 51.37% respectively. Adding a purge stream for produced hydrogen at the system downstream improves the efficiencies to 74 and 55.48% respectively. At atmospheric pressure and 525℃, the system model suggests that a stack roundtrip of 82% is achievable, and overall system efficiency increases by reducing the energy consumption by the balance of plant components for steam generation and storage. Economic analysis of the process gives levelized cost of methane as $2.24/MMBtu lower than the conventional production route that range between $3.46/MMBtu and $9.85/MMBtu. The lifecycle analysis shows that the global warming potential for the production of methane and hydrogen from the RePCEC system is 3.83 kg CO2 eq which is lower than 9.35 kg CO2 eq emission during steam methane reforming for hydrogen production. This answered both the environmental and economic concerns in the raised research question.

The proposed RePCEC configuration and analysis carried out in this dissertation to address the surge in renewable energy and challenges with PCEC technology hold significant potential in achieving large-scale energy storage while simultaneously reducing carbon emissions. These advancements, coupled with suitable governmental policies and incentive programs, have the potential to economically disrupt the natural gas industries by using RePCEC systems for methane production, thereby making them more favorable for eventual implementation and commercialization.

CHAPTER 1 INTRODUCTION

The increase in the development and deployment of renewables coupled with their intermittency and of the grid power supply has called for the design of large-scale energy storage for the management of this energy perturbation. Energy production by renewable energy sources like wind and solar fluctuate with time and natural conditions and the societal energy demand also varies with time. Therefore, efficient energy storage system is required to use the electricity produced from these sources and maintain a stable electrical energy grid and ensure a continuous supply to meet demand. Energy can be stored in different forms including chemical, mechanical and electrical energy. Several energy storage technologies (ESTs) are developed in tandem with different energy storage forms. The various ESTs include the pump hydro storage (PHS), Compressed Air Energy Storage (CAES), Flywheel Energy Storage (FES) and Gravity energy storage (GES) which are mechanical. Batteries and other electrochemical devices like fuel cells are chemical and capacitors are electrical. A detailed review of their operation concepts and conditions, emphasizing their merits and demerits, is available in the literature [1-6]. However, a critical storage metric that helps to understand the value of energy lost in the technology is the round-trip efficiency, values above 70% are promising. The range for batteries and PHS is 70-95% [7] which are the most widely used technologies. Storing electrical energy in the form of chemical energy is highly appealing and advantageous, primarily because of its substantial storage capacity [1, 6]. This approach enables electrical energy to be stored in form of chemical fuel and back to electrical energy at the time of need. This concept is called power to chemical (PtX) and its reverse chemical to power (XtP) are usually facilitated by electrochemical technologies- electrolysis and fuel cells. Electrochemical devices have shown in recent times to be an excellent alternative energy technology for electrical energy storage (EES) which will play a significant role to control this perturbation. This is due to their ability to produce clean energy, high efficiency, versatility, and integration with renewables. Furthermore, as the penetration of renewable energy increases driven by global decarbonization goal, innovative pathways are required to generate fundamental chemical energy and crucial industrial chemicals like hydrogen for green economy. Other valuable

chemicals like ammonia, syngas and methane can benefit from this production route [8, 9]. This presents an opportunity to integrate the energy storage industry with the chemical synthesis sector and brings about a change in operation paradigm in those industries.

1.1 The importance of energy storage for the future

The global energy production in the last three decades has grown tremendously, most especially the last decade has witnessed a growth in energy mix which has no precedence. As of 2021, the global total energy consumption which is usually three-quarter of the total production of 176,431 TWh compared to its approximate value of 152, 966 TWh in 2010 [10] which results in 14.7% increase. Fossil fuels which include natural gas and oil, coal and peat contributed to 80% of the production in 2012 [11] and 63% in 2022 as more renewable energy sources are explored. Despite the huge increase in energy production to cater for the growing global population as shown in Fig. 1.1 [12], there is a drop in the percentage of fossil fuel which is replaced by renewables. Meanwhile, the fossil fuel power plants have been used in managing the load balance to maintain power network stability. With this diminishing percentage production of energy from fossil fuel sources, there will be less reliance on them which will eventually enhance in achieving the CO_2-emission target. This climatic issue mitigation goal can be attained with continuous progression in the generation of energy from renewable sources whose capacity is expected to grow by 85% in the next five years. This growth is equivalent to almost what was added in the past 20 years [13]. This increment is huge and needs to be prepared for to optimize its energy production and benefits. However, majority of these renewable energy sources are intermittent by nature as depicted in Fig. 1.2, this poses challenges for their use in the production of energy, stability of power network and its reliability.

There have been some objections and disputes in the past for need for energy storage system due to few and poor implementation because of limitations which include;

a. High generating source of the conventional energy supply which can be managed to cater for the load demand.

b. Shortage of technical-know-how of implementation and tools for adequate economic and operational feasibility studies.

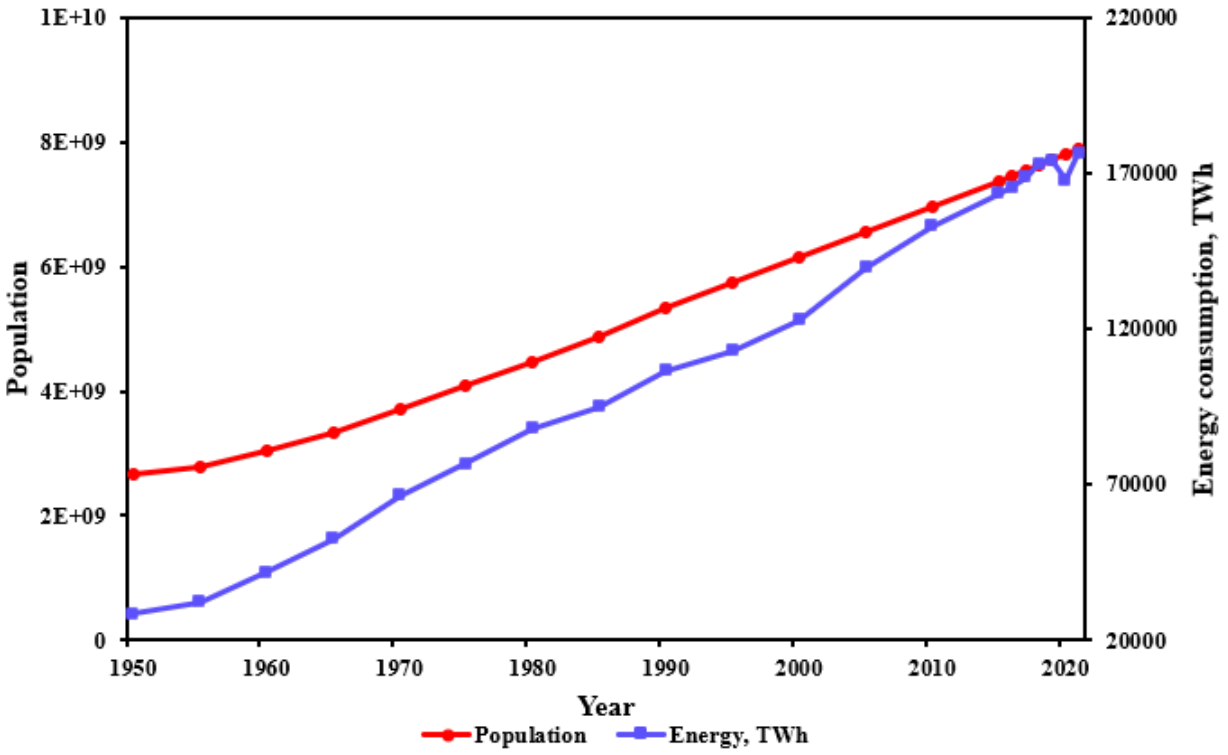

Fig. 1.1: Relationship between growing global population and consumed energy

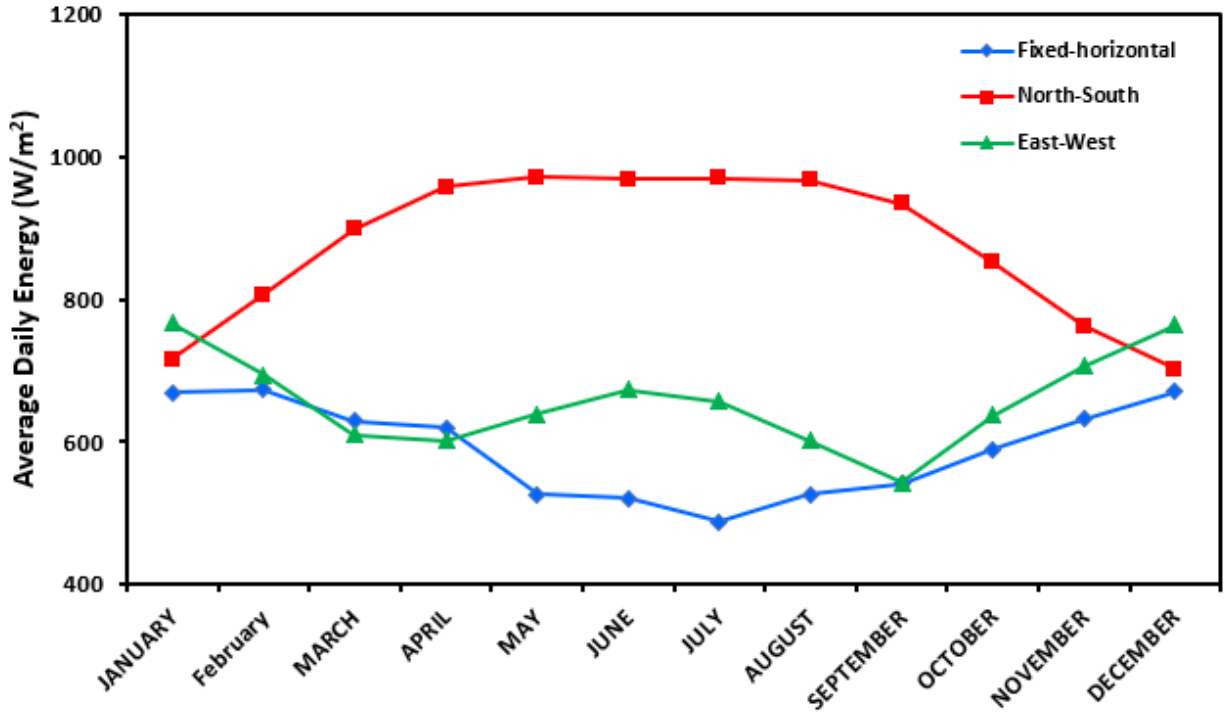

Fig. 1.2: Average monthly solar radiation energy at latitude 35 degree for a year

It has however been concluded by the International Energy Agency (IEA) that installing efficient energy storage system will enhance the reduction of global warming by 2℃, if the installation capacity reached 450GW by 2050 [14].

Recently, the increased penetration of the renewable energy sources (Fig. 1.3) and multiple uncontrollable generating sources have reinvigorated the interest towards the development of cheap and efficient energy storage technologies. However, the energy generated through this medium is constrained by intermittence and fluctuation. For example, while wind and solar have been reported to be potentially viable in the energy industry their fluctuation needs to be stabilized by the integration of energy storage system.

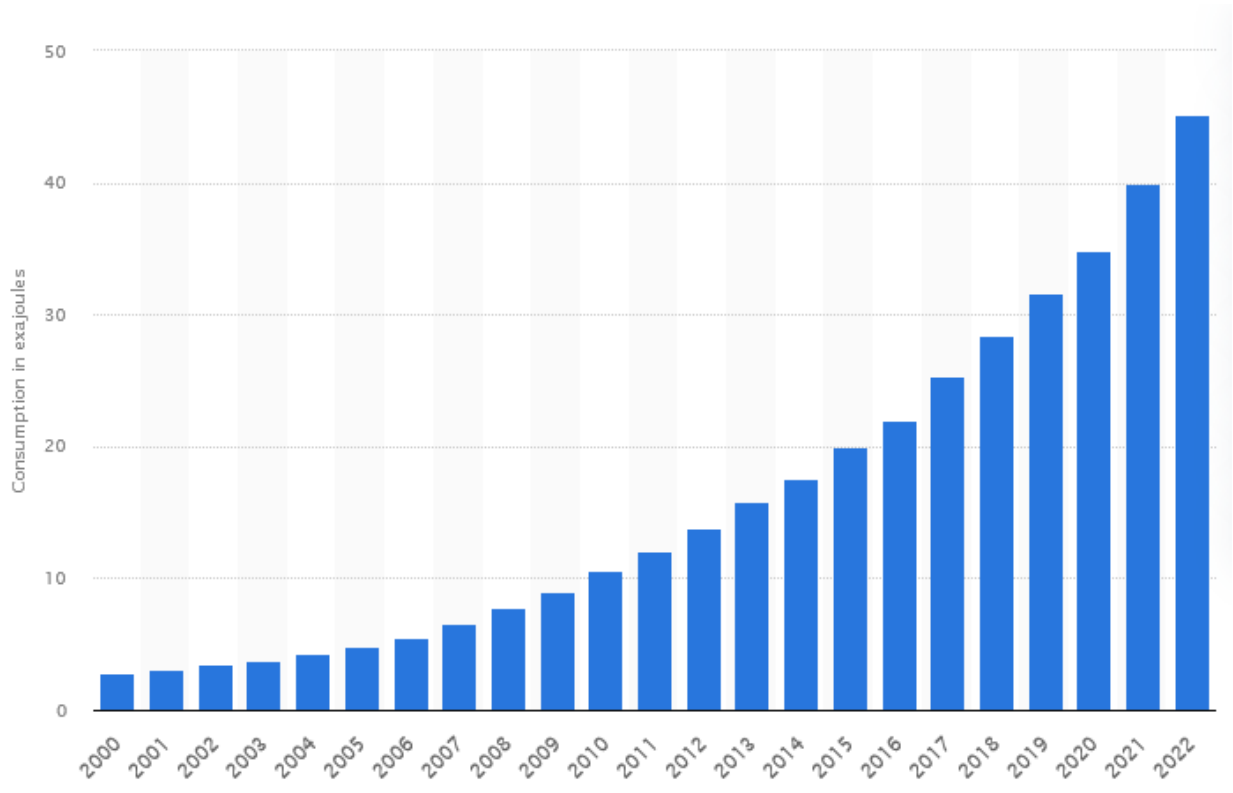

Fig. 1.3: Global renewable energy consumption (2000-2022)

Likewise, Fig. 1.4 shows an estimated wind data in April 2014 with energy storage charged with wind power and supplying energy during low wind supply. Large-scale energy storage system is very essential for temporal fluctuation of demand in an inexpensive manner. Efficient storage

system will maintain the supply of electricity during severe storms like the Texas incident in 2021. This will help avoid double generation of electricity during peak demand and reduce the financial burden of the consumers and enhance low utility rates.

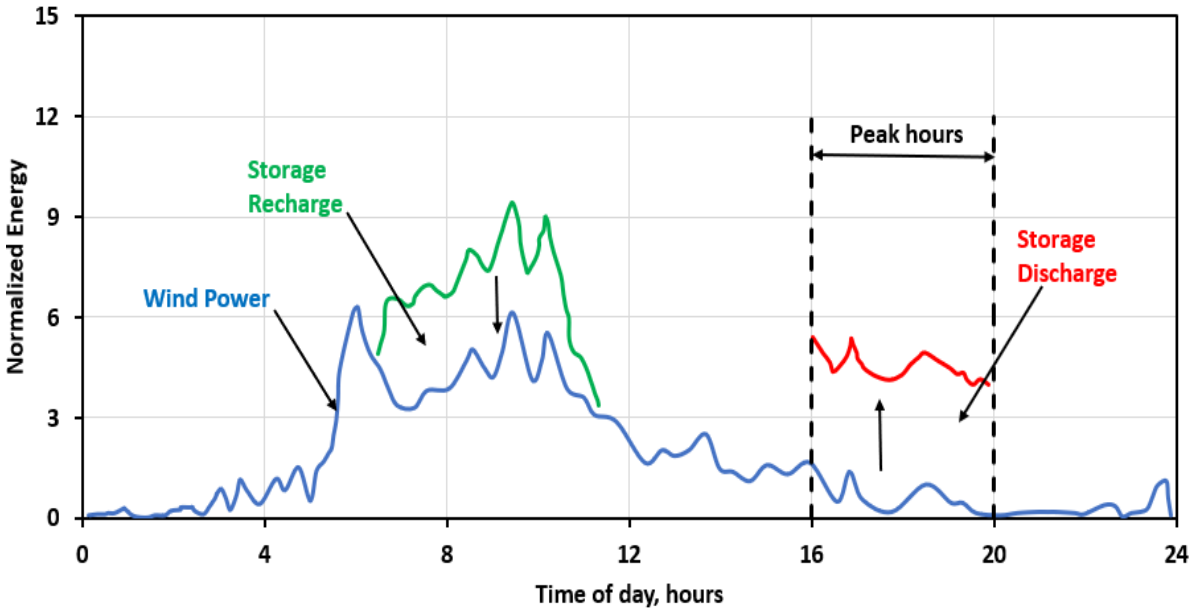

Fig. 1.4: Energy storage serving as a peaking resource

1.2 Types of energy storage

Currently, there are many types of energy storage technologies with different comparisons among them. Fig. 5 shows the general overview and comparison of these technologies from Sandia National laboratories with respect to their discharge times and power size.

Additionally, the US Department of Energy (DOE) made a high-level broader classification of all of them and their use cases as shown in Fig. 1.6 [15]. For instance, the electrochemical category includes Lead acid, Li-ion, Na-ion and so on. The main categories usually discussed in the literature are the electrochemical, electrical, mechanical, thermal, and chemical [1, 6, 16, 17]. There is remarkable increase in the deployment of some of the energy storage technologies with the pumped hydro storage (PHS) system leading and taking up to over 95% of the globally installed energy storage system (ESS) and others making up to less than 5% as of 2018 [1]. The need to

sustain the growing energy and net zero economy demands significant advancement and improvements. Some other attracting mechanical energy storages are compressed air energy storage (CAES), it has potential consideration for wide range of application with just only two globally deployed but produces CO_2 emissions [18, 19]. Flywheel energy storage (FES) has high energy performance mainly for standby power and not suitable for long time energy storage [20] and gravity energy storage (GES) system. Other ESS technologies geared towards advancement and

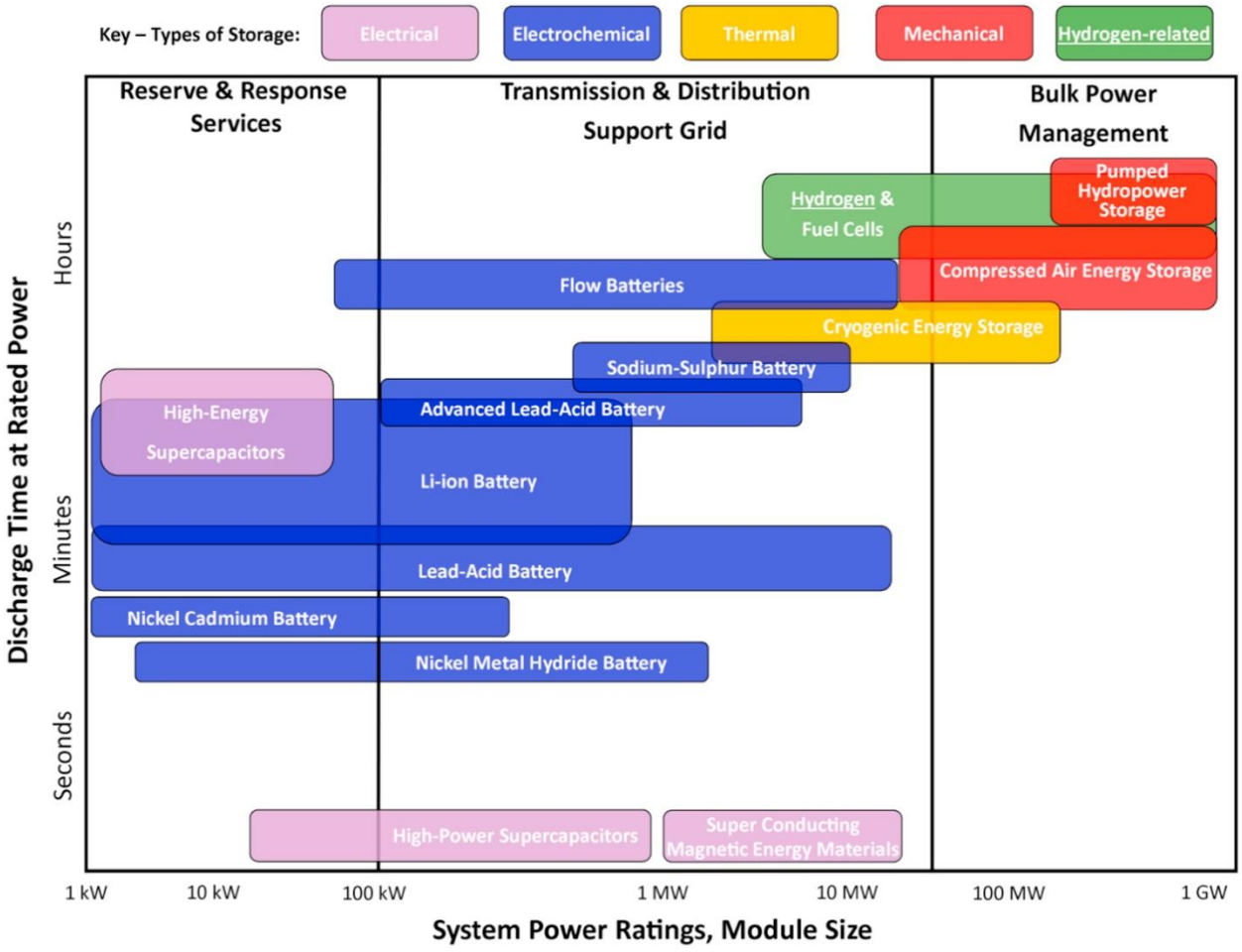

Fig. 1.5: general overview and comparison of existing energy storage technologies [21]

commercialization include batteries (conventional and advanced batteries). Examples of the conventional batteries are lead-acid (flooded type and valve regulated), Nickel cadmium (NiCd), lithium, zinc-carbon batteries and so on. The advanced batteries include redox flow batteries, lithium-ion, and metal-Air batteries [16]. Examples in the electrochemical storage category include capacitors and supercapacitors. While some of these technologies have the potential to solve some

specific energy storage problems, they are faced with very unique challenges that have hindered their development making the PHS have the lead in the energy storage industry.

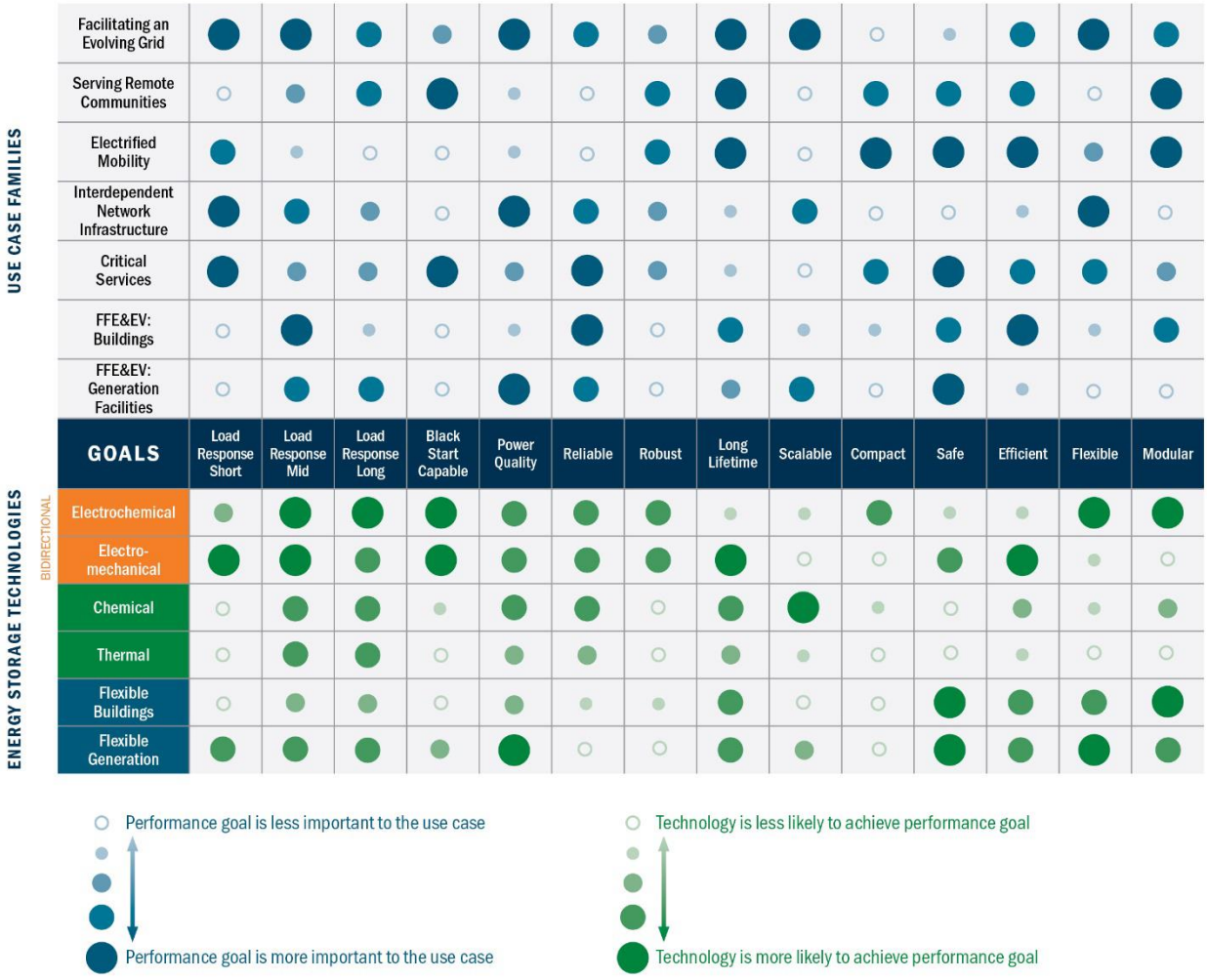

Fig. 1.6: Illustration of energy storage technologies and their performance functional framework [22]

Technical and economical evaluations of these technologies make it known that most of them do not meet the requirements (which include cost, efficiency, and durability) for viable ESS technology. For large scale application of the ESS, the following criteria is key; high efficiency, longer life span, cheap and high energy density. Energy storage is required for both small scale and large-scale functionality, it is therefore critical to prioritize our requirement as it is difficult to find a single ESS that satisfy all these characteristics and some other evolving metrics.

For a stationary energy storage system, roundtrip efficiency, levelized cost, capital cost and energy density has been chosen to be their main performance metrics. The US DOE has paid close attention to energy storage system technology and has continuously set criteria for operational acceptance most especially for micro-grid level application because of their importance. The need for ESS can be summarized into the following.

a. changing in the load characteristics
b. energy production for consumers distant from the grid
c. increase in the deployment renewable energy source
d. Carbon dioxide emissions abatement

This dissertation uses the recent DOE targets to analyze and establish the feasibility of PCEC as a potential large scale energy storage technology.

1.3 Introduction to reversible protonic ceramic electrochemical cells

The reversible protonic ceramic electrochemical cell is a single electrochemical device that combines the operation of PCEC and protonic ceramic fuel cell (PCFC) in a standalone device and possesses similar physical structure as them. It carries out the electrolysis mode of operation and the fuel cell mode of operation independently. Unlike the low-temperature reversible PEMECs (RePEMEC) which could either be Unitized Regenerative Fuel Cell system (URFC) or Discrete Regenerative Fuel Cell system (DRFC) depending on design need [23] that operate at 30 to 180 ℃ [24-26] and high-temperature rSOC that operate 500-1000 ℃ [27, 28], it operate at an intermediate temperatures of 300-600 ℃ [29, 30]. For RePCEC to operate in either of these modes, it only requires alternation of polarity as depicted in Fig. 1.7 and Fig. 1.8.

The RePCEC membrane electrolyte assembly (MEA) structure is basically composed of proton-conducting electrolyte membrane used to partition the positrode (electrolysis anode) and negatrode (electrolysis cathode) electrodes. Both electrodes are porous that they enable the transport of gases and simultaneous conduction of protons and electrons. The porous positrode is made up triple-conduction oxide (TCO), $BaCo_{0.4}Fe_{0.4}Zr_{0.1}Y_{0.1}O_{3-\delta}$ (BCFZY). The TCO is permits the transport of protons, electrons, and oxygen vacancies. Likewise, the porous negatrode is a composite of Ni (for electronic conduction) and $BaCe_{0.7}Zr_{0.1}Y_{0.1}Yb_{0.1}O_{3-\delta}$ (BCZYYb) (the ionic conduction) [31, 32]. The electrolyte is a proton-conducting ceramic membrane that allows the transport of H^+ from the

steam electrode to the fuel electrode as shown in Fig. 1.8. Several proton-conducting ceramic materials have been studied and used for MEA layers [33].

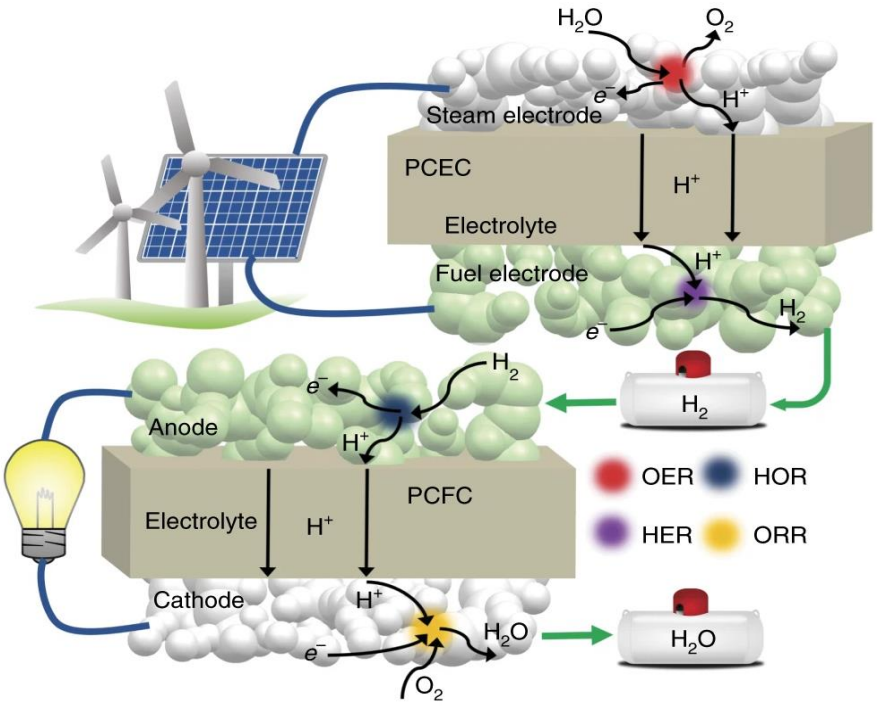

Fig. 1.7: Schematic reversible protonic ceramic electrochemcal cell operations adapted from Ref [29].

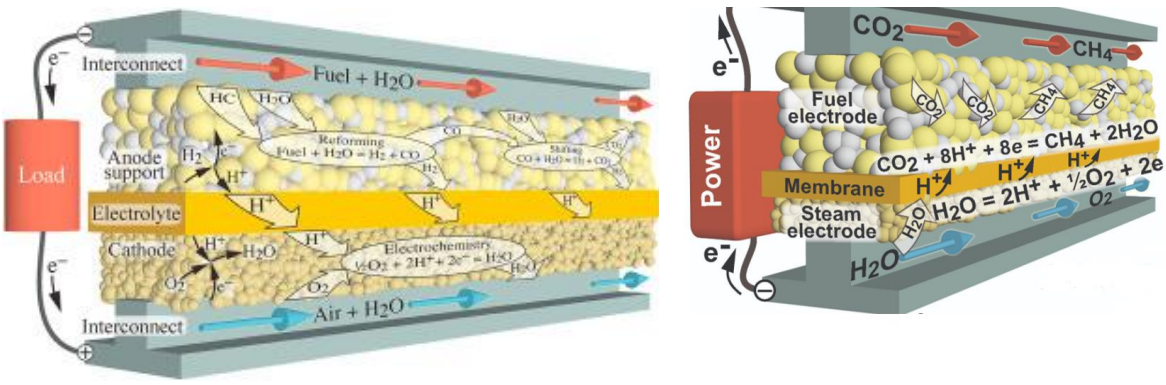

a. b.

Fig. 1.8: Single channel planar reversible protonic ceramic electrochemical cell illustration adapted from Ref [34].

However, the most studied of all are the perovskite-structure oxides on which the RePCEC designed, and data used in this dissertation is based. The perovskite structure is generally represented with chemical formula ABX3. The A, B and X usually represent a divalent cation (like Sr^{2+} and Ba^{2+}), tetravalent cation (like Ce^{4+}, Zr^{4+}), trivalent cation (like Yb^{3+}, Y^{3+}) and anions (frequently oxide) respectively [33, 35, 36].

The PCEC technology has the capability to function as a reactor for several reactions, which can vary depending on the feedstock employed. Furthermore, the same feedstock can undergo multiple reactions within the PCEC system, influenced by factors such as the operating conditions. In the operating mode, reactants are fed to the fuel electrode (the negative electrode called negatrode). These reactants could be hydrogen or syngas in the PCFC mode, and water or water-CO_2 in the PCEC mode. This work focuses the production of methane from H_2O and CO_2 molecules and therefore the two compounds are invariably the reactants for the PCEC operation in a process called co-electrolysis. Steam is passed into the steam electrode (the positive electrode called positrode) of the PCEC and CO_2 co-fed into the PCEC fuel electrode (the negative electrode called negatrode). Methane and steam are typically produced at the fuel electrode of the PCEC while oxygen is produced at the steam electrode. These products are then correspondingly passed to the fuel and air electrodes in the PCFC mode for a reverse operation.

A standalone RePCEC unit typically operates in a voltage range of 0.1-1.5V [29, 37, 38]. However, attaining a functional voltage output from the unit necessitate cell stacking. The stacking process comes along with additional requirements like the need for electronically conductive materials for the interconnects and robust sealing mechanism that prevent leakage or gas crossover within the stack. Generally, cell stacking becomes more complex at high temperature, and this does not absolve the RePCEC intermediate temperature of this complexity. This due to the potential inequalities in thermal expansion of the make-up materials used in the stack design. The are several feasible configurations for RePCEC considering its structural versatility, they include series-segmentation, tubular and planar configurations which are typical for rSOC. While the planar and tubular are the most studied configuration for most electrochemical cells [39], the planar configuration has been generally reported to be superior and outperform the tubular configuration. This has been traced to more uniform gas distribution coupled with ease of production of the planar cells. It also offers the benefit of power (volumetric) densities and low cost of production [40, 41].

Likewise, taking into account the lower power density associated with tubular design due to increased current path, the planar design geometry is considered in this dissertation.

The integration of the endothermic steam electrolysis reaction with the exothermic CO_2 hydrogenation reaction facilitates thermal balancing of the process and enhance high efficiency in the PCEC operation mode. Likewise, the electrochemical reaction in the PCFC mode like other types of fuel cells is exothermic and requires excess air or other external cooling to ward off thermal stress in the stack. This thermal imbalance in the reversible operation modes poses critical challenge in the use of integrated RePCEC system for a system level design and impair its performance. In order to enhance the system efficiency, a thermal management approach is adopted in this study which require strategic selection of the operating conditions (like temperature and compositions) for RePCEC stack. This will simultaneously stimulate the production of methane and steam electrolysis in the PCEC mode and efficiently maintain the temperature required for the PCFC operation mode.

1.3.1 Distinguishing features of RePCEC

The technology proposed here offers distinguished features, especially in comparison with other reversible fuel cells (e.g., reversible solid oxide cells, reversible proton exchange membrane fuel cells), which include and are not limited to;

(1.) The reversible PCERs integrated system ensures long-term energy storage and enhances on-demand power generation and sustainable feedstock for fossil industries.

(2.) PCERs exhibit high H_2S and coking tolerance, implying that they can directly utilize “dirty” flue gas or exhaust gas from fossil-fuels plants for energy storage without employing additional complex purification units.

(3.) They exhibit a theoretical round-trip efficiency of up to 100%.

(4.) Lower (compared to SOC) operating temperatures facilitate integration with a wider range of waste heat sources, easing the limitations on cell stack and balance of plant components. This potentially reduces the costs while simultaneously enhancing reliability, dynamic responsiveness, and tolerance to thermal cycling.

(5.) PCERs can achieve remarkable faradaic efficiency ranging from 90% to 98%. They operate as a highly efficient endothermic process, achieving an outstanding overall electric-to-hydrogen energy conversion efficiency of 97% (using the lower heating value

(LHV) of hydrogen) at -1.0 A/cm^{-2} current density. Interestingly, more exceptional efficiencies are achieved during the co-electrolysis of H2O and CO2 for methane production.

(6.) A consistent round-trip efficiency exceeding 75% along with stable operation, with a degradation rate of less than 30 mV over 1,000 h. This outstanding performance makes PCERs an attractive and ideal candidate for the energy storage application.

1.3.2 Protonic ceramic electrochemical cells: The ongoing advancements and the current technological status

The electrochemical cells are expected to play a significant role in the production of chemicals and fuels for energy storage in the nearest future [42] due to their potential to generate high-purity hydrogen that is carbon-free [43]. This can be in form of a fuel cell which is a solid-state electrochemical conversion device that directly transform the chemical energy stored in fuel species to generate electrical power. It can also be electrolysis cell where oxidized feedstock are electrochemically converted into fuels and other useful chemical products. It can also combine the first-two mode of operations to form a cyclic mode called reversible cells [39].

The regenerative electrochemical cells, which operate in a reversible manner for storing renewable energies by interchanging chemical energy like hydrogen from water electrolysis with electricity and back to the latter in the fuel cell mode have received little attention until later in less than a decade [44]. While there are several developed and designed fuel cells analyzed by researchers [45] there are three prominent ones like the polymer exchange membrane fuel cell (PEMFC) and aqueous alkaline (AFC), which operate at low temperatures and hydrogen is usually employed as fuel. But unfavorably, the PEMFC performance depreciates due to the susceptibility of the platinum catalyst at its anode to CO poisoning, which accompanies the supplied hydrogen fuel as bulk of its production is from steam methane reforming (SMR). The last of them, the solid oxide fuel cells (SOFC) explore their high temperature operating condition to use non-noble metal catalysts and present some other benefits like fuel flexibility. In fact, the CO impurity which is unwanted in PEMFC is a usable fuel in SOFC. Nonetheless, only these fuel cells have been studied for reversible operation for the energy storage systems [29, 45].

After the breakthrough in material sintering and device fabrication of proton-conducting oxides which find its application in the protonic ceramic electrochemical cells, it regained prominence and has been of greater attention in less than a decade ago [46]. This work is led by Babilo and Haile in 2005 [47]. In 2010, a cluster of research is carried out in improving the sinterability of the protonic ceramics using different metallic oxides like CoO, CuO, NiO, and ZnO as sintering aids [48-50]. Interestingly, the PCEC is an evolving and attractive energy storage system that switches operation from the fuel cell to the electrolyzer mode without adjustment, a stand-alone regenerative operation. It is a proton-conductor-based solid oxide cell that is designed to operate at moderate temperatures and overcome some of the challenges in the previous regenerative fuel cell (RFC) technologies [51]. It is often used to produce hydrogen in the electrolysis mode, and hydrogen is used as fuel in the reverse mode (fuel cell). However, using some other fuel like methane can give some fascinating benefits like increasing the round trip efficiency as no energy would be required for the vaporization of supplied water [46]. Correspondingly, methane generation through Sabatier reaction or process has however been perceived to be of immense importance for storing excess electricity in a renewable-energy controlled setup [52] in place of the direct hydrogen usage for energy storage [53] and the operation of the PCEC would be highly required. The PCEC evolved because of the inability of the most of current technologies to meet the requirements for off-, micro-grid and grid-scale system that can be used for energy storage to enhance the stable and efficient electricity.

The alkaline electrolytic cell (AEC) is regarded as the fundamental process for splitting water and is the most mature technology of all the electrolytic production of hydrogen [54]. It suffers some setbacks like low current density, low-pressure operation, and partial load. These challenges plaguing this electrolyzer were overcome by the advent of the polymer electrolyte membrane (PEM) electrolytic cell (PEMEC) [55]. The PEMEC is faced with high capital cost, pure water requirement, and high system complexity which stems from its operational pressure [55, 56], which brought about the emergence of solid oxide electrochemical cell (SOEC) as a solution. Insufficient long-term stability has hindered the widespread of this technology, most especially at high current densities, which is expected to be resolved with reversibility [57].

Customarily, the focus on chemical-to-electrical energy interconversion has been unidirectional in the electrochemical device of interest [58]. The electrolyzer is a mature technology, thus is the

reverse operating device, the fuel cell which gains attraction due to its use of hydrogen for carbon-free electric power generation [59]. The combination of these functionalities in a single reversible cell, will enhance a long-tern storage and stability, which will support a large-scale reversible cell technology deployment [44]. Based on this observation and projection, there is a switch toward this bifunctional technology. Researchers started working assiduously on reversible solid oxide cell (SOC) to get the best out of this technology. Graves et al [57], in their work on eliminating degradation in SOC, showed that reversible operations play a vital role in achieving higher efficiency and a better understanding of the degradation mechanism. Srikanth et al. [60] also worked using the regenerative SOC (rSOC) by exploring the flexibility of the technology by using coal in the generation of hydrogen. Kazempoor and Braun [27] used a modeling approach to assess the performance of rSOC and its validation using mathematical models and showed that the electrochemical losses differ based on the operating mode. Wendel et al [28, 61] critically make technological assessment and use of rSOC for large scale energy storage and system level integration. However, high operating temperature that enhance cell degradation and diminish durability has been a major challenge for its commercialization.

In seeking improvements for the rSOC and lowering its operating temperature resulted in the evolution of the proton ceramic electrochemical cell (PCEC) which is an SOC with a proton-conducting electrolyte. The PCEC has been rigorously studied in recent times as a potential solution for efficient and sustainable chemical synthesis, energy storage and power generation.

Protonic ceramic fuel cell (PCFC) is an efficient device to convert chemical energy into electrical power. Hydrogen and hydrocarbons is usually the proposed used fuel with precedence given to hydrogen due to its generation of COx-free ehaust [30].Depending on the fuel used, it is also poised for cogeneration of some beneficial products with the electric power. For example, when ethane is used as the anode feedstock, dehydrogenation reaction takes place to produce ethylene and hydrogen [62, 63].

Additionally, to the power-generating ability of the PCECs, they have been explored for chemical production via electrolysis. The reverse operation of the H_2-air PCFCs is used in hydrogen production through steam electrolysis. In 2019, the protonic ceramic electrolysis cells (PCECs) showed very high efficiency for hydrogen production in work by Duan et al. [29], and they demonstrated similar efficiency for the reversible protonic ceramic electrochemical cells

(RePCECs). More fascinating is the versatility of the PCEC in producing broad range of chemicals from the abundant naturally available earth resource (like N_2, H_2O) and captured or stored greenhouse gases (e.g CO_2 and CH_4). [64-66]

It is worthy to note that recent studies revealed that if the protonic ceramic electrochemical cells (PCECs) is properly harnessed have several distinguishing features over the SOECs both in the generation of electricity as protonic ceramic fuel cell (PCFC) [67] and in the storage of energy as protonic ceramic electrolytic cell (PCEC) [68]. These advantages include lower cell and stack temperature (300-600℃), optimization of air ratio, revamped cell voltage, enhanced fuel utilization, diversified and efficient chemical production [29, 65, 69].

As with previous electrochemical technologies, a lot of works have focused on the improvement of the materials used to design PCEC as their development is of great significance to its maturity and reaching its technological readiness level. Like the development of high-entropy $Pr_{0.2}Ba_{0.2}Sr_{0.2}La_{0.2}Ca_{0.2}CoO_{3-\delta}$ (HE-PBSLCC) air electrode for the oxygen reduction reaction (ORR) during water electrolysis. The ORR is considered to be most critical reaction during water electrolysis and only efficient electrodes for the reaction can facilitate the commercialization of the PCEC [70]. Kang et al [71] in their study answered the same call designing heterostructure air electrode for ORR. Due to the infancy of the technology, most efforts have been geared towards lab-scale material design and development. However, there have been several calls pushing for the pilot and commercial scale design and fabrication due to the prospect of the technology and to enhance its commercial deployment.

The design and operation of PCEC is quite challenging as its common to other regenerative electrochemical technologies due to their bi-functionality and the intertwining of the operating conditions in both operational modes. Additionally, material selection to fulfill both backward and reverse reaction is another key challenge. Likewise, the operation paradigm of designed PCEC changes when it is integrated to some other resources like renewables and power plants. All these factors are interdependent and greatly influence the PCEC performance, manufacturing cost and implementation. These challenges need to be overcome which suggest a detailed computational analysis of process and system to enhance its viability as an excellent energy storage system, therefore justifying this dissertation.

1.4 Research motivation and rationale for choosing PCEC for energy storage

The highlight in the distinguishing characteristics is one of the key motivations for this work. While focus have been on renewables integration, the fossil fuels which are no doubt would dominate the energy industry for some decade to come needs to be store and have received limited attention. As such, this work combines between storing fossil and renewable energies using RePCEC. Literature revealed that previous work mostly revolved the development of a standalone PCFC and PCEC for power generation and hydrogen production respectively. The ability of the RePCEC to combine these two operations in cyclic standalone device has geared up its use as potential energy storage technology as previously mentioned. Enormous efforts have been dedicated to this area study mostly especially in the last five years.

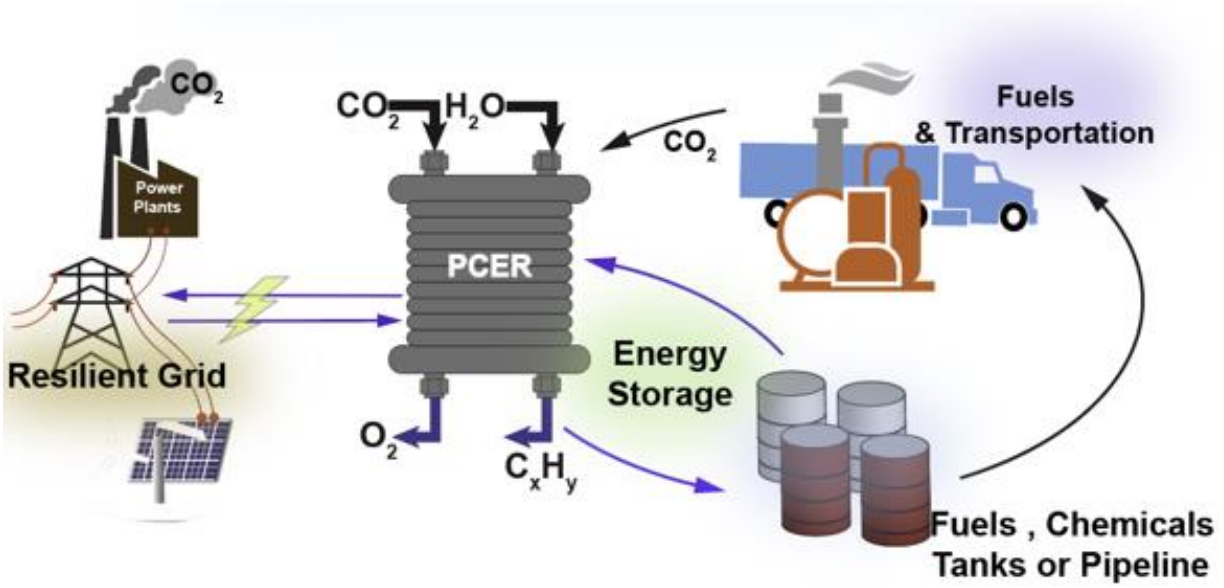

Fig. 1.9: Operation of RePCEC for methane production as a typical fossil and renewable energy storage technology. RePCEC is Protonic ceramic electrochemical reactor (PCER).

Fig. 1.9 shows a diagrammatic representation of the operation of RePCEC in both forward and backward mode for energy storage and generation respectively. In the energy storage mode, the surplus electrical energy from the fossil power plant or renewable resources is supplied to RePCEC stack for charging it. This stack operates as a PCEC whereby the captured CO_2 (using carbon

capture technology like a membrane) from fossil power plant and nontraditional water sources (from powerplant or wastewater system) are supplied to the negatrode and positrode of the stack respectively to produce CH_4-rich gas. This gas can be stored in fuel tanks, injected into natural gas pipeline, immediately used as feedstock for fossil industries or supplied for the reverse operation. In the PCFC mode, the polarity of the cell switches and the device is discharged as chemical energy in the CH_4-rich supply gas is converted to electrical energy while the fuel flows from the "fuel tanks" through the RePCEC stack where it is electrochemically oxidized. The exhaust species which are mainly CO_2 and H_2O can be cyclically reused or put or stored in a pressure tank. It worthy to note that air from the ambient environment is used in both mode of operations either as a sweep gas in case of PCEC where it flushes out the produced oxygen at the positrode and reduce its partial pressure or as an oxidizer in the PCFC mode.

As shown in Fig. 1.10 as well, the technology can also be use in the synthesis several other valuable chemicals like ammonia, syngas and some high-value hydrocarbons which have been demonstrated extensively on a lab-scale [65, 69, 72].

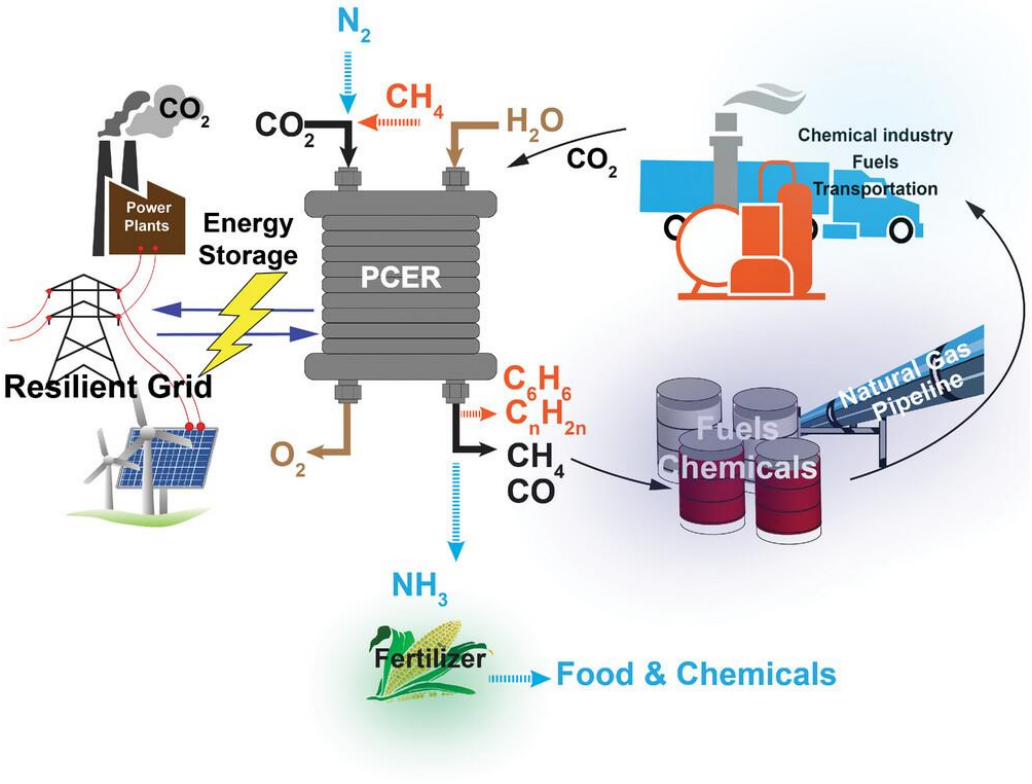

Fig. 1.10: Demonstration of the RePCEC for chemical storage and synthesis [68]

Fig. 1.9 depicts the major operation of RePCEC in this work, some other components briefly discussed its description are not shown. The overall operation of the integrated system which involves the balance of plants (BoP) and different configurational structure are not shown.

To understand the interplay between storage and conversion functions, especially with thermal management, it is necessary to conduct comprehensive system design analysis. As previously mentioned, bulk of this research endeavor is focused on designing appropriate system configurations to demonstrate the suitability and future advancement and integration of reversible methane electrochemical reactors as a highly efficient energy Storage system with different energy sources.

1.5 Problem statement and research objectives

The protonic ceramic electrochemical cell (PCEC) is a novel technology that can be used to produce chemicals and in the reverse operation for generating electricity. Previous studies have concentrated on establishing PCEC's potentiality as an individual electrochemical reactor and its materials development. However, integration of PCEC with fossil fuel power plants, renewable feedstock, and equipment as energy storage system is not studied. As a new and standalone technology, there are several challenges that accompany its operation ranging from its reaction and the charge defect transport. So, there is need to address these complexities and comprehensively answer the PCEC integration requirements with fossil fuel power plants, performance requirements, technical and non-technical gaps for it to be used as large-scale energy storage and eventual implementation at system level.

The overall objective of this dissertation to conduct comprehensive research to demonstrate the suitability and future advancement and integration of reversible methane electrochemical reactors as a highly Efficient Energy Storage (EES) system with fossil powerplants and renewable energy sources. Fundamental process and system models are developed to conduct a preliminary conceptual study. As a new and standalone electrochemical cell technology, there are several challenges that accompany its operation ranging from its reaction, the charge defect transport and coupled with its interaction with external components. So, this dissertation addresses these complexities and comprehensively answers the RePCEC integration requirements with fossil fuel power plants and renewable energy sources, performance requirements, technical and non-

technical challenges for it to be used as large-scale energy storage and eventual implementation at system level.

A significant part of this work is focused on devising and the idealization of the RePCEC system for various large-scale applications, crafting approaches for system integration, conceptualizing several system configurations, identifying crucial design, and operating parameters and devising RePCEC system simulation methodology. Summarily, the following research questions are answered which lead to significant contributions and generation of new knowledge.

- **RQ1**: What is the current status, challenges, and progress of PCFC, PCEC and RePCEC technologies?
- **RQ2**: How is the complexity of the reactions and ion-defects transport addressed at the cell level to capture the PCEC activities?
- **RQ3**: Can the PCEC stack be integrated with fossil fuel power plants and renewables and be used as an energy storage?
- **RQ4**: What are the optimum conditions and their influence for designing a cost-effective integrated energy storage system?
- **RQ5**: What are the impacts of renewables on the carbon footprint of the system and the types of uncertainties attached to the net energy usage and designing of energy storage systems?

Each research question refers to one aspect of the problem. The proposed approach in this work to step-wisely achieve these objectives involves using the systems engineering concepts such as the end-state approach to completely define the technology.

- **Objective 1**: Literature review in the PCEC field (**RQ1**)

Approach: A comprehensive review of literature is carried out to give insight into the ongoing advancements, the current technological status and identify the gaps in the development and commercialization of the PCEC technology

New knowledge: Overview of recent progress, advancement and highlight of gaps with PCEC technology.

- **Objective 2**: cell level model of PCEC for co-electrolysis reaction (**RQ2**)

Approach: Firstly, technical modeling of the RePCEC unit cell and stack using engineering equation solver (EES). This model is designed to represent details of reactive porous-media transport, elementary catalytic chemistry, electrochemistry and the high proton and oxygen

vacancy transport at intermediate temperature within unit cells of stacks. The EES is an excellent tool for solving the numerous systems of simultaneous non-linear equations. So, it is used for detailed modeling of the unit cell and PCEC stack. This detailed model is simplified to a reduce-order model that can be used for fundamental analysis of the proposed concept. These models are specifically used for the production of hydrogen and then translated for reversible PCECs as the energy storage system core. In all cases, the experimental results from our collaborators and national laboratories are used to determine performance characteristic curves and for validating our simulated models in EES.

New knowledge: Standardized and satisficing design of PCEC unit cell for the production of methane, hydrogen and other chemicals.

- **Objective 3**: Stack and system level model of RePCEC for co-electrolysis reaction (**RQ3**)

Approach: The cellular and stack level models are followed by a system level simulation in Aspen HYSYS. The main goal here is for comprehensive large-scale simulation of different balance of plant (BoP) components with the validated PCEC stacks. This is integrated with fossil fuel power plant and the renewables for hydrogen and methane production. Aspen HYSYS is chosen for modeling and simulation of the integrated system being a leading process simulation software with numerous specialized physical properties and comprehensive property databank. This enhances seamless thermodynamic modeling. Aspen HYSYS has integrated tools for equipment design, costing, energy management, safety analysis and sustainable operations. The PCEC stacks would be singly modelled in Aspen HYSYS transferring the results from the EES and validated to achieve the same results as the EES. The fossil fuel power plant and the BoP components which include evaporator, condenser, heat exchanger, compressor, heater, cooler and pump are thermodynamically simulated. These are integrated to generate the required feedstock into the PCEC stack in the integrated system.

New knowledge: Development of stack model and optimal design of integrated RePCEC systems for improved net energy usage and large-scale energy storage using water-energy nexus framework.

- **Objective 4**: Economic feasibility study of integrated RePCEC system operation for possible commercialization (**RQ4**)

Approach: Parametric studies are carried out with an in-built excel sheet and a separate excel tool linked with the system for techno-economic analysis and net energy analysis is implemented with aspen energy analyzer in Aspen HYSYS.

New knowledge: A comprehensive techno-economic analysis (TEA) of large-scale RePCEC operation that can predict the levelized cost of hydrogen and methane with the influencing factors. The first levelized cost of methane through co-electrolysis of CO_2 and H_2O in PCEC technology.

- **Objective 5**: Estimation of integrated RePCEC system operation carbon footprint (**RQ5**)

Approach: For sustainability assessment, it is very crucial to address the environmental impact of the newly integrated system and quantify the carbon footprint. To achieve this, SimaPro which is a powerful and global leading lifecycle analysis (LCA) solution software built on robust science and life cycle thinking is used. It requires four chronological strata for successful analysis. The scope of this work will begin with raw materials for the manufacturing of the RePCEC and the BOP. The LCA level is from cradle-to-gate, as such waste and material disposal are not discussed. The decommissioning of the plant is beyond the scope of this work as it is a new technology. The PCEC inventory and manufacturing processes are not readily available in SimaPro due to the infancy of the technology. These are modeled in SimaPro for PCEC system operation. Other BoP components not available in SimaPro are modeled which gives room for the full analysis of the integrated system. Sensitivity analysis and comparison of different energy feedstock for the process would be entrenched in this analysis to measure the climatic and carbon emission impact of the technology.

New knowledge: A comprehensive lifecycle analysis (LCA) of large-scale RePCEC operation and the balance of plant components for the integrated system to determine their global warming potential. Damage impact of coal-fired powerplant on human, environment and resource compared to solar photovoltaic.

The validations in this work are in stages similar to the model levels and are as follows.

-The PCEC cell and stack level validations: in this case analytical and experimental works from Kansas State University and national laboratories would be used validate:

---Hydrogen production from water electrolysis and

---Methane production from co-electrolysis of water and CO_2

-The system level validation: Here, the system sub-component and balance of plant components validation which would be carried out by comparing with data from controlled and real-world operations. Reasonable prediction of the quantity of hydrogen and methane produced with promising levelized cost in a reliable uncertainty window.

1.5.1 What is not addressed in this work

Due to the scope of this dissertation, complexity of the technology and the system coupled with time constraint, there are several areas not and cannot be addressed in this single work. The system operation is in steady state, the unsteady state operation of the stack and the system is not considered in this work. Furthermore, while energy storage typically involves some sort of disturbance and dynamism in its operation like start-up, shutdown, mode switching and load following, these are out of scope for this work and as a result dynamic operation of the system is not addressed.

1.6 Dissertation structure

After the detailed introduction to RePCEC in this chapter, subsequent ones address the highlighted objectives in a step-by-step manner. It is noteworthy to mention that these chapters entail in a whole or in parts some published or to-be published peer-reviewed journal papers. As such, each chapter is structured in paper format with its reference.

Firstly, **chapter 2** gives additional insight into the background of the technology and detailed review of most relevant and recent literature related to PCEC, PCFC, RePCEC and integrated systems. Research gap analysis based on the challenges and literature survey. **Chapter 3** addresses the design and modelling of the PCEC unit cell. Detailed the assumptions, equations, and methodology used in the cell-level modelling in these studies. **Chapter 4** delves into the design and modelling of the reversible protonic ceramic electrochemical cell (RePCEC) stack and the system. This involve the modelling of the fossil fuel powerplant and balance of plant components and integrated with the RePCEC system. Considering the need to capture CO_2 from the atmosphere and powerplants, a two-stage membrane carbon capture system is incorporated into the system. This chapter also embodies detailed RePCEC system analysis, highlight desirable operating conditions, and establish the limits of theoretical roundtrip efficiency. This chapter is also dedicated to model verification and validation. Comparing the models with experimental

results from our collaborators, literature, and national laboratories. The model is use for laboratory and large-scale prediction of processes and operating conditions. **Chapter 5** presents the economic analysis (EA), net energy analysis (NEA) and lifecycle analysis (LCA) of the system. It compares the system level operation of SOEC and PCEC. Levelized cost of hydrogen in both technologies and their carbon footprint are analyzed. The net energy requirement and heat integration potential at the system level are also analyzed. **Chapter 6** addresses cradle-to-gate analysis of the RePCEC system and levelized cost of methane production from the integrated system and parametric studies. Lastly, the dissertation is concluded with **chapter 7** which presents the dissertation summary and answers to the research questions. Added to this chapter is the research contributions and finalized with suggestions and future works. Fig. 1.7 Shows the outline of the dissertation and the relevant research questions and new knowledge.

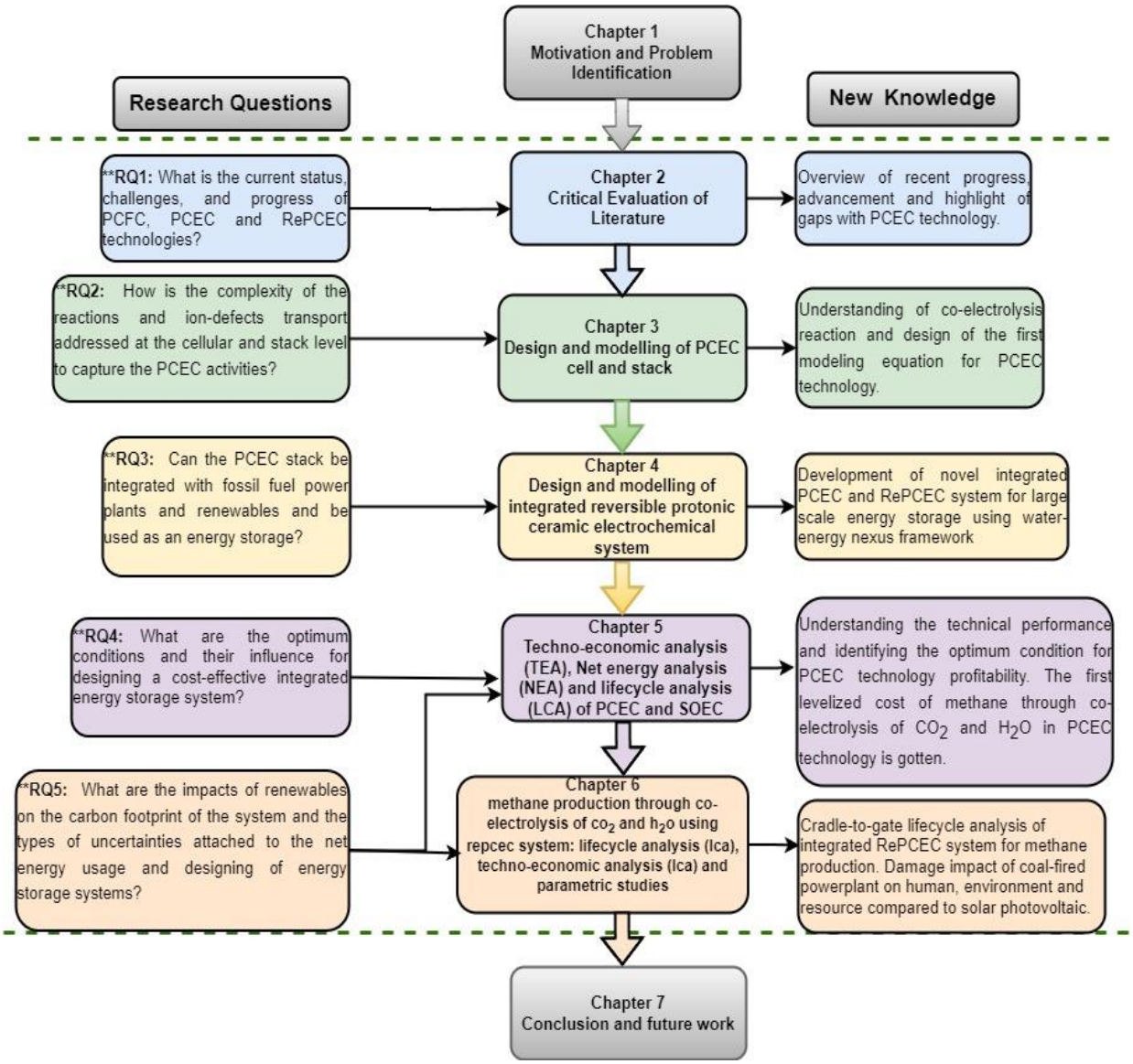

Fig. 1.11: Dissertation structure with relevant research questions and new knowledge.

CHAPTER 2 CRITICAL EVALUATION OF LITERATURE

? Research Question, RQ1: What is the current status, challenges, and progress of PCFC, PCEC and RePCEC technologies?

- **Objective 1**: Literature review in the PCEC field.

✓ **New knowledge**: Overview of recent progress, advancement and highlight of gaps with PCEC technology.

2.1 Literature review

The application of electricity to dissociate water into hydrogen and oxygen was dated back to the proper discovery of the British scientists William Nicholson and Sir Anthony Carlisle in the eighteenth century using a voltaic pile. This idea was informed after the first demonstration of hydrogen production from water in 1789 by two Dutchmen, Johan Rudolph Deiman – a medical doctor and Adriaan Paets van Troostwijk – a merchant using electrostatic generator as electricity source [73, 74], and the invention of the voltaic pile by Alessandro Volta in 1800 [75].

In 1839, William Groove discovered the fuel cell, its principle of operation, generating electricity from hydrogen and oxygen-reverse water electrolysis- only, remains the same. Fuel cells are not thermodynamically restrained by maximum thermal efficiency, and as a result, are very efficient in the conversion of chemical energy to electrical energy, also they are clean energy engines and they do not require recharging and use hydrogen as reactant [76].

The invention of the Gramme machine for the generation of direct current by Zenobe Gramme in 1869 made the production of hydrogen via water electrolysis very cheap. Although, the industrial synthesis method for large-scale hydrogen production from water was developed almost a century after the initial invention by a Russian engineer, Dmitry Lachinov in 1888 [77]. And in less than two decades, over 400 industrial alkaline water electrolyzers were globally available and functioning [78].

In the mid-to-late 1960s, the proton exchange membrane (PEM) electrolysis process was described and developed for the Gemini space program by General Electric (GE) using an acidic fluorinated

ionomer solid polymer electrolyte [55, 79]. This work on PEM cells was continued by GE till mid-1970s, when a PEM water electrolysis technology was developed for undersea life support which birthed the United States Navy oxygen generating plant. By the late 1980s it became an attractive technology due to the challenges faced with alkaline electrolyzers [80]. At almost the same time, the first high-temperature water electrolysis using a solid oxide electrolyzer (SOEC) was reported by Dönitz and Erdle [81] in the Hot Elly project in Germany. The commercialization of these two types of electrolyzers was futile despite all the technical progress made [75] due to a number of factors like the drop in the price of fossil fuels and governmental policies[82].

The interest in water electrolysis was revitalized in the 1990s because of the global need to decarbonize the world, and hydrogen was already considered as a green energy vector which could be used for renewables for a green economy [83].

However, J.B.S. Haldane, another British scientist, introduced the concept of renewable hydrogen as an electrochemical energy storage means in 1923 as proposed in his work science and the future. He suggested water electrolysis for hydrogen generation using excess energy from windmills which can be use at a later time to generate electricity [84, 85]. The focus of electrical energy storage has been on hydrogen generation, and more work were done after with different novelty. Shortly before this is the advent of Sabatier reaction in 1897 by two French chemists, Paul Sabatier and Jean-Baptiste Senderens. They produced methane from carbon dioxide and hydrogen using a nickel catalyst. This methane generation process has, however been perceived to be of immense importance for storing excess electricity in a renewable-energy controlled setup [52] in place of the direct hydrogen usage for energy storage [53].

The electrochemical cells are expected to play a significant role in the production of chemicals and fuels for energy storage in the nearest future [42] due to their potential to generate high-purity hydrogen that is carbon-free [43]. Presently, there are three major commercialized and conceptualized electrolyzing cells for hydrogen generation [86]. These include the alkaline electrolytic cell (AEC), which is regarded as the fundamental process for splitting water and is the most mature technology of all the electrolytic production of hydrogen [54] yet suffers some setbacks like low current density, low-pressure operation, and partial load. These challenges plaguing this electrolyzer were overcome by the advent of the polymer electrolyte membrane (PEM) electrolytic cell (PEMEC) [55]. Although, there are some recent claims that the advanced

alkaline electrolyzer showed superior efficiencies to the PEM water electrolyzer even while it is yet to reach its technological readiness level (TRL) [86, 87]. The PEMEC is as well faced with high capital cost, pure water requirement, and high system complexity which stems from its operational pressure [55, 56], which brought about the emergence of SOEC as a solution. Insufficient long-term stability has hindered the widespread use of this technology, most especially at high current densities, which is expected to be resolved with reversibility [57].

Customarily, the focus on chemical-to-electrical energy interconversion has been unidirectional in the device of interest [58], the electrolyzer is a mature technology, thus as the reverse operating device, the fuel cell which gains attraction due to its use of hydrogen for carbon-free electric power generation [59]. , The combination of these functionalities in a single reversible cell, will enhance a long-tern storage and stability, which will support a large-scale reversible cell technology deployment [44]. Based on this observation and projection, there is a switch toward this bifunctional technology, and researchers started working assiduously on reversible solid oxide cell (SOC) to get the best out of this technology. Graves et al [57], in their work on eliminating degradation in SOC, showed that reversible operations play a vital role in achieving higher efficiency and a better understanding of the degradation mechanism. Srikanth et al. [60] also worked using the regenerative SOC (rSOC) by exploring the flexibility of the technology by using coal in the generation of hydrogen. Likewise, Kazempoor and Braun [27] used a modeling approach to assess the performance of rSOC and its validation using mathematical models and showed that the electrochemical losses differ based on the operating mode. In seeking improvements for the rSOC and lower its operating temperature resulted in the evolution of the proton ceramic electrochemical cell (PCEC) which is an SOC with a proton-conducting electrolyte.

The development in the proton-conducting oxides (PCOs), which find its application in the protonic ceramic electrochemical cells, can be schematically represented as shown in Fig. 2.1 [46]. The light on the concept of proton conduction in a ceramic using $LaAlO_3$ was first mentioned by Forrat et al. in 1964 [88] in their work on a fuel cell. Even though the first power generation from this kind of fuel cell using hydrogen-air was proposed by Iwahara et al. in 1983 but suffered some setbacks due to poor sinterability of the protonic ceramics and fabrication complexities which made it to be abandoned [89]. But after the breakthrough in material sintering and device

fabrication led by Babilo and Haile in 2005 [47], PCOs picked up again and have been of greater attention in the past decade [46]. In 2010, a cluster of research was carried out in improving the sinterability of the protonic ceramics using different metallic oxides like CoO, CuO, NiO, and ZnO as sintering aids [48-50].

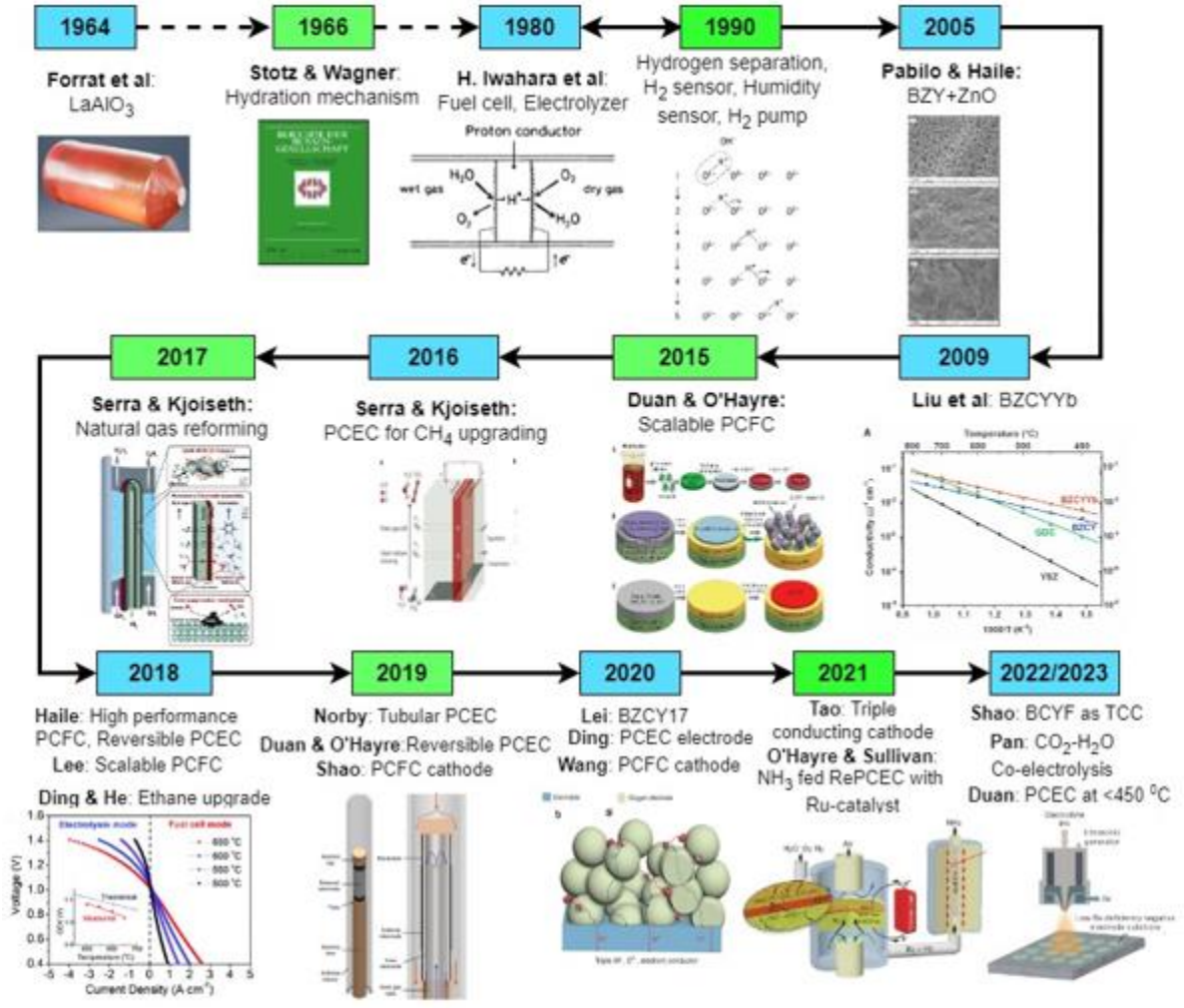

Fig. 2.1: History of proton conducting oxide and applications [46, 47, 65, 88, 90-95]

Additionally, to the power-generating ability of the protonic ceramics, they have been explored for chemical production via electrolysis. The reverse operation of the H_2-air PCFCs is used in hydrogen production through steam electrolysis. In 2019, the protonic ceramic electrolysis cells (PCECs) showed very high efficiency for hydrogen production in work by Duan et al. [29], and they demonstrated similar efficiency for the reversible protonic ceramic electrochemical cells (RePCECs). The PCEC is a proton conductor-based SOC that is bifunctional in its ability to store

energy and renewables, utilizing water electrolysis to produce hydrogen in its electrolyzer mode and using the produced hydrogen in its fuel cell mode to generate electricity [96]. With the considerable progress that has been made in solid-state proton conductors and their application in electrochemical cells in the last decade [97, 98], PCEC seems to be a promising technology in accomplishing the cheap energy storage and conversion goal, as it offers higher efficiencies (faradaic and roundtrip) at low temperature [99] coupled with its low-cost materials [100] and longer system durability property [101]. Despite all these, the PCEC is yet to be deployed on a large scale due to some serious limitations in the developing efficiently robust electrodes that can withstand high-steam concentration at an intermediate temperature [102]. This setback motivated Ding et al. [51] to use a triple conducting electrode to develop a PCEC with a self-sustainable operation that generates hydrogen at a fast rate that is sufficient for the reverse operation to generate electricity without an external hydrogen feed. As of 2021, over twenty review articles give comprehensive analysis of several novels and scientific contributions towards the PCEC, including the only detailed bibliometric review by Idris et al [103]. Other than the reviews, several works have been done of late due to the resurgence of this technology and the most relevant ones for future development would be summarized below. The review will cover and recapitulate the protonic ceramic oxides (PCO), protonic ceramic fuel cell (PCFC), protonic ceramic electrolysis cell (PCEC) and reversible protonic ceramic electrochemical cells (RePCECs).

2.2 Proton-conducting oxides (PCO)

The proton-conducting oxides (PCOs) which are simply called protonic ceramics are typically oxides with oxygen-deficiency (shortage of oxygen atom) which results in oxygen vacancies. These vacancies are extrinsic defects mainly induced through doping. The PCOs possess numerous advantages like high proton conductivity at a relatively low temperature range of 300-700 ℃ and are cheap [98, 104]. These materials are well known to the materials research community and have been the subject of active research for decades with recorded history of development as shown in Fig. 2.1. The first report by Iwahala and co-workers in 1980s on proton conductivity in oxides, especially in 1981 on the revelation of proton conduction in variants of the perovskite SrCeO3 ignited several decades of research on PCOs. By the end of 1980s, they had identified yttrium-doped barium cerate (BCY) as the leading proton conductor for electrochemical devices. This is due to its exceptional attributes which include minimal electronic leakage, easy sintering, and high proton conductivity [46]. However, it became evident that BCY and other barium cerates had a

notable drawback such as thermodynamic instability when exposed to water and CO_2, rendering them unsuitable for various applications. Consequently, researchers redirected their efforts and focus towards barium zirconates, particularly BZY, owing to its impressive proton conductivity and significantly improved chemical stability. Among the studied examples, yttrium-doped barium zirconates and cerates have been the most extensively researched due to their impressive protonic conductivity and stability [35, 98, 104, 105]. The BCY and BZY properties have been synergized to produce BCZY which seems to possess the attributes of both with performance compromise [106]. The PCO generally exhibit high chemical resistance to coking and poisoning, thus negating the necessity for an initial separation process when used [107].

The PCOs have different classifications based on active temperature range, transport nature, arrangement of oxygen deficit and oxide structures. Several PCO structures have been studied, they include mayenite- $A_{12}B_{14}X_{33}$, brownmillerite- $A_2B_2X_5$, apatite- $A_{10}B_6X_2$, fluorite and perovskites [108] which is the material of focus in this work. The perovskite structure ABX_3 (Fig. 2.2) has been mostly adopted and studied for proton conductors (the electrolyte and the electrodes) of PCECs. The A, B and X usually represent a divalent cation (like Sr^{2+} and Ba^{2+}), tetravalent cation (like Ce^{4+}, Zr^{4+}), trivalent cation (like Yb^{3+}, Y^{3+}) and anions (frequently oxide) respectively. The degree of proton passage and uptake for perovskite materials of the type $(Ba,Sr)(Ce,Zr,Y,Yb)O_{3-\delta}$ is a function of oxygen basicity [109].

Among the range of candidate elements such as Gd, Yb,Sc,Dy,Nd and others, Yttrium (Y) has been firmly recognized as most effective acceptor dopant for the B-site for both barium zirconates and cerates [46]. Proton conduction differs from that of oxygen ion and other charge carriers due to the small size and strong polarizing effects of proton which make its transport mechanism got attention. The PCO materials are majorly employed in electrochemical cells as electrolyte and serve as supports for electrocatalysts there in. Due to high protonic conductivity, they are fast becoming promising as a prospective material for the upcoming generation of electrochemical storage and energy conversion [110-112]. This has prompted ongoing and immediate research on PCO in the electrochemical community towards developing and advancing the creation of low-cost and long-lasting devices with excellent and efficient energy conversion and its storage.

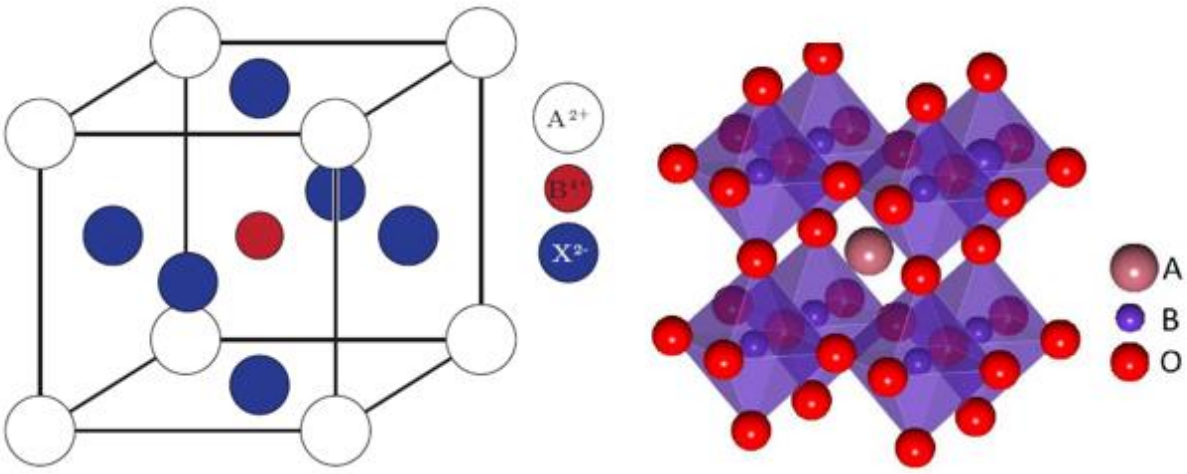

Fig. 2.2: The perovskite cubic and crystal structure [113]

The synthesis and processing of the protonic ceramics have been extensively discussed in literature [46, 114-116]. The primary uses of PCO can be categorized based on the electrochemical conversion processes and the intended end products, the include PCFC, PCEC and RePCEC which would be the subject of discussion in subsequent sections.

2.3 Protonic ceramic fuel cell (PCFC)

Generally, the protonic ceramic electrochemical cells are types of the solid oxide cell. As such, the protonic ceramic fuel cell (PCFC) can be classified as a sub-category of the solid oxide fuel cell (SOFC). Basically, the SOFC has been divided into two primary categories; the customary oxide ion-conducting fuel cell (O-SOFC) which utilize oxygen ion conductors as electrolytes. The second category is the PCFC (often written as H-SOFC) that employs PCOs as electrolytes. Some of the advantages of using the PCO as electrolyte over the oxygen-ion conducting oxide is that it offers the potential to lower the ohmic resistance, particularly when operating <600℃. This falls within its lower operating temperatures of 300-600 ℃ which has some other economic and durability merits [39]. Most of the advantages the SOFCs possessed over other fuel cells is similarly shared by PCFCs. However, the PCFC also offers several distinct benefits beyond the popularly known lower operating temperatures gained with use of the PCO which include outstanding stability and exceptional resistance to coking.

The first supposed to be PCFC was initiated in 1983, when Iwahara et al utilized PCO in their fuel cell design for generating power with hydrogen as reactant. Research towards the technology almost went into extinction and faded until a sintering solution was found by Babilo and Haile in 2005 [47]. They used ZnO to enhance the sintering of PCO used as electrolyte in the device. This concept was leveraged, and this invigorated the attention toward the PCFC. In 2015, O'Hayre firstly employed and adopted the Solid-State Reactive Sintering (SSRS) as a key technique for manufacturing PCFC [98]. This also added to the interest toward this technology. This renewed attention is driven by their inherent benefits coupled with the previously mentioned like low operating temperatures, which include low cost of raw materials. Their operating temperatures proffers solutions to the SOFC stability challenges at high temperatures and effectively address the concerns related to the slow kinetics observed in PEMFCs. This section of the work will be summarizing works on PCFC using tables and figures. Using the web of science (WoS) for the data collation on studies done on PCFC for the past two decades after typing protonic ceramic fuel cell and PCFC as keywords, Fig. 2.3 was generated. From the figures, an overview and analysis of total of 177 articles is highlighted by WoS and were randomly examined. The area of interest, research focus and problem addressed on PCFC by these studies would be summarized in the following paragraphs.

Fig. 2.3a shows that there is a growing interest in the technology as an alternative to SOFC as more work are being published since its resurgence. Most of these studies focused on the design, development, production and improving the PCFC material components, ranging from the electrolyte [117, 118], cathode [119-122] and the anode [123, 124] depending on the reaction goal. The PCFC technology has been used to generate electricity using different fuels including H_2

which has become conventional and mostly used in the earlier works on PCFC [92], ammonia [125, 126], methane [127] and ethanol[128]. Some of these works have also focused on the geometry and structural configuration of the materials to drive their performance. The geometry structure includes material size and thickness [118] while the configuration put the planar and tubular configuration into perspective. Several computational and numerical analysis [129] were employed and adopted in the model of PCFC using different model like Nernst-Planck-Poisson model[130]. Most often than not, some of these works compared between the base SOFC and the improved PCFC [131] for performance and economic analysis.

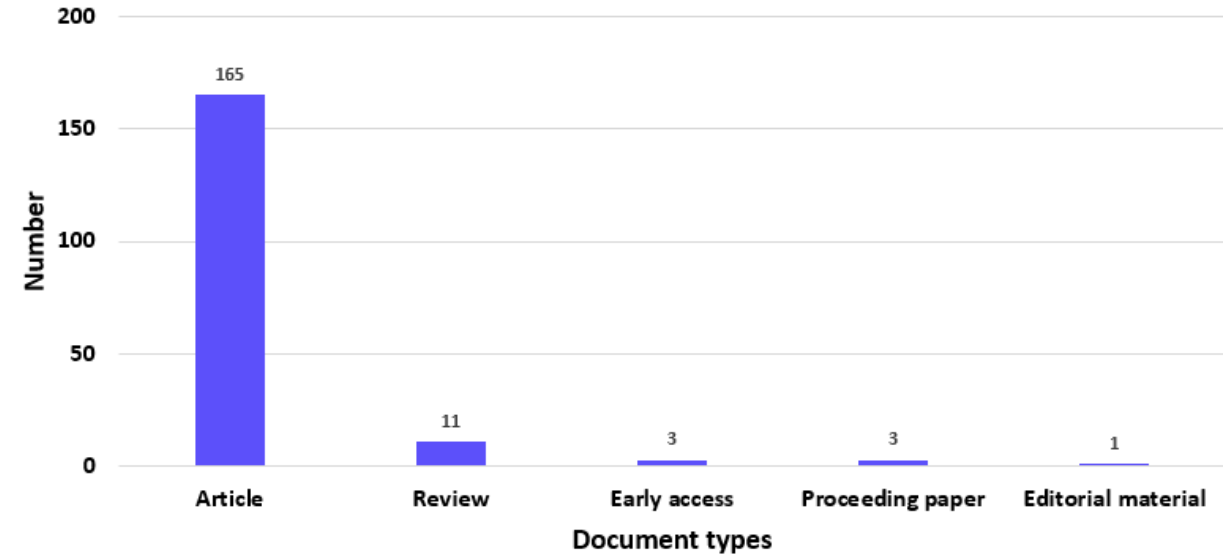

(a)

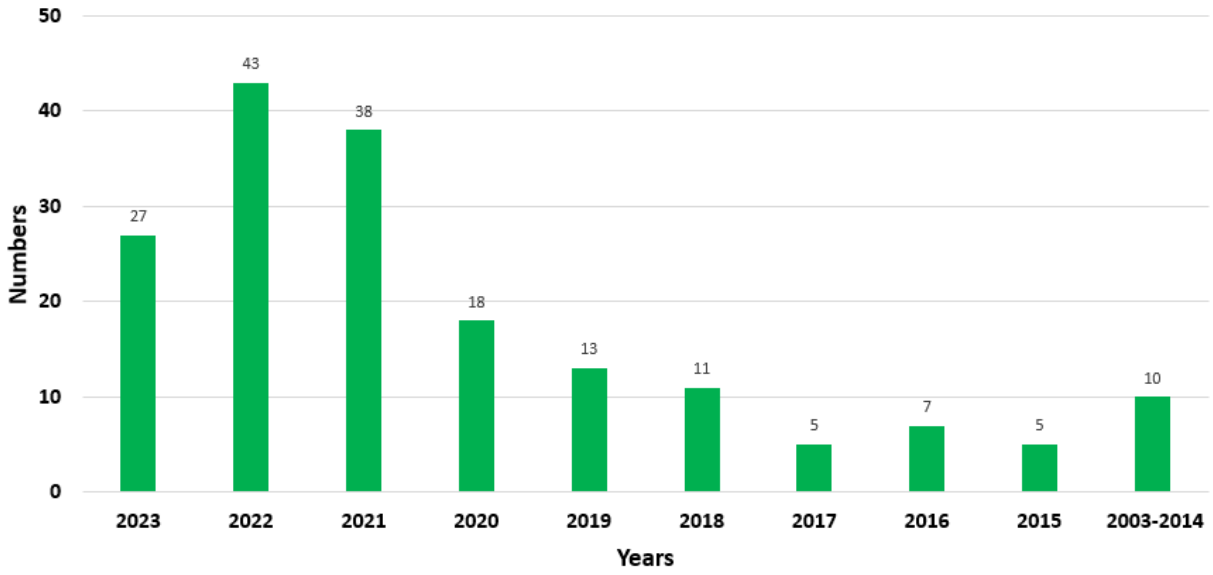

(b)

Fig. 2.3: PCFC research output for two decades (a) Document types (b) Years

Others have focused on improving the durability of PCFC to address the issue of degradation [132, 133]. Prior to this, critical analysis of the PCFC and PCEC at the cellular level for their electrochemistry and energy conversion was carried out to drive hydrogen economy and global decarbonization[134]. Some others, however, combine the assessment of the PCFC and PCEC in a single work to show the growing interest in the twin technology and sometimes include RePCEC

[135]. From the numerous ongoing research initiatives dedicated to tackling the material challenges encountered by PCFC, its design and the use of several feedstock for its operations, only one has partly addressed its economics [136]. In this work by Dubois et al [136] about six years ago compared the competitiveness of PCFC production cost with that of SOFC. It was assumed that SOFC at its operating temperature would produce a power density that is almost 1.5 times what is produced by PCFC. This implies three PCFC is required to produce the equivalent of two SOFC which still gives SOFC an edge economically. Interestingly, the immense efforts toward material development have yielded good results and there are PCO that are used in PCFC that gives higher power density than the SOFC [117] which makes PCFC a better option. However, a critical techno-economic analysis is urgently required to give an excellent detail of progress made with the PCFC manufacturing in enhancing its large-scale implementation. To date, nobody has attempted to address the lifecycle analysis and carbon footprint of this technology. Likewise, limited efforts have been made to explore the steady and dynamic modeling of PCFC [137] in the computational arena and its thermodynamics. Even though more attention has been given to the steady state modeling and perhaps the study by Albrecht et al [137] is the only reported wok on the dynamic model of PCFC. Kyle et al [67] pioneered the first integrated system model with PCFC in 2021 and not much has been seen in literature afterwards. PCFC system integration is part of the areas of direct application of the technology that needs more attention for successful implementation of this technology and the final outcome and fruits of previous research efforts that have been expended on the design of PCO and other PCFC materials. Some of the work done after its resurgence are tabulated in table 2.1 with their performance geared toward the power density of the PCFC. The operation of the PCFC is diagrammatically illustrated in Fig. 2.4.

Table 2.1: PCFC selected works to address performance

Title	efficiency	Ref	Fuel	Level	Components type	Material	Temperature, C	Power density, W/cm2
Probing oxygen reduction and water uptake kinetics of $BaCo_{0.4}Fe_{0.4}Zr_{0.1}Y_{0.1-x}Zn_xO_{3-\delta}$ cathodes for protonic ceramic fuel cells		[119]	H_2	cell	Cathode	$BaCo_{0.4}Fe_{0.4}Zr_{0.1}Zn_{0.1}O_{3-\delta}$ (BCFZZn)	600	0.49
Ceramics breakthrough		[117]	H_2	cell			500 & 600	0.55 & 1.1
High performance protonic ceramic fuel cell systems for distributed power generation	70%	[67]	H_2	system		$BaZr_{0.8}Y_{0.2}O_{3-\delta}$ (BZY20)	550 & 600	
Exceptionally high performance of protonic ceramic fuel cells with stoichiometric electrolytes		[138]	H_2			$BaZr_{0.4}Ce_{0.4}Y_{0.1}Yb_{0.1}O_{3-\delta}$ (BZCYYb)	550 & 650	1.01 & 1.9
Exceptional power density and stability at intermediate temperatures in protonic ceramic fuel cells		[111]	H_2		PBSCF	BZCYYb4411	500	0.5
The $BaCe_{0.16}Y_{0.04}Fe_{0.8}O_{3-\delta}$ nanocomposite: a new high-performance cobalt-free triple-conducting cathode for protonic ceramic fuel cells		[139]	H_2		$BaCe_{0.16}Y_{0.04}Fe_{0.8}O_{3-\delta}$	$BaZr_{0.1}Ce_{0.7}Y_{0.1}Yb_{0.1}O_{3-\delta}$	650	0.29

operating at reduced temperatures								
Direct ethanol-fueled protonic ceramic fuel cell with reforming layer operating at low temperature		[128]	H_2				500	0.184
Steady-State and Dynamic Modeling of Intermediate-Temperature Protonic Ceramic Fuel Cells		[137]	H_2			BCZYYb	500	0.125
Characterization of direct ammonia proton conducting tubular ceramic fuel cells for maritime applications		[140]	NH_3			$BaCe_{0.7}Zr_{0.1}Y_{0.16}Zn_{0.04}O_{3-\delta}$	750	
A New Durable Surface Nanoparticles-Modified Perovskite Cathode for Protonic Ceramic Fuel Cells from Selective Cation Exsolution under Oxidizing Atmosphere		[141]	H_2				650	1.04

High performance tubular protonic ceramic fuel cells via highly-scalable extrusion process		[142]	H_2		BSCF		600	0.534
Zr and Y co-doped perovskite as a stable, high-performance cathode for solid oxide fuel cells operating below 500 °C		[143]	H_2		$BaCo_{0.4}Fe_{0.4}Zr0.1Y_{0.1}O_{3-\delta}$	BSCF	500	0.97

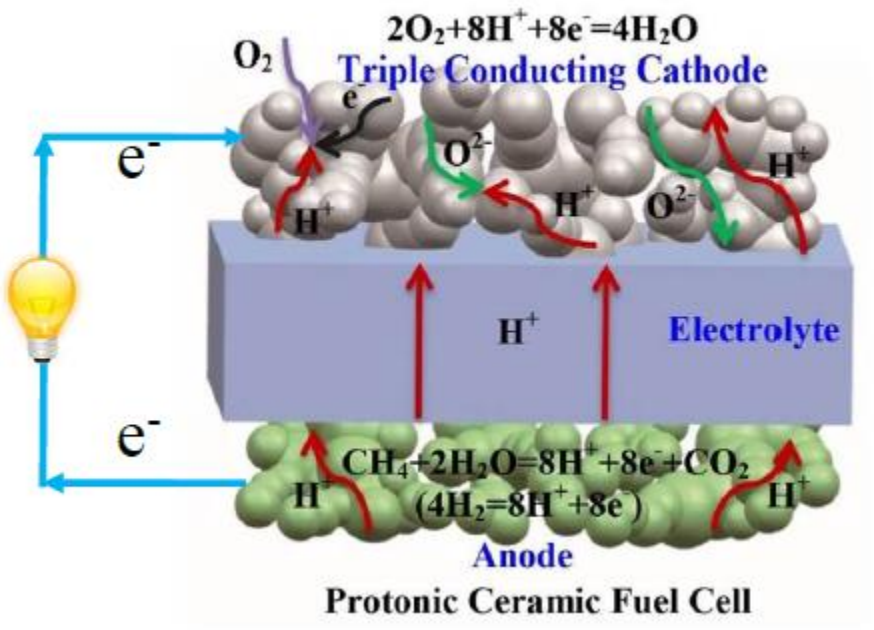

Fig. 2.4: PCFC operation

2.4 Protonic ceramic electrolysis cell (PCEC)

In seeking improvements for the solid oxide electrochemical cells (SOEC, SOFC and rSOC) and lower its operating temperature resulted in the evolution of the proton ceramic electrochemical cell (PCEC) which is an SOC with a proton-conducting electrolyte. This is also called Proton conducting solid oxide electrolysis cell (H-SOEC). The development in the proton-conducting oxides, which find its application in the protonic ceramic electrochemical cells was first mentioned by Forrat et al. in 1964 in their work on a fuel cell while using $LaAlO_3$. This concept suffered some setbacks due to poor sinterability of the protonic ceramics and fabrication complexities which made it to be abandoned [92]. But after the breakthrough in material sintering and device fabrication which was led by Babilo and Haile in 2005 [47] then, it picked up again and has been of greater attention less than a decade ago [46]. In 2010, a cluster of research was carried out in improving the sinterability of the protonic ceramics using different metallic oxides like CoO, CuO, NiO, and ZnO as sintering aids [49, 50]. Additionally, to the power-generating ability of the protonic ceramics, they have been explored for chemical production via electrolysis. The reverse operation of the H_2-air PCFCs is used in hydrogen production through steam electrolysis. In 2019,

the protonic ceramic electrolysis cells (PCECs) showed very high efficiency for hydrogen production in work by Duan et al. [29, 97], and they demonstrated similar efficiency for the reversible protonic ceramic electrochemical cells (RePCECs). With the considerable progress that has been made in solid-state proton conductors and their application in electrochemical cells in the last decade [98]. PCEC seems to be a promising technology in accomplishing the cheap energy storage and conversion goal. As it offers higher efficiencies (faradaic and roundtrip) at low temperature [99] coupled with its low-cost materials [100] and longer system durability property [101]. Despite all these, the PCEC is yet to be deployed on a large scale due to some serious limitations in the developing efficiently robust electrodes that can withstand high-steam concentration at an intermediate temperature [102]. This setback motivated Ding et al. [144] to use a triple conducting electrode to develop a PCEC with a self-sustainable operation that generates hydrogen at a fast rate that is sufficient for the reverse operation to generate electricity without an external hydrogen feed. Another appealing characteristics of PCEC is being an efficient energy transition technology that can operate at intermediate temperatures [145]. They operate at temperatures lower than the conventional SOECs, typically between 400°C and 600°C. At these lower operating temperatures, a proton-conducting electrolyte is used in place of traditional oxygen ion-conducting ceramic electrolyte. A schematic diagram of the electrolytic mode of operation using a proton-conducting electrolyte is shown in Fig. 2.5.

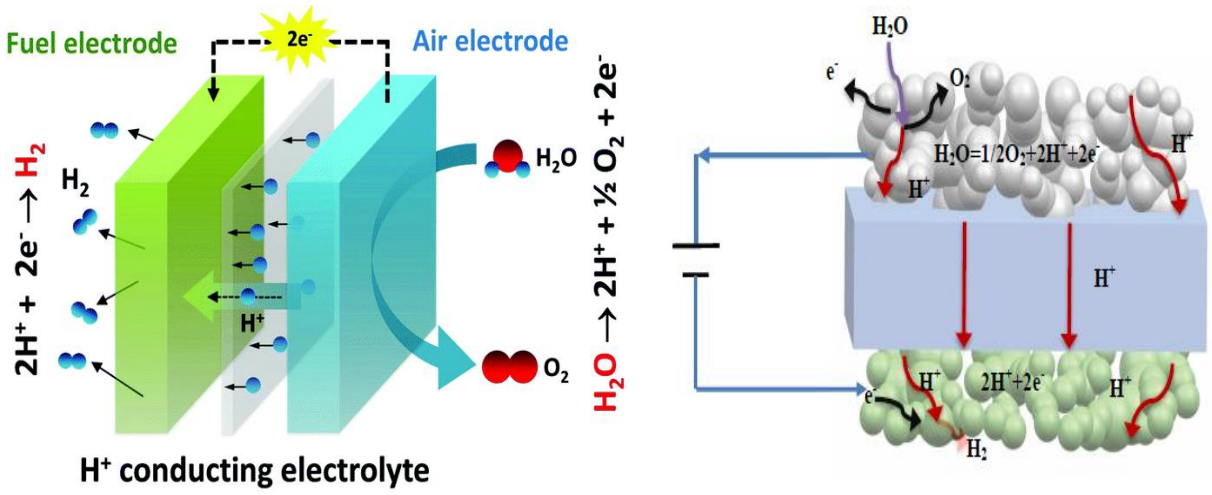

Fig. 2.5: Water electrolysis with a proton-conducting electrolyte [44].

The operation of PCECs for co-electrolysis of H_2 and CO_2 is similar to that of SOECs; steam is electrochemically oxidized at the anode and simultaneously departs into oxygen and protons (equation 1). When protons diffuse across the electrolyte to the cathode, they produce pure hydrogen at the interface (equation 2). At the same time, CO_2 fed to the cathode reacts with hydrogen via the reverse water-gas-shift (RWGS) reaction (equation 3), producing CO on the cathode side [146].

Anode $H_2O \rightarrow 2H^+ + 0.5O_2 + 2e^-$ ……..(1)

Cathode $2H^+ + 2e^- \rightarrow H_2$ ……(2)

$CO_2 + H_2 \leftrightarrow CO + H_2O$ ……(3)

PCECs have the potential to improve the efficiency and reduce the cost of hydrogen production because of their lower operating temperatures and reduced material degradation.

As of 2021, over twenty review articles gave comprehensive analysis of several novel and scientific contributions towards the PCEC, including the only detailed bibliometric review by Idris et al [103]. In recent times, huge efforts have been expended in the improvement of electrode and electrolyte materials of this technology. Yet, inadequate attention is paid to the fundamental design of H-SOEC, and it is less explored for the synthesis of chemical products. Some of these issues were comprehensively addressed by Liu et al [147]. However, PCECs are still in the early stages of development, and several technical challenges need to be addressed to achieve commercial viability, such as improving the proton conductivity and stability of the electrolyte, reducing electrode polarization, and optimizing the cell design for high performance and durability. Nonetheless, PCECs are a promising area of research for the development of low-temperature, efficient, and cost-effective hydrogen production technology.

The PCEC mode of operation with water as feedstock to produce hydrogen and electricity can be represented by,

Electricity (electrolysis)

$$Overall: H_2O \leftrightarrow H_2 + \frac{1}{2}O_2 \qquad (1)$$

Electricity (fuel cell)

A schematic diagram of this electrolytic mode of operation using a proton-conducting electrolyte is shown in Fig. 2.5.

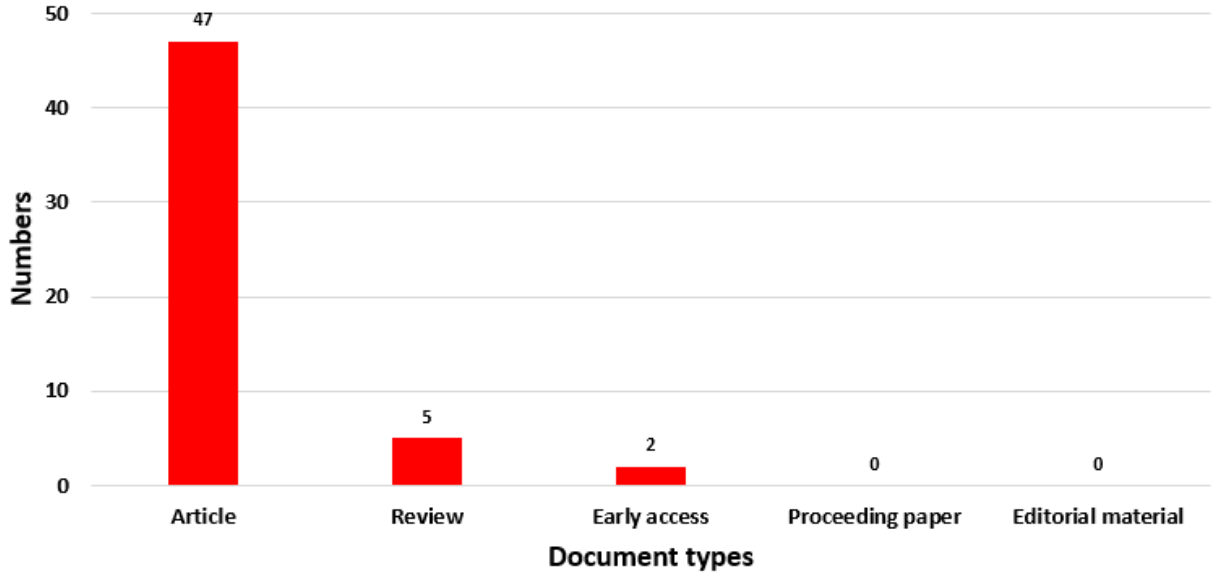

(a)

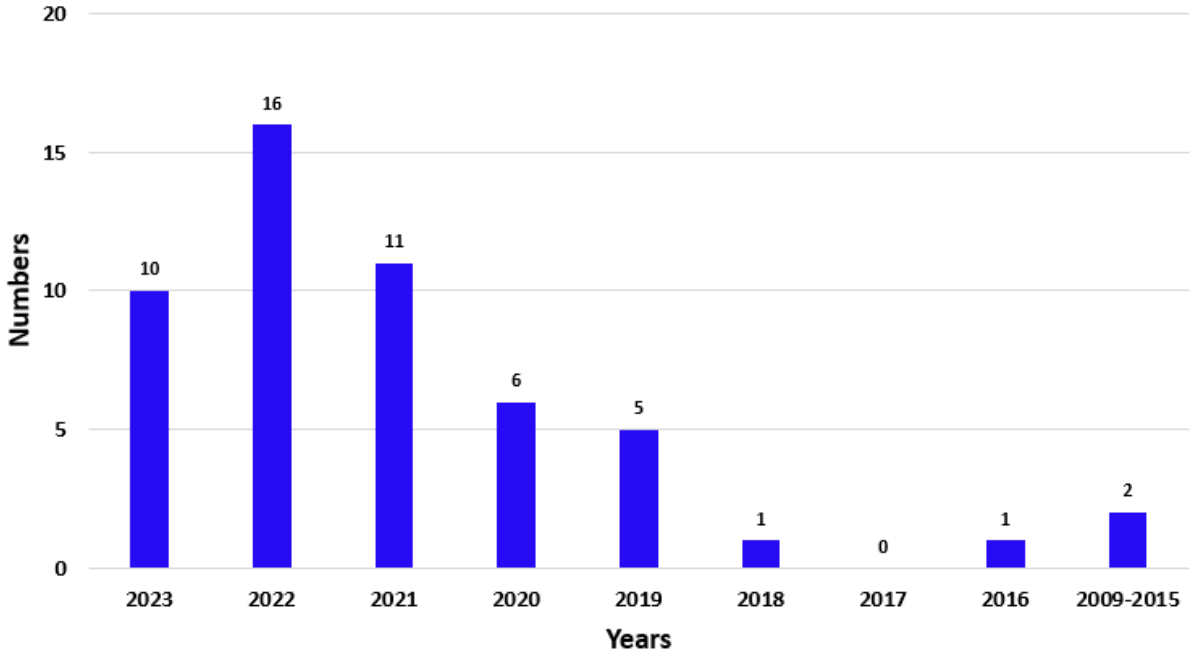

(b)

Fig. 2.6: PCEC research output for a decade (a) Document types (b) Years

The web of science is also used in gathering information on PCEC as done with PCFC using the keywords Protonic ceramic electrolysis cells and PCECs gave a total of 26 articles. With in-depth review of literature, there have been discrepancies in the number of words used in describing the PCEC. As a result, some other keywords were added and they include "proton-conducting electrochemical cells", "protonic ceramic electrochemical cell" and "protonic ceramic electrolyzer cell". This doubles the number of outcomes to 52 documents. Obviously, comparing Fig. 2.3 and Fig. 2.6 more studies have been done on PCFC than the PCEC which is the norm in the electrochemical community. Attention is usually focused on developing the fuel cells for a particular technology before the electrolysis. This is intuitively understandable because there is higher clamoring and need for energy and electricity generation than the need to store them or need to use electrochemical cell to produce useful chemicals which have alternative reactors for their production. Since this technology is in its infancy, focus has been on the development of its component materials and studies have shown that some materials that give high performance with PCFC did the same with PCEC [94]. So, it can be partially concluded that material development for PCFC is material development for PCEC even though experience have shown that it is not always the case due to difference in reactions. For example, in catalysis, Fe is good catalyst for ammonia synthesis but it is not for its decomposition [148]. So, the materials for ammonia fueled PCFC might give a high-power density and energy conversion and the production of ammonia using the PCEC might have low efficiency. From all the published documents, only one has discussed the small-scale integration of PCEC with methanal synthesis system [149]. Unfortunately, none has discussed the integration of the PCEC for a large-scale operation like powerplant and some other fossil fuel assets. Likewise, the economies of the PCEC and its lifecycle analysis are black areas that have not been touched and critically examined. These areas should be of interest for researchers as they are key for driving sustainability and wide range implementation. The following section is going to be a review of literature on the RePCEC which is a standalone device that combines the activity of PCFC and PCEC in one technology.

2.5 Reversible protonic ceramic electrochemical cells (RePCECs)

As shown in the introductory chapter of this dissertation, that there has been an unprecedented growth in renewable energy and this trend is envisaged to continue. So, this called for the need for energy storage system to store these renewables due to their intermittency during the low demand period. There are criteria set for a potential energy storage system and reversible electrochemical

cells like the RePCEC is believed to have the potential to fulfill these criteria. Consequently, researchers have set out in the last decade studying this technology and the work so far is summarized in Fig. 2.7. It is presumed that for global energy sustainability that there is need for integration of equipment and processes, this drives the competitive research between PCEC (52 documents) and RePCEC (47 documents) as reflected in the research output in both Fig. 2.6 and Fig. 2.7.

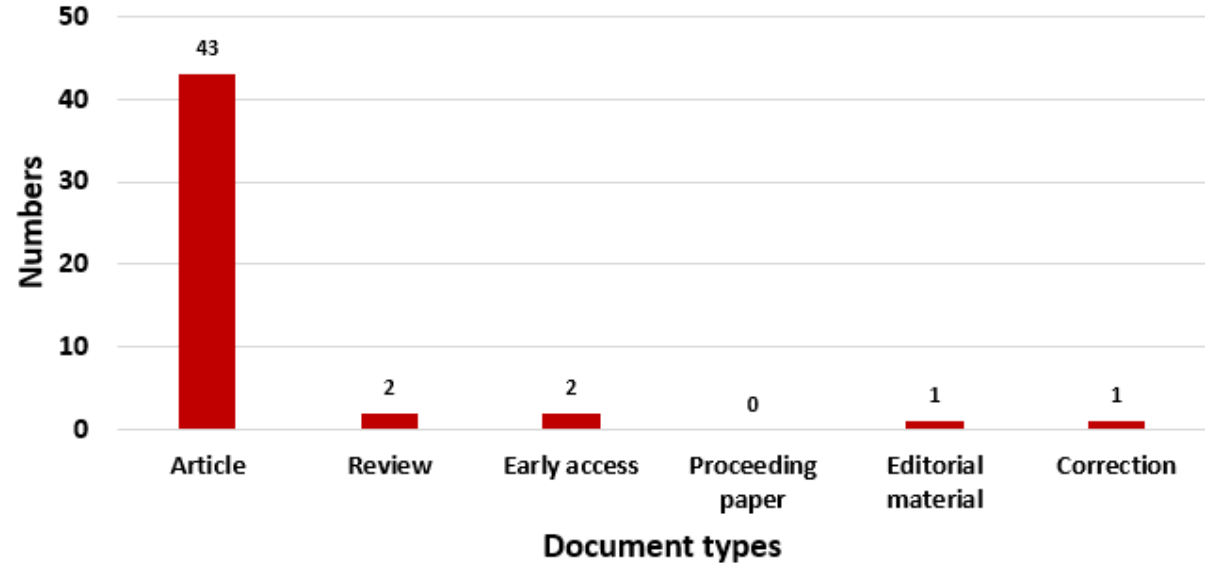

(a)

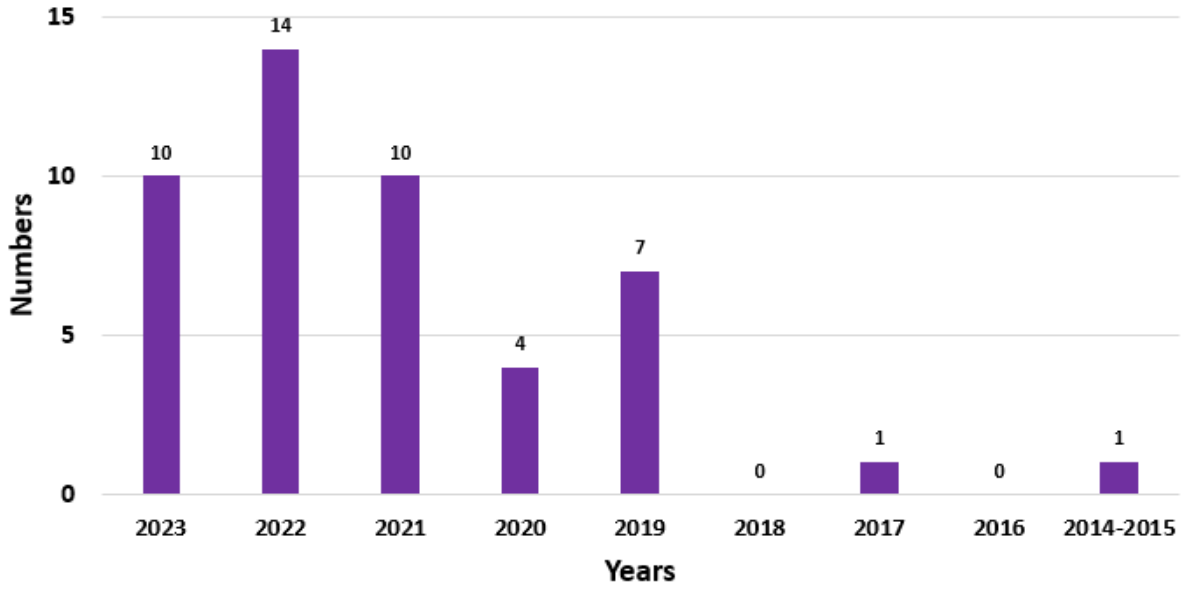

(b)

Fig. 2.7: RePCEC research output for a decade (a) Document types (b) Years

One of the big challenges faced with this technology is developing and designing electrodes that would be bifunctional, that it is works excellently well if used in both the PCFC and PCEC modes of operation. This is highly challenging because most often than not the kinetics and thermodynamics for a forward and backward reaction are different. Now, designing a single electrode that keys into both operations is the big task ahead. However, researchers are unravelling this bottleneck which is said to be hindering the performance of this technology. Zhou et al [150] in their work coated the conventional LSCF air electrode with barium cobaltite (BCO) to enhance its stability and improve the sluggish kinetics of the oxygen reduction reaction (ORR) and oxygen evolution reactions (OER). He et al [37] in an attempt to solve the same problem of slow ORR and OER kinetics optimized the interaction between BCMN and BCO to develop $Ba_2Co_{1.5}Mo_{0.25}Nb_{0.25}O_{6-\delta}$ (BC1.5MN) composite air electrode. Several studies [71, 151, 152] are steered towards the improvement of the oxygen electrode because of its importance on the cell reaction kinetics and eventual performance. Recently, Pei et al [153] also coated a double-perovskite $PrBaCo_2O_{5+\delta}$ (PBC) air electrode with $Pr_{0.1}Ce_{0.9}O_{2+\delta}$ (PCO) to reduce its area-specific resistance to 0.096 Ωcm^2 which further enhance the fuel electrode and overall cell performance. Steam and hydrogen are most used fuel for both PCEC and PCFC operations respectively in this technology even though there is report of CO2 and hydrocarbon been used [29, 46]. In 2021, Zhu et al [65] reported the first ammonia-fed RePCEC which at 650℃ gives a peak power density of 0.877Wcm^{-2} in the PCFC mode. In the PCEC mode under 75% steam concentration, it gives almost 100% H_2 Faradaic efficiency in the current density rage of 0.5-1.0 A/cm^2. Immense efforts have been channeled more towards the development of the electrodes especially the oxygen/air electrode as shown in the keyword network visualization generated using VOSviewer software for RePCEC literature in Fig. 2.8 and studies are still ongoing in this direction. Some of these key research outputs are summarized in table 2.2. This praiseworthy, as the Faradaic efficiency in the PCEC mode must be greater than 90% and the roundtrip efficiency must be above 75% [46] for this technology to be competitive and economically viable. So, the reason for this continuous strive on developing RePCEC materials that can achieve these targets. Perusing the literature, it shows that there is currently no documentation on the anticipated integratiom of this technology into any

fossil fuel or renewable energy sources, a potential breakthrough that has yet to be explored.

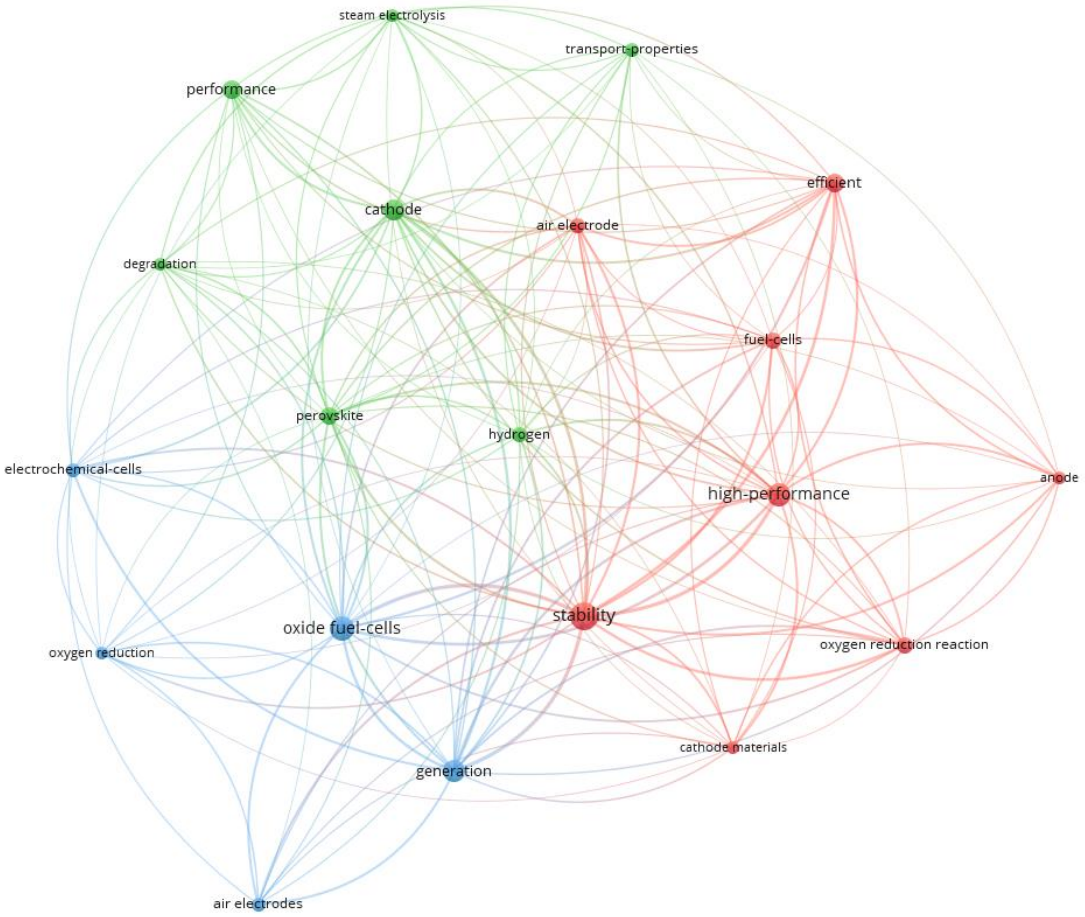

Fig. 2.8: Keyword clusters and network visualization for RePCEC literature for a decade

applications. Likewise, this technology is devoid of detailed techno-economic and lifecycle analysis which are among the biggest drivers of sustainability. This dissertation will be addressing some of these knowledge gaps in detail.

Table 2.2: RePCEC literature summary

Authors	Title	Voltage, V	Current density, A/cm^2	Temperature, °C	Materials	Ref	Year	Peak Power density, W/cm^2
Kang et. al	An Efficient Steam-Induced Heterostructured Air Electrode for Protonic Ceramic Electrochemical Cells	1.3	2.148	550	$PrBaCo_{1.6}Fe_{0.2}Nb_{0.2}O_{5+\delta}$	[71]	2022	1.059
Yucun et al.	An Efficient Bifunctional Air Electrode for Reversible Protonic Ceramic Electrochemical Cells	1.3	1.8	600	$La_{0.6}Sr_{0.4}Co_{0.2}Fe_{0.8}O_{3-\delta}$ (LSCF)	[150]	2021	1.16
Yucun et al.	An Active and Robust Air Electrode for Reversible Protonic Ceramic Electrochemical Cells	1.3	1.51	600	$PrBa_{0.8}Ca_{0.2}Co_2O_{5+\delta}$	[154]	2021	1.06
Duan et al.	Highly efficient reversible protonic ceramic electrochemical cells for power generation and fuel production	1.45	2	600	BCZYYb-based	[29]	2019	0.65
Choi et al.	Protonic ceramic electrochemical cells for hydrogen production and electricity generation: exceptional reversibility, stability, and demonstrated faradaic efficiency	1.3	1.8	600	$PrBa_{0.5}Sr_{0.5}Co_{1.5}Fe_{0.5}O_{5+\delta}$	[44]	2018	0.8

Niu et al.	Highly Active and Durable Air Electrodes for Reversible Protonic Ceramic Electrochemical Cells Enabled by an Efficient Bifunctional Catalyst	1.3	1.82	600	$(La_{0.6}Sr_{0.4})_{0.95}Co_{0.2}Fe_{0.8}O_{3-\delta}$ (LSCF)	[155]	2022	1.04
Pei et al.	Surface restructuring of a perovskite-type air electrode for reversible protonic ceramic electrochemical cells	1.3	2.8	650	$Ba_{0.9}Co_{0.7}Fe_{0.2}Nb_{0.1}O_{3-\delta}$ (BCFN)	[38]	2022	
Liang et al.	Magnesium tuned triple conductivity and bifunctionality of BaCo0.4Fe0.4Zr0.1Y0.1O3-δ perovskite towards reversible protonic ceramic electrochemical cells	1.3	1.244	600	$Ba(Co_{0.4}Fe_{0.4}Zr_{0.1}Y_{0.1})_{0.95}Mg_{0.05}O_{3-\delta}$ (BCFZYM)	[156]	2022	
He et al.	Catalytic Self-Assembled Air Electrode for Highly Active and Durable Reversible Protonic Ceramic Electrochemical Cells	1.3	2.04	650	$Ba_2Co_{1.5}Mo_{0.25}Nb_{0.25}O_{6-\delta}$ (BC1.5MN)	[37]	2022	1.17
Lee et al.	Tailoring an Interface Microstructure for High-Performance Reversible Protonic Ceramic Electrochemical Cells via Soft Lithography	1.3	1.7	650	$BaCe_{0.7}Zr_{0.1}Y_{0.1}Yb_{0.1}O_{3-\delta}$	[157]	2022	1.136
Pei et al.	Constructing an active and stable oxygen electrode surface for reversible protonic ceramic electrochemical cells	1.3	2.69	650	$PrBaCo_2O_{5+\delta}$ (PBC)	[153]	2023	1.21

Zhu et al	A surface reconfiguration of a perovskite air electrode enables an active and durable reversible protonic ceramic electrochemical cell	1.3	2.336	650	GCO-BGPC	[151]	2022	0.909
He et al.	An Efficient High-Entropy Perovskite-Type Air Electrode for Reversible Oxygen Reduction and Water Splitting in Protonic Ceramic Cells	1.3	2.63	650	HE-PBSLCC	[70]	2023	1.5
Liu et al.	High-Entropy Perovskite Oxide: A New Opportunity for Developing Highly Active and Durable Air Electrode for Reversible Protonic Ceramic Electrochemical Cells	1.3	1.95	600	PLN-BSCC	[158]	2022	1.21
Ding et al	Self-sustainable protonic ceramic electrochemical cells using a triple conducting electrode for hydrogen and power production	1.4	1.31	600	$PrNi_{0.5}Co_{0.5}O_{3-\delta}$	[144]	2020	0.528

The operation of RePCEC is typical of a PCEC and PCFC standalone operations in a single device. The PCEC operation using steam as feedstock is shown in Fig. 2.5. The fuel cell mode is exactly the reverse operation. However, if there is additional feedstock like carbon dioxide with the water feed in a co-electrolysis reaction, the PCEC can also work well. Fig. 2.9 shows a typical schematical representation of RePCEC for both operations using different fuels in an integrated system. Some of the distinguishing features of this technology have been highlighted in the previous chapter.

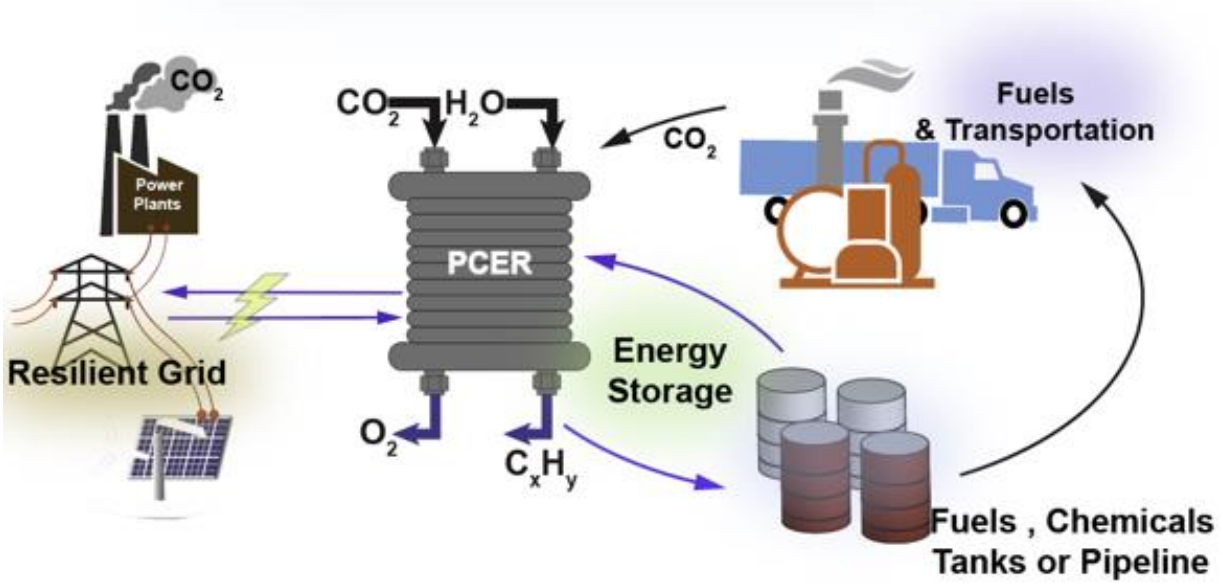

Fig. 2.9: RePCEC (PCER) operations in an integrated system

2.6 System integration studies

A reliable energy storage system is a unique solution to the challenges of linking the renewable power generation system to the power grid. While many studies and research groups have investigated the integration of ReSOC and it's like for energy storage, only a few works have been done about PCEC integration due to the recency in its acceptance. Most of the previous works focused both on laboratory scale experiments and computational studies using ideas and lapses in existing technologies as a pivot. The studies cut across the type of energy, geological conditions, the accuracy of the models, intended uses, and heat management techniques. Due to the

intermediate temperature of PCECs, it has a upper hand in tackling the challenges of stability and thermal integration posed by SOECs which is a major concern during the endothermic reactions in the system in the electrolysis mode. The PCECs integration is a work in progress as its development. However, the studies on heat management in the stack have taken different dimensions and these will be summarized here. Also, due to its ability to withstand poisoning, the generated fuels in the systems are different, and all relevant integration studies related to the PCECs will be highlighted in this section.

In work by Duan et al [29], they designed a RePCECs with an overall round trip of over 75%, which is close to that of many batteries. In exploring this technology, they proposed that its operational characteristics are favorable for integration with wind and solar-based renewable energy. This is because the roundtrip efficiency of their system can be maximized in the electrolysis mode when run for a shorter period at high current densities under the control of the equal charge-transfer operation and at lower current densities in the fuel cell mode. In this work, they successfully used this system to co-convert carbon dioxide and steam to methane. In order to strike a balance between CO_2 hydrogenation with an optimal temperature of 300 ºC and methane selectivity, a separate fixed-bed reactor was incorporated downstream at this temperature. In comparison, the PCEC operates at 600 ºC. At atmospheric pressure, this integration resulted in CO_2 conversion rate of 79.7% and CH_4 selectivity of 99.1%.

Long Q. et al [34] work is the first to be performed on PCECs scaled up above the size of the button-cell and their integration into small stacks. They used a conventional fabrication method to build PCFCs which gave prospective results. At 600 ºC, using air as an oxidizer they generated a maximum power density of 690 mW cm^{-2} and 470 mW cm^{-2} using hydrogen and internally reformed methane fuel, respectively. Efforts were made to reduce the rates of stack degradation by substituting BCZYYb electrolyte material in place of BCZY and switching to pure oxygen as oxidizer. The lowest rate was achieved by including a gadolinium-doped ceria interlayer between the BCZYYb electrolyte and the electrodes with no report of the round-trip efficiency.

Braun et al. [159] designed a PCFC operated with natural gas for stationary power uses. They adopted a semi-empirical approach to design and analyze a 25 kW system and modeled the BoP components for the reactant generation with the PCFC stack. A preheated mixture of natural gas and steam was sent into the stack after it was pre-reformed to prevent the depletion of hydrogen at

the stack inlet and to get rid of the heat sink from the stack while reducing large temperature gradients. Steady-state performance of the system shows an approximate electric efficiency of 58% at LHV, which is close to that of SOFC.

More studies have been done on the integration of PEMFC and SOFC, and PCEC working at an intermediate temperature between these technologies offers a lot of advantages and has taken dominance in recent times which were mentioned in literature [114],[160]. In view of this, it will be worthwhile to leverage the integration of these two to design and model several energy integration systems based on PCEC.

2.7 PCEC's research and development critical to energy storage applications

The infancy in the acceptance of the PCEC as an energy storage system has not given a chance to capture and establish all the fundamental system requirements for its consideration. Therefore, various challenges need to be resolved to make it ready for use at the desired efficiency and integration. The limited number of studies performed show that challenges linger around on achieving high roundtrip efficiency, stack scale up and the operating materials-material design and synthesis. A detailed understanding of its chemistry and mode of operation, especially the heat and gas need of this technology, is required to give insight into its modeling and simulation for accurate design configuration. Couple with these is the integration of catalysts, intensifying the technological processes and improving durability, stability, and flexibility. Though more work has been done in the PCFC mode than in the electrolyzer mode, and the former has shown higher performance than the latter. For the energy storage purpose, a balance needs to be reached for efficient operation in both modes with a proximal performance. While there has been a focus on the generation of hydrogen, this technology has shown prospects for the production and utilization of hydrocarbons that are more economically viable as fuel than hydrogen.

Duan et al. [46], in their review, made several proposals for achieving higher technological performance, which can be summarized as follows;

a) Improved mechanical property knowledge about PCEC, which will help in scale-up and manufacturing

b) Reduction in PCEC degradation risk and failure by matching the expansion coefficients of electrodes and sealing materials

c) Rational design of PCEC positive electrodes to enhance ORR and/or OER activities and bulk proton conductivity.

d) Catalyst modification and integration to enhance the desired electrochemical reaction.

Duan et al. [29] proposed a PCEC device coupled with an external fixed bed methanation reactor. The experimental result shows that using CeO_2 with 10% Ni as catalyst yield almost 80% conversion of CO_2 with 99% selectivity for methane at a current density of 2308 mA/cm^2. This is typically double the conversion and over 14 times the selectivity that was gotten without the external reactor. Generally, the CO_2 and CH_4 selectivity are enhanced with increased current density, however, the optimum temperature for the methanation catalyst is 250 ºC. In the same work, the durability and evaluation of PCEC performance working in both modes were carried out. They demonstrated a consistent round-trip efficiency (>75%) in the conversion from electricity to hydrogen and back to electricity, coupled with stable operation. The degradation rate remains below 30 mV over a period of 1,000 hours.

The PCFCs have been reported to have a prospect of simultaneously providing high efficiency distributed energy generation and increasing the grid penetration of renewable sources due to their high per-pass utilization and flexibility while maintaining their performance [161], [136], [162]. As PCFCs are envisioned to offer solutions to the challenges of high cost and slow start-up and shutdown experienced in the previous fuel cell technologies, Albrecht et al. [163] developed new engineering models and investigated the steady-state and dynamic performance characteristics of PCFCs. The model was designed for easy experimental calibration, which does not necessitate future experiments to validate the transport properties of mixed conductors. The counter-flow of the reactant gas in the steady-state shows better electrochemical performance than the co-flow but the latter might be preferred due to its uniform current density and degradation advantage. At current densities of $0.15A/cm^2$, they both gave an approximate performance of 0.75V with low power density of $0.113W/cm^2$ which is small compared to SOFCs but of greater benefit for load-following activities. It causes slow thermal response which prolong the cell life and enhances rapid transient response. Building capacity with PCFC with high efficiency will enhance its use as distributed energy generation device.

Motylinski et al. [164] investigated the transient behavior of renewable energy system integrated rSOC while inter-switching between its two modes of operation. A model was designed to show the feasibility of balancing the grid by connecting rSOC to the grid. It was shown that the wind input power into the system resulted in similar output power. The dynamic model was designed to capture the energy balancing on the grid while switching from the fuel cell mode to the electrolyzer mode and vice versa, and the result shows this operation can be continuous. The study did not address the challenges of the electrical grid but focused on how energy can be a balance on the grid during the time of low and excess supply. While the results are optimistic, transferring this to a PCEC might likely generate better results due to some of its superiorities over the rSOC as Sihyuk et al [44] studied the cyclic operation of the PCEC with no observable performance degradation after 12 cycles.

CHAPTER 3 MODELING AND EXPERIMENTAL PERFORMANCE OF PROTONIC CERAMIC ELECTROCHEMICAL CELLS FOR H2O AND CO2 CO-ELECTROLYSIS FOR METHANE PRODUCTION

? **Research Question, RQ2**: How is the complexity of the reactions and ion-defects transport addressed at the cellular and stack level to capture the PCEC activities?

- **Objective 2**: cell level model of PCEC for co-electrolysis reaction

✓ **New knowledge:** Standardized and satisficing design of PCEC unit cell for the production of methane, hydrogen and other chemicals.

The original draft is solely by the author and the experimental results are from Kansas state university.

Abstract

This study presents the development of a one-dimensional button-cell model for protonic ceramic electrochemical cell (PCEC) using the Engineering Equation Solver (EES). The model focuses on the co-electrolysis of CO_2 and H_2O for methane production, providing insights into the effects of overpotentials on cell performance. The results obtained from the model highlight the potential of PCECs as efficient CO_2 sinks for decarbonization purposes and as a means of methane production. Furthermore, the model's findings offer valuable guidance for the design, selection of stacks, and choice of building materials in PCEC systems. The potential applications of PCECs as real-life fuel utilization technologies are justified, opening doors for scale-up and eventual commercialization. These findings contribute to the development of sustainable energy systems and advance the pursuit of decarbonization goals.

3.1 Introduction

The global energy production in the last two decades has grown tremendously, most especially the last decade has witnessed a growth that has no precedence. As of 2021, the global total energy consumption which is usually the three-quarter of the total production is 176,431 TWh compared to its approximate value of 152, 966 TWh in 2010 [10] that results in 14.7% increase. Fossil fuels which include natural gas and oil, coal and peat contributed to 80% of the production in 2012 [11] and 63% in 2022 as more renewable energy sources are explored. The growing deployment and

use of renewable energy sources and their intermittent nature highlight the necessity for a reliable energy storage solution. Several works have reported the solid oxide electrolytic cells (SOECs) to be a good storage device most especially through water electrolysis to useful hydrogen [27, 165]. However, recent studies revealed that the protonic ceramic electrochemical cells (PCECs) if properly harnessed have several distinguishing features over the SOECs both in the generation of electricity as protonic ceramic fuel cell (PCFC) [67] and in the storage of energy as protonic ceramic electrolytic cell (PCEC) [68]. These advantages include lower cell and stack temperature, optimization of air ratio, revamped cell voltage, enhanced fuel utilization, diversified and efficient chemical production [29, 65, 69].

The PCECs system is a proton conductor-based SOC and can work as a standalone technology called the reversible protonic ceramic electrochemical cells (RePCECs) that is bifunctional in its ability to store energy and renewables and produce electricity[96]. It offers higher efficiencies both faradaic and roundtrip at low temperature [99] which is a crucial parameter for the design of energy storage systems. Moreover, it utilizes low-cost materials [100] and exhibits enhanced system durability [101], which makes it more appealing. In achieving this, most work focused on the production of hydrogen through water electrolysis and its reuse [144, 166-168] except for few that use and produce other fuels and chemicals [29, 34, 107]. The co-electrolysis of CO_2 and water to produce methane has not been explored with this technology which is key in a bid to reducing industrial and environmental carbon footprint. In this way, the technology would be solving two fundamental societal issues simultaneously through decarbonization and energy storage. While the SOEC shows some economic prospects in this realm, it is essential to exploit the eccentric properties of the PCEC for direct methane production at cell and stack level for energy storage system. Most of the previous work on PCEC focused largely on laboratory scale experiments and very few computational studies using ideas and lapses in existing technologies as a pivot. A computational framework for PCEC comes with several challenges and not limited to evaluating the mixed charged conductors, open circuit voltages and other similar conditions.

However, it is imminent to develop cell and stack models with great degree of precision to enhance the design of energy storage at the system level. This model should be able to predict both steady-state and dynamic performance in such a way that operating conditions (e.g., T, P, composition, utilization) of the PCEC, heat management of the system, operating strategies for load change and

mode-switching, stability and thermal integration, desired tank storage state points (T, P, and composition) [169] can be evaluated to high level of exactness. This work presents the first modelling tool for co-electrolysis of CO_2 and H_2O to serve the above-mentioned functions.

Albrecht et al. [137] investigated the steady-state and dynamic performances of PCFC at cell level by developing a distinct engineering models using the latest PCFC technology. Despite the limited research conducted on this topic compared to its solid oxide counterparts, a number of researchers have pursued this area of study. Zhu and Kee [170] modeled a button-cell configuration of PCFC that uses porous composite electrodes to predict its performance. This arises in a complex model due to the formation of mixed ionic-electronic conductors (MIEC) from the doped electrolyte materials. For a genuine performance prediction, the model put into consideration porous electrode chemistry and accounted for the defect transport within the MIEC. In order to project the PCFC technology beyond the cell level demonstration, Long et al [34] worked on its scale up and integrations of the cells into a stack using hydrogen and methane fuel with low performance degradation almost 1.5% k/h after running it over 100 days. While the PCFC modeling is still its rise, huge progress has been made in the prediction its performance and more work is still ongoing. The PCFC reverse operation (PCEC) just like the case of SOFC and SOEC, the latter had a big setback in its adoption both at experimental and computational level.

The PCEC is getting its utmost attention in recent times, most especially with the considerable progress that has been made in solid-state proton conductors and their application in electrochemical cells in the last decade [39, 97, 98]. PCEC seems to be a promising technology in accomplishing the cheap energy storage and conversion goal with its higher efficiencies, low temperature, durability, and low-cost materials requirement. Despite all these, the PCEC is yet to be deployed on a large scale, due to some serious limitations in developing efficiently robust electrodes that can withstand high-steam concentration at an intermediate temperature [102]. This setback motivated Ding et al. [51] to use a triple conducting electrode to develop a PCEC with a self-sustainable operation that generates hydrogen at a fast rate that is sufficient for the reverse operation to generate electricity without an external hydrogen feed. Most of this work is empirical and have focused mainly on the production of hydrogen from water. Even at that, there are not enough reliable data for both experimental and numerical prediction of PCEC performance. As a new and standalone technology, there are several challenges that accompany its operation ranging

from its reaction and the charge defect transport. Computational analyses are very important in addressing some of these problems to prevent repetition and enhance scalability for the technology to be considered for energy storage and to produce valuable chemicals. To serve as a reliable storage system, the round-trip efficiency for the forward and backward operation modes of the system should be significantly high and will help in understanding the intricacy of PCEC operating mechanisms. Duan et al [29] demonstrated this experimentally with electrolysis of water to produce hydrogen with faradaic and round-trip efficiencies exceeding 95% and 75% respectively at high stability. This has also made the standalone reversible protonic ceramic electrochemical cells (RePCEC) to get some attention. Using the same PCEC set up, they co-electrolysed water with CO_2 to produce methane though at a lower yield. This methanation (methane production) reaction is one of the over seventeen CO_2 hydrogenation reactions [171] that are very critical for the decarbonization of the planet. However, to enhance the renewability of the CO_2 hydrogenation reactions, the supplied hydrogen must be coming from water splitting using renewables, like water electrolysis using solar or wind [172, 173] as shown in equations 1 and 2.

$$xCO_2 + yH_2O \rightarrow product + zO_2 \qquad CO_2\ hydrogenation \qquad 3.1$$

$$2H_2O \rightarrow O_2 + 2H_2 \qquad Water\ splitting \qquad 3.2$$

Methanation technology is very promising due to higher combustion value of CH_4, its stability and ease of transportation by the readily available infrastructure [174] and thereby enhances faster implementation.

Co-electrolysis of H_2O and CO_2 has numerous advantages over the CO_2 or CO hydrogeneration by hydrogen from water electrolysis as mentioned in the literature [175, 176]. Most of the previous works done on the co-electrolysis of water and CO_2 have used the SOEC technology [177-180], and one of the pioneering work in recent times using the PCEC technology is that reported by Duan et al [29] as previously mentioned followed by Pan et al [94] which are all empirical. In order to fulfill the large-scale production and integration of this technology into the existing infrastructure as posited, numerical research activities are highly required to drive the progress. As far as the author's knowledge is concerned, this is the first work addressing the co-electrolysis of H_2O and CO_2 in PCEC numerically.

This present work shows that there are many issues to be resolved to model a PCEC for reliable prediction of reality for a regenerative technology. The initial work in this modeling series

highlights the importance of validation, revealing that minor modifications made to SOFC model for reverse operation in the SOEC mode can compromise precision due to difference in reaction pathways and favorable catalysts. This paper focuses on the design of steady-state PCEC models which represent details of reactive porous-media transport, elementary catalytic chemistry, and electrochemistry within unit cells and stacks. The model examines the effect of the feed gas and operating conditions, and the results are calibrated and validated with experimental and the available numerical data.

3.2 Theory of operation of PCECs

3.2.1 Principles of operation

The PCEC technology has the capability to function as a reactor for several reactions, which can vary depending on the feedstock employed. Furthermore, the same feedstock can undergo multiple reactions within the PCEC system, influenced by factors such as the operating conditions. This work involves the production of methane from H_2O and CO_2 molecules in a process called methanation reaction. Its operational concept illustrated in Figure 1 demonstrates a button-cell electrochemical technology employing the Sabatier process, also known as the reverse methane steam reforming. As shown in the Figure 3.1, steam is passed into the steam electrode (the positive electrode called positrode) of the PCEC and CO_2 co-fed into the PCEC fuel electrode (the negative electrode called negatrode). An external energy source is used to drive the electrolysis of water at the positrode to produce O_2 and protons an in Equation 3.3 using the Kröger–Vink notation [109] and can be conventionally written as in Equation 3.44. The protons are transported across the protonic-ceramic membrane to the negatrode side of the cell while the produced O_2 is removed it as an exhaust waste and can be used for other commercially beneficial purposes.

$$H_2O(g) + 2O_O^X(el) \leftrightarrow 0.5\,O_2(g) + 2OH_O^{\bullet}(el) + 2e'(ed) \qquad 3.3 \text{ Kröger–Vink notation}$$

- Steam channel (Positrode/electrolysis anode)

$$4H_2O \rightarrow 8H^+ + 2O_2 + 8e^- \qquad 3.4$$

At the negatrode, the protons electrochemical react with the fed CO_2 to produce methane, CH_4 and water, H_2O as in Equation 5

- Fuel channel (Negatrode/electrolysis cathode)

$CO_2 + 8H^+ + 8e^- \rightarrow CH_4 + 2H_2O$ 3.5

In one of the experimental works conducted for the validation of our model, it is important to highlight that the steam channel was supplied with air containing 21% O_2 and N_2 as the balance, while the fuel channel was fed with CO_2 along with argon as a sweep gas. The integration of the endothermic steam electrolysis reaction with the exothermic CO_2 hydrogenation reaction facilitates thermal balancing of the process and enhance high efficiency.

Generally, the possible chemical reactions in a PCEC fed with CO_2 and steam are:

a) Reverse water gas shift reaction (RWGSR):

$CO_2 + H_2 = CO + H_2O$ ΔH=-41kJ/mol 3.6

b) Co-electrolysis process:

$2H_2O = 2H_2 + O_2$ ΔH=241.7 kJ/mol 3.7

$2CO_2 = 2CO + O_2$ ΔH=-110.5 kJ/mol 3.8 and

c) methanation

$CO_2 + 4H_2 = CH_4 + 2H_2O$ ΔH=-164 kJ/mol 3.9

$CO + 3H_2 = CH_4 + H_2O$ ΔH=-206 kJ/mol 3.10

The methanation reaction or reverse methane steam reforming which is the focus of this work adopt the Sabatier process as previous mentioned. However, the typical electrochemical reaction for CO_2 reduction can be written as in Equation 3.5

The overall reaction in the PCEC for this operation can be presented by combining Equations 3.4 and 3.5:

$CO_2 + 4H_2O \rightarrow CH_4 + 2H_2O + 2O_2$ 3.11

And the steam further decomposes as;

$2H_2O \rightarrow 2H_2 + O_2$ 3.12

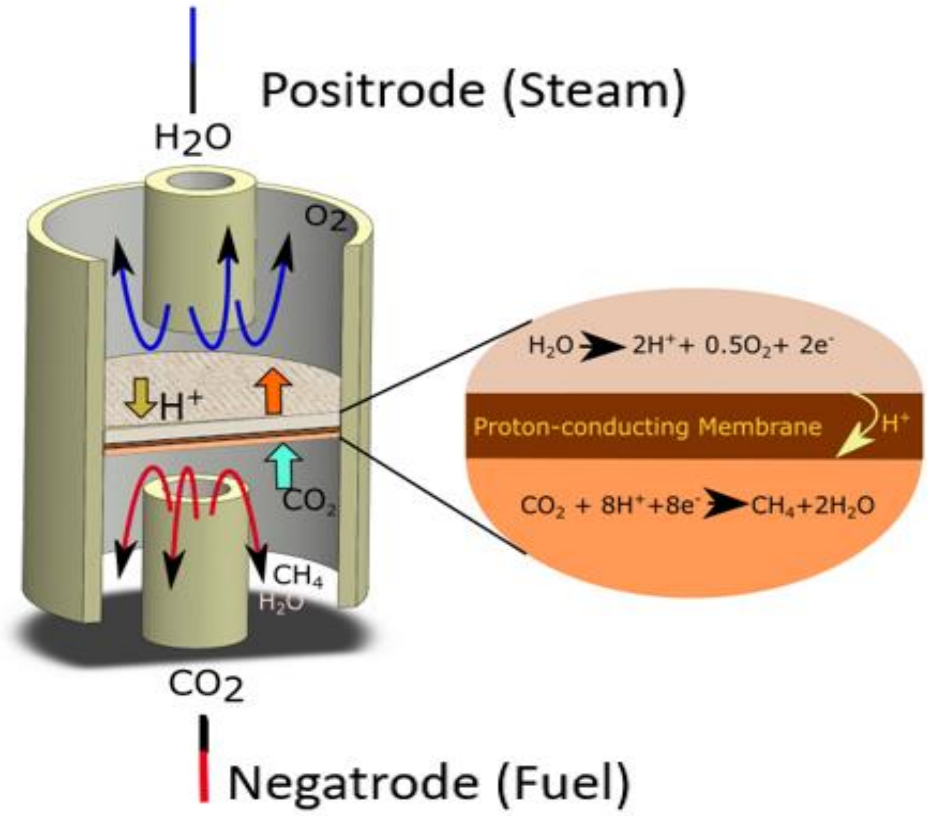

Fig. 3.1: PCEC button-cell for methane production

3.3 PCEC materials

Generally, similar materials have been employed for the protonic ceramic electrochemical cell either for a standalone operation or the reversible case, and most often the same geometrical configurations. Therefore, the PCEC materials is typical of what is used for PCFC and RePCEC. The perovskite structure ABX3 has been mostly adopted and studied for proton conductors (the electrolyte and the electrodes) of PCECs. The A, B and X usually represent a divalent cation (like Sr^{2+} and Ba^{2+}), tetravalent cation (like Ce^{4+}, Zr^{4+}), trivalent cation (like Yb^{3+}, Y^{3+}) and anions (frequently oxide) respectively. The degree of proton passage and uptake for perovskite materials of the type $(Ba,Sr)(Ce,Zr,Y,Yb)O_{3-\delta}$ is a function of the oxygen basicity [109]. Electrolyte-supported PCECs employ effective pure ion conductor as electrolyte materials the likes of the perovskites previously discussed and others with different crystal structures. The perovskite structured electrolytes have dominant applications for this technology due to their chemical stability and high conductivity [115]. Their conductivity stem from both proton and oxygen ion transport, oxygen ion contributes significantly to conductivity at high temperatures

above 600℃. However, for PCECs that operate at lower temperatures below 600℃, the protonic conductivity dominates and that of oxygen ion becomes negligible. For higher faradaic efficiency, there is need to optimize the protonic conductivity and minimize that of the O-site polarion [33, 36]. The negatrodes are mainly made up of porous ceramic-metallic composites like BCZY which act as the ion-conducting phase and Ni that serves as the electron-conducting phase and has been validated experimentally for CO_2 reduction. Duan et al [29] used $BaCe_{0.7}Zr_{0.1}Y_{0.1}Yb_{0.1}O_3$ (BCZYYb7111) and Ni as negatrode for CO_2 reduction reaction to CO and CH4. Pan et al [94] in their study which is one of the experimental works for the validation of our model used $BaCe_{0.4}Zr_{0.4}Y_{0.1}Yb_{0.1}O_3$ (BCZYYb4411)+Ni for the co-electrolysis of H_2O and CO_2. The positrode is expected to possess some special qualities like chemical stability in humid oxidizing surroundings, compatibility with the electrolyte materials, adequate protonic and electronic conductivities to reduce polarization resistances. It has the greatest effect on the performance of the PCEC and its durability and must be able to function as an excellent catalyst for the H_2O oxidation [109]. Similarly, Duan et al [29] and Pan et al [94] used $BaCo_{0.4}Fe_{0.4}Zr_{0.1}Y_{0.1}O_{3-\delta}$ (BCFZY) and 80% $BaCo_{0.4}Fe_{0.4}Zr_{0.1}Y_{0.1}O_{3-\delta}$ (BCFZY)+ 20% $BaCe_{0.4}Zr_{0.4}Y_{0.1}Yb_{0.1}O_{3-\delta}$ (BCZYYb) as positrodes in their works respectively and the commonly used materials are highlighted in ref. [109]. As shown in Figure 1, the electrolyte which is proton-conducting membrane is closely packed in between the porous positrode and negatrode. These electrodes are made up of electronically conducting phase and mixed ionic-electronic conducting phase (MIEC). A typical design of button cell PCEC is done by our collaborator in the Materials Research Laboratory for Sustainable Energy, its morphology and dimension are detailed in the following section.

3.4 Single button cell dimension and morphology

Figure 3.2 shows a designed PCEC single button cell with its dimension measurement as built from the Materials Research Laboratory for Sustainable Energy at Kansa state University. The diameter of the negatrode and electrolyte is approximately 14 mm. The positrode is painted on the electrolyte with a diameter of 8 mm (the effective area is 0.5 cm^2). We have left a space of 3-4mm on the electrolyte edge for sealing, it will be covered by sealing glass and will not contribute to the ohmic resistance. To gain a better visualization of the microstructure and morphologies of this button cell, cross-sectional area scanning electron microscopy (SEM) images are presented in Figure 3.3. The overall thickness of this button cell is ~ 460 um, as shown in Figure 3a. The porous

positrode consists of nano-sized $PrBa_{0.5}Sr_{0.5}Co_{1.5}Fe_{0.5}O_{5+\delta}$ (PBSCF, with the thickness of ~30 um in Figure 3b), one

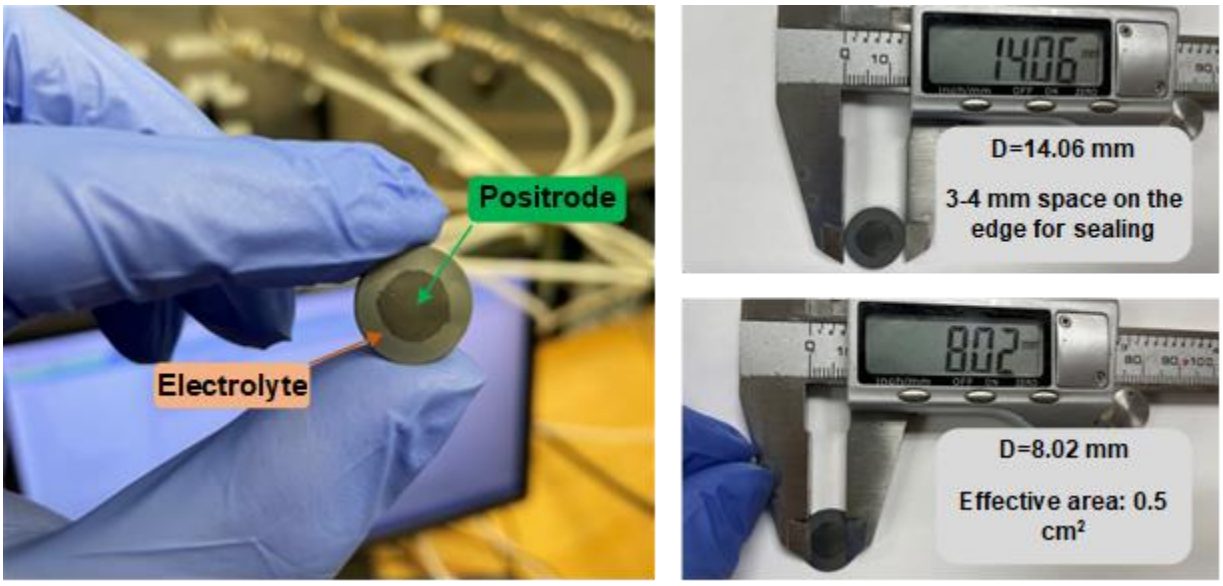

Fig. 3.2: Photos of a lab scale PCEC.

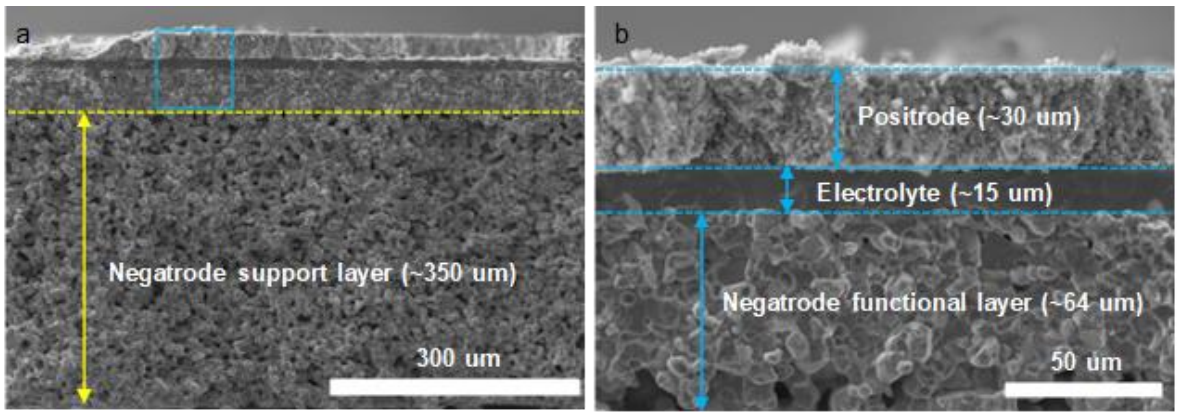

Fig. 3.3:Cross-sectional area SEM images of the single button cells (Figure 3.3b is the enlarged image from the blue box in Figure 3.3a)

The porous positrode consists of nano-sized $PrBa_{0.5}Sr_{0.5}Co_{1.5}Fe_{0.5}O_{5+\delta}$ (PBSCF, with the thickness of ~30 μm in Figure 3.3b), one of the-state-of-art positrode materials of PCECs, is screen printed on a thin BCZYYb4411 electrolyte, which is supported on a multilayered Ni-BCZYYb7111 negatrode. The thickness of electrolyte is around 15 μm, without any pinhole, ensuring gas tightness and preventing electronic short circuits. The upper-layer of the Ni-BCZYYb7111 is a dense negatrode functional layer (~64 μm) designed to maximize the triple phase boundaries for

electrochemical reactions. The bottom porous layer (~350 μm) serves as the support layer, providing both mass transport and mechanical strength. Additionally, to further tune the yield and selectivity of the CO_2 conversion in PCEC, a catalytic layer normally developed and then painted on the negatrode support layer (not shown in the SEM images).

For the examination of the material properties of the PCEC and the cell configuration, our model can adequately simulate the PCEC.

3.5 Model description

This section gives a comprehensive description of the button-cell PCEC model. This model details the reactive porous-media transport, elementary catalytic chemistry, and electrochemistry. It is used for the calibration of electrochemical parameters to the data gotten from the laboratory experiment. These parameters describe the activities taking place at the positrode, electrolyte and the negatrode. They include the overpotentials (activation, concentration and ohmic) diffusion and Butler-Volmer equation. The global methanation, RWGSR and water electrolysis reactions are included to estimate the rate of production of CH_4, CO, O_2 species respectively and the consumption of H_2O and CO_2.

3.5.1 Model assumptions

In the design of an electrolyte-supported single button-cell PCEC, it assumed that the flow in the steam and fuel channels are counter-current, and the protons passed across the electrolyte membrane fast to ensure the immediate reduction of CO_2 in the fuel channel. It is assumed that the sweep gas and fuel flows distribute uniformly in the cell channels. Other key assumptions in this work include:

1. Adiabatic boundaries at the cell ends
2. All gases are ideal gases
3. At steady state
4. Lumped temperature of the cell structure
5. Uniformly distributed cell temperature
6. At constant pressure
7. One-dimensional cell representation along the streamwise direction
8. Channels act as a continuously stirred tank reactor (CSTR).

9. One-dimensional cell representation along the streamwise direction
10. Selective reduction of CO_2 for methane production at the fuel electrode

3.6 Electrochemical model

In calculating the PCEC model open-circuit voltage, the reaction in both the steam and fuel channels are put into consideration. The steam electrolysis is given preference in some SOEC modelling work, but in this case the electrochemical reduction of CO_2 is an integral part of the overall reaction and in fact the system is modelled for a preferential selectivity of methane production in the fuel channel as per the cell catalyst and material design. The model incorporates both the steam electrolysis and the methanation reactions occurring on the electrodes and electrolyte membrane. These reactions are divided into two half-reactions, corresponding to the functioning electrodes in the channels, as depicted in Equations 3.3 and 3.4. The electrochemical potential at each electrode is estimated using the Nernst potential equation based on the active species in each channel. For the positrode, it is estimated thus:

$$E_{Nernst,O2,ps} = E^0_{O2} + \frac{RT_{PEN}}{n_e F} ln\left(\frac{P^4_{H2O}}{P^2_{O2} * P^4_{H2}}\right) \qquad 3.13$$

At the negatrode, it is estimated as:

$$E_{Nernst,CH4,ng} = E^0_{CH4} + \frac{RT_{PEN}}{n_e F} ln\left(P_{CO2} * \frac{P^4_{H2,ca}}{P_{CH4} * P^2_{H2O,ca}}\right) \qquad 3.14$$

Where E_{Nernst} denotes the Nernst cell potential and E^0 is standard equilibrium potential. Also, n_e, R, F, P_i, and T represent the Number of electrons transferred, gas constant, mole fractions, Faraday constant, partial pressures of the participating species, and PCEC operating temperatures respectively, i= CO_2, CH_4, H_2O, O_2, H_2. Ps is the positrode and 'ng' is the negatrode. As opposed to the SOEC, which has a single oxygen-ion conductor [43], the PCEC contains multiple conductors, including mobile charged defects such as protons, polarons, and oxygen vacancies. Due to this distinction, the difference in electrochemical potentials between the triple phase boundary (TPB) and the mixed ionic-electronic conductors (MIEC) of the two electrodes cannot accurately determine the cell's open circuit voltage under equilibrium conditions. Equation 3.15, which is based on the mixed potential theory and represents the superposition of potential differences resulting from electrochemical reactions at the electrodes, may not provide an accurate estimation in the case of the PCEC.

$$E_{Nernst,tot} = E_{Nernst,O2,ps} - E_{Nernst,CH4,ng} \qquad 3.15$$

This is due to the continual charge defect mobility observed in PCEC in these conditions. A charge-balanced ionic current is shown by these defects even when the net electronic current is zero [32]. This implies the OCV of a PCEC is not in a state of equilibrium and subsequently the energy needed to drive the defects' mobility reduce the OCV below what we have in Equation 14 based on the equilibrium thermodynamics [181]. To capture this condition in our electrochemical model, we introduce the adjustment factor, δ for all potentials in the PCEC cell.

The final cell operating voltage is estimated putting into consideration all the cell overpotentials both during operation and for an open circuit due to the peculiarity of PCEC as explained and as a function of the adjustment factor, δ that serves in place of transference number [137] in its PCFC counterpart. The initial operating voltage, $E_{op,i}$ in our analysis considering the overpotentials is given by

$$E_{op,i} = E_{Nernst,tot} - (\eta_{ohm} + \eta_{act} + \eta_{conc}) \qquad 3.16$$

Where $\eta_{ohm}, \eta_{act}\ and\ \eta_{conc}$ are the ohmic, activation and concentration overpotentials respectively and $E_{op,i}$ represents the initial cell operating potential. Adapting the $V_{op,i}$ with the adjustment factor, δ which is a function of temperature makes the actual and final cell operating voltage to be expressed as;

$$E_{op,f} = \delta * E_{op,i} = \delta * [E_{Nernst,tot} - (\eta_{ohm} + \eta_{act} + \eta_{conc})] \qquad 3.17$$

δ =0.00218*T_{PEN}-1.0683 3.18

And T_{PEN} is the cell operating temperature in Kelvin.

3.6.1 Ohmic overpotential

The main sources of ohmic overpotential loss in electrolytic cells are due to resistance to ion and electronic flow in the electrolyte and the electrodes respectively. The electrodes are usually made up of highly conductive materials which limit their resistance to electronic flow. Thus, the ohmic resistance in the MEA is dominated by the ionic resistance by the electrolyte. The PCEC cell's geometry follows a typical design similar to the one employed by Kazempoor and Braun [169] and Zhu and Kee [170] in their SOEC and PCFC models respectively. Other properties from the work by Albrecht et al [137]. The PCEC geometry parameters for this work are detailed in Table 1. The Ohm's law is employed to evaluate the cell ohmic overpotential:

$$\eta_{ohm} = i\, R_{eq,ohm} \qquad 3.19$$

Where i is the cell current and R_{eq} is the equivalent resistance which is dependent on the cell geometry and cell material components. The solid structure resistance is given by [182].

$$R_{PEN} = \frac{sr_{ng}\delta_{ng} + sr_{El}\delta_{El} + sr_{ps}\delta_{ps}}{A} \qquad 3.20$$

Here, A represent the active area in the PEN layer where current flows, and δ_i and sr_i are the corresponding current flow length and specific resistivity of the negatrode, electrolyte, and positrode respectively. In addition to the geometry, Table 3.1 also entails the operating parameters, material properties and diffusion polarization parameters that are used for the model calibration.

Table 3.1: PCEC model parameters [137, 169, 170]

Geometry parameters	
Positrode thickness (m)	30×10^{-6}
Negatrode thickness (m)	64×10^{-6}
Electrolyte thickness (m)	15×10^{-6}
Interconnector thickness (m)	0.19×10^{-3}
Cell active area (width × height) (mm^2)	80 × 80
Channel height, fuel side (m)	1.09×10^{-3}
Channel height, sweep gas side (m)	1.09×10^{-3}
Channel width, fuel side (m)	2×10^{-3a}
Channel width, sweep gas side (m)	2×10^{-3a}
Flow configuration	Co-flow
Material properties	
Conductivity of PEN (W m^{-1} K^{-1})	2.16
Conductivity of interconnector (W m^{-1} K^{-1})	27
Interconnector specific resistivity (Ω m)	1.176×10^{-4}
Negatrode specific resistivity (Ω m)	8.856×10^{-6}
Electrolyte specific resistivity (Ω m)	$1.07\times10^{-4}\exp(7237/T_{PEN})$

Positrode specific resistivity (Ω m)	1.425×10^{-4}
Contact resistances (Ω m^2)	10^{-4}–0.2×10^{-4}
Diffusion polarization	
Pore diameter of positrode (m)	1×10^{-6}
Pore diameter of negatrode (m)	1×10^{-6}
Porosity of negatrode	0.4
Porosity of positrode	0.4
Tortuosity of positrode	3.0
Tortuosity of negatrode	3.0
Operating conditions	
Pressure (Pa)	101,325 (atmospheric pressure)
Average current density (A m^{-2})	0–10000
Temperature (°C)	450–600

3.6.2 3.5.2. Activation overpotential

The activation overpotential in the PCEC associated with charge-defect transport and reactions during its operation is characterized using the popular Butler-Volmer (BV) equation. Since there is species concentration variation in both the reactants and the product in the bulk and TPB at the negatrode, the BV equation is modified to capture this and given by Bard et al [183].

$$I = i_{0,ng}\left\{\frac{C_{CO2,TPB}}{C_{CO2,b}} exp\left(\alpha \frac{n_e F\, \eta_{Act,ng}}{RT_{PEN}}\right) - \frac{C_{CH4,TPB}}{C_{CH4,b}} exp\left(-(1-\alpha)\frac{n_e F\, \eta_{Act,ng}}{RT_{PEN}}\right)\right\} \quad 3.21$$

Where I and i_0 represent the current density and the exchange current respectively. A similar approach is adopted for the positrode as there is significant species concentration variation from the bulk flow to the TPB as well and the oxygen impact is needs to be included which made it a mix. It is given as

$$I = i_{0,ps}\left\{\frac{C_{H2O,TPB}}{C_{H2O,b}} exp\left(\alpha \frac{n_e F\ \eta_{Act,ps}}{RT_{PEN}}\right) - \frac{C_{O2,TPB}}{C_{O2,b}} exp\left(-(1-\alpha)\frac{n_e F\ \eta_{Act,ps}}{RT_{PEN}}\right)\right\} \quad 3.22$$

The charge transfer coefficient, α in the above equation, measures the fraction of potential to lower the activation energy of the reaction at the TPB and bulk interface, this give the overpotential fraction that influence the current density [183]. It is usually assumed to be 0.5 in electrochemical cells. The activation overpotential, η_{Act} is given by

$$\eta_{Act=}\eta_{Act,ps} + \eta_{Act,ng} \quad 3.23$$

The exchange current densities, $i_{0,ng}$ and $i_{0,ps}$ in equations 20 and 21 for the reactions at the negatrode and positrode respectively is given by

$$i_{o,ps} = \gamma_{ps} X_{O2}^{a} X_{H2O}^{b}\ X_{H2}^{c} exp^{\frac{(-E_{act,ps})}{RT}} \quad 3.24$$

$$i_{o,ng} = \gamma_{ng} X_{CO2}^{d} X_{H2O}^{e} X_{CH4}^{f} X_{H2}^{g} exp^{\frac{(-E_{act,ng})}{RT}} \quad 3.25$$

Where a, b, c, d, e, f and g are constants. E_{act}, X_i, γ_{ps} and γ_{ng} represent the activation energy of reaction at each electrode, the species fractional concentration, positrode and negatrode pre-exponential factors respectively.

3.6.3 Concentration overpotential

To capture the concentration overpotential due to the mass transport of species the bulk phase in the channels to the TPB in the porous electrodes, we use a transport model for the diffusion resistance. Diffusion overpotential at positrode and negatrode side channels can be calculated as:

$$\eta_{conc,ps} = \frac{RT_{PEN}}{nF} ln\left(\frac{X_{H2O,b} X_{O2,TPB}}{X_{O2,b} X_{H2O,TPB}}\right) \quad 3.26$$

$$\eta_{conc,ng} = \frac{RT_{PEN}}{nF} ln\left(\frac{X_{CO2,b} X_{CH4,TPB}}{X_{CH4,b} X_{CO2,TPB}}\right) \quad 3.27$$

Where X_i is the molar fraction of species in both bulk phase and TPB. So, for diffusion overpotential, it is important to calculate the reactants and products' concentrations in both phases. The mole fractions in the bulk flow can be estimated using material balance while two diffusional steps need to be considered for the estimate on TPB [182]. The Fick's law is adopted for the bulk phase-electrode surface estimation:

$$X_{O2,s} = 1 + \left(X_{O2,b} - 1\right) exp\left(\frac{RT_{PEN}J}{4FP_{ng}\, D_{O2,N2}} \frac{H_{CH,A}}{2}\right) \qquad 3.28$$

$$X_{H2O,s} = 1 + \left(X_{H2O,b} - 1\right) exp\left(\frac{RT_{PEN}J}{4FP_{ng}\, D_{H2O}} \frac{H_{CH,A}}{2}\right) \qquad 3.29$$

$$X_{i,s} = X_{i,b} + K\frac{RT_{PEN}J}{4FP_{ps}\, D_i} \frac{H_{CH,F}}{2} \quad where \quad i \in [CH_4(K=1), CO_2\ (K=-1)]$$

While the Dusty-Gas model (DGM) is mostly adopted in the description of gas diffusion through porous media (electrodes), we use used Fick's model which gives reasonable approximation and given as

$$X_{i,TPB} = 1 + \left(X_{i,s} - 1\right) exp\left(\frac{RT_{PEN}J}{4FP_{ng}\, D_{i,eff}} \delta_{ng}\right) \qquad 3.30$$

$$where \quad i \in [O_2, H_2O\ ]b$$

$$X_{i,TPB} = X_{i,s} + K\frac{RT_{PEN}J}{4FP_{ps}\, D_{i\ ,eff}} \delta_{ps} \qquad 3.31$$

$$where \quad i \in [CH_4(K=1), CO_2\ (K=-1)]$$

3.7 Material balances

The PCEC experimental work considered in this dissertation uses several gases as the feedstock in its operation. These gas mixtures and their supply to the electrodes is as described in section 2.1. The general continuity equation is used to relate the materials balance in the cell channels, and expressed as:

At the negatrode

$$\frac{\partial C_i}{\partial t} = -\frac{\partial (u_{ng} C_i)}{\partial x} + \sum_J v_{i,j} r_j \frac{1}{H_{ng}} \qquad 3.32$$

$$i \in \{\ CO_2, H_2O, CO, H_2, Ar\ (or\ N_2), CH_4\}\ \ j \in \{Red, Methanation\}$$

At the positrode,

$$\frac{\partial C_i}{\partial t} = -\frac{\partial (u_{ps} C_i)}{\partial x} + \sum_j v_{i,j} r_j \frac{1}{H_{ps}} \qquad 3.33$$

$$i \in \{N_2, O_2, H_2O\}\ j \in \{Ox, \quad steam\ electrolysis)\}$$

Where C_i, is molar concentration of species i, $\nu_{i,j}$ and r_j are the species stoichiometric coefficient for reaction j and its rate respectively, and H is the height of the gas channels.

If the imposed electric current, I in the cell is totally used for the full species conversion in the PCEC, the electrochemical rate of reaction at the electrodes can be given as:

$$r_{Ox} = r_{Red} = \frac{I}{2F} \quad 3.34$$

Again, the PCEC global chemical reaction for co-electrolysis of CO_2 and H_2O are:

$CO_2 + H_2 \rightarrow CO + H_2O$, ΔH=-41kJ/mol 3.35

$CO + 3H_2 \rightarrow CH_4 + H_2O$, ΔH=-206 kJ/mol 3.36

$CO_2 + 4H_2 \rightarrow CH_4 + 2H_2O$, ΔH=-164 kJ/mol 3.37

There have been different expressions formulated to estimate the global rate of steam reforming (SR) and water gas shift (WGS) reactions, their reverse reactions was adopted at equilibrium for methanation and reverse WGS respectively. This give rise to the following general expressions:

$$r_{SR,meth} = -K_{SR}\left[P_{CH4}P_{H2O} - \frac{P_{CO}P_{H2}^3}{K_{eq,SR}}\right],\ K_{eq,SR} = \frac{K_{SR}}{K_{Methanation}} \quad 3.38$$

$$r_{WGS,RWGS} = -K_{WGS}\left[P_{CO}P_{H_2O} - \frac{P_{CO_2}P_{H2}}{K_{eq,WGS}}\right] - r_{SR},\ K_{eq,WGS} = \frac{K_{WGS}}{K_{RWGS}} \quad 3.39$$

where K_i denotes the rate of forward (SR and WGS) and backward (methanation and RWGS) reactions. K_{eq} is the equilibrium constant of each reaction. Generally, based on the Arrhenius first order kinetic expression, the rate of forward SR and WGS reactions can be estimated as [184]:

$$K_{SR\ or\ WGS} = K_o(P_i)^{n_i}\ exp\left(-\frac{E_{act}}{RT}\right) \quad 3.40$$

$$where\ i = CO, CH_4, CO_2, H_2O$$

where k_o, E_{act} , P_i are pre-exponential constant, activation energy, and species partial pressure of mixture respectively, while n_i denotes the gas species partial pressure effect. And specifically as,

$$K_{SR} = 2395\ exp\left(-\frac{-231266}{RT}\right)\ \ (mol.m^{-3}pa^{-2}s^{-1}) \quad 3.41$$

$$K_{WGS} = 0.0171\ exp\left(-\frac{103191}{RT}\right)\ (mol.m^{-3}pa^{-2}s^{-1}) \qquad 3.42$$

And the equilibrium constants estimated as [185]:

$$K_{eq,SR} = 1.0267 \times 10^{10}\ exp(-0.2513\ Z^4 + 0.3665\ Z^3 + 0.5810\ Z^2 - 27.134\ Z + 3.2770) \qquad 3.43$$

$$K_{eq,WGS} = exp(-0.2935\ Z^3 + 0.6351\ Z^2 + 41.788\ Z + 0.3196) \qquad 3.44$$

$$Z = \frac{1000}{T_{PEN}} - 1 \qquad 3.45$$

3.8 Model performance parameters

The fuel utilization (FU) ratio considering the reactants molar inflow rate and their outflow rate suggest the species electrochemical consumption and can be expressed as;

$$FU = 1 - \frac{\dot{n}_{H2O,out} + \dot{n}_{CO2,out}}{\dot{n}_{H2O,in} + \dot{n}_{CO2,in}} \qquad 3.46$$

The PCEC area specific resistance (ASR) can be written as:

$$ASR = \frac{E_{Op} - E_{Nernst}}{I_{ave}} \qquad 3.47$$

3.9 Results and discussions

Engineering equation solver (EES) being an excellent tool for solving the numerous systems of simultaneous non-linear equations is used for the modeling of the PCEC and it is used for all calculations in this study. The computational work is typical of the theoretical description in the previous sections.

3.9.1 Experimental results for validation

Fig. 3.4 displays the polarization curves depicting the methane production rate obtained from the experimental results of co-electrolyzing CO_2 and H_2O in PCEC operation mode. These results are of particular significance as they serve as validation for our model, as further elaborated in the subsequent sections. Operating cell potential differences of 1.78, 1.63, 1.50 and 1.36V were applied at 400, 450, 500 and 550℃ respectively to realize a current density of -10000A/m^2. The highest production of methane was achieved at this current density at 450℃ at a rate of 0.13 sccm cm^{-2}.

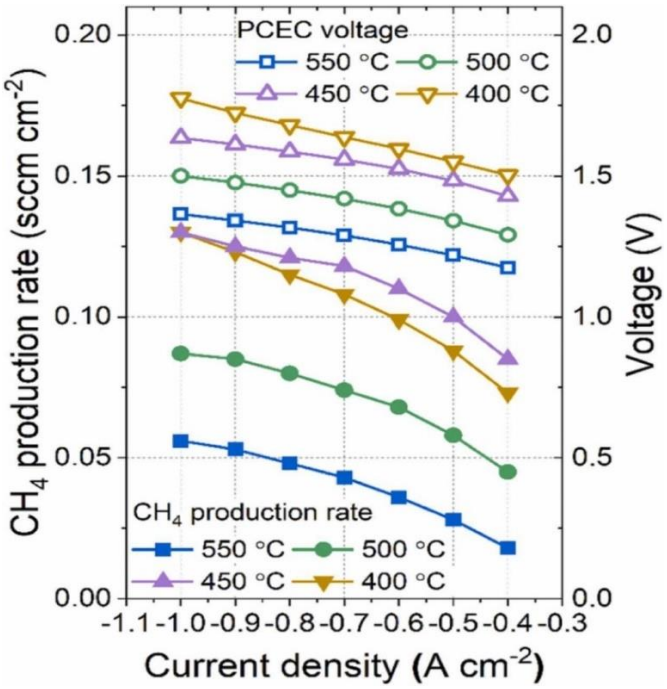

Fig. 3.4: Experimental characterization curves for PCEC co-electrolysis of water and CO_2 and methane production rate. Copyright, Elsevier 22 [94]

3.9.2 Model performance validation

The PCEC technology is still in its infancy stage, and one major challenge in the simulation of such technology is getting enough empirical data for its detailed modeling. Very limited experimental data are available in literature for hydrogen production which is the most research application for PCEC and just one or two for other chemicals like methane [29, 94]. In this work, we validate the OCV of modeled perovskite-supported PCEC for co-electrolysis of water and CO_2 for methane production and compare it with the only available experimental results by Pan et al [94] and Duan et al [29]. The polarization curves for the electrolysis-methane synthesis at 500℃ and other temperatures compared with the empirical data are shown in Fig.3.5a.It is reported that the operating temperature range for efficient operation of the PCEC is from 400-600 [29], so the average of these temperatures (500 ℃) is chosen as a base and reference validation temperature. As depicted in Fig. 4a, there is non-linear increase in the operating voltage from 0.69 to 1.44 V as the current density increases from -1 to -8286 Am^{-2} as expected. The same trend is observed in the empirical data (Fig. 3.4) and the model prediction at other temperatures as shown in Fig. 3.5b. Due to the intricacy and the complexity of the co-electrolysis reaction in the PCEC, the empirical study supplies the negatrode with is a gas mixture of CO_2 and N_2, without H_2. Thus, the reducing

environment during the operation is only maintained by the H_2 produced from the electrolysis process at the positrode. Therefore, to avoid possible oxidation of the Ni catalyst and maintain continuous co-electrolysis reaction due to limiting reactant, the minimum current density during the test was set as 4000 A/m^2. However, due to the versatility of the model we are able to predict a situation where the nickel catalyst is not oxidized or an alternative non-oxidizable catalyst of similar activity is used. Consequently, we extend the polarization curves to a current density of 1 A/m^2 for different temperatures as shown in Fig. 3.5b. The Fig. 3.5b further compares the experimental data and our model in this work at 450, 500 and 550℃. At 450℃, the model is limited by the amount of reacting species at higher current density, this is due to the high rate of methanation as elaborated in section 3.9.3. To probe if our model is a good representation of the experimental results, errors between the two data were estimated as shown in Fig. 3.6. The errors at all temperatures fall below the highly significant error reference of 0.001 which is strong evidence for the reliability of our model. Likewise, statistically comparing our model with the empirical data using the Wilcoxon signed rank test, at the 0.05 level shows that there is no significant difference between the two.

For better understanding of the behavior of the PCEC operation during the co-electrolysis reaction for methane production, the variation of the activation, concentration and ohmic overpotentials were studied at different operating current densities as depicted in Fig 3.7. It is obvious that the ohmic overpotentials are dominant of all there overpotentials and increase with current density which expected obeying the ohm's law (v=IR), though the rate of increase diminishes at higher current densities. The ohmic overpotential is in manifolds of others as be seen for example at a current density of 3000 A/m^2 the ohmic, concentration and activation overpotentials are 0.65, 0.004 and 0.19v respectively. This is due to the thickness of the electrolyte (0.14 mm) and the interconnectors (0.19 mm) used. The higher ionic conductivity of the proton-conducting electrolyte results in a pronounced activation overpotential. On the other hand, the concentration overpotential is less prominent due to the increased hydrogen diffusivity resulting from water electrolysis at the positrode, which is the controlling reaction. The quasi-linear behaviour of these two dominant overpotentials explains the reason why the PCEC polarization curve (I-V curve) almost follows a quadratic relationship. To further explore the factors that can influence the low concentration overpotentials in PCEC, the effects of temperature and increased current density are parametrically studied as shown Fig. 3.8. At higher operating temperatures, there is non-linear

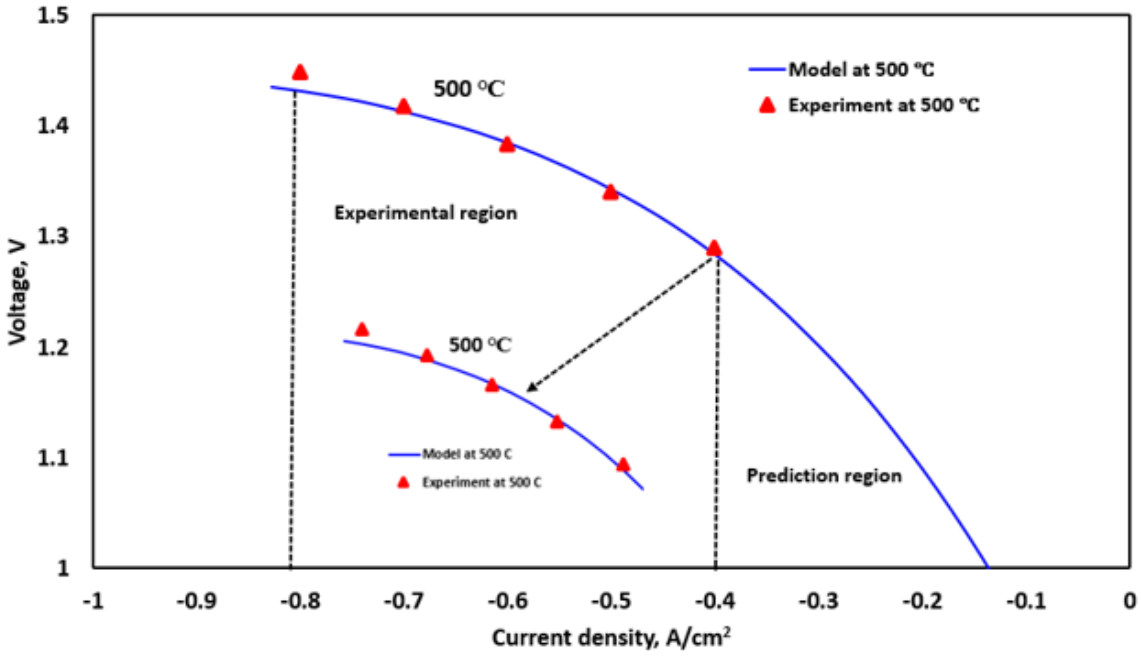

(a)

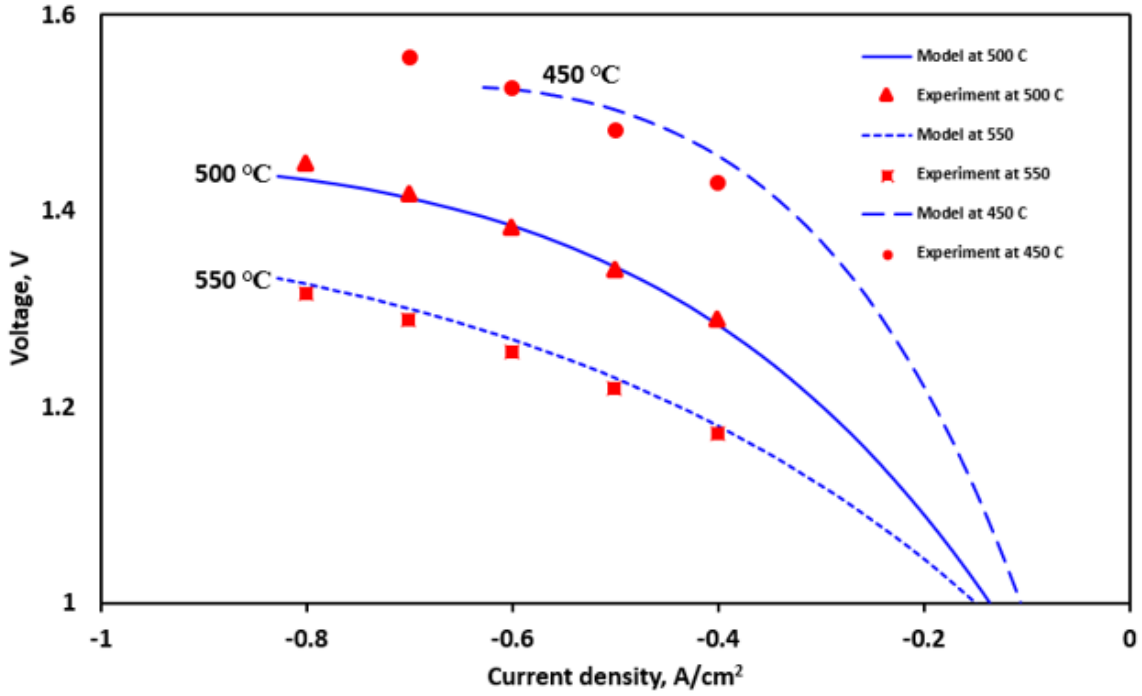

(b)

Fig. 3.5: Comparison between the polarization curves of model simulation results and experimental data a) comparing at 500°C b) prediction at other temperatures and lower current densities

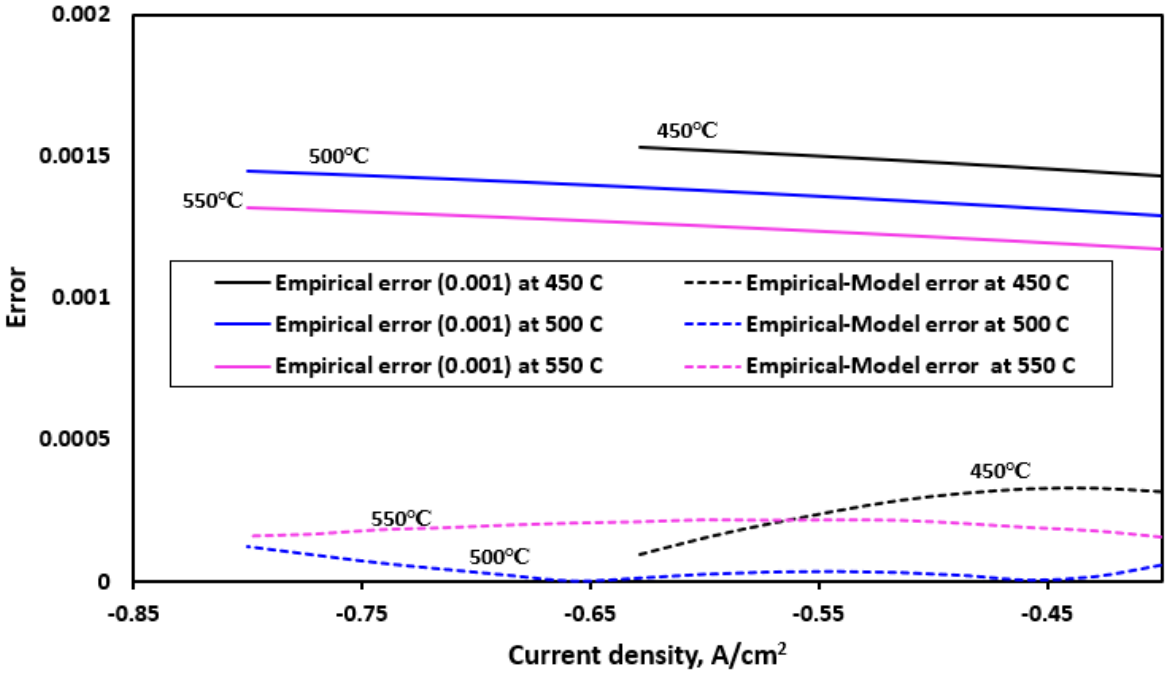

Fig. 3.6: Error curve for the empirical and model results

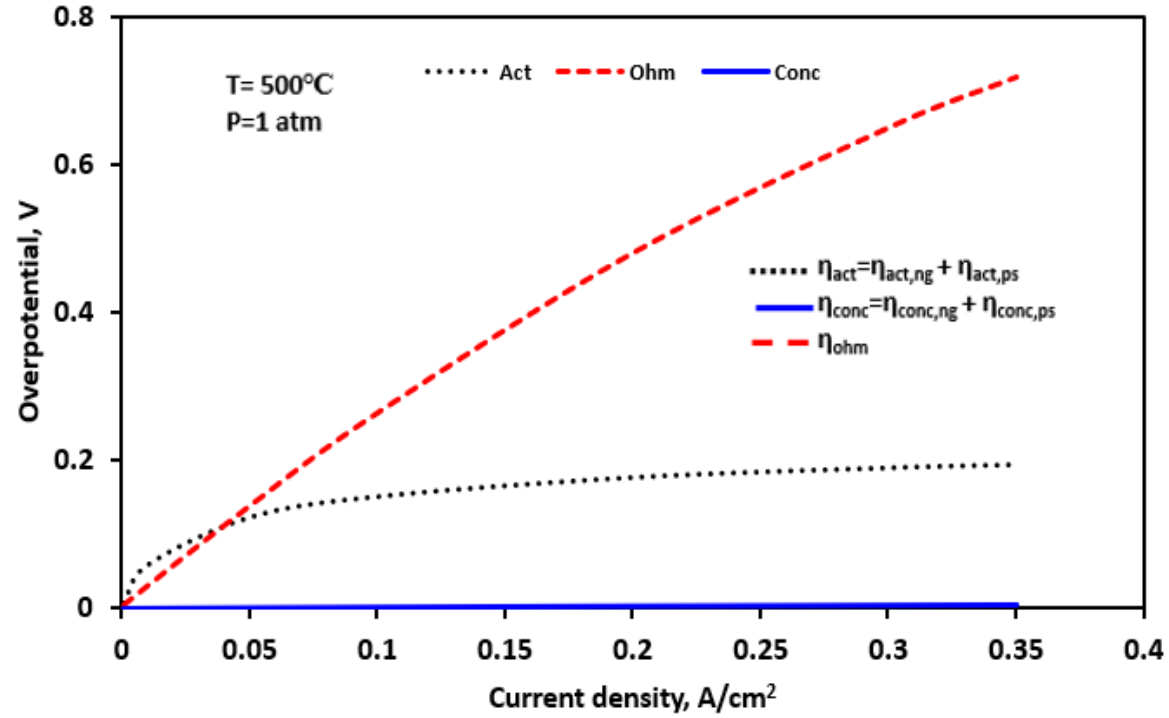

Fig. 3.7: The overpotentials at varying current densities

increase in concentration overpotential due to the increase in the mass transfer resistance resulting from higher effective diffusion coefficient.This reduces the molar diffusion rate and contributes to the variation in the gas concentrations which is reflected by the non-linearity in the curve [27, 146]. The effect of temperature seems to be more pronounced at higher operating current densities. Likewise, higher current densities increase the overall concentration overpotentials of the cell as shown in Fig. 3.7 and made apparent in Fig. 3.8. The current density plays a key role in driving the electrochemical kinetics of the cell, as it increases, it drives and increases the reaction rate at the electrodes. This results in fast consumption of the reactants and reduces their concentrations electrode surface due to inability to keep up and sustain the consumption rate [186]. This decrease mass transport towards the reaction site increases as current density increases which is proportional and directly related to the concentration overpotential. However, these effects are not obvious in the operating cell voltage due to the overriding effects of the activation and ohmic overpotentials, they are in higher multiples of the concentration overpotential in all cases. Generally, the concentration overpotential seems to be lower in PCEC compared to SOEC which merit of the PCEC. This typically is reasonable since SOEC operates at higher temperature which favors increased concentration overpotential unlike the PCEC with medium operating temperatures. As expected, overpotentials increases

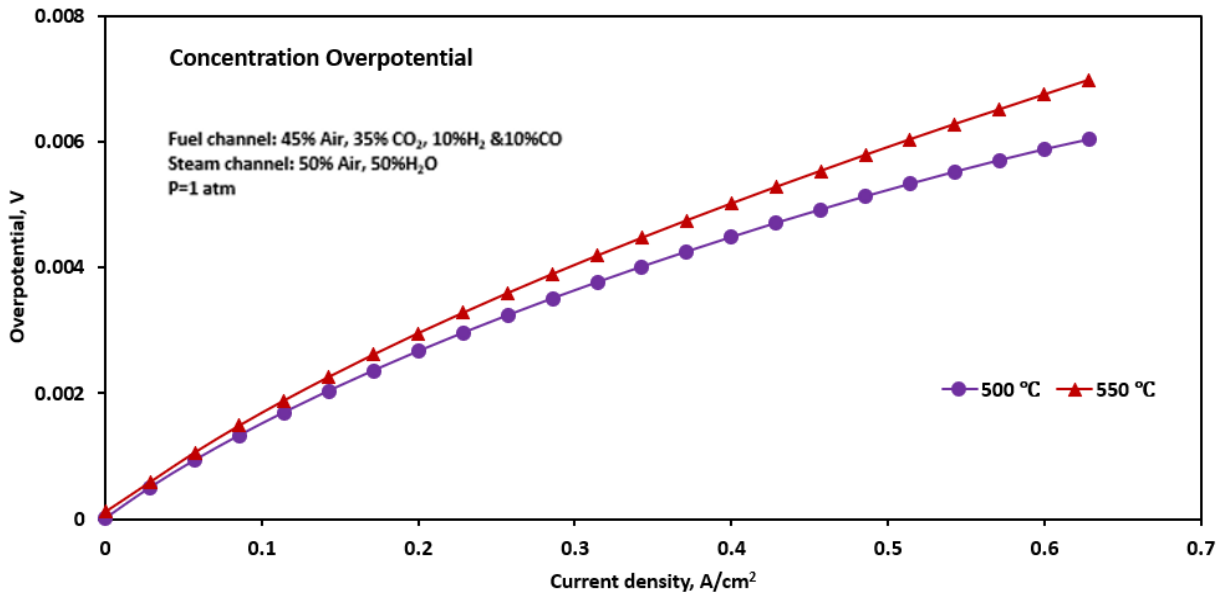

Fig. 3.8: Effects of temperatures and current densities on concentration overpotential.

proportionally with current densities as depicted in Fig. 3.7. However, unlike the concentration overpotential that increases with increasing temperature, the ohmic and activation overpotentials decreases as temperature goes higher as shown in Figures 3.9 and 3.10. From the nonlinear polarization curve in Fig. 3.9, there is a sharp rise in the activation overpotential at low current density due to the need to overcome the resistance posed by the rate determining step of the reaction. It increases very at lower densities and dominates other overpotentials, its dominant is obvious in Fig. 3.7. The activation overpotential must be surpassed for reaction to proceed and the activity of the electrodes play significant role in determining its value. It is evident in Fig. 3.9 that at higher temperature there is a decrease in the activation overpotential as expected, when the operating temperature increases the electrochemical kinetic energy and the rate of reaction at the electrode surfaces increase. Consequently, this lower the activation overpotential. A similar temperature effect is observed with ohmic overpotential as detailed in Fig. 9, it decreases with increase in temperature. The protonic conductivity of the electrolyte increases at higher temperature which lowers the electrolyte resistance and enhance the transport of protons across the electrolyte. This protonic conductivity is very sensitive to temperature that leads to a drastic drop in the ohmic overpotential as observed in Fig. 3.10. This literarily reduces the operating cell potential as supported by Fig. 3.5b.

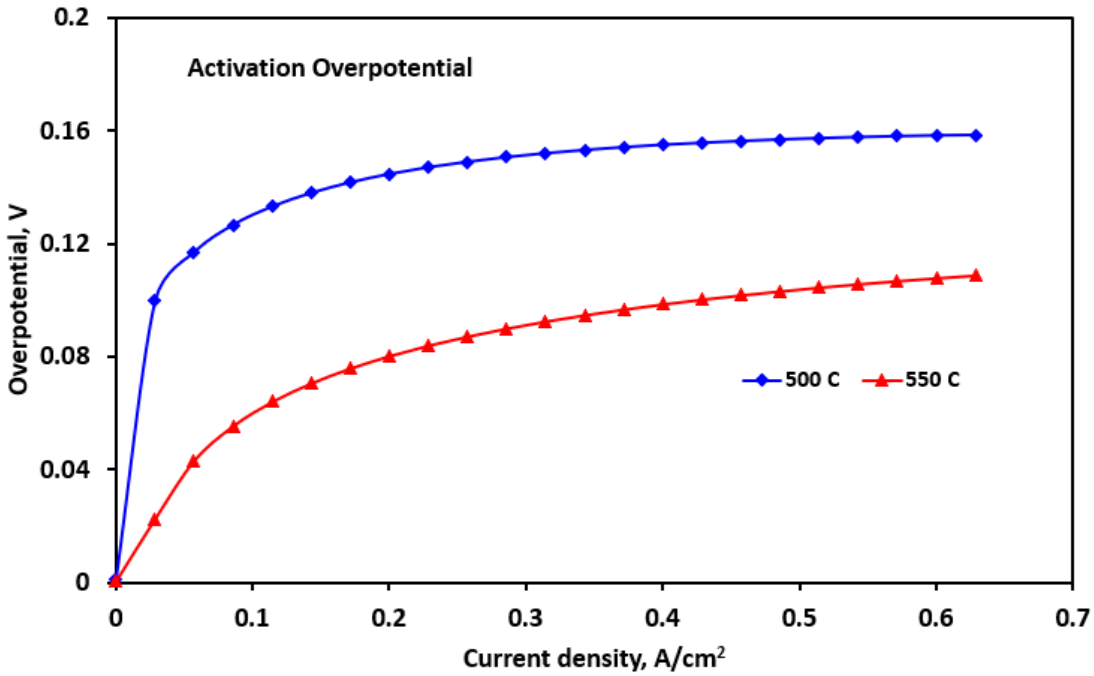

Fig. 3.9: Effects of temperatures and current densities on activation overpotential.

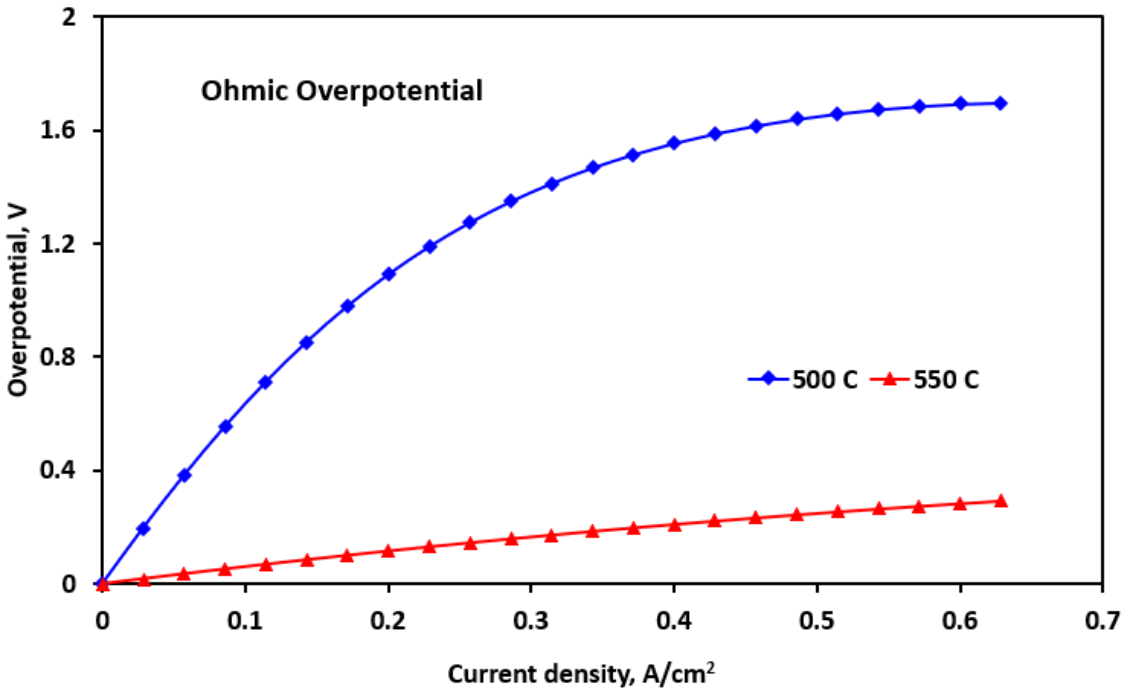

Fig. 3.10: Effects of temperatures and current densities on ohmic overpotential.

3.9.3 Rate of methane production with temperature

In Fig. 3.11, the molar flow rate of methane production from the PCEC is presented at various operating temperatures. The plot illustrates the combination of the electrolysis and methanation reactions at a current density of 2000 A/m^2, with a steam inflow rate of 50 cm^3/min. The production of methane has been studied to be very low at high temperatures and this is one of the reasons for lower yield in high operating temperature electrolyzers like the oxygen-ion-conducting SOECs, 0.03% was reported by both Li et al [187] and Luo et al [188] at 550℃ and 600℃ respectively. Xie et al [189] also recorded a low yield of 0.2% at 650 ℃, all these can be ascribed to the exothermicity of the methanation reaction. However, with the PCEC which generally operates at intermediate temperatures with better efficiency in the range 400-600℃ [29] lies a solution and thermodynamic prediction by Pan et al [94] gives similar temperature range. In further studies of the characteristics behavior of our model, we estimate the rate of methane production at varying temperatures as depicted in Fig. 3.11. The results revealed that higher rate of production at the operating conditions lies approximately between 420-470℃ with the optimum production rate of 0.0391 moldm^{-3}min^{-1} at 450℃ in support of previous findings and this result is corroborated by the experimental results by Pan et al [94]. Additional investigations in this field are necessary to

determine the optimal operating temperatures under different conditions. These analyses will be conducted in future works to provide comprehensive insights within the series of this study.

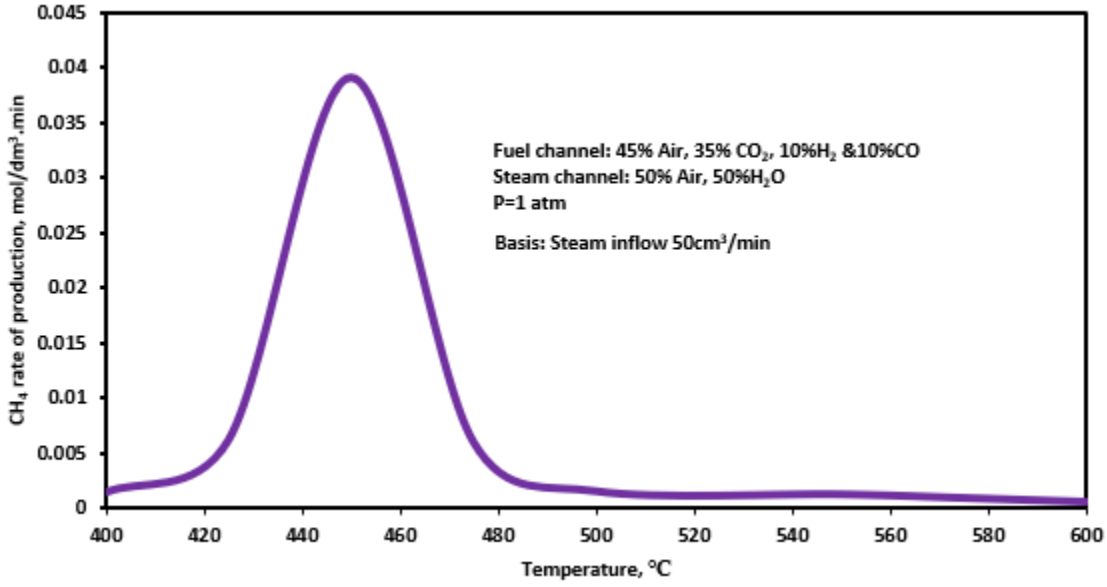

Fig. 3.11: Rate of methane production at varying temperature

The mole ratio of methane and other reactant species at the cell and stack outlet after the reactions is also investigated at different current densities and the result is shown in Fig. 3.12. In Fig. 3.12a the downward slope of H_2O shows that with increase in current density more steam is consumed and same is observed for the CO but narrower. The observed trend can be attributed to the production of CO from CO_2 and its subsequent consumption in methane production. As expected, methane displays a positive slope in the plot, indicating increased production. Exceptionally, the mole ratio of CO_2 also exhibits a positive slope with increasing current density, despite being consumed in the reaction. This can be misleading since the plot shows a ratio of reactant and product species, which implies that other reactants are being consumed more rapidly than CO_2. To clarify the increased consumption of CO_2, an independent rate measurement is conducted as illustrated in Fig. 3.12b, which clearly demonstrates that its consumption increases with higher current density, leading to a decline in its concentration.

The I-V polarization curve at varying CO_2 concentration is studied to know its effect on the operation of the cell and production of methane. Fig. 3.13a and b are detailed curves depicting the effect of the CO_2 feed composition at the negatrode of the PCEC. At fixed H_2O mole fraction the

cell voltage does not significantly change with variation of CO_2 mole fraction, though it thus shows a higher voltage at lower CO_2/H_2O ratio and lower at higher voltage.

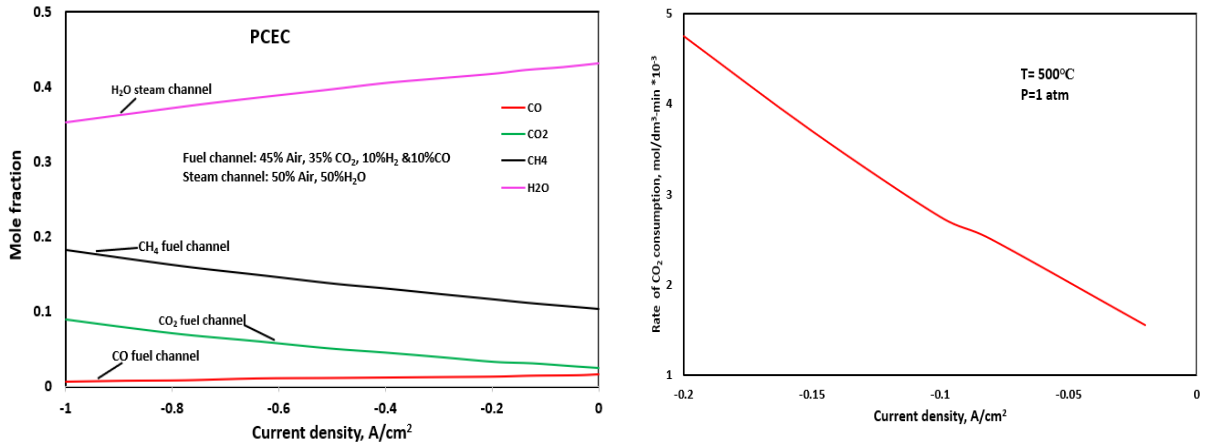

(a) (b)

Fig. 3.12: Mole ratio of CH_4 and the reactant species at 500°C with varying current densities a) product and reactant ratio b) consumption rate of CO_2

As expected, there is higher production of methane in all cases. It is worth to note that at higher current densities both the voltage and methane production increases. To further understand the effect of CO_2/H_2O ratio, the mole fractions of the CO_2 and H_2O are varied at different current densities. Fig. 3.14a and b shows that there is a significant change in the cell voltage and the amount of methane produced compared to when H_2O mole ratio was fixed in Fig. 3.13a and b. Lower ratios show higher voltage and methane production, and higher ratios show the reverse.

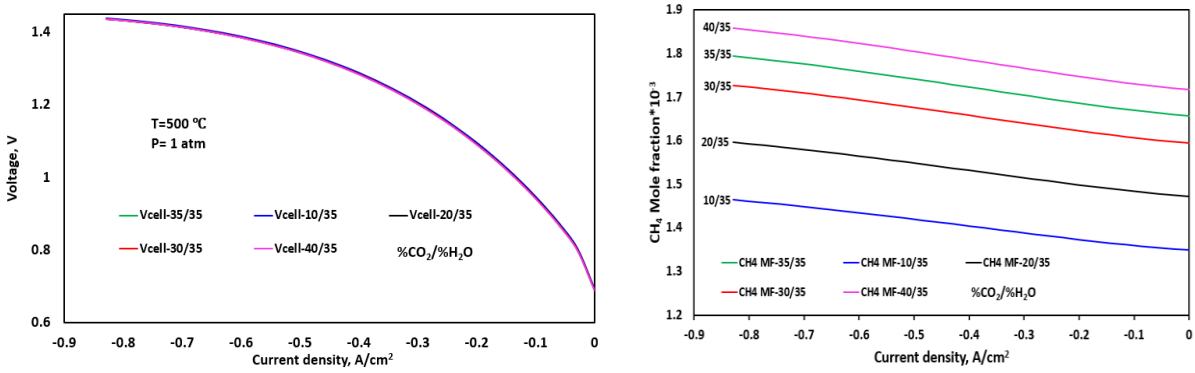

(a) (b)

Fig. 3.13: Effect of CO_2 concentration on a) I-V polarization curves b) produced CH_4 mole fraction

At higher H_2O mole ratio of 60% (10% CO_2) there is higher production of CH_4 with an output mole fraction of 0.005 compared to 35% (40%CO_2) with molar fraction of 0.0019 which is over 2.5 times lower. This might be showing the dominance of effect of the water electrolysis in the co-electrolysis reaction and possibly rate determining step as mentioned in extant literature. It can also be inferred that perhaps more H_2O is available for the other side reactions and more proton and water can react with CO_2 for more methane production.

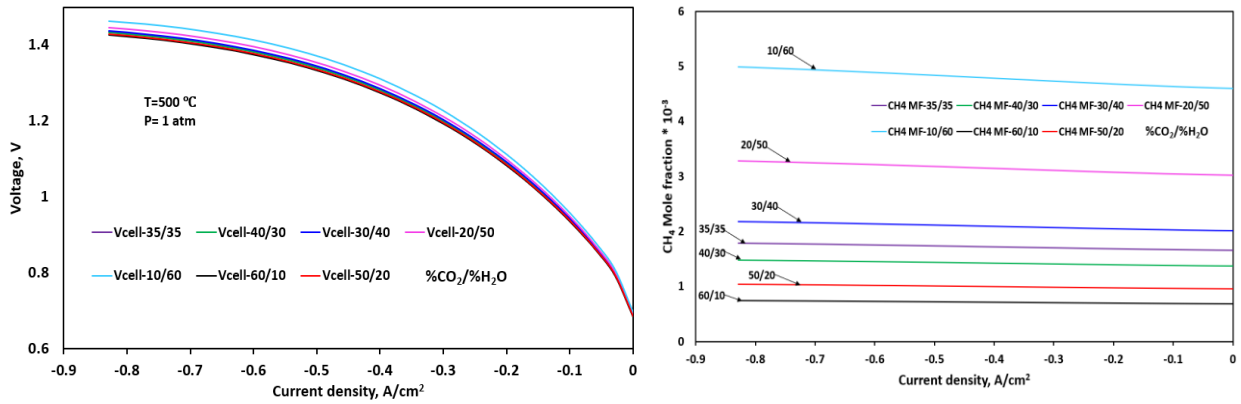

(a) (b)

Fig. 3.14: Effect of CO_2 and H_2O concentration on a) I-V polarization curve b) produced CH_4 mole fraction

3.10 Conclusion

In this study, we have constructed a one-dimensional button-cell model for protonic ceramic electrochemical cells (PCECs) using the Engineering Equation Solver (EES). The model specifically focuses on the co-electrolysis of CO_2 and H_2O to produce methane. The model detailed the operation of a unit cell and stack of PCEC in the electrolysis mode in steady state. The model is validated and calibrated with experimental results. Therefore, a new conceptual formulation and satisficing semi-empirical PCEC model is established which would save time against future experimental procedures to demonstrate reactive porous-media transport, elementary catalytic

chemistry, and electrochemistry properties in the cell. The model shows lower voltage output as the operating temperature increases and predict the cell potentials at lower operating current densities. It also gives insight on of the effect on the overpotentials on the cell output which will enhance dexterity in its design and choice of stack and building materials. The model presents the rate of methane production at different temperatures and revealed that efficient PCEC for co-electrolysis of CO_2 and H_2O is operated in the temperature range of 420-470℃ and the optimum being 450℃ at the rate of 0.0391 $moldm^{-3}min^{-1}$. Presumably from the model, it shows there is need for enough water for higher CH_4 production and the water electrolysis is the rate determining step in co-electrolysis of CO_2 and steam in PCEC The outcomes of this model rationalize the potential utilization of the PCEC as a CO_2 sink for decarbonization purpose and methane production that can be transferred into real life fuel utilization. Furthermore, the model's findings create opportunities for scaling up the technology and eventual commercialization.

CHAPTER 4 DESIGN AND MODELING OF AN INTEGRATED REVERSIBLE PROTONIC CERAMIC ELECTROCHEMICAL SYSTEM

? **Research Question, RQ3**: Can the PCEC stack be integrated with fossil fuel power plants and renewables and be used as an energy storage?

- **Objective 3**: Stack and system level model of RePCEC for co-electrolysis reaction.

✓ **New knowledge**: Development of stack model and optimal design of integrated RePCEC systems for improved net energy usage and large-scale energy storage using water-energy nexus framework.

This chapter stands at the core of this dissertation, addressing research questions one to three and bridging significant gaps in the utilization of RePCEC as an energy storage system for large-scale grid applications. The chapter is written wholly by the author in an intended journal format.

4.1 Broader

Reliance on fossil fuels will continue for the next decades even though there are global pushes away from it to mitigate the overarching climate challenge, most especially by its highest consumers. While there is a hastening global shift away from fossil fuel, integrating its assets into this technology helps limit the risk and future losses of stranded assets and reduce the cost of investment in the new technologies. Moreover, the generation of electricity from intermittent renewable sources like solar and wind has witnessed a significant surge in recent years, leading to a pressing demand for practical energy storage systems. Reversible electrochemical cells (RECs) offer a promising option for addressing the fossil fuel assets integration and energy storage challenges through the interconversion between electrical and chemical energy and concurrent utilizing carbon emission. In their electrolysis mode, the RECs convert electricity into durable, storable, and portable valuable chemical fuels (like syngas and methane). Conversely, the produced chemical fuels are used as reactants in the fuel cell mode to generate electricity on demand with minimal (hydrocarbons) or zero (when H_2 or NH_3 is used) emissions. However, a challenging goal for this type of technology remains to achieve optimal operation and high roundtrip efficiencies, which has hindered the deployment of previous ones. This work demonstrate how reversible protonic ceramic electrochemical cells (RePCECs) can be integrated with fossil fuel powerplants and renewable energy sources as a potential energy storage system.

We thereby address the performance requirements, technical and non-technical challenges for it to be used as large-scale energy storage, and its eventual implementation at the system level to enhance net-zero economy.

4.2 Introduction

The International Energy Agency (IEA) revealed in 2023 [190] that there would be an estimated 33% increase in the global installation of renewable capacity. In addition to the climate challenge mitigation drive, this surge is attributed to several factors, including rising fossil fuel costs, supporting policy, and heightened concerns about energy security, all spurring the extensive deployment of solar photovoltaic and wind power technologies. The year 2023 is set to witness an unprecedented surge in world renewable capacity additions, with a remarkable increase of 107 GW, bringing the year total to almost 500 GW. This trend is poised to continue in 2024, with the global cumulative capacity for renewable electricity projected to reach 4,500 GW (4.5 TW). To put this in perspective, this capacity is equivalent to the entire power output of the United States and China. This is huge and more than quadruple of the 2050 projection by the National Renewable Energy Laboratory (NREL) in 2006 [191], as shown in Fig. 4.1

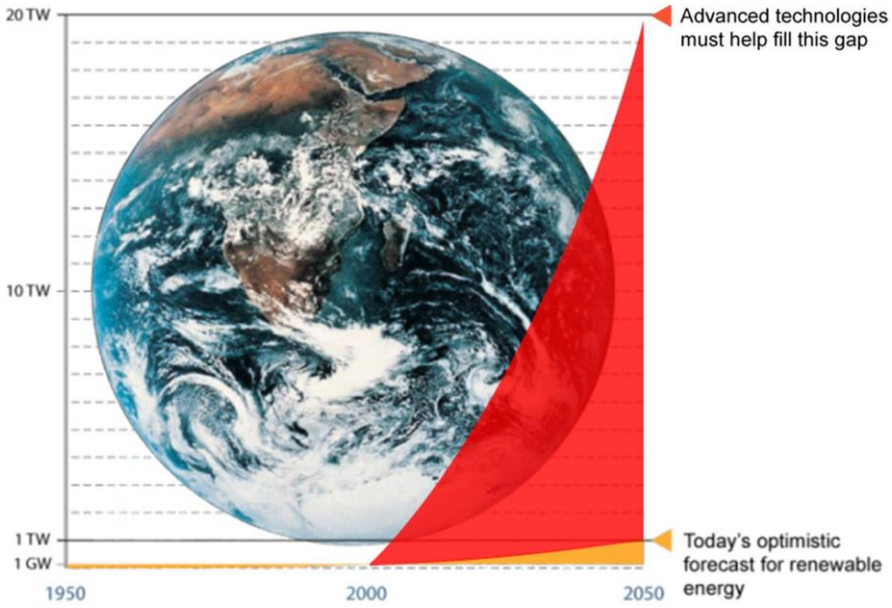

Fig. 4.1: Magnitude of energy challenges and 2050 renewables projection in 2006 [191]

Likewise, Fig. 4.2 shows that the world is currently producing the projected amount of renewables in 2035, which shows it over ten years ahead. Maintaining this level of concerted effort can make the global net-zero dream comes to fruition earlier than expected and likely fill up the gap in Fig.1

by 2040. The interesting thing about this renewable energy production mix is that over 90% of the produced RE is coming from solar and wind. As mentioned, this kind of growth is unprecedented, and increasing utilization is expected as there are drives for it. However, a significant challenge with these deployments is the intermittency of these two primary sources.

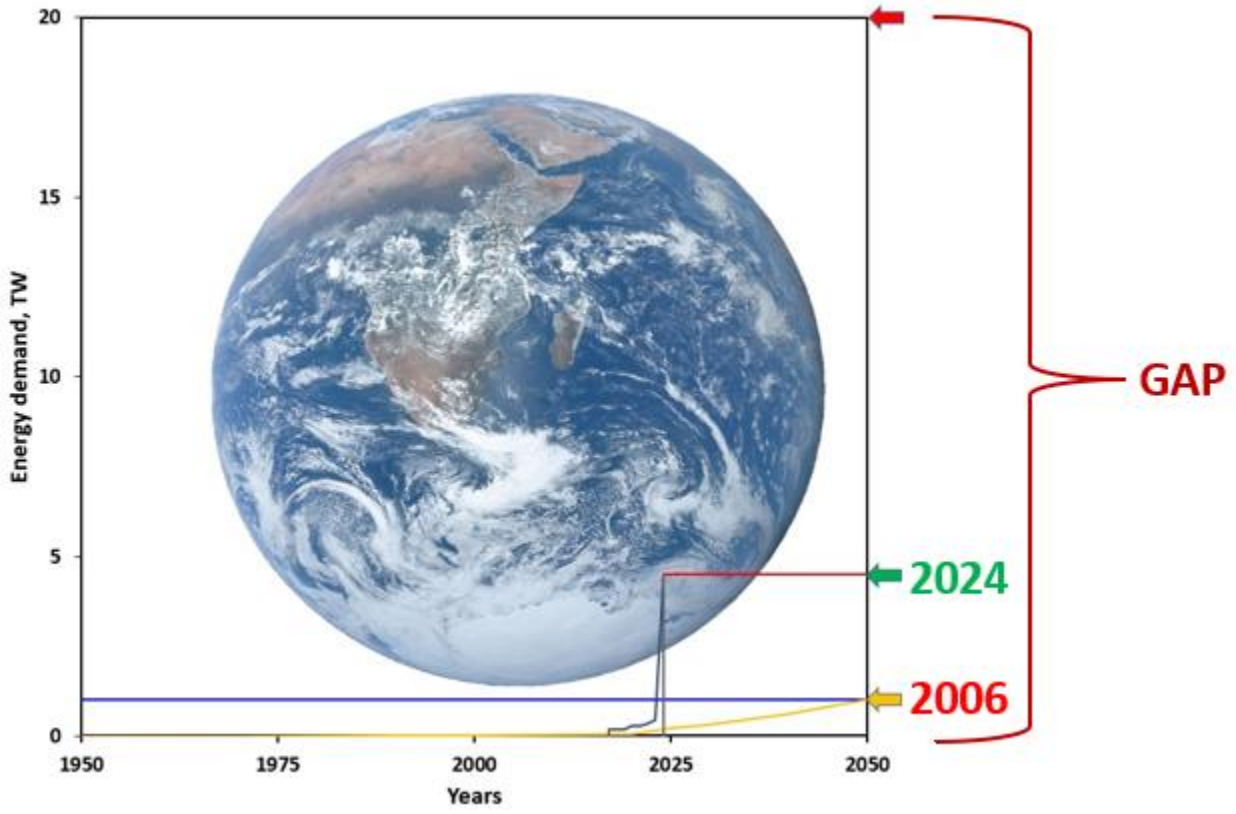

Fig. 4.2: Current state of global renewable energy production (red line shows the 2024 RE deployment, blue line is the 2006 RE production projection limit, yellow line 2006 projection rate, black line indicates the actual trend from 2017-2023 before the jump in 2024)

To enhance the continuous use and integration of renewable wind and solar sources into the electricity grids, there will be an urgent and growing need for expanded energy storage capacity to effectively handle these consequential variations and intermittence in power generation and consumption [165, 192]. The periodic change in energy demand that usually leads to disparities between demand and supply, in addition to interruptions to the power supply, will benefit immensely from a sophisticated energy storage system. This is required for balancing a load that changes at different times. To address these concerns, the future energy storage requirements

estimation of 15-20% of the annual load must be met [193]. This is in tandem with the 20% storage backup rule of thumb agreed on by utilities and grid operators for going completely renewable [194]. An average of 670 GW of energy storage demand is anticipated for 2-3 billion kWh energy demand in China [195] which falls almost in the same range. The current energy storage systems are faced with several critical challenges when it comes to providing long-term storage solutions; this stems from problems like high costs, low efficiency, and large-scale requirements [3, 196]. These challenges have been broadly classified into technology and economic constraints [1]. While numerous storage technologies and approaches are currently explored, enough attention has not been given to reversible electrochemical cells (RECs) used for interconversion between chemical and electrical energy [39]. From the limited studies on RECs, focus have been on reversible solid oxide electrochemical cell (ReSOC) technology due to its latest developments [196] and advantages (like high roundtrip efficiency, >70%, poison tolerance and cost-effective) [61] over the older ones like Reversible Proton Exchange Membrane Electrochemical Cell (RePEMEC) and Reversible Alkaline Electrochemical Cell (ReAEC). However, the recent advancements and improvement of the solid oxide cells birthed another technology, the reversible protonic ceramic electrochemical cell (RePCEC) [39, 46] which is the focal point of this study.

The RePCEC is a bifunctional standalone device that combines the functions of the protonic ceramic electrolysis cell (PCEC) and the protonic ceramic fuel cell (PCFC). In the electrolysis mode, it stores energy and renewables, utilizing water, CO_2, and other reactants to produce hydrogen and valuable chemical fuels, and its fuel cell mode uses the produced hydrogen and fuels to generate electricity [38, 68]. This work uses RePCEP for co-electrolysis of H_2O (steam) and CO_2 for methane (desired product), H_2, and CO production. The two global reactions in the PCEC (forward) mode are the exothermic methanation reaction and the endothermic steam electrolysis reaction. Combining the heat-consuming steam electrolysis reaction with the heat-producing CO_2 hydrogenation reaction enables effective thermal management of the process, which results in an improved overall efficiency. The same thermal management concept is adopted in the PCFC (reverse) mode for the endothermic steam reforming and exothermic H_2O production. This typically will minimize heat loss from the system and enhance the roundtrip efficiency of the RePCEC, similar to what was reported by Duan et al. [29]. Being able to achieve this at high fidelity makes it a potential storage solution that is similar to rechargeable batteries in their chargeability. The effective incorporation of these functionalities in a standalone device would

enable the development of a long-term storage technology whose deployment scale is primarily constrained by the capacity of the fuel storage tanks.

As the world rapidly transitions away from fossil fuels, which will still dominate the energy industries in the coming decades, the integration of existing fossil fuel assets into the RePCEC technology serves to mitigate the risks and potential future losses associated with stranded assets while also reducing the upfront investment costs in this emerging technology. However, significant capital expenditures and uncertainty regarding future cost and efficiency improvements pose challenges to investing in RePCEC. Our comprehensive exploration of integrating RePCEC system with fossil fuel assets and renewable energy sources demonstrates its potential as an economically viable energy storage device for the future, especially when renewables are adopted and dominate the energy industries.

4.3 Stack model

The previous chapter focused on the design of PCEC (typical of RePCEC) at a single cell-level, which is relatively simple and particularly suitable for a laboratory-scale experiment. Nevertheless, for a large-scale application, it is necessary to assemble multiple cells for a stack-level design. The stack-level modeling is employed to simulate the PCEC stack, comprising multiple single-cell units, interconnects, manifolds, frames, and seals [39]. The overarching goals of this dissertation require the development of models that can precisely predict the technical performance of the system. This section outlines the underlying assumptions, equations, and modeling approach adopted to design RePCEC stack and system-level implementation. A critical aspect of this work is to determine the optimal RePCEC operating parameters for grid-scale integration. Hence, the modeling of RePCEC stack is carried out at a higher level of precision compared to the balance of plant (BoP) components in the system design. Here, we established a physically grounded channel-level RePCEC model, allowing us to account for the performance fluctuations under different cell operating conditions and methods, drawing from empirical performance data using BCZYYb as the electrolyte membrane. This strategy enhances the quick scaling up of the RePCEC from the button-cell level to the channel-level model. Each of the BoP components is singly modeled and thermodynamically integrated into the system.

The primary purpose of the stack model created in this study is to simulate the performance of RePCEC stack used in the system-level model. Some of these performance parameters include the amount of electric power generated or consumed, species concentration, and other operating conditions influenced by other BoP components. Building on the approach used for the button cell and validation, it is easy to transcend to the channel-level. The species (reactant and product) mixture's composition changes (decrease for reactant and increase for product) along the channel's length because of the electrochemical reactions. Thus, to determine the axial changes in species concentration, physical properties (like pressure and temperature), and transport properties (like diffusion and thermal conductivity) in the cell channel, the governing equations like conservation of mass, species, momentum, and energy must be solved. This work adopted the methods used by Refs. [27, 197] in their modeling of ReSOC to achieve the RePCEC stack model. A detailed PCEC cell model is developed in chapter three. The scope of this cell model is extended to create a generic RePCEC stack model. However, the stack energy conservation equation at the channel-level is addressed here.

4.3.1 RePCEC stack configuration

Electrochemical cell stack configuration picks after its unit or single cells, which are systematically arranged in an order. The smallest RePCEC units can either be planar or tubular configurations similar to others, like polymer electrolyte membrane (PEM) and SOEC. Generally, the planar configuration has been reported to be superior and outperformed the tubular designs and has been adopted in many models. This has been traced to more uniform gas distribution coupled with ease of production of the planar cells. It also offers the benefit of power (volumetric) densities and low cost of production [40, 41]. Likewise, considering the lower power density associated with tubular design due to increased current path, the planar design geometry is considered in this work.

4.3.2 Channel-level model

The RePCEC model is detailed in this section in addition to the button cell model in Chapter 3; it entails the channel geometry parameters, conservation equations (mass, species, momentum, energy), and the numerical solution approach.

4.3.2.1 The channel geometry

Fig. 4.3 depicts the geometry of the channel-level model, illustrating the dimensions of the rectangular positrode (the positive electrode) and negatrode (the negative electrode) channels, along with the cell components' thickness and that of the interconnectors and the PEN. The PEN comprises the positrode, electrolyte membrane, and the negatrode, thus its thickness is the sum of the MEA materials' thickness combined. The terms positrode and negatrode are always the positive and negative electrodes respectively and are the same, independent of the operating mode. Likewise, the positrode or negatrode can be the electrochemical cell anode or cathode depending on the operating mode and vice versa.

This model is built to define the stack and its performance.

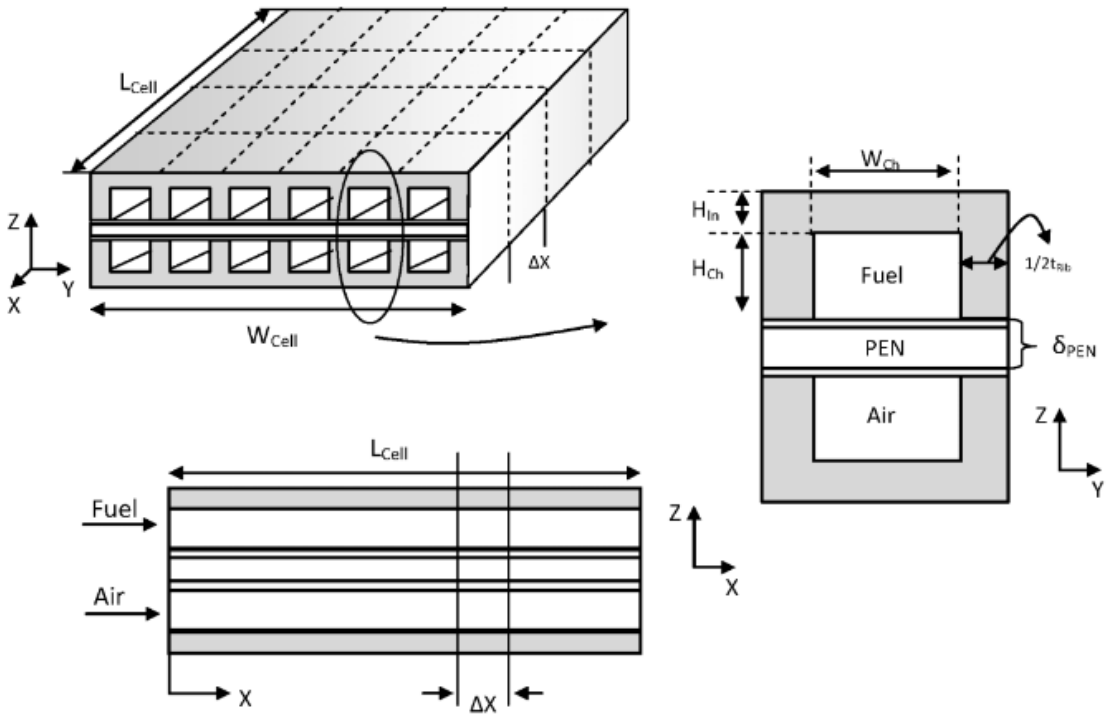

Fig. 4.3: Schematic channel geometry [182]

4.3.3 Model assumptions

In the design of the planar PCEC model, it assumed that the flow in the steam and fuel channels are concurrent, and the protons passed across the electrolyte membrane fast to ensure the immediate reduction of CO_2 in the fuel channel. The PCEC physiochemical conditions for its development are uniquely defined by extrapolating certain modeling concepts used with SOECs, while adopting some assumptions made in references [165, 169]. To represent the entire cell unit, an extended interface charge-transfer channel model is employed. It is assumed that the sweep gas and fuel flows distribute uniformly in each cell channel. Other key assumptions in this work include:

11. Adiabatic boundaries at the cell ends.
12. All gases are ideal gases.
13. At steady state.
14. Lumped temperature of the cell structure.
15. Uniformly distributed cell temperature.
16. At constant pressure.
17. Plug flow across the channels.
18. One-dimensional cell representation along the streamwise direction.
19. Channels act as a continuously stirred tank reactor (CSTR).
20. One-dimensional cell representation along the streamwise direction.
21. Selective reduction of CO_2 for methane production at the fuel electrode.

4.3.4 Material balance

The RePCEC operation in this work uses several gases as the feedstock, and the mass balance computes their compositions in each channel resulting from the electrochemical reaction taking place there. These gas mixtures and their supply to the electrodes are as described in Chapter 3. While it has been assumed that the channels are a CSTR (uniform mix at each node of the x direction), they act as a plug flow reactor, PFR (varying composition across the length), as shown in Fig. 4.4.

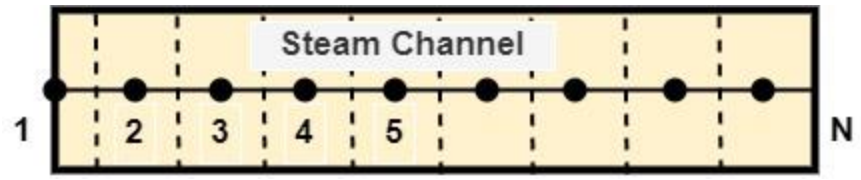

Fig. 4.4: Species movement and variation across the channel

The general continuity equation is used to relate the mass balance in the cell channels and expressed as:

At the negatrode (Fuel channel)

$$\frac{\partial C_i}{\partial t} = -\frac{\partial (u_{ng} C_i)}{\partial x} + \sum_j v_{i,j} r_j \frac{1}{H_{ng}} \qquad 4.1$$

$$i \in \{ CO_2, H_2O, CO, H_2, Ar\ (or\ N_2), CH_4 \}\ j \in \{Red, Methanation\}$$

At the positrode (Steam/Air channel),

$$\frac{\partial C_i}{\partial t} = -\frac{\partial (u_{ps} C_i)}{\partial x} + \sum_j v_{i,j} r_j \frac{1}{H_{ps}} \qquad 4.2$$

$$i \in \{N_2, O_2, H_2O\}\ j \in \{Ox, \quad steam\ electrolysis)\}$$

Where C_i, is the molar concentration of species i, $v_{i,j}$ and r_j are the species stoichiometric coefficient for reaction j and its rate, respectively, u is the velocity of species at both the negatrode and positrode, and H is the height of the gas channels.

The formulation in equations 4.1 and 4.2 are typically used in this work. However, for comprehensive benefits, an alternative formulation for the material balance starting from the first principle is expressed below and it is alternatively called overall mass conservation here.

4.3.4.1 Overall mass conservation

In a multicomponent system as we have in the electrochemical reactor channel, considering a component i undergoing electrochemical reaction in the channel with volume element WHΔx and moving across in the x-direction, the continuity equation is given by

$$\frac{\partial \rho_i}{\partial t} = -(\nabla . n_i) + r_i \qquad 4.3$$

$$\frac{\partial \rho_i}{\partial t} = -\frac{\partial (\rho_i v_x)}{\partial x} + r_i \qquad 4.4$$

This gives the continuity equation for species i in a multicomponent reacting mixture. Where ρ is its density and n= ρv is the mass flux across constant area WH and v is the velocity and r is the rate of production or consumption of species i per unit volume. W and H are the channel width and height respectively.

In the x-direction and reaction across the bottom plate with area WΔx through which species leave and enter the volume element,

$$\frac{\partial \rho_i}{\partial t} = -\frac{\partial (\rho_i v_x)}{\partial x} + \frac{r_i}{H} \qquad 4.5$$

This gives the continuity equation with mass unit. Its corresponding derivative with a molar unit can be written as,

$$\frac{\partial c_i}{\partial t} = -(\nabla . N_i) + R_i \qquad 4.6$$

$$\frac{\partial c_i}{\partial t} = -\frac{\partial (c_i v_x)}{\partial x} + R_i \qquad 4.7$$

$$\frac{\partial c_i}{\partial t} = -\frac{\partial (c_i v_x)}{\partial x} + \frac{R_i}{H} \qquad 4.8$$

For all required species,

$$\frac{\partial c}{\partial t} = -\frac{\partial (c v_x)}{\partial x} + \sum \frac{R_i}{H} \qquad 4.9$$

$$\frac{\partial c}{\partial t} = -\frac{\partial (c v_x)}{\partial x} + \frac{1}{H} \sum R_i \qquad 4.10$$

The molar flow across each node as shown in Fig. 4 can be estimated using the discretization of channel length in the x-direction as depicted in Fig. 3. Simplify equation 4.7 at steady state,

$$\frac{\partial (c_i v_x)}{\partial x} = R_i \qquad 4.11$$

The relationship between the concentration c_i and the molar $\dot{N}_i$ flow can be written has,

$$C_i = \frac{\dot{N}_i}{(A_x v_x)} \qquad 4.12$$

Where cross-sectional area, WH in x-direction and v_x is the velocity. Substituting 4.12 in 4.11

$$\frac{1}{A_x}\frac{\partial(\dot{N}_i)}{\partial x} = R_i \qquad 4.13$$

It is worthy to note that R_i is the rate of reaction per unit elemental volume WHΔx and can be related to the general reaction rate as

$$R_i = \frac{\sum r_i}{WH\Delta x} \qquad 4.14$$

Combining 4.13 with 4.14, we have

$$\frac{\partial(\dot{N}_i)}{\partial x} = A_x \frac{\sum r_i}{WH\Delta x} \qquad 4.15$$

Discretizing 4.15 with the discretized length Δx for explicit finite difference with forward differencing, 4.15 becomes,

$$\frac{\dot{N}_{i,j+1} - \dot{N}_{i,j}}{\Delta x} = A_x \frac{\sum r_{i,j}}{WH\Delta x} \qquad 4.16$$

$$\dot{N}_{i,j+1} = \dot{N}_{i,j} + \sum v_{i,j} r_{i,j} \qquad 4.17$$

Where $\nu_{i,j}$ and r_j are species i stoichiometric coefficient for reaction j and its rate respectively.

4.3.5 Energy balances

To determine the temperature distribution in the cell channels, thermal energy equations are used. In this model, energy balance is carried on five cell functional compartments, which include positrode and negatrode streams, their interconnects, and PEN. The associated energy transport mechanisms and sources are electrochemical reactions, heterogeneous reactions, convective energy transport, and gas-solid convection, respectively.

The energy balance for the fuel channel, which includes the convective heat transferred to the interconnects and PEN, enthalpy flux due to the electrochemical reaction, and the bulk flow enthalpy:

$$\rho_{F,ave}V_F CP_{F,ave}\frac{\partial T_F}{\partial t} = (\dot{E}_{in,F} - \dot{E}_{out,F}) + q^{conv}_{ICF,F}A_{conv} + q^{conv}_{ICF,F}A_{conv} + \dot{E}_{CO_2} - \dot{E}_{H_2O} - \dot{E}_{CH_4} \quad 4.18$$

Similar to the fuel channel, the energy balance for the steam channel is written as;

$$\rho_{S,ave}V_S CP_{S,ave}\frac{\partial T_S}{\partial t} = (\dot{E}_{in,A} - \dot{E}_{out,A}) + q^{conv}_{PEN,S}A_{conv} + q^{conv}_{ICS,S}A_{conv} + \dot{E}_{H_2O} - \dot{E}_{O_2} \quad 4.19$$

where $\dot{E}_i and\ q_{i,j}$ are given as:

$$\dot{E}_{React,i} = r_{Ox\,(or\,Red)}h_i(T = T_{PEN}, P = P_{cell}) \quad 4.20$$

$$where\ \ i = H_2, CH_4\ H_2O, O_2, CO_2$$

$$q_{i,j} = h_{conv}\left(T_i - T_j\right) \quad 4.21$$

where $h_{conv} = Convection\ heat\ transfer\ coefficient$

For the PEN, the energy balance, which includes convective heat transfer between the gas flows and the PEN; heat conduction, radiation heat transfer between PEN and interconnectors are given by;

$$\rho_{PEN,ave}V_{PEN}CP_{PEN,ave}\frac{\partial T_{PEN}}{\partial t} = \lambda\frac{\partial^2 T_{PEN}}{\partial x^2}V_{PEN} - q^{conv}_{PEN,F}A_{conv} - q^{conv}_{PEN,S}A_{conv} + q^{rad}_{PEN,ICS}A_{rad} + q^{rad}_{PEN,ICF}A_{rad} - \dot{E}_{CH_4} + \dot{E}_{H_2O} - \dot{E}_{O_2} + \dot{E}_{CO_2} \quad 4.22$$

For the interconnect, convective heat transfer with streams, internal heat conduction, and heat radiation to the PEN are considered for its energy balance. For both the steam side and fuel side interconnectors, respectively, it is given by;

$$\rho_{ICS,ave}V_{ICS}CP_{ICS,ave}\frac{\partial T_{ICS}}{\partial t} = \lambda\frac{\partial^2 T_{ICS}}{\partial x^2}V_{ICS}A_{Cond} - q^{conv}_{ICS,S}A_{conv} - q^{rad}_{PEN,ICS}A_{rad} \quad 4.23$$

$$\rho_{ICF,ave}V_{ICF}CP_{ICF,ave}\frac{\partial T_{ICF}}{\partial t} = \lambda\frac{\partial^2 T_{ICF}}{\partial x^2}V_{ICF}A_{cond} - q^{conv}_{ICF,A}A_{conv} - q^{rad}_{PEN,ICF}A_{rad} \quad 4.24$$

The governing equations for the PCEC model are summarized in Fig. 4.5

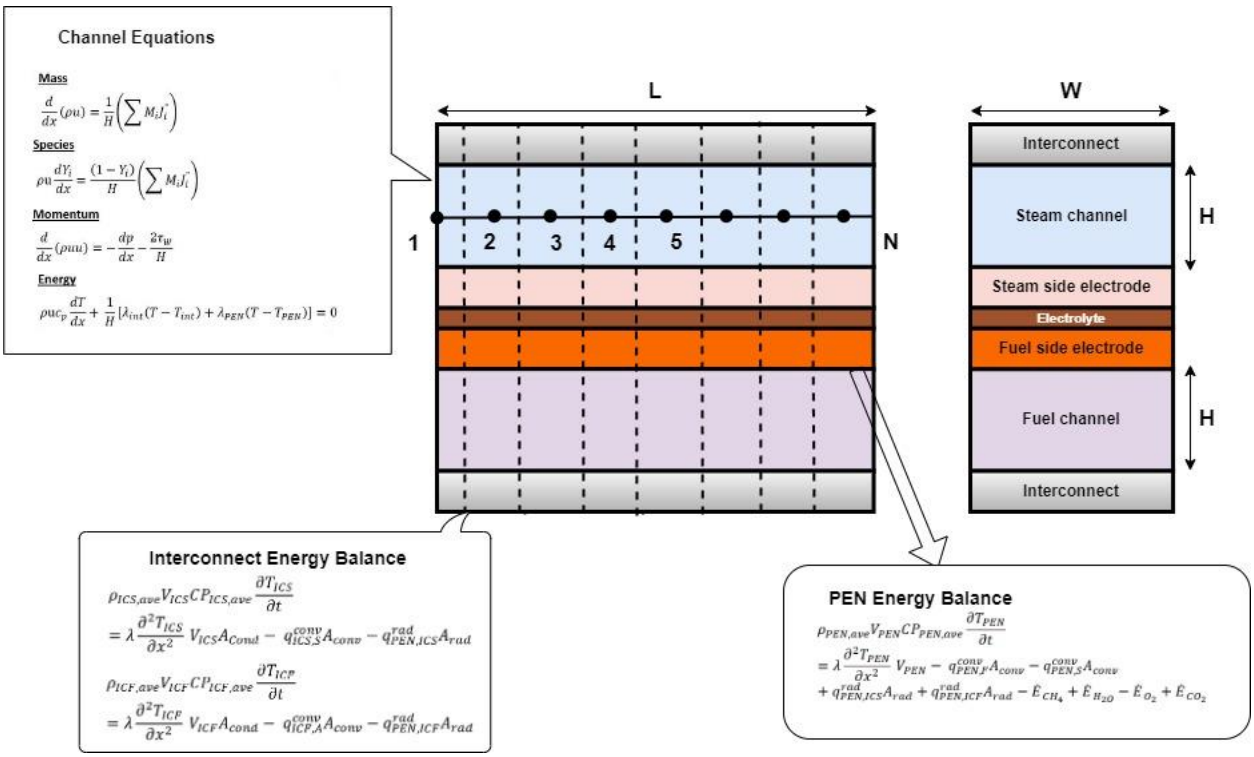

Fig. 4.5: PCEC model governing equations

4.3.6 Cell to stack model

The cell level model as described in chapter 3 is the fundamental model on which higher level models are built. The stack on the other hand houses several numbers of the cells. For a large-scale application, it is necessary assembling multiple cells for a stack-level modeling and design. However, to represent the performance of the cell-stack more accurately, additional layer of conditions and assumptions are required. For the stack design, other than the multiple cells, several other materials would be needed for its packaging which contribute to its performance. The compatibility between protonic-ceramic materials (Fig. 4.5a) and stack packaging components such as current collectors, metallic interconnects, glass-ceramic sealants, and gaskets is critical for the design and their assembling for its modeling. Considering the modeled stack is having several cells in array, a unit cell stack (Fig. 4.5b) has been used for model validation with some assumptions.

The following assumptions are made to for the cell to stack model.

1. The model is based on highly idealized operation.
2. It is carried out under isothermal condition.

3. No leak in stack package.
4. Minimal pressure loss across stack.
5. No contact resistance

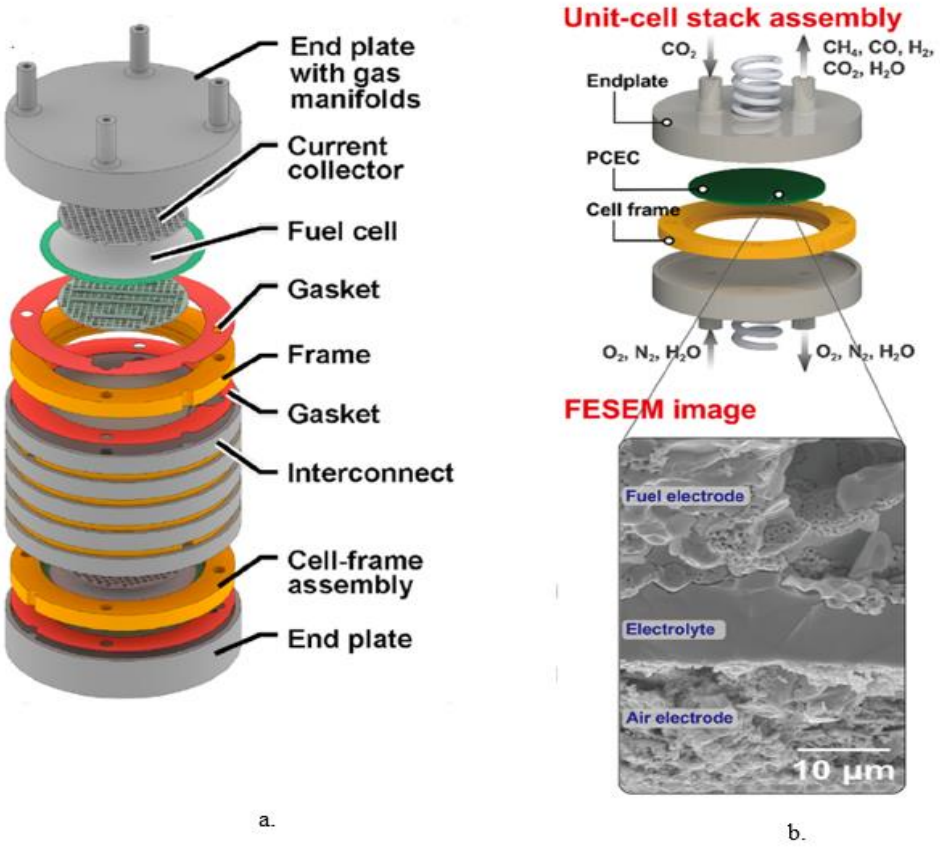

Fig. 4.6: Complete stack schematic for protonic ceramic electrochemical cells (a) The PCFC stack schematic with materials' labeling (b) Unit-cell stack assembly of the PCEC with Cross-sectional morphology of a freshly prepared and reduced PCEC [34, 126]

4.3.7 Definitions of parameters

This section describes some performance parameters that are peculiar to electrochemical cells and storage system, some of which are used in subsequent sections of this work.

4.3.7.1 Roundtrip efficiency

The efficiency of an energy storage RePCEC integrated system relies on two key factors:

a. the efficiency of the RePCEC (for both forward and backward operation) itself, and
b. the supplementary power needed for the balance of plant (BoP) components.

The roundtrip system efficiency, denoted as $\varepsilon_{\_RT,system}$, is defined and expressed as the ratio of the energy produced during the discharge of the system to the energy needed for charging the system.

This is calculated by dividing the net energy generated in PCFC mode by the total energy supplied in PCEC mode [28, 196] and given by,

$$\varepsilon_{RT,system} = \frac{E_{PCFC} - E_{BoP,PCFC}}{E_{PCEC} + E_{BoP,PCEC}} = \frac{V_{PCFC}Q_{PCFC} - E_{BoP,PCFC}}{V_{PCEC}Q_{PCEC} + E_{BoP,PCEC}} \qquad 4.25$$

Where V_{PCFC} and V_{PCEC} are the operating nominal cell voltages for the forward (PCFC) and backward (PCEC) operations of the integrated stack, $Q_{PCFC,}$ and Q_{PCEC} are the total charge transferred across the protonic ceramic electrolyte, and it is worth noting that the electrical energy term by the stack is E=QV. $E_{BoP,PCFC}$ and $E_{BoP,PCEC}$ are the total BoP energy required during PCFC and PCEC modes, respectively. The BoP supplementary power or energy encompasses the power losses from components like compressors, coolers power generated by heaters, and the energy introduced into the system through fuels or process streams.

As indicated by the definition in equation 4.24, to achieve a high roundtrip efficiency, there is a need to have a higher numerator and a lower denominator. Therefore, it is advantageous to run the system at a high cell voltage during PCFC mode and a low applied voltage during PCEC mode and run at low overpotentials. Additionally, it is essential to minimize the energy consumption associated with the BoP in both modes of operation. Defining efficiency in terms of energy rather than power is advantageous as it accommodates varying operating durations in SOFC and SOEC modes. Nevertheless, to ensure consistent and self-sustaining energy storage operation, the system must be cycled back to its initial state of charge; that is it must be recharged. After expending energy in PCFC mode, it should be able to return and operate in PCEC mode. The state of charge (SoC) is determined by the hydrogen equivalent of the gas stored for the PCFC operation, and it is directly related to the amount of charge transfer needed for the complete oxidation of the stored fuel. Therefore, to guarantee the repeatability of the operation, the total charge exchanged during the PCEC mode should match the charge exchanged when the system is discharged in SOFC mode. Such that Q_{PCFC} and Q_{PCEC} are equal. Neglecting the BoP energy from equation 4.24, another performance metric within the system can be obtained. Simplifying this equation gives the RePCEC stack roundtrip efficiency, $\varepsilon_{RT,stack}$ given as,

$$\varepsilon_{RT,stack} = \frac{V_{PCFC}Q_{PCFC} - E_{BoP,PCFC}}{V_{PCEC}Q_{PCEC} + E_{BoP,PCEC}} \quad 4.26$$

0

$$\varepsilon_{RT,stack} = \frac{V_{PCFC}Q_{PCFC}}{V_{PCEC}Q_{PCEC}} \quad , Q_{PCFC} = Q_{PCEC} \quad 4.27$$

$$\varepsilon_{RT,stack} = \frac{V_{PCFC}}{V_{PCEC}} \quad 4.28$$

The RePCEC stack roundtrip efficiency is a valuable metric for assessing system performance as it quantifies the efficiency implications of both the RePCEC stack and the BoP components separately.

4.3.7.2 Fuel Utilization

The fuel utilization (FU) measures the portion of the reactant supplied to the stack that undergoes electrochemical conversion. In the case of a reversible system, it is also valuable to assess utilization in the context of oxygen transport across the electrolyte. Therefore, FU parameters are employed to establish mathematical relationships between the "fuel" and "exhaust" compositions.

In fuel cell mode, FU or U_F is determined by the ratio of the molar rate of electrochemical fuel (e.g H_2, CH_4, etc) consumption to the corresponding molar flow of fuel provided to the fuel channel of the PCFC stack. This is written as,

$$U_F = \frac{N_{CH_4,consumed}}{\left(N_{CH_4} + N_{H_2} + N_{CO_x} + H_2O\right)_{PCFC,inlet}} \quad 4.29$$

where Ni is the molar flow of species i and $N_{CH4,consumed}$ is the molar rate of methane consumed in the PCFC fuel electrode. On the other side, for electrolysis operation, reactant utilization, RU or U_R can be expressed as the ratio of the CO_2 consumed at the cathode to the total CO_2 content within the reactant species entering the fuel channel. This is given as,

$$U_R = \frac{N_{CO_2,consumed}}{\left(N_{CO_2} + N_{CO_x} + H_2O\right)_{PCEC,inlet}} \quad 4.30$$

In a co-electrolysis reaction, the steam utilization is evaluated separately in the same format. Since this is a reversible reaction, both equations 4.28 and 4.29 influence themselves as the amount of reactant conversion in one direction determines the amount of fuel in the other direction.

4.3.7.3 Faradaic efficiency

Faradaic efficiency (FE) is a measure of the efficiency of an electrochemical process in converting electrical energy into chemical energy or vice versa. It describes the overall selectivity of an electrochemical process and is defined as the amount (moles) of collected product relative to the amount that could be produced from the total charge passed [198]. Faradaic efficiency is typically expressed as a fraction or percentage and provides insight into how effectively the desired electrochemical reactions occur within a system.

For example, in the context of a fuel cell or an electrolyzer, the Faradaic efficiency measures the extent to which electrical energy is converted into the chemical energy of the desired products. A high Faradaic efficiency indicates that a significant portion of the electrical current is used for the intended chemical reactions. In contrast, a lower Faradaic efficiency suggests that some of the current may be lost to side reactions or other forms of energy loss. Faradaic efficiency measurements are of particular significance for reactions like carbon dioxide reduction reaction (CO_2RR) and nitrogen reduction reaction (N_2RR), where it is not possible to exclude the competing Hydrogen Evolution Reaction (HER) based solely on thermodynamic considerations. Faradaic efficiency is crucial in evaluating the performance of electrochemical devices, as it helps determine the overall effectiveness of the system in converting energy. It is an important parameter when assessing the feasibility and sustainability of electrochemical technologies, especially in applications related to energy storage, fuel production, and emissions reduction. The FE can be given as,

$$FE = \frac{n * F * concentration}{Current * Time} \qquad 4.31$$

In a continuous mode,

$$FE = \frac{n * F * Xi * molar\ flow\ rate}{Current} \qquad 4.31$$

Where n, F are the number of electrons transferred and the Faraday constant, respectively. X_i is the mole fraction, which is ppm times 10^6 for gases. Details on simplification for gases can be obtained in the ref. [199].

4.3.7.4 Thermoneutral voltage

A very crucial parameter for electrochemical cells that is used for the determination of the theoretical operation point at thermal equilibrium in the system is known as the thermoneutral voltage, E_{tn}. This is described as the voltage at which there is no exchange of heat with the environment i.e. all the thermal energy needed for the steam electrolysis is mainly gotten from the heat of reactions within the cell or only from the electrical energy input. It is generally given as;

$$E_{tn} = \frac{\Delta H_R}{nF} \qquad 4.32$$

Here ΔH= lower heating value of hydrogen, n= number of electrons involved in the overall reaction F= Faraday's constant

For pure steam electrolysis, the thermoneutral voltage was estimated to be [200];

$E_{tn} = \frac{\Delta H_R}{2F} \approx 1.287$ V at 800 ºC

Where ΔH_R= enthalpy of steam reduction

Three different cases are possible with these potentials and the occurrence of the electrolysis reaction [201];

Case 1: When $E^0 > E_{cell}$, this reaction will not occur.

Case 2: When $E_{tn} > E_{cell} > E^0$, this is an endothermic operation- the reaction takes place with an external heat requirement to maintain an isothermal operation.

Case 3: When $E_{cell} > E_{tn}$, this is an exothermic operation, excess heat not needed for the reaction will be generated due to irreversibiltes and its removal is required for isothermal operation.

Where E^0 = standard electromotive force (EMF), the reference open-cell potential given by

$$E^0 = \frac{\Delta G_R}{nF} \qquad 4.33$$

And ΔG_R is the Gibb's energy of reaction.

In general, electrolysis reaction releases heat when operated above the thermoneutral voltage and absorbs heat when operated below it. With the cell stack operating near or at the thermoneutral voltage has the tendency to streamline the thermal management of the stack, as it minimizes both external heat inputs and thermal stresses at this voltage [169, 200].

However, when the reactant is not a pure compound as shown for pure steam, most especially with gas species containing carbon are introduced to the cell feed gases, dealing with the thermal behavior becomes increasingly difficult. For example, in the co-electrolysis of H_2O and CO_2 in this work, with several reactions like the methanation, reversible water-gas shift (RWGS) and

water electrolysis reactions, the total heat of reaction will be different depending on selectivity, yield ratio or the extent of reaction. A fixed isothermal assumption would mean a constraint on the reaction and local temperatures. But in reality, there is tendency for temperature gradient within the system. Noting that the thermoneutral voltage, E_{tn}, exhibits only slight sensitivity to variations in temperature (+5 mV /200℃). For this work, it is assumed that the thermoneutral voltage is the voltage when the temperature difference between the stack inlet and outlet temperatures is less than 25℃.

4.3.8 Stack validation

The stack model for the RePCEC is calibrated and validated using the experimental results from Pan et al. [94]. This is the only work on the co-electrolysis of CO_2 and H_2O using PCEC, and it is co-authored with our collaborator [94]. The cell is validated for 5 cm^2 unit stack PCEC with BCZYYb electrolyte (almost 8μm) and 60 wt % NiO and 40 wt% BCZYYb fuel electrode (about 0.8mm) composition. The air electrode composition is 80 wt% BCFZY and 20 wt% BCZYYb; details about the materials and their geometries are discussed in chapter three of this dissertation. Table 4.1 shows the calibration and validation parameters. The validation is carried out individually on both modalities, as shown in Fig. 4.6a and b. In all cases, it is assumed that there is adequate sealing of the stack and no significant gas leakage to minimize the resistance losses. In the experimental test at these temperatures, methane is directly fueled into the PCFC using a fuel mixture of CH_4, steam, and N_2 with flow rates 20, 67 and 80 sccm, respectively. This composition resulted in a steam-to-carbon ratio of 3.35. A high N_2 flow rate is supplied to lower the concentration of steam and mitigate its flow rate fluctuations. However, it is anticipated this might reduce the performance of the cell due to the dilution effect caused by the excess of non-reactive nitrogen gas. Fig. 4.6a shows the PCFC operation polarization curve for comparing the experimental results with the model results at different temperatures 400-550 ℃. Here, the cathode composition is made up of 10% H_2O and 90% O_2 and the anode composition is 12% CH_4, 48% N_2, and 40% steam. The model exhibits high degree of precision and minimal error across a wide range of current densities, and the stack voltage takes into account all the significant types of polarizations and overpotentials, the ohmic, concentration, and activation overpotential.

Likewise, Fig 4.6b shows the PCEC mode operation polarization curves comparing this model and experimental results. It was reported that the operating temperature range for efficient operation

of the PCEC is from 400-600℃ [29], however, the experimental work uses temperatures 400-550℃. As depicted in Fig. 4.6b, there is a non-linear increase in the operating voltage from 1.3 to 1.5 V as the current density increases from -4000 to -10000 Am^{-2} at 500 ℃ as expected. The same trend is observed in the empirical data and the model prediction at other temperatures as shown in the figure. Due to the intricacy and the complexity of the co-electrolysis reaction in the PCEC, the empirical study supplies the fuel electrode with is a gas mixture of CO_2 and N_2, without H_2. Thus, the reducing environment during the operation is only maintained by the H_2 produced from the electrolysis process at the steam electrode. Therefore, to avoid possible oxidation of the Ni catalyst and maintain continuous co-electrolysis reaction due to limiting reactant, the minimum current density during the test was set as 4000 A/m^2. However, due to the versatility of the model we are able to predict a situation where the nickel catalyst is not oxidized or an alternative non-oxidizable catalyst of similar activity is used. Consequently, we extend the polarization curves to a current density of 0 A/m^2 at 500℃ shown in Fig. 4.7 to address the open-circuit voltage (OCV) for both modalities. A correlation between the experimental results and this model as depicted in Fig. 4.6a shows the degree of precision in the model. At all temperatures and current densities, the maximum error observed in the model compared to the experimental results is 2% which can be statistically considered as accurate most especially in the electrochemical community.

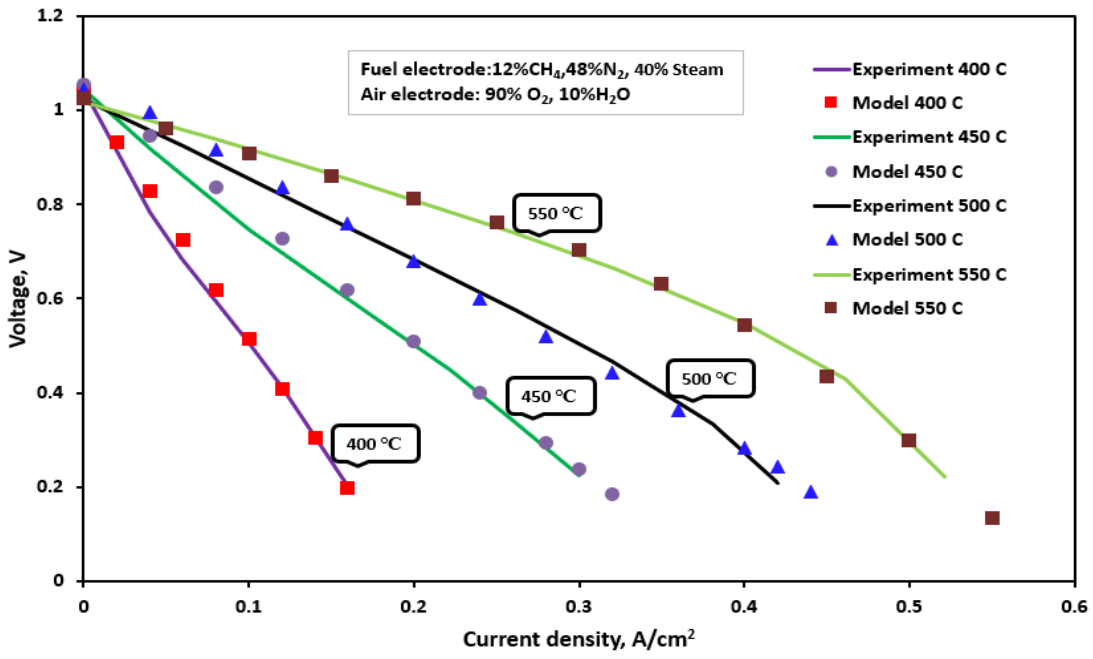

(a)

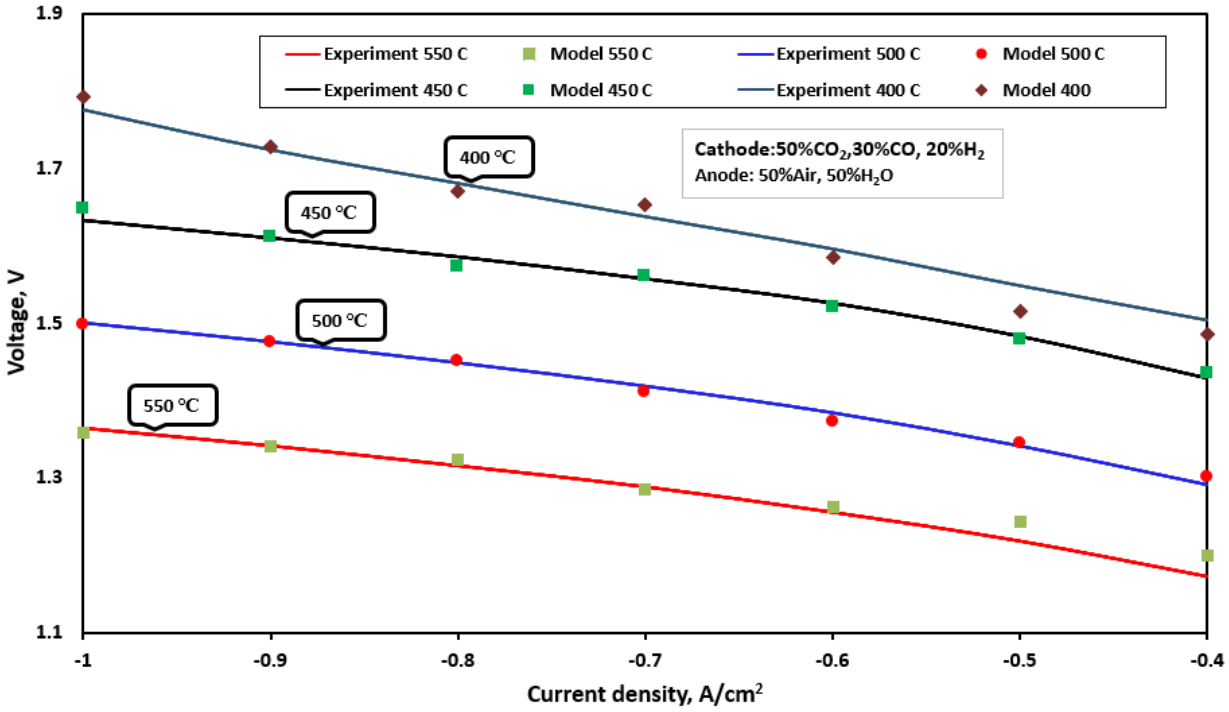

(b)

Fig. 4.7: PCFC stack validation I-V curve and Polarization curve (a) PCFC (b) PCEC

Table 4.1: PCEC model parameters [137, 169, 170]

Geometry parameters	
Positrode thickness (m)	30×10^{-6}
Negatrode thickness (m)	64×10^{-6}
Electrolyte thickness (m)	15×10^{-6}
Interconnector thickness (m)	0.19×10^{-3}
Cell active area (width × height) (mm^2)	80 × 80
Channel height, fuel side (m)	1.09×10^{-3}
Channel height, sweep gas side (m)	1.09×10^{-3}
Channel width, fuel side (m)	2×10^{-3a}
Flow configuration	Co-flow
Material properties	
Conductivity of PEN ($W\ m^{-1}\ K^{-1}$)	2.16

Conductivity of interconnector (W m^{-1} K^{-1})	27
Interconnector specific resistivity (Ω m)	1.176×10^{-4}
Negatrode specific resistivity (Ω m)	8.856×10^{-6}
Electrolyte specific resistivity (Ω m)	$1.07 \times 10^{-4} \exp(7237/T_{PEN})$
Positrode specific resistivity (Ω m)	1.425×10^{-4}
Diffusion polarization	
Pore diameter of positrode (m)	1×10^{-6}
Pore diameter of negatrode (m)	1×10^{-6}
Porosity of negatrode	0.4
Porosity of positrode	0.4
Tortuosity of positrode	3.0
Tortuosity of negatrode	3.0
Operating conditions	
Pressure (Pa)	101,325 (atmospheric pressure)
Average current density (A m^{-2})	0–10000
Temperature (°C)	450–600

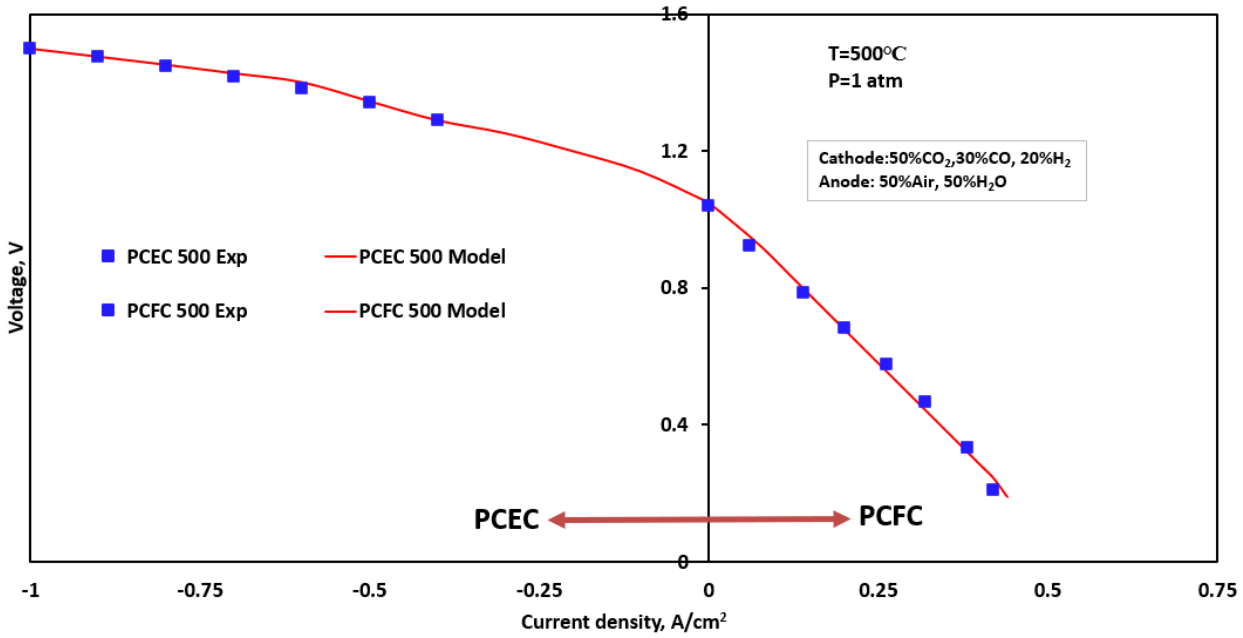

Fig. 4.8: The reversible operation of RePCEC

The stack model is used to predict the operation of the cell in PCFC mode with a different fuel composition and temperatures as shown in Fig. 4.8. The polarization characteristics curves as different temperatures shows that the power density increases with temperature. The peak operating power density for co-electrolysis of CO_2 and H_2O is 0.22 W/cm^2 at 0.63 V and 550 ℃ which is similar to what is reported by Pan et al [94]. This performance is superior to the reported power density of 0.18 W/cm^2 at 0.8 V and 600 ℃ by Kyle et al [67] which reveal a developmental progress in the PCFC design and its materials. The power densities at other temperatures 500, 450 and 400 ℃ are 0.144, 0.1 and 0.05 W/cm^2 respectively.

With thermoneutral voltage being the voltage when the temperature difference between the stack inlet and outlet temperatures is less than 25℃. The model estimates the thermoneutral voltage to be approximately to be 1.19V. Additionally, the temperature variation across the cell and stack at 500℃, 0.2 A/cm^2 with species molar ratio of 45% Air, 35% CO_2, 10%H_2 and 10% CO are shown in Fig. 4.9a. It is obvious from the figure that there is an initial sharp rise in cell temperature at the beginning of the channel which subsided towards the end of the cell channels, and it becomes flat and stable. This can be rooted to the endothermicity of the water electrolysis reaction in the cell which must be firstly initiated for the methanation reaction (exothermic) to occur and presumed to be the dominating and controlling reaction. Figs. 4.9b and c show number of mole variations across

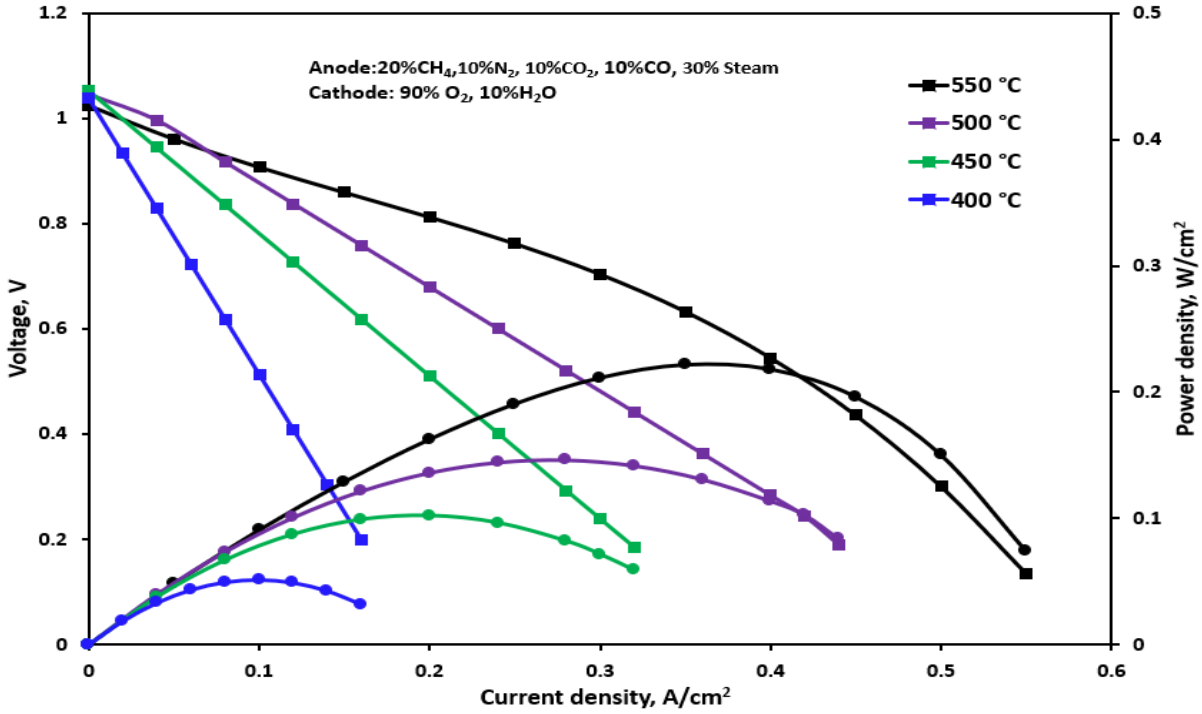

Fig. 4.9:The I-V and P-V curves of the PCFC stack from the model

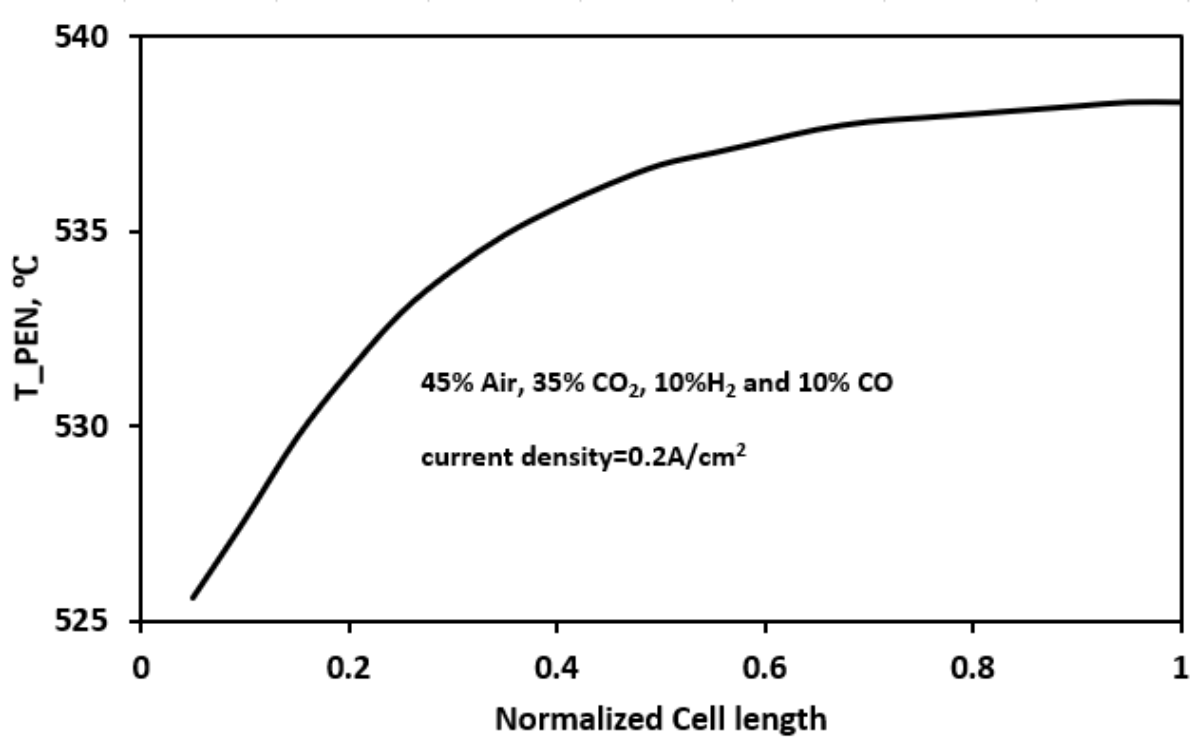

(a)

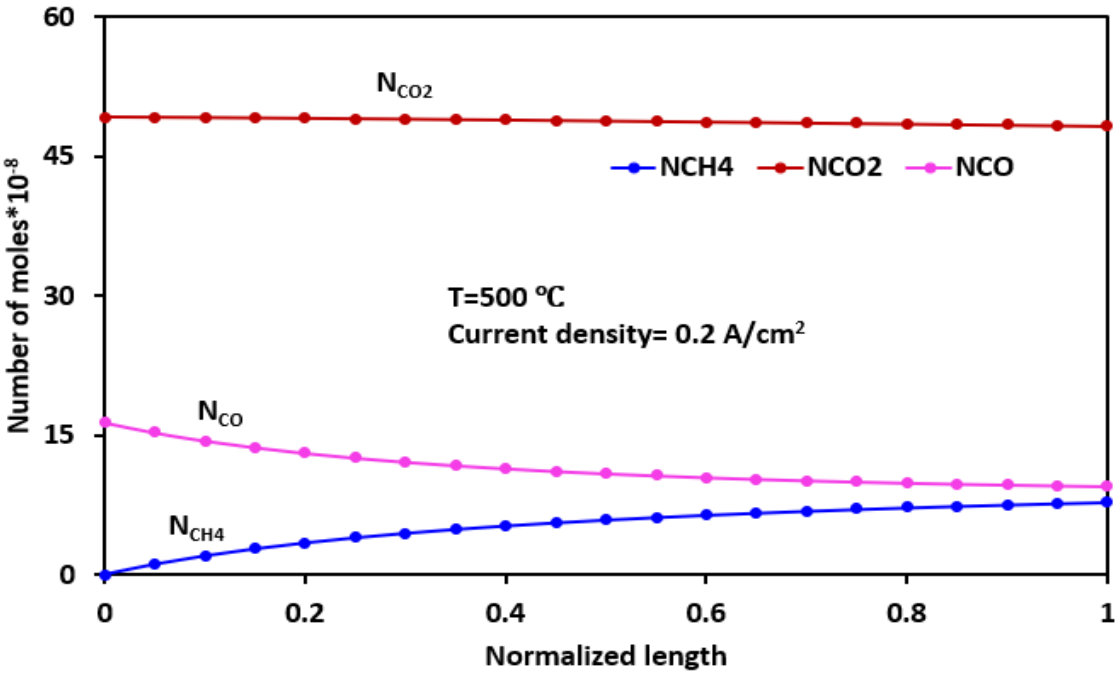

(b)

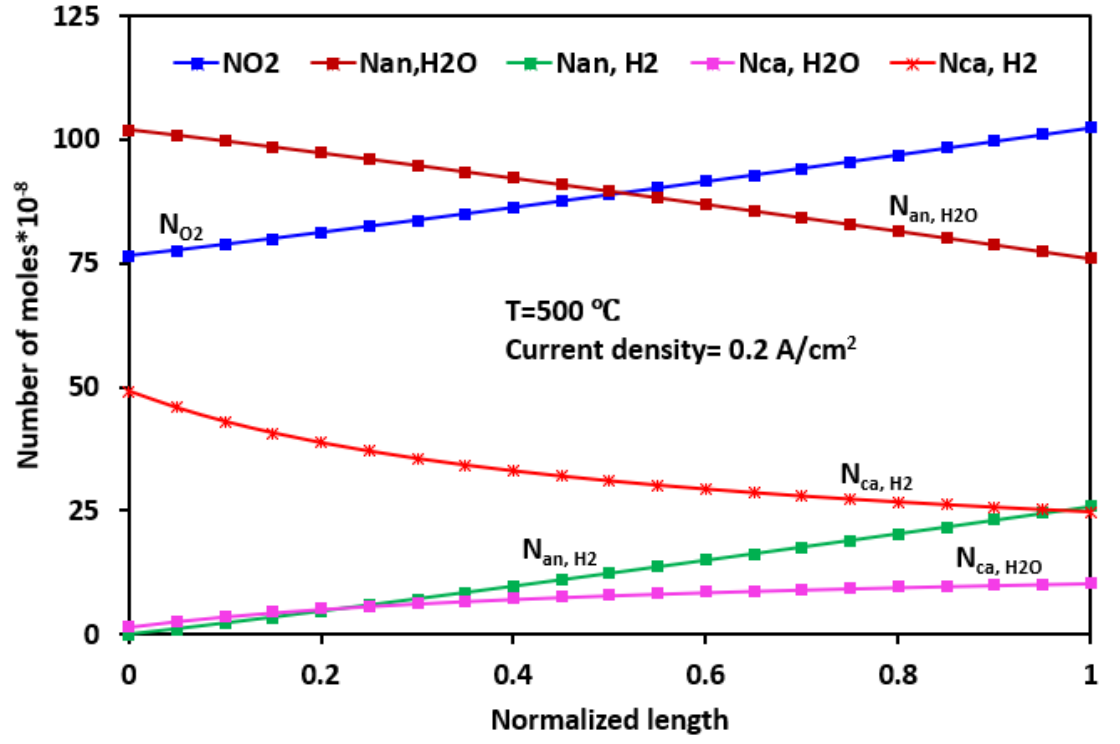

(c)

Fig. 4.10: Parameter variations across the unit stack during co-electrolysis of H_2O and CO_2 (a) Temperature (b) species (CO_2, CO and CH_4) number of moles (c) species (H_2O, O_2 and H_2) number of moles

the channel at 500°C, 0.2 A/cm^2. In Fig. 4.9b, the declining curve of CO shows the decrease in in its number of moles across the channel, this indicates CO rate of consumption. This is higher compared to CO_2 rate of consumption as evident in its slightly declining curve, this perhaps due to CO_2 stability. This shows that the affinity of CO for the proton ion is higher compared to CO_2. It suggests that CO_2 utilization during CO_2 and H_2O co-electrolysis is enhanced in the absence of CO. Fig. 4.9c shows the decline in number of moles of the H_2O as evidence of its decomposition and consumption for water electrolysis reaction along the channel. This is reflective in the sharp rise in number of moles of the O_2 and the H_2 produced at the anode. Likewise, Fig. 4.9c shows there is a sharp decline in the cathodic H_2 consumption for methane production at the beginning of the channel and almost steady at the remaining channel length. This is signifying that the methanation reaction is fast at the beginning and becomes slow at the middle of the channel. The anodic H_2 production (proton ion generation) that moves across the electrolyte to the cathode is slow at the beginning and becomes faster compared to its utilization for methanation after the one-third of the channel length.

4.4 System models

A literature review shows that there are different ways of categorizing electrochemical models. Based on its geometric dimension and simulation purpose [202, 203]. The geometric classification can be a zero-dimension (0D), 1D, 2D and three-dimension (3D) model. The grey-box model is adopted in the modeling of the PCEC stack in this work for its performance prediction as a large-scale storage system is required. The modeled stack is validated using a unit cell stack as previously mentioned. However, the stack system houses numerous cells of the PCEC, which comprise the cells as described in chapter three and re-iterated in section 4.3.

After detailed calibration and validation of the stack model, this is model is integrated into a larger and detailed process system model. The integrated system model is expected to evaluate the RePCEC stack efficiency, voltage and output conditions at various given input parameters. While other stack model and design is still valid, the system model implemented in this dissertation using Aspen HYSY. Within the Aspen HYSYS, the balance of plant (BoP) components are modeled using mass balance and thermodynamic equations, incorporating energy and entropy balances. The BoP components include tank storages (fuel and exhaust), compressor, mixer, heater, evaporator, blower, heat exchanger, electrostatic precipitator, separator, pump, two-stage membrane-based

carbon capture system (TSMB CCS) and the wastewater treatment and recovery unit (WTRU). Further discussion on each of them is given in section 4.4.2. A very crucial aspect of the system design involves the integration of the heat exchange network (HEN) among these system components. The selected minimum pinch temperature across all components is 10 ℃ for an energy efficient HEN in the system. The following assumptions are made for the system model simplification.

4.4.1 System model assumptions

The flow distribution of fluids are uniform, and other assumptions similar to that of ref. [169] is adopted with slight additions, and they are as follows:

(1) All gases are ideal gases

(2) Steady state condition is considered

(3) Parameter evaluation at a given temperature

(4) Uniformly distributed cell temperature.

(5) The electrolysis reaction is at a constant pressure i.e no pressure loss across the stack.

(6) No side or reverse reaction of species

(7) Lumped temperature of the solid cell structure

(8) Adiabatic boundaries at the stack ends

(9) Other fluids in the system are assumed to be Newtonian

The system model is made up of several balance of plant (BoP) components in addition to the PCEC reactor and detailed about the BoP is discussed in the following section

4.4.2 Balance of Plant components

4.4.2.1 Condenser (Cooler) and Evaporator

The condenser is modeled to fulfill the goal of complete water vapor condensation from the flue gas continuously. It is of different types, and the used in this work is modeled based on shell and coil condenser. The fluid inflow is used by Aspen HYSYS for the estimation of the removed heat since the target temperature is known and is given as

$$Q = mC_{p,avg}\Delta T \qquad 4.34$$

Where Q is the rate of heat removal from the condenser in kJ/h and m is the flue gas mass flow rate in kg/h and ΔT is the change in the inlet and output temperature. The $C_{p,avg}$ is average specific

heat of the flue gas due to its constituent. The evaporator is modeled similarly to the condenser, but it has only one flow specie, so the $C_{p,avg}$ becomes C_p.

4.4.2.2 Heater and Heat Exchanger

The heater is modeled similar to the cooler above, and two of it is used in this study, steam and air pre-heaters. Aspen HYSYS performs two-sided mass and energy balances in the heat exchanger, and it is used for water boilers. A single shell and tube heat exchanger used in this work is modeled at a steady-state using the Log Mean Temperature Difference (LMTD) method to solve its thermo-hydraulic performance analytically. This method is suitable for our case as the target temperature is known, Kay and Nedderman [204] detailed the LMTD method.

4.4.2.3 Compressor and Pump

In our system, a centrifugal pump and compressor are typically modeled using the power to drive the pump and operate the compressor at predefined adiabatic and isentropic efficiencies respectively. This power is given by

$$P_i = \frac{\rho g V H}{\eta} \qquad 4.35$$

Where P_i is the power in kW, ρ is the fluid (water for pump and air for the compressor) density in kg/m^3, g is the acceleration due to gravity m/s^2, V is the fluid flow rate m^3/s and H is energy head in m and is the sum of all losses due to bends in pipes or valves, friction, and static lift.

4.4.2.4 Mixer

The mixer is modeled as a three-way pipe connector. A fixed length of 1m and 0.05m diameter is assumed, and the model was built basically on the mass balance as below

$$M_o = M_{i,1} + M_{i,2} \qquad 4.36$$

And M_o is the output mass flow rate in kg/h, $M_{i,1} and M_{i,2}$ are the inlet mass flow rates.

The energy balance is typical of equation 4.36 for the mass balance and given as

$$E_o = E_{i,1} + E_{i,2} \qquad 4.37$$

Where E_o is the output energy flow rate in kJ/h, $E_{i,1} and E_{i,2}$ are the inlet energy flow rates

4.4.2.5 Water Treatment and Recovery Unit (WTRU)-Evaporator

This is modeled as an evaporator to generate high pressurized steam, see section **4.4.2.**1. This has been assumed for simplicity since the feedstock needed by the PCEC is steam which does not require high level of purity as required in alkaline and proton electrolyte membrane electrolyzers. It is assumed that the wastewater has passed through the primary treatment which makes eveaporation easier. This approach is of economic benefits since it cheapest of the levels wastewater treatment when compared to secondary and tertiary treatment [205].

4.4.2.6 Separator

The separator is used to remove liquid water from the condensed flue gas stream that enters into it from the cooler, it is modeled like a cylindrical pressurized vessel equipped with a mist extractor. At a steady-state, the vessel is maintained at atmospheric pressure, and its contents are split into its vapor and liquid constituents. The design procedure mentioned in the GPSA data book [206] is used for the main vessel and the gas outlet nozzle [207].

4.4.2.7 Tank storage

The tanks in the system are modeled as straightforward sources and sinks with properties that remain constant since steady-state is considered in this work. At steady-state and isothermal condition, the tank volume is given as [208];

$$V_{tank} = \frac{v(T,p_{max}) * N_{evacuation} t_{evacuation}}{1 - \frac{v(T,p_{max})}{v(T,p_{min})}} \qquad 4.38$$

Where v(T; p) represents the molar specific volume calculated at temperature, T and pressure,p. $t_{evacuation}$ and $N_{evacuation}$ denote the duration and molar flow during tank discharging, T signifies the tank temperature, and p_i corresponds to either the maximum or minimum tank pressure.

4.4.2.8 Electrostatic precipitator (ESP)

The ESP uses electrostatic forces to remove fine and suspended particles from gas streams like air, dust, smoke and flue gas. The ESP is very selective as it applies energy only to the particulate matters causing minimum obstruction to the flow of gases through the unit. The modeling of the ESP is simplified by relating the induced electrostatic force, F to the mass, m of the collected particles using Newton's law,

$$F = ma \qquad 4.39$$

Where the electrostatic force, F can be obtained from the two electrodes using the common Coulomb's law of electric force and a is the acceleration of particles in the direction of force. An attracting characteristic property of the ESP is its low pressure drop which is usually in the range 0.001-0.01 bar, the model implementation is built around it.

4.4.3 Thermodynamics

Aspen HYSYS is used for the system model, and it is heavily dependent on for the thermodynamic calculations based on the selected equipment. Thus, its thermodynamic model for a component predicts outlet composition and temperature by assuming that thermodynamic equilibrium has been reached. The equilibrium state is calculated at the specified temperature of the selected components and reactors especially Gibbs reactor which is extensively used as representative PCEC stack reactor incorporated with the stack model discussed. This equilibrium calculation is derived through a routine that minimizes Gibbs energy. At the outlets, the gas components which include, CO_2, H_2O, CH_4, H_2, CO, O_2 and N_2 are taken into account in all cases. The outlet temperature of every component in the system is determined by solving the overall energy and mass balances according to the equations adopted by the selected package in Aspen HYSY, taking into consideration adiabatic conditions. Inlet conditions are either input parameters or derived from the output of the preceding system component. Initial temperature into the stack and current density are specified input variables.

4.4.4 System description

There are different configurations for the integrated system, nevertheless the base configuration is described in this section. Other configurations will be discussed in section 4.5. The process flow diagram for the integrated system for hydrogen production is shown in Fig. 4.10. The system is based on RePCEC connected to two different sources of high pressurized steam (HPS) and CO_2 from power plant aimed at being integrated into the grid. In this process, 500 m^3/s flue gas from combined cycle power plant with 600 MW total capacity is passed through an electrostatic precipitator to remove the particulate matters with insignificant pressure loss. The outlet from the precipitator is sent to the water removal. Other flue gas composition (CO_2, N_2, O_2) is stored in the exhaust tank and passed through the heater to increase its temperature to the PCEC cathode inlet

temperatures of 400-550℃. Likewise, water from a wastewater/ freshwater reservoir at ambient temperature and atmospheric pressure is pumped to the water treatment and recovery unit (WTRU) at a pressure of 250kpa with the goal of evaporating it to generate steam. The recovered water from the flue gas is pumped to a heat exchanger where it is superheated and evaporated for high pressurized steam generation, and the HPS here is mixed with that obtained from the WTRU. The mixed HPS stream is stored in the exhaust tank and enters the PCEC stack anode after passing a pre-heater where it is heated to the inlet temperature range of 400-550 ºC. This lower the required entropic heat to decompose the steam endothermically when compared to the liquid water [209] and as a result reduces power consumption [210]. The heater is designed to utilize waste heat from the PCEC's product lines, leaving the system considering that a larger percentage of the heat added to the feed stream is retained in the exit gas stream. Waste heat from external sources also works suitably with the heater. The heat integration recuperation is carried out such that the heat from the stored gases in both the exhaust and fuel tanks are used by the heaters and heat exchanger at the stack inlets and outlets respectively. Likewise, the heat removed from the flue gas is used by the WTRU, water heater and evaporator as the case may be. Air from the ambient environment is compressed, preheated, and supplied to the system to flush out the produced oxygen from the electrolysis reactions in the PCEC. This also serves as a medium for carrying heat into the stack to meet the boundary conditions, and the streams exit the stack. An external source of heat ($T\Delta S$) is essential as it reduces the required electricity per volume of hydrogen gas produced compared to other electrolyzer technologies [165]. The change from liquid water to steam electrolysis enhances an appreciable drop in the demand for electricity followed by a steady decrease with increasing temperature [209]. This is due to its operation at a high temperature which is kinetically and thermodynamically favorable for the reaction. For the thermodynamic advantage, there is a drop in the molar Gibbs energy of the reaction as the temperature increases and the molar enthalpy remains virtually constant. Therefore, the external source would be supplying a significant part of the energy required for the electrolysis reaction at the anode. The cathodic reaction requires less heat which balance up for the heat needed at the anode. The exiting gases at the anode and cathode is then passed into the stack again after reversing polarity to supply cathode and anode respectively for the PCFC operation for electricity generation. Analysing this base case system modeling via steady-state computational techniques using a physically designed RePCEC stack model and

thermodynamic models for the BoP components gives some insight into the determining the favorable configurations and operating conditions.

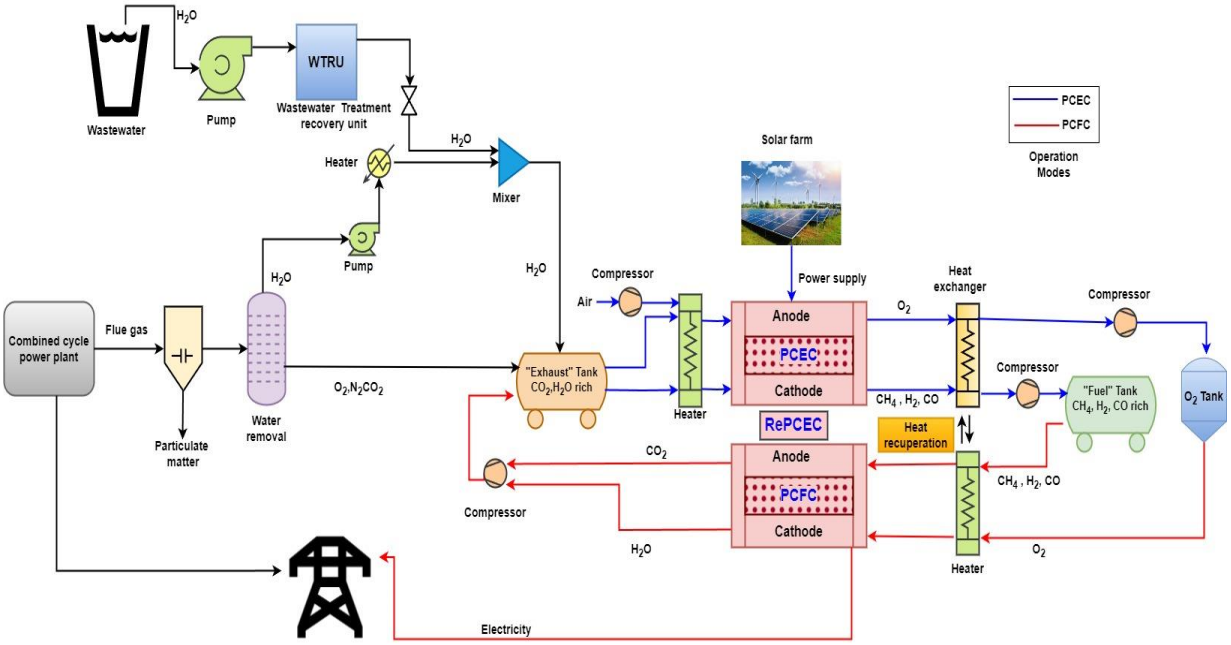

Fig. 4.11: The RePCEC integrated system for co-electrolysis of CO_2 and H_2O (base case, BC)

The operating conditions considered for this base case is detailed in section 4.6 and Table 4.2. In this case, reactants from the flue gas are stored in tanks and are kept at an elevated temperature to sustain the vapor phase of stored reactants most especially water with highest boiling point. The feedstock stored in tank for the stack operation is highlighted in Table 4.2

Table 4.2: Feedstock for base case 1 without CCS

Base case 1- without CCS					
		131000	kmol/hr	kmol/hr	Fraction
Exhaust flow, ton/hr	3706.56 ton/hr	kmol/hr	To anode	To cathode	Cathode
O_2 mol%	12.4	16244		16244	0.136
CO_2 mol%	3.9	5109		5109	0.043
H_2O mol%	8.5	11135	11135		0
N_2 mol%	74.3	97333		98512	0.821
Ar mol%	0.9	1179			0
		131000	11135	119865	1

The results show that the percentage conversion of CO_2 is 55.7%. The rate of methane production, its percentage production and its selectivity are 1795 kmol/h, 35.9% and 62.6% respectively. The stack and system roundtrip efficiencies for this base case are 65.18% and 42.79% respectively, suggesting that there is a notable decrease in efficiency due to the BoP energy consumption for the process. This higher energy can also be traced to the huge volume of non-participating gases like nitrogen from the flue gas that needs to be heated and passed across the components along with the participating gas like CO_2. The exhaust tank requires higher energy to maintain its isothermicity with this quantity of gases in the PCEC mode. Another challenge with the tank in the PCEC mode is the required tank volume to contain the exhaust from the flue gas. The gases from the powerplant and steam are at higher temperatures compared to the tank storing temperature which can be explored to reduce the energy consumption by the BoP. The fuel tank experiences similar unnecessary storage of the inert gas during operation as its content is dependent on what the exhaust tank is passing to the stack. Depending the on the grid energy demand and storage time before utilization, conducting a more detailed analysis with increased accuracy is essential to investigate the transient effects of the storage tanks (particulary the exhaust tank), considering specified tank geometry and materials. This is necessary to finalize this aspect of the system design. However, applying some cleaning equipment and reconfiguring this base case might give better stack and system efficiencies and performances.

4.5 Configurations

The aim in this section is to assess the technical performance of stand-alone reversible protonic ceramic electrochemical cell systems, with the goal of identifying the optimal system configurations and operational conditions for use in a large-scale energy storage application. This goal is accomplished by utilizing steady-state computational modeling to simulate the roundtrip operation of a RePCEC system. The simulation involves calibration and validation of a physically-based RePCEC stack model as previously discussed in section 4.3 and thermodynamic models for system components as mentioned in section 4.4.3. As previously mentioned, there are different configurations for the integrated system which influence the overall and PCEC stack efficiency. This ranges from the input feed generation from the BoP configuration and returning of the products from the downstream back into the stack. Following the base case discussed in section 4.4.4, this system is without a carbon capture system. It can be observed in this base case that the feedstock to the fuel channel has only 4.3 mol% CO_2 which is one of the primary reactants. Having

a system that can remove higher percentage of the CO_2 might improve the system both technically and economically. In the work by Asadi and Kazempoor [211], the designed two-staged membrane carbon capture system (TSMCCS) with relatively cheap cost of CO_2 capture of 27.35 \$/tCO_2. From their study, the retentate having higher concentration of the inactive gases exit at higher pressure and can replace the compressed air in the base case without carbon capture system (CCS). There is dual economic benefit of this, reduction in both capital and operating costs. The capital cost saves from none-procurement of compressor. Likewise, the operating cost saves from the compressor operational cost and energy required to keep these inert gases at the stack and BoP components operating temperatures. However, an extra tank is required to store them. This seems milder as the needed quantity might be stored and put the remain for an immediate use. Adding a carbon capture system to this base configuration gives a new one shown in Fig. 4.11. The system here is based on RePCEC connected to two different sources of high pressurized steam (HPS) and CO_2 from two-staged membrane carbon capture system (TSMCCS) integrated into the grid and renewable energy sources. In this case, higher mol% of the CO_2 captured from the power plant goes to the cathode side of the stack with O_2 and N_2 serving as sweep gas. While there are several runs and powerplant loading carried out for CCS, 100% loading is used in this case. The results of the CCS operational runs with their permeate and retentate are given in section 4.9. The permeate outcome from the CCS which serves as the stack feedstock is highlighted in Table 4.3. Additional steam is added to the one from the previously removed water and the WTRU is added to the one from the permeate as the anodic feedstock.

From Table 4.3, the mol% of CO_2 fed into the stack is over 60% unlike the base case with just 4.3%. Running the system under this condition results in the percentage conversion of CO_2 of 73.3%. The rate of methane production, its percentage production and selectivity are 3100.6 kmol/h, 62.01% and 92.27% respectively. The stack and system roundtrip efficiencies for this base case are 72.1% and 51.37% respectively. While all the performance metric parameters are higher with the CCS system, the overall system efficiency is low. This typically shows the influence of the BoP energy requirement on the overall system efficiency as the additional energy demand by the CCS system plays it role. It noteworthy to mention that the RePCEC stack itself is highly energy consuming. However, the total moles of CO_2 available for reaction is lower than the base case.

Table 4.3: Feedstock for base case 1 with CCS

Base case with CCS						
Permeate			9467	kmol/hr	kmol/hr	Fraction
permeate flow, kg/hr	321691.4	ton/hr	kmol/hr	To anode	To cathode	Cathode
O_2 mol%	4.9	182	464		464	0.061
CO_2 mol%	48.4	1794	4582		4582	0.603
H_2O mol%	19.7	730	1865	1865		0
N_2 mol%	27	1001	2556		2556	0.336
Ar mol%	0	0	0			0
		3707	9467	1865	7602	1

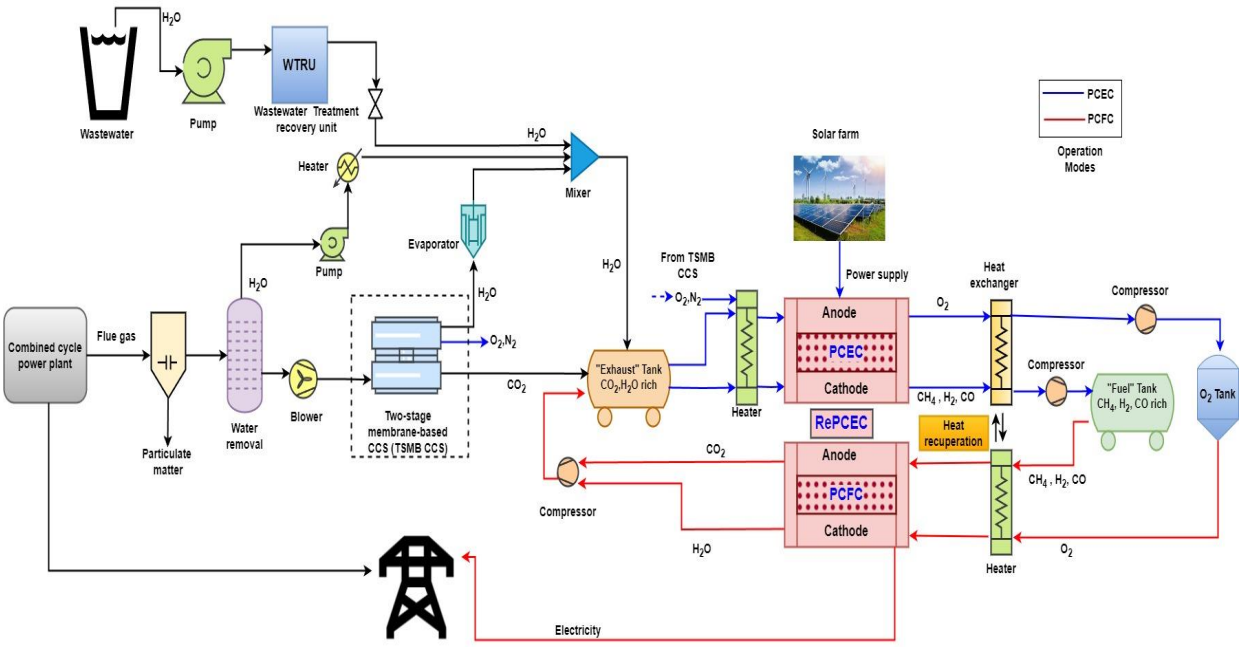

Fig. 4.12: The RePCEC integrated system for co-electrolysis of CO_2 and H_2O with carbon capture system (BC +CCS)

Making more CO_2 for reaction is likely to increase both the stack and system performance. This can be achieved by adding more exhaust tanks reserved for CO_2 storage. Likewise, the efficiency of the CCS is key to high stack and system performance. High level energy recovery design among the BoP is very critical for system performance, most especially among the heater, cooler, water separator and the compressors. This needs to carefully managed at the system upstream.

Comparing between the base case without and with CCS, the results show that the latter outperformed by all metrics. So, the focus and attention is the improvement of this base case with CCS.

The inclusion of recycle, bypass, purge streams and several cleaning systems at strategic part of the operation system is essential for high productivity which therein gives different configurations. However, the system economics required adequate attention to decide which of this addendum equipment is needed and place to put them in the process stream. After diligent management of the upstream with the previously suggested strategies ranging from additional tanks and heat integration to enhance the availability of active reactant and reduce energy demand, then the improvement of the downstream is necessary.

Segregating the reactants generation section at the upstream of the base configuration with CCS, further configurations will focus on the downstream. While dealing with the downstream, stringent measures need to identify possible area heat integration and energy demand. Also, the upstream would be run simultaneously with the downstream at different operating conditions to quickly identify point of needs and improvement. This will also enhance synchronization. Three additional configurations are added to the two base cases. Different system design setups are assessed using roundtrip efficiency and stored energy density as evaluation criteria. The first of the three configurations is recycling of the upstream product for the PCEC operation mode as shown in Fig. 4.12. It has been mentioned that the base case with CCS is the focal configuration, however, to study the effect of product recycle, recycles are attached to the two base cases. This recycle stream configuration is typical of the previous two configurations, what differs is the addition of the recycle stream to the product of the PCEC mode operation. The simulations are carried out at the same operating conditions. As stated in the results for the two cases, the amount of unreacted CO_2 in the product streams is 44.3% and 26.7% for the base case (BC) and the BC with CCS (BC+CCS) respectively. The recycle stream takes this unreacted CO_2 in part or as whole back to the feed stream for reaction. This enhances more production of methane, and also saves energy from generating fresh CO_2 to the required feed temperature. Even though energy is expended in the recycle stream, this is not comparable to what is required to generate the same amount of CO_2.

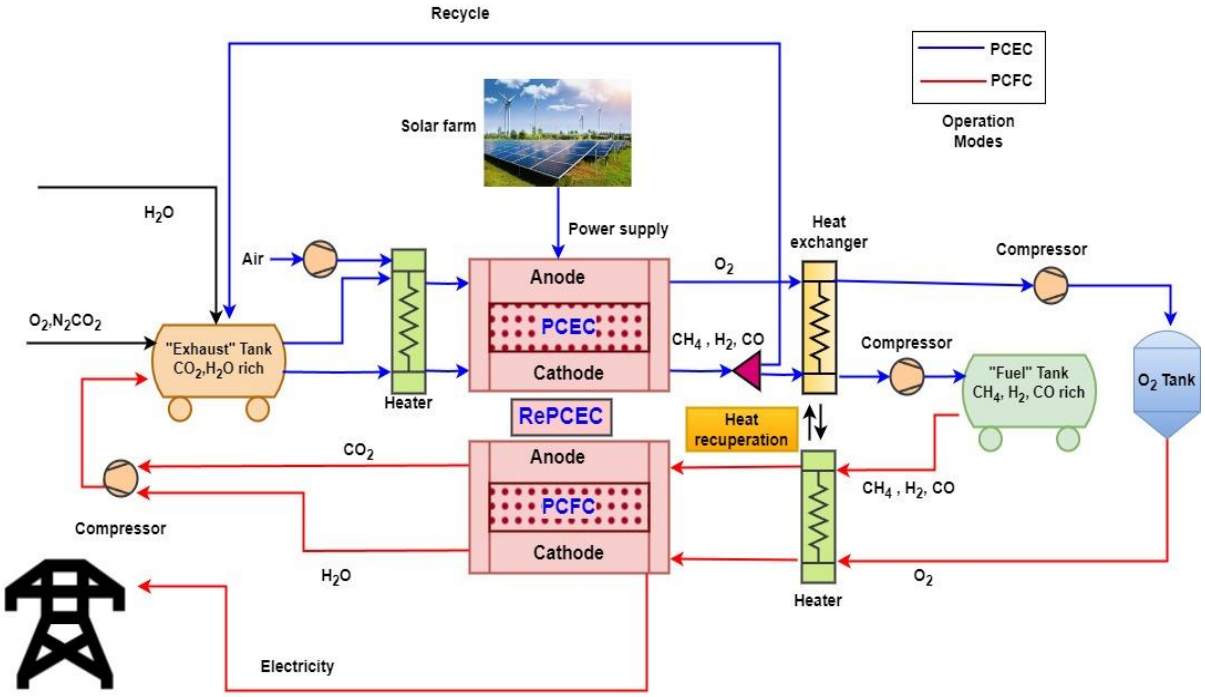

Fig. 4.13:Downstream configurations for the RePCEC integrated system, base case with CCS and recycle stream (BC+CCS+ RS)

The second configuration after the base cases, is the use of additional storage tank to support the exhaust tank which makes CO_2 abundantly available for the stack as shown in Fig. 4.13. The CO_2 for the extra storage tank is gotten from the TSMB CCS retentate and addition from an external source can also be used. The last configuration considered is this work is addition of purge to the exit streams as shown in Fig. 4.14. The exiting oxygen from the anode is purged and put to other uses. The heat from the high temperature oxygen can be integrated in other part of the system or sent to the plant for use. In this case, the required O_2 tank volume required is smaller compared to when it is not purged which definitely serve an economic purpose. Likewise, hydrogen is purged from the cathodic channel of the PCEC operational mode. This seems to have both economic and environmental benefits; it reduces competition between the combustion of methane and hydrogen in the stack. While purged hydrogen can be used for other green purposes, the system also reduces the quantity of unreacted methane. In all purging cases, energy is saved from maintain the

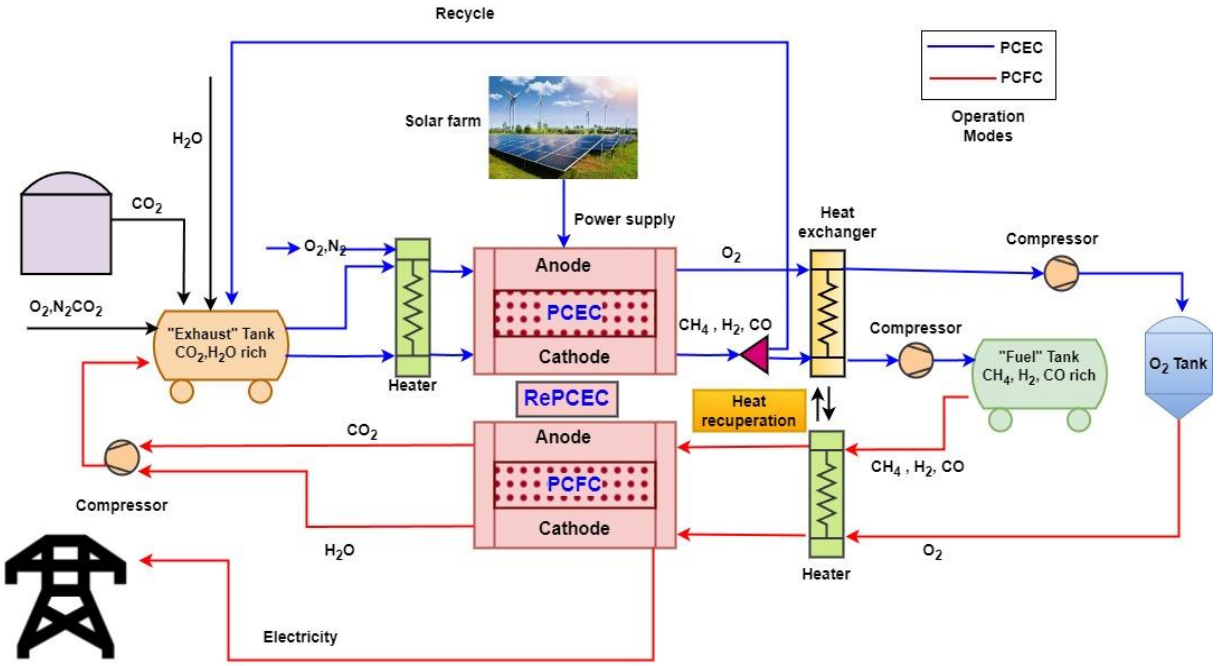

Fig. 4.14: Downstream configurations for the RePCEC integrated system, base case with CCS, recycle stream and CO_2 tank. (BC+CCS+RS+ Tank)

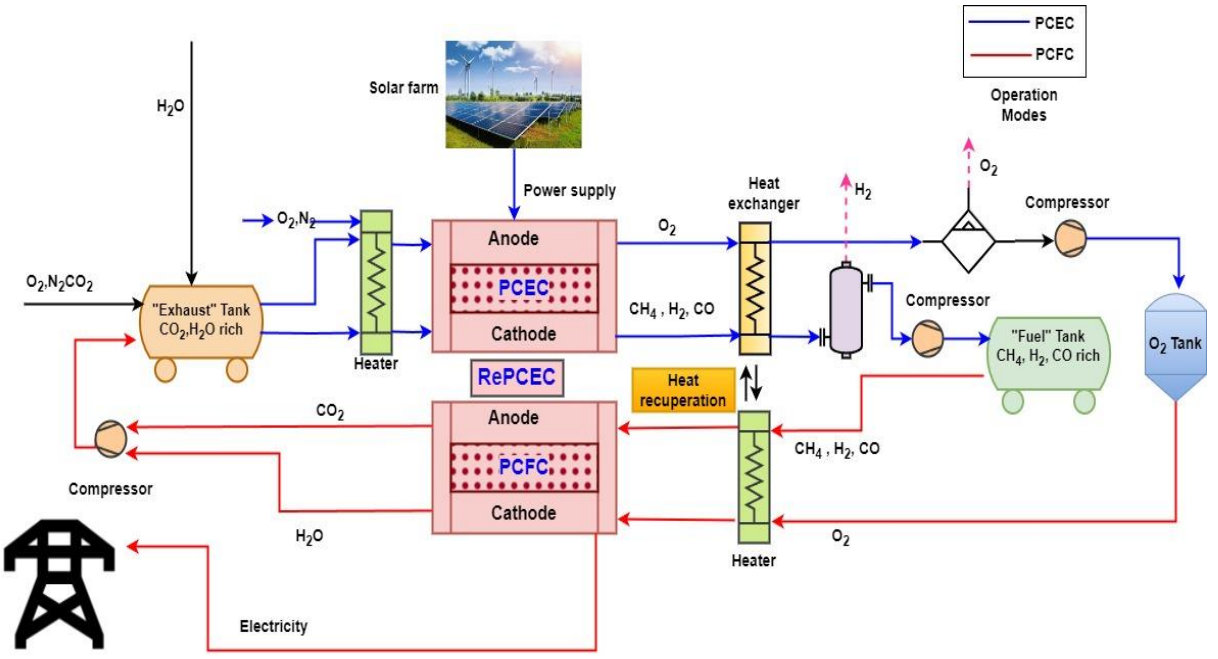

Fig. 4.15: Downstream configurations for the RePCEC integrated system, base case with CCS and purge stream (BC+CCS+PS)

isothermicity of the tanks and capital is saved from buying and maintain bigger tanks. Section 4.9 gives further discussion on the results of these configurations.

4.6 Operating conditions

Operating parameters play crucial roles in electrochemical system as with many engineering unit and process operations. Several parameters influence the performance and efficiency of electrochemical cells, stacks and systems. They include temperature, pressure, flow rate, molar composition, current density and operating voltage. The behavior of the system is examined under single operational pressure, and that is the atmospheric pressure. As presented in chapter three and in section 4.3.6, the substantiated current density range for co-electrolysis reaction in the RePCEC is operation is 0.1-0.5 A/cm^2 in the PCFC mode and 0.3-1.0 A/cm^2. The other operating parameters for the base cases are highlighted in Table 4.2. Details about the effects of these parameters are elaborated in the results section.

Table 4.4: Operating parameters for the base cases

Parameters	value
Inlet temperature	500℃
Stack pressure	1 atm
Flow configuration	Co-flow
Sweep gas composition	21% O_2 / 79% N_2
Current density	0.3 A/cm^2 -PCEC, 0.15 A/cm^2 -PCFC,
Steam molar flow from external source	9000kmol/hr
Oxygen molar flow from fuel tank to stack	1000kmol/hr
Recycle ratio, rr	0.2

4.7 Gas compositions

Choosing suitable reactant compositions for the PCFC and PCEC operation for higher system performance requires high level of process astuteness and stack operational know-how. This necessitates taking into account factors such as cell electrical performance, heat generation, electrochemical reaction and kinetics, energy density, durability and the source of gas feedstock. Moreover, in RePCEC, as the reactant composition in one mode is essentially produced by operating in the reverse mode, these compositions are contingent on the stack's operating

conditions. And in order to optimize operation in a mode, this might necessitate changing the gas composition in the process stream which further dictate the upstream and downstream configuration of the system.

4.8 Efficiencies

The efficiencies (equations 4.24-4.29) to be discussed for this system are detailed in section 4.3.5

4.9 Results

This section discusses one of the core objectives of this dissertation. It addresses the RePCEC stack integration requirements with fossil fuel power plants, performance requirements, technical and non-technical gaps for it to be used as large-scale energy storage and eventual implementation at system level. The goal is accomplished by utilizing steady-state computational modeling to simulate the roundtrip operation of a RePCEC system. The simulation involves a physically based RePCEC stack model and thermodynamic models for system components. The following sections will discuss the effects of the operating parameters, thermal management, and system configurations.

4.9.1 System Configurations.

Five main configurations with two supplementary ones have been considered in this work namely and iniatialized respectively as follows,

a. Base case (BC)
b. Base case with carbon capture system (BC+CCS)
c. Base case with recycle stream (BC+RS)
d. Base case with carbon capture system and recycle stream (BC+CCS+RS)
e. Base case with carbon capture system, recycle stream and extra water stream (BC+CCS+RS+H_2O)
f. Base case with carbon capture system and purge stream (BC+CCS+PS)
g. Base case with carbon capture system, purge stream and exhaust tank (BC+CCS+PS+Tank)

The cases c-e is considered as one main one, to study the impact of recycle stream on the system performance. The base operating parameters for all cases are highlighted in Table 4.4 and the feedstocks for base case, BC is as given in Table 4.2. Configurations having the CCS use the

feedstock in Table 4.3. The storage tank is typically used to store the balance of CO_2 from the powerplant with flowrate of 450kmol/hr. Recycle ratio of 0.2 is chosen as the base parameter across all configurations to avoid accumulation of unused reactants. For the purging configuration, 5000 kmol/h of hydrogen is purged from the process stream after the PCEC mode operation. Table 4.4 shows the oxygen input of 1000kmol/hr for the PCFC operation for all the configuration, indicating there is a purge from the PCEC operation. This value is reduced continually to evaluate the purging from the base case. Fig. 4.15 and Table 4.5 show the results of the simulation for these configurations at the described system operation and parameters.

Again, the PCEC global chemical reaction for co-electrolysis of CO_2 and H_2O are:

$CO_2 + H_2 \rightarrow CO + H_2O$, ΔH=-41kJ/mol 4.40

$CO + 3H_2 \rightarrow CH_4 + H_2O$, ΔH=-206 kJ/mol 4.41

$CO_2 + 4H_2 \rightarrow CH_4 + 2H_2O$, ΔH=-164 kJ/mol 4.42

Correspondingly for the reverse operation, The following reactions are possible in PCFC depending on the gas concentration of the fuel feed :

$CH_4 + CO_2 \rightarrow CO + 2H_2$, ΔH=247 kJ/mol ---Dry CH_4 reforming 4.43

$CH_4 + H_2O \rightarrow CO + 3H_2$, ΔH=206kJ/mol --- Steam CH_4 reforming 4.44

$CO + H_2O \rightarrow CO_2 + H_2$, ΔH=-41kJ/mol ---Water gas shift reaction 4.45

Equations 4.40-4.42 are reverse water gas shift (RWGS), reverse steam reforming and Sabatier reactions respectively, can occur in the PCEC mode. However, the cell and thermodynamics favor the methanation reactions as evident in its percentage selectivity for all configurations. Likewise, steam methane reforming is favored in the PCFC mode which finally generate CO_2 and H_2O in the presence of excess oxygen [46].

The performance of the first-two configurations has been detailed in sections 4.4.4 and 4.5 respectively. The case c-e, however considered the impact of recycling the PCEC operation exit products into the feedstock for all the three cases. Table 4.5 shows that there is a mild increase in the stack roundtrip efficiency with a decrease in the % CO_2 conversion.

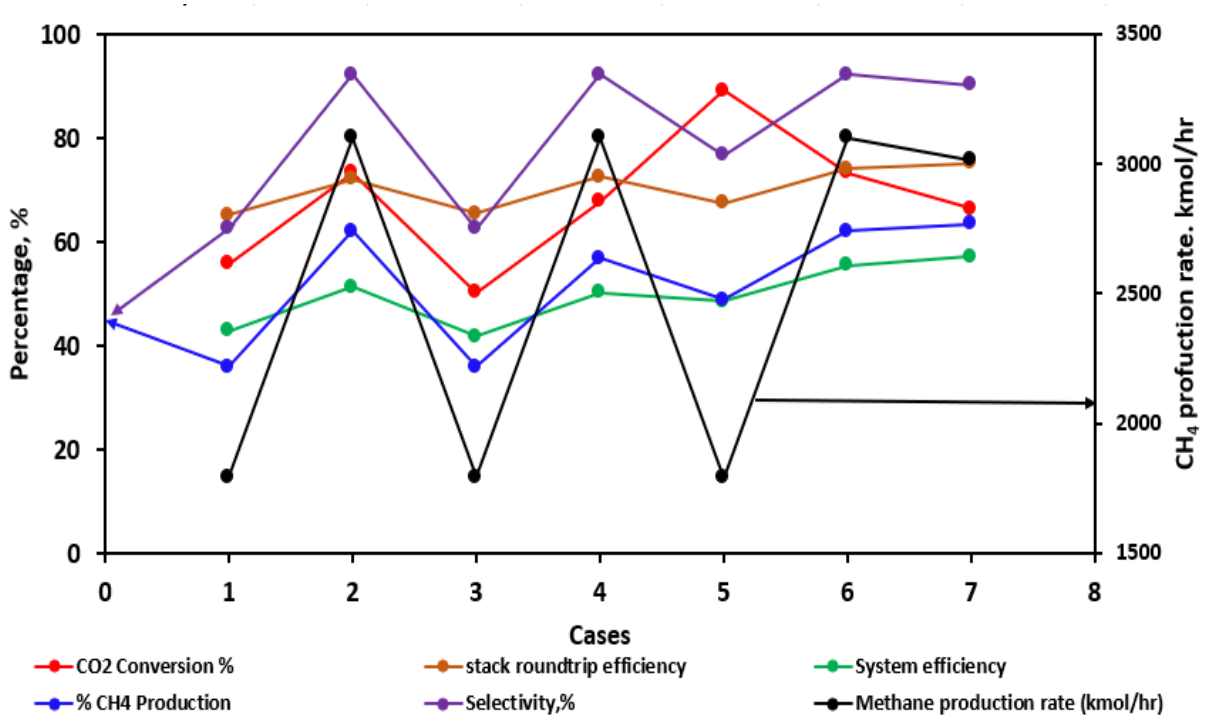

Fig. 4.16: Simulation result of cases. 1= Base case, BC, 2= BC with CCS, 3= BC +RS, rr=0.2, 4= BC+CCS+RS, rr=0.2, 5= BC+CCS+RS+ H_2O, 6= BC+CCS+PS and 7= BC+CCS+ PS+Tank

From the table, there are situations whereby the flowrates of the produced methane are the same. This can be traced to the depletion of one of the reactants and the steam in this case. Addition of CCS as previously posited enhance the stack and system performances. However, excess steam is not favorable for the stack and mild for the overall system performance. As shown in the table, purging some of the exit gases before storage is both beneficial to the stack and system performance. Identifying this, further studies is carried out on these cases with some other operating parameters and detailed in later part of this section.

Using the CCS permeate alone for the base case with CCS gives CO_2 conversion, methane production rate and Selectivity of 15.1%, 162.1 kmol/hr and 23.43% respectively. However, the RePCEC stack roundtrip efficiency of 66.6% for this configuration is higher than the 65.2% for base case. The higher values of other metric other than the stack efficiency for the base case is expected due to higher feedstock flow rate permitted by the configuration in the system.

Table 4.5: Simulation results for various configurations

Configurations	CO_2 Conversion %	Stack roundtrip efficiency	System efficiency	% CH_4 Production	Methane production rate (kmol/hr)	Selectivity,%
Base case, BC	55.7	65.18	42.79	35.9	1795	62.59
BC with CCS	73.3	72.1	51.37	62.01	3100.6	92.27
BC +RS, rr=0.2	50.16	65.5	41.81	35.9	1795.1	62.59
BC+CCS+RS, rr=0.2	68.72	72.48	50.24	56.8	3100.6	92.27
BC+CCS+RS+ H_2O	89.11	67.41	48.52	48.47	1795	76.7
BC+CCS+PS	73.3	74.1	55.48	62.01	3100.6	92.27
BC+CCS+ PS+Tank	66.42	75.08	57.22	63.49	3015.6	90.19

rr= Recycle ratio

Table 4.6 shows the exhaust flue gas from the power plant at different loadings. Using the two-stage membrane-based carbon capture system in the work by Ref [211] to capture CO_2 and separate the flue gas from the combined cycle powerplant under study at varying power plant loading gives the results in Table 4.7. The 100% power plant loading is used for this study. The total feedstock flow rate from the table is 131000 kmol/hr which is over ten folds of the permeate in Table 4.6 used in BC with CCS as previously detailed. The high roundtrip efficiency despite the low feedstock makes it fascinating and this typically shows there is prospect in modular deployment and integration of the RePCEC stack with the power plant.

Table 4.6: Results for two-stage membrane carbon capture system (TSM-CCS) for 600MW combined cycle power plant (CCPP).

CCPP load	100%	90%	80%	70%	60%	50%
Generated power (kW)	421052	378262	336334	291796	252662	208586
Exhaust gas flow (tonne/hr)	3706.56	3460.32	3211	2964	2781.2	2567.2
Exhaust gas O_2 mol%	12.39	12.38	12.36	12.42	12.64	**12.91**
Exhaust gas CO_2 mol%	3.9	3.90	3.91	3.88	3.78	3.66
Exhaust gas H_2O mol%	8.42	8.43	8.45	8.39	8.2	7.96
Exhaust gas N_2 mol%	74.4	74.39	74.39	74.41	74.48	74.58
Ar mol%	0.9	0.9	0.9	0.9	0.9	0.9
Permeate flowrate (kg/hr)	321691.4	300895.8	279557.1	256928.2	237762.7	215504.3
CO_2 mole%	0.48	0.48	0.49	0.48	0.48	0.468
H_2O mole%	0.2	0.2	0.2	0.25	0.2	0.208
N_2 mole%	0.27	0.27	0.27	0.27	0.28	0.28
O_2 mole%	0.049	0.045	0.045	0.045	0.047	0.049
	3222503	3007273	2789901	2577533	2425396	2246824

Retentate flowrate (kg/hr)						
CO_2 mole%	0.0045	0.0046	0.0046	0.0045	0.0044	0.0043
H_2O mole%	0.0011	0.0011	0.0011	0.0011	0.0011	0.0011
N_2 mole%	0.843	0.854	0.854	0.854	0.852	0.85
O_2 mole%	0.152	0.140	0.140	0.141	0.143	0.145

Nevertheless, when the water removed before the carbon capture system is re-introduced into the system to increase the steam channel feedstock, there is a remarkable increase in the system performance. Further addition of water from external sources like the wastewater treatment unit also increases the system performance metric, so it can be concluded from the system that water is the limiting reactant which is previously mentioned and supported by thermodynamics. It is noteworthy to mention that recycling some of the stack products increases system performance and the roundtrip efficiency for all configurations especially with addition of external CO_2. Separating CO_2 from the PCEC exit products and recycling only CO_2 from the exiting gas from the stack as well increases the methane production and roundtrip efficiency as shown in Fig. 4.16. This is achieved by using another separating equipment in the process downstream as mentioned in the system configurations. While results using the CCS have shown to be higher for configurations, base case is a bit competitive in some cases, but lower system efficiency does not make it a good fit for consideration.

Table 4.7: Feedstock for BC

Base case 1- without CCS					
		131000	kmol/hr	kmol/hr	Fraction
Exhaust flow, ton/hr	3706.56 ton/hr	kmol/hr	To anode	To cathode	Cathode
O_2 mol%	12.4	16244		16244	0.136
CO_2 mol%	3.9	5109		5109	0.043
H_2O mol%	8.5	11135	11135		0
N_2 mol%	74.3	97333		98512	0.821
Ar mol%	0.9	1179			0
		131000	11135	119865	1

Table 4.8: Feedstock for BC+ CCS

Base case with CCS						
Permeate			9467	kmol/hr	kmol/hr	Fraction
permeate flow, kg/hr	321691.4	ton/hr	kmol/hr	To anode	To cathode	Cathode
O_2 mol%	4.9	182	464		464	0.061
CO_2 mol%	48.4	1794	4582		4582	0.603
H_2O mol%	19.7	730	1865	1865		0
N_2 mol%	27	1001	2556		2556	0.336
Ar mol%	0	0	0			0
		3707	9467	1865	7602	1

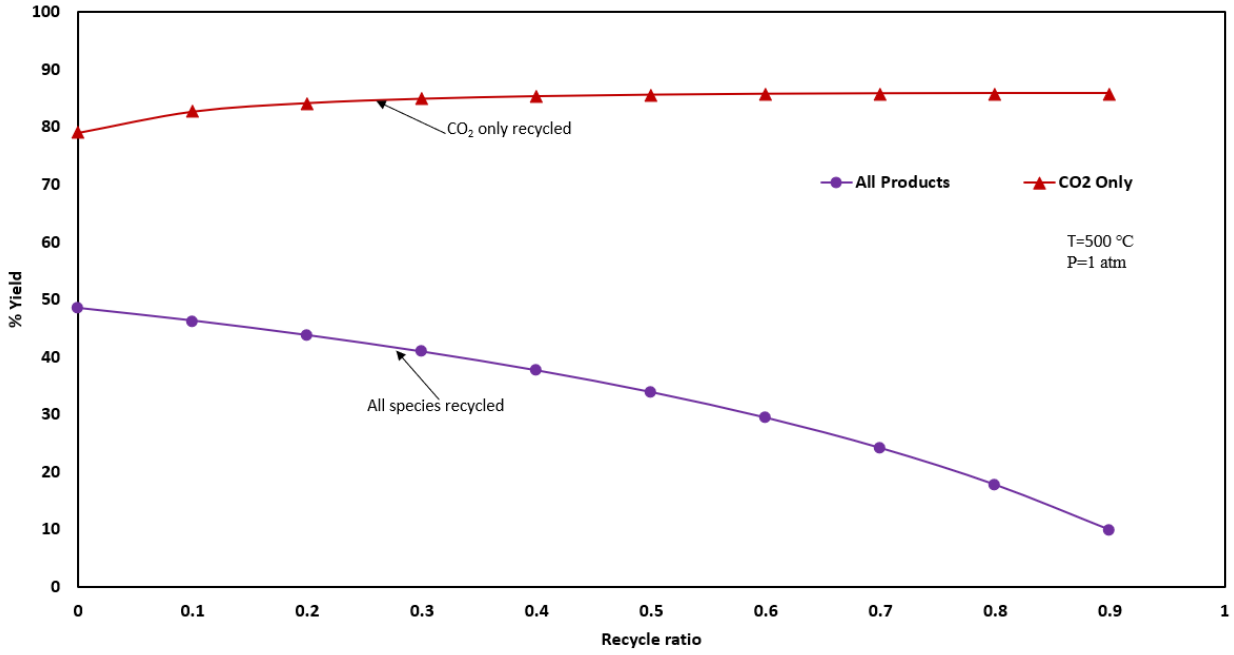

Fig. 4.17: Recycling only CO_2 from the exiting gases compared with recycling all species

Using the base case with the CCS (BC+CCS), the effect of some operating parameters would be study in the following sections.

4.9.2 Effect of recycle ratio

There is a rise in performance for all the system configurations with recycle ratio of 0.1 as shown in Table 4.5. This is the same at different temperature as depicted in Fig. 4.17. The figure compares two scenarios for the BC+CCS for its efficiency, the case having recycle ratio of 0.1 shows a higher roundtrip stack efficiency compared to case without recycle. However, the optimal recycle ratio is unique for each configuration and dependent on other operating conditions like temperature and feed composition. At it can be seen from Fig. 4.17 that there is deviation from the trend at 550 °C. The recycle ratio coupled with the recycle composition is another factor that can influence the productivity and efficiency of the system. Fig. 4.16 and 4.18 compared the recycle ratio and the percentage reaction yield in the stack. As previously mentioned, when all the exiting species is recycled the stack reaction yield decreases as shown in Fig. 4.18. Nevertheless, when the active reactant like CO_2 alone is recycled the yield increases as depicted rising curve in Fig. 4.16. This expected as there is decrease in the concentration of the reacting species as the new products continuously mix with old reactants and increase in the flow rate. However, it shows there is an increase in yield when only CO_2 is recycled from the exiting gas. This yield increases with recycle

ratio till it reached 0.65 where it remains almost steady. This might be due to the exhaustion of the limiting reactant, steam in this case. The recycle at the process downstream is focused on the PCEC operation mode exit product as previously mentioned and shown in Fig. 4.12 A different outcome using recycle for the PCFC mode is expected and that will birth another configuration. This is anticipated to affect performance and exhaust species since a commonly employed operational approach in internal reforming SOFCs involves recycling the products from the fuel channel. This recycling process is utilized to supply the necessary steam content for methane reforming [28]. The recycle ratio can typically impact the performance of the system by affecting its electrical attributes, thermal behavior, and the compositions of the local gases. The influence of recycling on the system also differs between the two operating modes, offering distinct advantages and/or trade-offs.

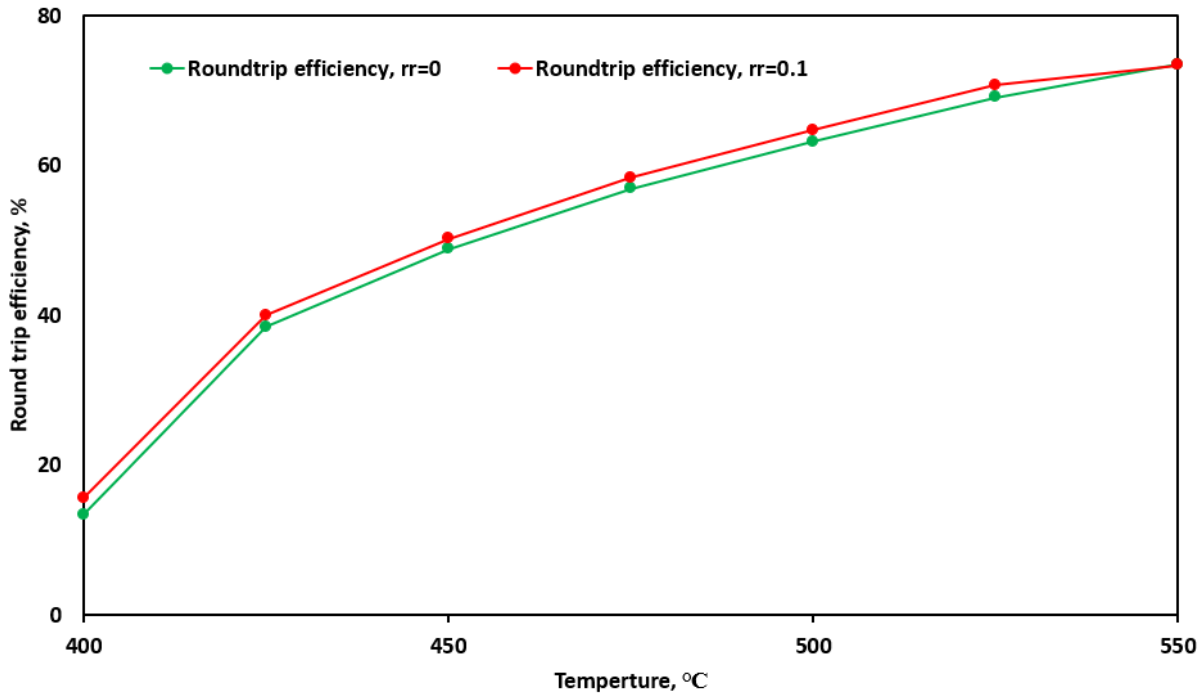

Fig. 4.18: Comparing the roundtrip efficiency at different recycle ratio, rr (rr=0 (green), rr= 0.2 (red)

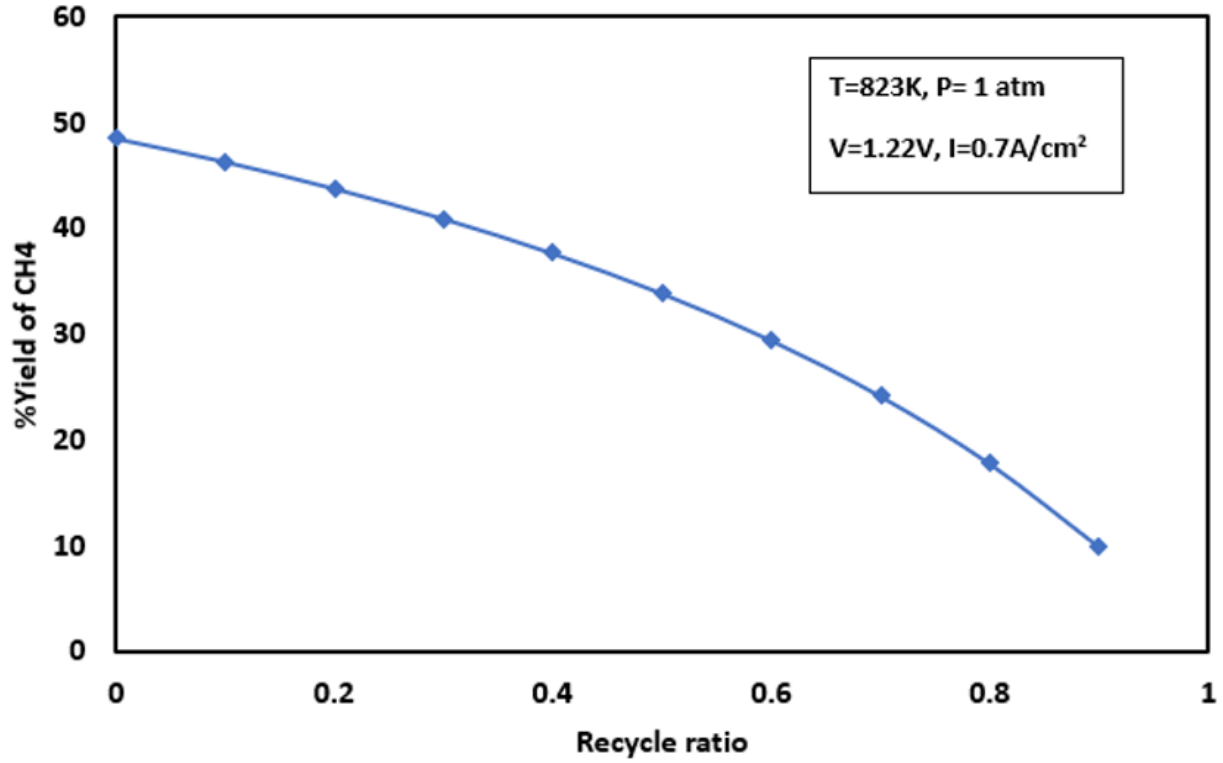

Fig. 4.19: Yield against recycle ratio

4.9.3 Effect of Stack operating temperature

Fig. 4.19 shows the effect of temperature on the roundtrip efficiency of the stack, methane production and the operation voltage during PCEC mode. In the co-electrolysis of CO_2 and H_2O, two major reactions occur namely, the decomposition of H_2O and CO_2 hydrogenation. The first reaction is endothermic and favored at higher temperatures while the latter is exothermic. The hydrogenation reaction is dependent on the H_2O decomposition to occur. So, at lower temperature only few hydrogen atoms would be available for CO_2 hydrogenation. As temperature increases, more hydrogen atoms become available for reaction. It is obvious from Fig. 4.19a that the stack round trip efficiency increases with temperature at the operating conditions. These results validate the credibility of the stack model in the integrated system. As temperature increases the cell voltage increases in the PCFC mode and decreases in the PCEC mode, which indicates an increased roundtrip efficiency. This increment continued to 525℃ that appear to be the optimum operating temperature at the given condition and started declining at 550℃. Cell voltage decreases with

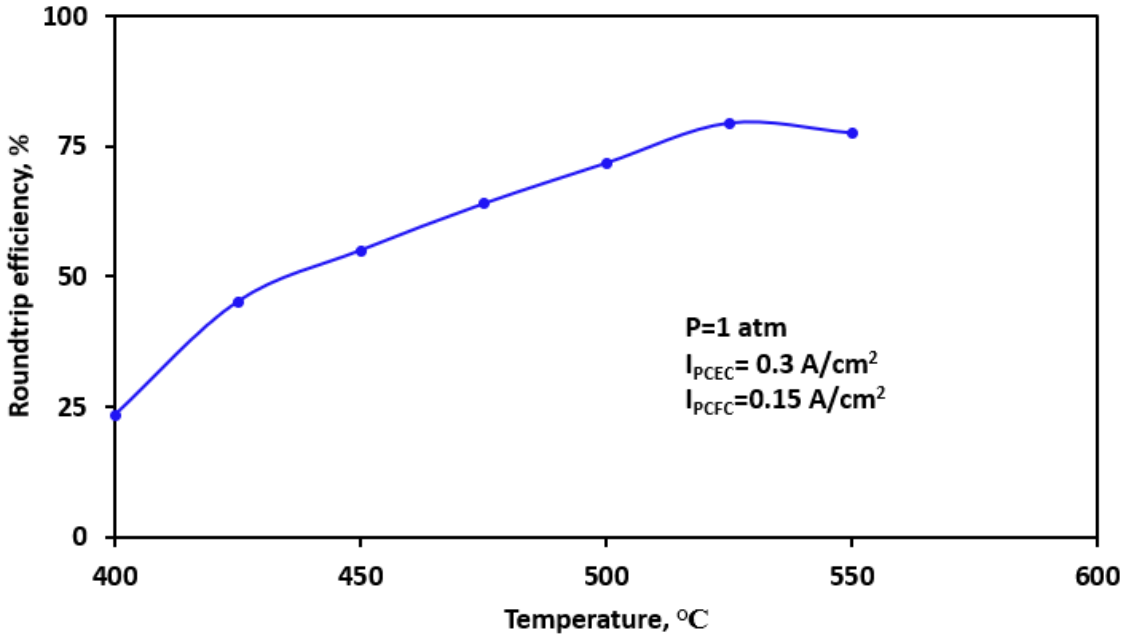

(a)

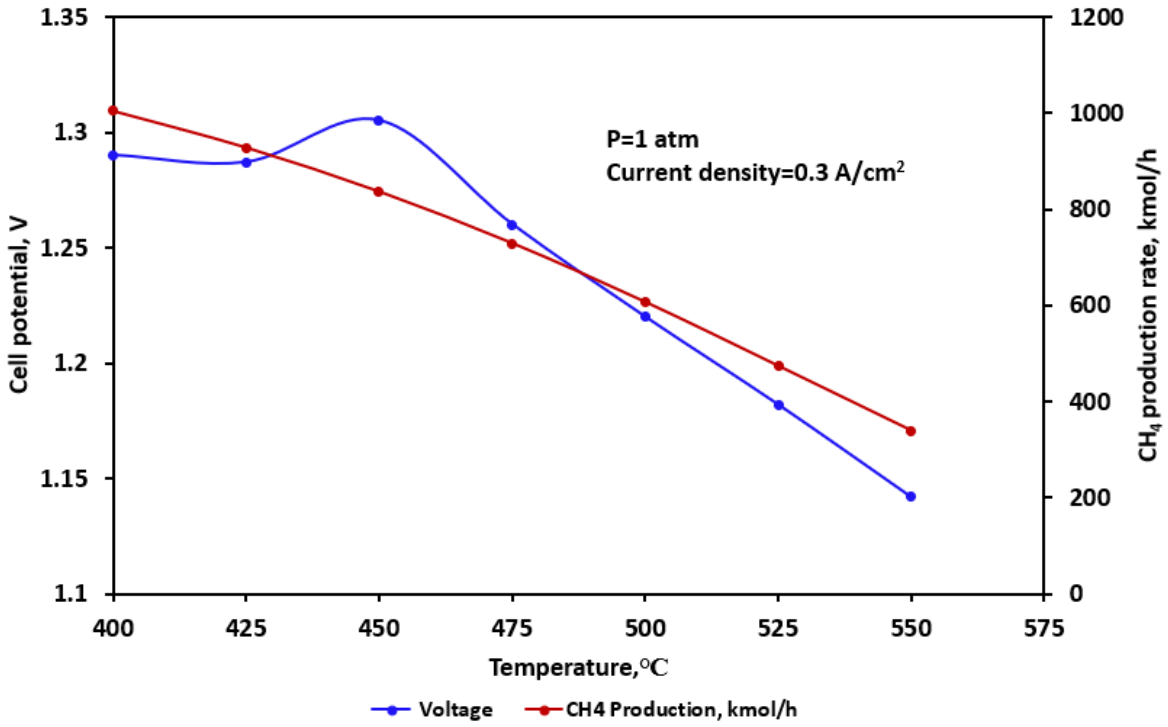

(b)

Fig. 4.20: Influence of operating temperature on (a) stack roundtrip efficiency (b) methane production and stack voltage.

temperature increase in the PCEC mode as shown in Fig. 4.19b with an offshoot at about 450 ℃ which perhaps might be due to a quick internal drop in stack temperature from reaction and species variation. It has been previously mentioned in chapter 3 of this dissertation, that the cellular level study for methane production shows that highest production of methane is at 450℃. Perhaps similar reaction phenomenon is what is observed in the stack. Likewise, there is a decrease in the methane production rate with increase in temperature. As previously mentioned, methane production is enhanced at lower temperature and increase in temperature makes the reaction to shift in the opposite direction based on the common Le Chatelier's principle.

In reaction engineering and kinetics, yield, reactant conversion and product selectivity are key parameters for assessing the reaction performance. Both the yield and CH_4 selectivity decrease with increase in temperature as depicted in Fig. 4.20. Similar explanation can be given as the effect of temperature on CH_4 production rate. The yield, selectivity and rate of production are directly proportional and related. However, there is a slight increase in CO_2 conversion with temperature increase, this might be attributed to the formation of side reactions that benefit from steam electrolysis as it increases with temperature through equilibrium shift. The competing reactions are given in equations 4.40-4.42

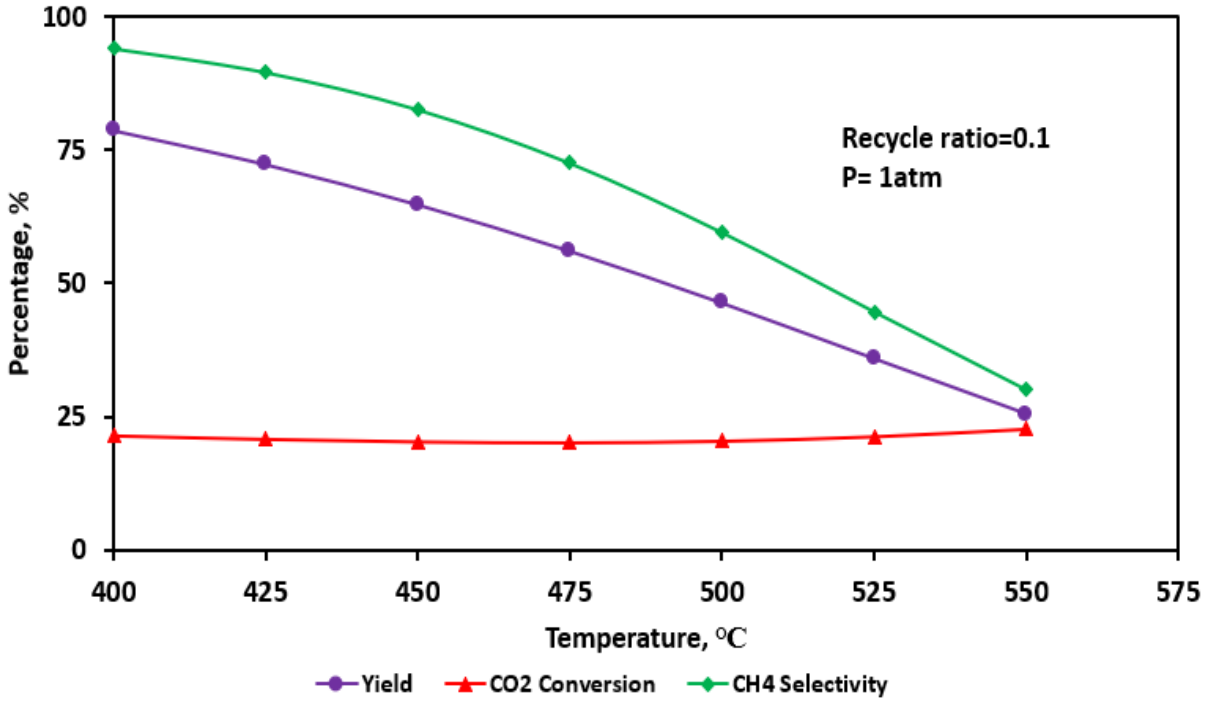

Fig. 4.21: Effect of temperature on yield, CH_4 selectivity and CO_2 conversion

Fig. 4.21 shows the effect of temperature on the reacting species in the stack. Considering the gas species at different temperatures shows that there is a drop in CO_2 remaining and CH_4 generated as temperature increase which emphasize the results of Fig. 4.18. As hypothesized that side reactions benefit from the increase in the CO_2 conversion as temperature increase, this inference can be assumed true as this is reflected in the amount of H_2, and CO produced as temperature increases.

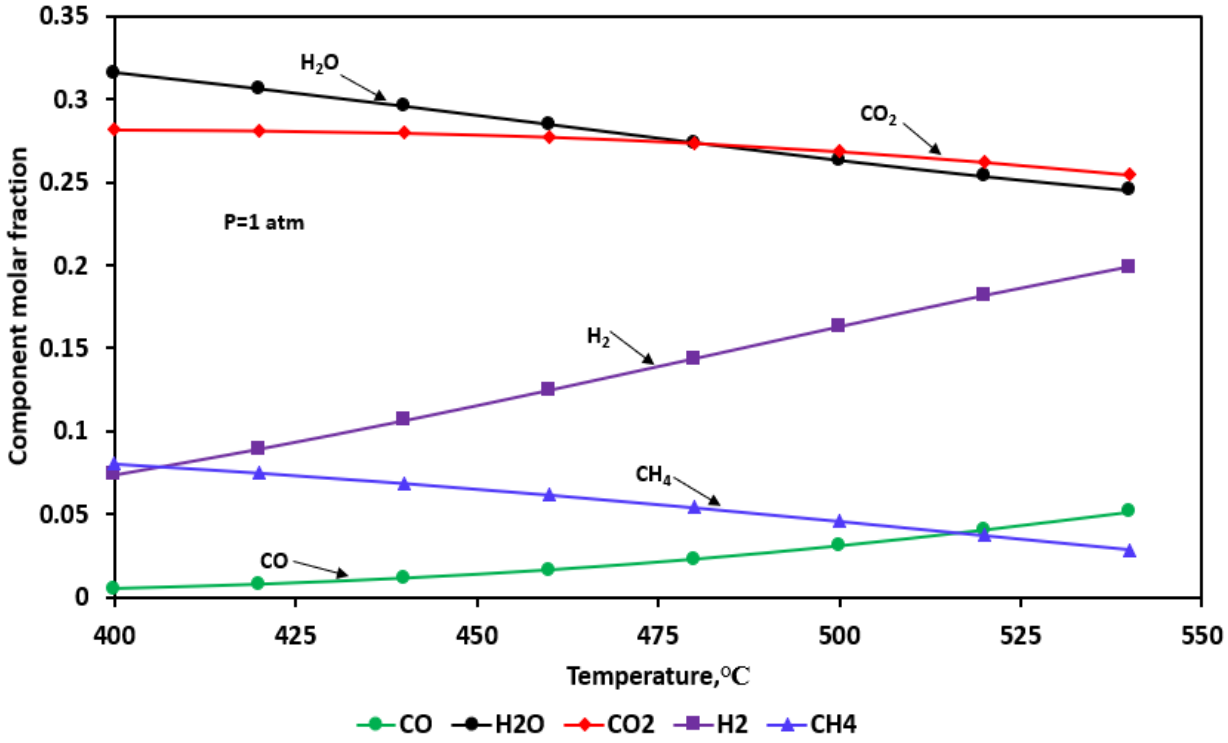

Fig. 4.22: Effect of temperature on gas composition

4.9.4 Effects of current density

Current density significantly influences cell efficiency as it affects overpotential in both operational modes. The roundtrip efficiency exhibits a nearly linear decrease as the PCEC mode current density increases, as depicted in Fig. 4.22 for the RePCEC stack. This analysis is carried out at constant PCFC current density while varying that of the PCEC as the current density in both operational modes can be tuned for optimal stack performance. This is expected because at an averagely constant PCFC voltage, increased PCEC current density brings about higher stack

overpotentials and eventual increase PCEC voltage. This results in the observed declining roundtrip efficiency. Nevertheless, the results reveal that high stack efficiency is possible by adjusting the current density between both modes of operation. While the PCFC mode current density is kept constant at 0.2 A/cm^2 and varying the PCEC mode current density, it is observed that an average of 75% and above roundtrip efficiency is achievable. This outcome indicates that enhancing stack performance by thoughtful design and reducing the internal resistances associated with cell stacking, that results in high overpotentials are essential steps to achieve high efficiency while maintaining reasonable current density. Due to the intricacy of the co-electrolysis reaction with the membrane electrode assembly (MEA), operating in the current density range of 0.4-0.8 A/cm^2 is highly recommended as suggested by this model and explained in chapter 3 of this dissertation for PCEC mode. This is corroborated in the study by Pan et al [94]. This also serves as an accommodation for the PCFC mode optimum operation range as shown in the section 4.3.6. The operating temperature is a very important parameter that influence the choice of current density selections. In all the temperatures examine, 525℃ has shown to be an optimum temperature to achieve and average of 80% roundtrip efficiency at all current densities.

Overall, the seventh case study configuration having the base case with CCS, purge and exhaust tank typically exhibits the highest stack and system efficiencies. Operating it at higher temperatures like the optimum suggested by the temperature analysis gives a stack roundtrip efficiency of 82.27%. This makes it more competitive with other energy storage devices like the U.S. utility-scale battery fleet with roundtrip efficiency of 82% on a monthly basis and pumped storage facilities with 79% [212]. The challenges in designing the system for all the scenarios are centered around minimizing the balance of plant components power requirements. The separation of water from the flue gas, cooling and reheating consumes a lot of energy. The WTRU is highly energy demanding, energy is required to evaporate water to steam at the stack inlet temperature. Reducing and regulating the generated steam from the WTRU is instrumental in sustaining high efficiency as excess steam is not favorable for the reaction going on in the stack. Likewise, saving the energy to for the excess steam maintains the system for higher efficiency. Moreover, several compressors are used for species compression into both the exhaust and fuel tank which is also energy demanding. Direct usage of reactant when needed and reducing the compressor pressures and operating temperatures. The optimum methane production is 450 ℃ and the optimum for stack roundtrip efficiency is 525℃, maintaining operation in this temperature range enhances system

efficiency. Achieving low energy demand by the BoP components benefits the system operation and the economics for the feasibility and implementation of the RePCEC technology as sustainable energy storage system. Most especially when integrated with fossil fuel assets and renewables.

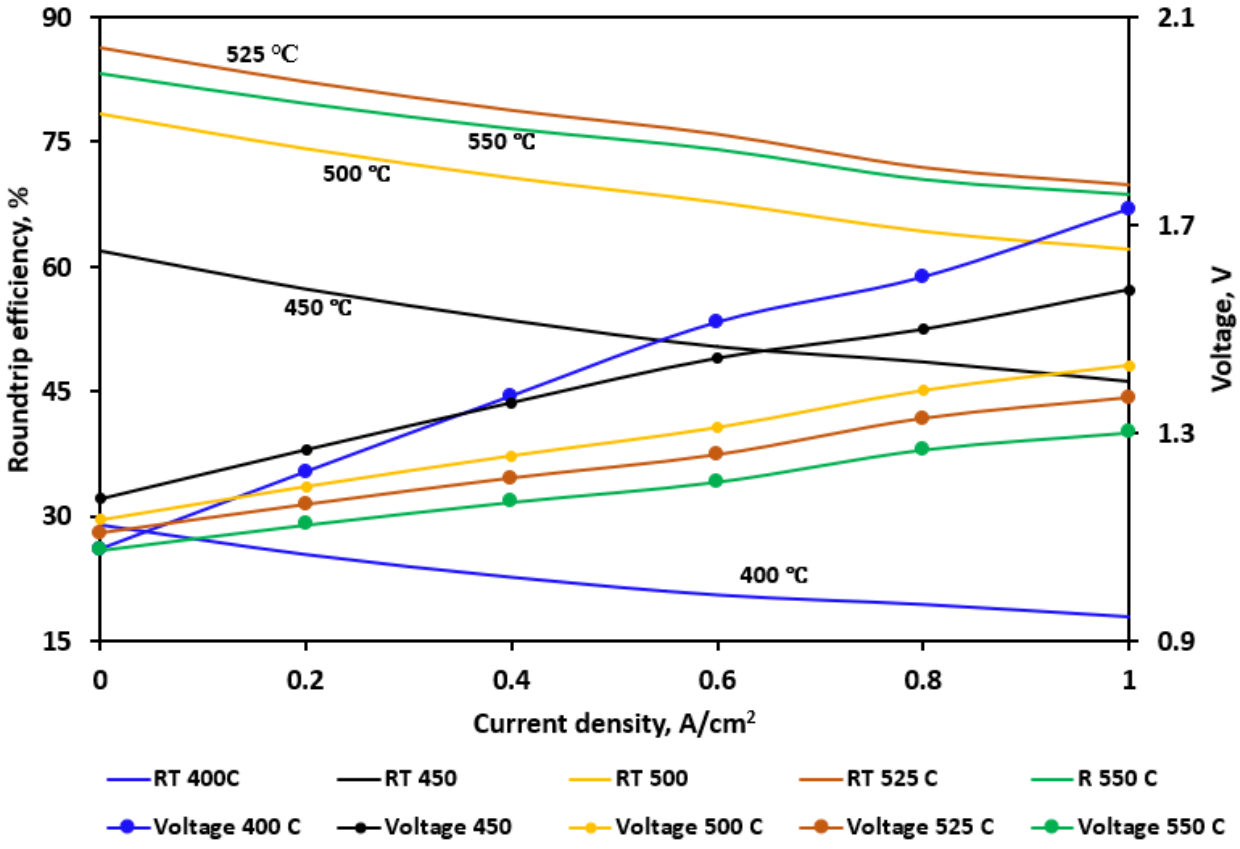

Fig. 4.23: Effect of current density on roundtrip efficiency

4.10 Conclusion

The stack model is simulated and its operation in a reversible protonic ceramic electrochemical cell system is evaluated through the use of a computational model. The system configuration to get as high quantity of the primary reactants (CO_2 and H_2O) into the stack during its integration for a system level design is key to achieving high methane production. While higher stack roundtrip efficiency of over 80% is achievable when integrated with combined cycle powerplant of 600MW, the overall system efficiency is limited by the BoP power demand. To achieve overall system level performance for an isothermal operation of this type, the BoP energy should be

appropriately integrated both at the upstream and downstream of the system to minimize energy consumption and heat loss. The stack isothermal operation benefits from high methane production for its heat to balance up with the demand during steam electrolysis which will eventually improve the system performance. To accomplish this, operations need to be within the temperature range of 450-525℃. Results show that 450℃ and 525℃ are the optimum temperatures for methane production and stack roundtrip efficiency respectively. The generation of heat within the RePCEC stack, especially during electrolysis mode, represents a significant limitation within the system and is influenced by factors like current density, reactant composition, and operating temperature. Analyzing these operational parameters parametrically uncovers trade-offs between stack durability, thermal management and finally stack and system efficiencies.

Another distinguishing advantage about the co-electrolysis in the RePCEC, is the potential to simultaneously generate hydrogen from the system. This give a dual chemical storage for renewables, as the hydrogen can be taken in parts from the system loop as posited in the system configurational design which gives the highest stack and system efficiencies. Detailed profitability analysis will reveal the economic value this will add to the process.

CHAPTER 5 ECONOMIC ANALYSIS (EA), NET ENERGY ANALYSIS (NEA) AND LIFECYCLE ANALYSIS (LCA) OF PCEC AND SOEC

? **Research Question, RQ4**: What are the optimum conditions and their influence for designing a cost-effective integrated energy storage system?

➢ **Objective 4**: Economic feasibility study of integrated RePCEC system operation for possible commercialization.

✓ **New knowledge**: A comprehensive techno-economic analysis (TEA) of large-scale RePCEC operation that can predict the levelized cost of hydrogen and methane with the influencing factors. The first levelized cost of methane through co-electrolysis of CO_2 and H_2O in PCEC technology.

This chapter is an extract of two published peer-reviewed papers titled "a novel green hydrogen production using water-energy nexus framework" [165] and "Life cycle analysis of a hydrogen production system based on solid oxide electrolysis cells integrated with different energy and wastewater sources" [213]. The original draft of both papers is solely carried out by the author. The chapter discusses and compare the levelized cost of hydrogen production using solid oxide electrolysis cells (SOECs) and protonic ceramic electrolysis cells (PCECs). It compared the energy requirement in both technologies and their carbon footprint during manufacturing and operations. Water electrolysis is used as a case study here due to the climatic friendliness of its by-products, hydrogen, and oxygen. Hydrogen has been globally accepted as one of the most promising alternative green energy sources transitioning away from fossil fuels, giving rise to the hydrogen economy. The goal of using hydrogen for global decarbonization is strongly driven in Europe and the United States.

Over time, hydrogen has shown to be a viable alternative energy source and vector due to its abundance and higher energy density, production of only water when used as fuel, and its convertibility to other valuable chemicals and electricity [214]. Hydrogen can be produced from a broad spectrum of primary energy sources [215, 216], such as solar [217], wind [218], nuclear [219], hydropower, and geothermal [220]. This option of diversity has made the production of hydrogen easy virtually in all parts of the world [221]. This is done using two major processes that can be categorized based on their separation from their feedstocks; the chemical and thermal and

the third one which is biological is under development [222]. Nearly all the produced hydrogen today (about 95% of produced hydrogen) uses the thermal process i.e. steam reforming (SR) of natural gas and many other hydrocarbons[223], and environmentally benign alternatives are in demand. Even though this steam reforming with greenhouse gas (GHG) emissions in the range 8.9-11.9 kg CO_2/ kg H_2 [224] serves as a benchmark to a lot of hydrogen production technologies including electrolyzers.

The following sections focus on the economic analysis (EA), net energy analysis (NEA), and lifecycle analysis (LCA) for hydrogen production using two electrolyzers, SOEC and PCEC. The PCEC is a low temperature (300-600℃) solid oxide electrochemical cell which makes it turn an anticipated alternative to SOEC (650-1000℃) [39]. High operating temperature comes with high capital, operating and maintenance costs. Ranging from buying equipment that can withstand and resist high temperatures and lasting durability to their maintenance. In addition to this is the cost of energy demand as high temperatures is proportional to higher energy requirement. Based on some of these premises it expected that PCEC to be more economic viable and environmentally friendly than SOEC. The system for all the analysis is described in section 5.1

5.1 System description

The schematic diagram for the integrated hydrogen production system to be considered for EA, NEA and LCA is shown in Fig. 5.1. The system is based on solid oxide electrochemical cell (SOEC) sourcing its steam feedstock from a coal power plant and a wastewater unit and aimed at being integrated with the grid. In this system, water from a wastewater source at 1 atm and ambient temperature is pumped to a water treatment and recovery unit (WTRU) that houses an evaporator to generate steam. Concurrently, flue gas from the power plant (PP) is cooled from its exhaust temperature of 120 ºC to room temperature in a condenser where the moisture content is recovered, and the heat regained in this process is used in the WTRU. The recovered water is sent to a heat exchanger where it is superheated and evaporated to generate high pressurized steam (HPS) mixed with that from the WTRU. The mixed HPS stream is pre-heated to the temperature range of 700-850 ºC to lower the needed entropic heat for the endothermic decomposition of the steam when compared to the liquid water [209]. This reduces power consumption [210] and the steam is sent to the SOEC stack where the reaction takes place. Air from the ambient environment is compressed, preheated, and supplied to the SOEC stack to flush out the produced oxygen from the

electrolysis reaction. It serves as a heat vector into the stack to meet the boundary conditions and exit the stack. An external source of heat (TΔS) is essential as it reduces the required electricity per volume of hydrogen gas produced when compared to some other electrolyzer technologies [209].

Thus, the external source is supplying a significant part of the energy required for the electrolysis reaction. The final hydrogen product is separated from the steam, and this exiting hydrogen gives up its heat for use in the heater and is stored in a compressed hydrogen storage tank at a desired pressure and can be used in solid oxide fuel cell (SOFC), when combined in a regenerative SOC. The separated steam is sent back into the cycle for reuse, and the O_2-rich stream can be utilized in the integrated fossil fuel power production facility to optimize the combustion process.

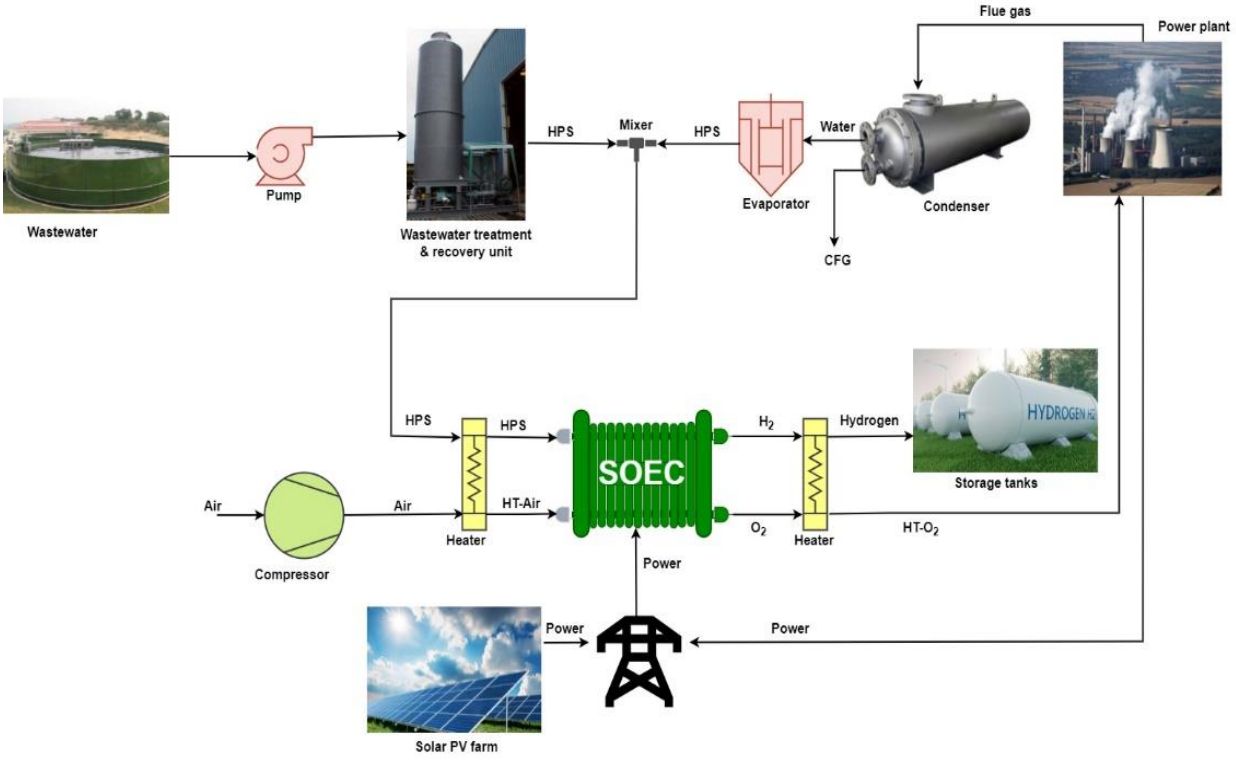

Fig. 5.1: The integrated system for hydrogen production

5.2 Economic analysis (EA)

The economic analysis is a technique used in examining the economic performance of a system and industrial product, process, and services. Usually, capital cost, operating cost, and revenue are estimated using software modeling built on financial input and technical parameters [225]. The goal of this work is to evaluate the viability of an integrated PCEC system for cheap hydrogen

production especially when compared to its rival counterpart, the SOEC system in similar operation. Therefore, the EA is performed to estimate the levelized cost of the produced hydrogen in an integrated electrolyzer system. Comprehensive cost estimates are carried out using data from the Aspen HYSYS model, and data from the literature for cost models. These results are compared using the DOE's H2A hydrogen production model, current central version 3.2018 [226] for the reliability of the outcomes.

5.2.1 Capital cost evaluation

The capital cost, which includes the cost of procuring the equipment, the SOEC cost with estimated size of 330MWh is obtained from the US DOE Hydrogen and Fuel Cells Program Record [227]. The auxiliaries, balance of plant (BoP) components are estimated using the cost equations as shown in Table 5.1 and the required input values from the Aspen HYSYS model. The wastewater treatment and recovery unit (WTRU) is modeled as an evaporator in our system in Aspen HYSYS, which is why the evaporator cost is only included in the EA. For some equipment for which equations are not readily available, the general equipment cost equation below was used in their formulations.

$$Cost = a + bS^{n} \quad (5.1)$$

The purchased equipment falls under the direct capital cost expenditure. Some others, like the installation cost and indirect cost, are shown in percentages of the total direct cost (TDC) [227]

Table 5.1: Equipment cost models and values for economic analysis

Equipment	**Cost model ($)**	**Value ($)**	**Reference**
Pump	$1120*W_{pump}\wedge 0.8$	2850	[228]
Condenser	$8000*(A_{cond}./100)\wedge 0.6$	9840	[228]
Heater 1	$7000+7100*W_{d}\wedge 0.8$	2892000	[229]
Compressor	$((71.7*m_{in})/(0.92-\eta_{comp}))*\pi_{comp}*\ln(\pi_{comp})$	2175000	[230]
Mixer	$780+62*V_{fl}\wedge 0.8$	1040	[229]
Evaporator	$330+36000*\ A_{sa}\wedge 0.55$	1037000	[229]
Heat Exchanger	$130*(A_{HX}/0.093)\wedge 0.78$	20300	[228]
Pump	$1120*W_{pump}\wedge 0.8$	2850	[228]

	$8000+240*V_{pf}^{\wedge 0.9}$		
SOEC		25560000	[227]
Separator	$20000+1200*m_{sh}^{\wedge 0.6}$	1566000	[229]
Heater 2	$53000+69000* W_d ^{\wedge 0.8}$	105000	[229]

Table 5.2: Estimates of the direct, indirect, depreciate, and non-depreciable capital cost

S/N	Expenditure	Value ($)	Value ($)
1	Direct expenses	SOEC	PCEC
a	Equipment free on board (FOB) cost	109140000	81860000
b	Installation materials (12%)	13100000	9823000
c	Labor (installation) (2%)	2183000	1640000
	Total direct cost, TDC	124420000	93320000
2	Indirect Expenses		
a	Freight, insurance, and tax (3%)	3733000	2800000
b	Construction overhead (2%)	2490000	1870000
c	Engineering and design expenses (10%)	12442000	9332000
3	Contingency and fee		
a	Contingency (7%)	8710000	6532000
b	Contractor fee (5%)	6221000	4666000
c	Legal fee (10%)	12442000	9332000
4	Auxiliary facilities		
a	Land acquisition and site development 5%	6221000	4666000
b	Auxiliary buildings 3%	3733000	2800000
c	Off-site and utilities 1.5%	1870000	1400000
	Total capital cost, TCC	306700000	230020000

5.2.2 Operational and maintenance (O&M) cost

Some assumptions are made for the estimation of the operating cost of the plant using several sources. Considering the similarities of the SOEC with the SOFC, estimates are based on Gerdes et al [231] and majorly from the DOE hydrogen analysis [227] and a recent work by Konor et al [232]. This estimating ratio for the SOEC has been adopted for the PCEC dealing with almost similar equipment and size. The operating costs include labor and overhead, licensing and permitting, rent payments, and feedstock costs. Depreciation is considered in the EA analysis using the Modified Accelerated Cost Recovery System (MACRS) type. Corrosion and other effects were put into consideration and the depreciation rate is high, making changing some units and lines to be twice within the 10 years of plant life as designed in the DOE H2A analysis tool. The production maintenance cost includes the cost of replacing the stack cell, repair, and royalties. The O&M costs are calculated as a percentage of the TDC, and the fixed, variable, and other operating costs and the maintenance cost are shown in Table 5.3.

Table 5.3: The O&M cost estimates [165]

Category	**Value ($)**	**Value ($)**
Operating costs	SOEC	PCEC
Fixed (1.5%)	1,870,000	1400000
Variable and others (95%)	118,200,000	88,650,000
Maintenance Cost (12%)	14,930,000	11,200,000

5.2.3 Levelized cost of hydrogen production

The levelized cost of hydrogen (LCOH), which is the average net present cost of hydrogen production for the entire lifetime of the plant, is given as [233];

$$LCOH = \frac{\dot{X}_{CapitalCost} + \dot{X}_{O\&M} + \dot{X}_{Fuel} + \dot{X}_{Electricity}}{\dot{M}_{annual,H_2}} \qquad (5.2)$$

where $\dot{M}$ is the mass flow rate and $\dot{X}_{CapitalCost} = investment\ cost\ rate$ and is given by

$$\dot{X}_{CapitalCost} = \frac{X_{total} * Capital\ recovery\ factor, CRF}{Total\ annual\ time\ (hours)} \qquad (5.3)$$

here X_{total} is the total capital investment (TCI), and for capital amortization with an assumed annual interest rate i, the capital recovery factor is:

$$CRF = \frac{i(1+i)^n}{(1+i)^n - 1} \qquad (5.4)$$

where n is the number of annuities (plant lifetime)

5.3 Life cycle analysis

Due to the attention that has been given to hydrogen by scientists and policymakers as a significant player in achieving a green economy and its several advantages, it is necessary to holistically access the environmental impact of the pathways of this must-produce energy vector.

One of the enhancing tools for organizational decision-making on sustainable resource management is the Life Cycle Assessment (LCA). The LCA is a standardized modeling approach for quantifying the cradle-to-grave environmental impacts of a product system and the net-energy impacts of its energy input and output systems [234], [235]. It addresses the collection and evaluation of inputs and outputs in a process and the future environmental impacts of a product system over its entire lifetime [236]. The assessment activities stem across extraction and transformation of the raw materials by manufacturing, operation, and marketing processes, the use, and re-use of the product and its maintenance and finally its recycling or disposal as waste. This method is globally accepted and has been well defined by the International Organization for Standardization (ISO) and peculiarly by ISO standards: ISO 14040 and ISO 14044 [236, 237]. Even though hydrogen is regarded as a clean fuel and energy vector, its production phase is not free of undesirable environmental impact. The application of LCA to hydrogen production, most especially through water electrolysis, is increasing rapidly in order to inform exigent decisions and determine promising and superior technology paths. From the three prominent electrolyzer technologies: PEM, AE, and SOEC, the LCA of the PEM and AE are well studied due to their high level of development. The AEs taking the lead and are the current technology for an industrial application while SOEC is the least developed of the three and its LCA has been seldomly studied [213, 238] that of the PCEC which is a proton-conducting SOC is virtually in existence. A standardized LCA for an SOC is expected to be a building tool for the LCA of PCEC.

5.4 Lifecycle analysis (LCA) frameworks

The LCA process entails four fundamental frameworks, namely

1. Goal and scope definition (system description and objectives)
2. Inventory analysis (data collation-knowing and quantifying the energy and materials in and out of the system)
3. Impact assessment (measuring the environmental effects of the system)
4. Interpretation (understanding and evaluation of result)

The fundamental frameworks are discussed in the following sections.

5.4.1 System definition

The proposed system described in section 5.1 and depicted in Fig. 5.1 is made up of an advanced solar photovoltaic (PV) system paired with an SOEC system integrated with a 334 MW coal power plant and a wastewater system from which it sources its water feedstock for hydrogen production. In this work, two scenarios are considered.

a. The solar PV system supplies the electricity and thermal energy required by the SOEC and the balance of plant (BOP) system.
b. The 334MW coal power plant supplies the electricity and the thermal energy required for plant operation, and oxygen is recycled to the power plant. Fig. 5.2 shows a generic LCA boundary under investigation.

The coal power plant supplies the system with a flue gas having 11.09 mol% CO_2, 67.13mol% N_2, 9.09 mol% O_2 and 12.69 mol% H_2O at a constant flowrate of 109548.13 kmol/hr generating 4911 kmol/hr of condensed water. This used in the SOEC system, and the wastewater system only supplies 100 kmol/hr to the electrolyzer. The energy splits between the electrolyzer system and the BOP components in both scenarios

5.4.2 System components

The overall hydrogen production facility comprises the SOEC and the BoP components, which includes condenser, heater, compressor, mixer, separator, heat exchanger, pump, water treatment and recovery unit (WTRU), which houses the evaporator.

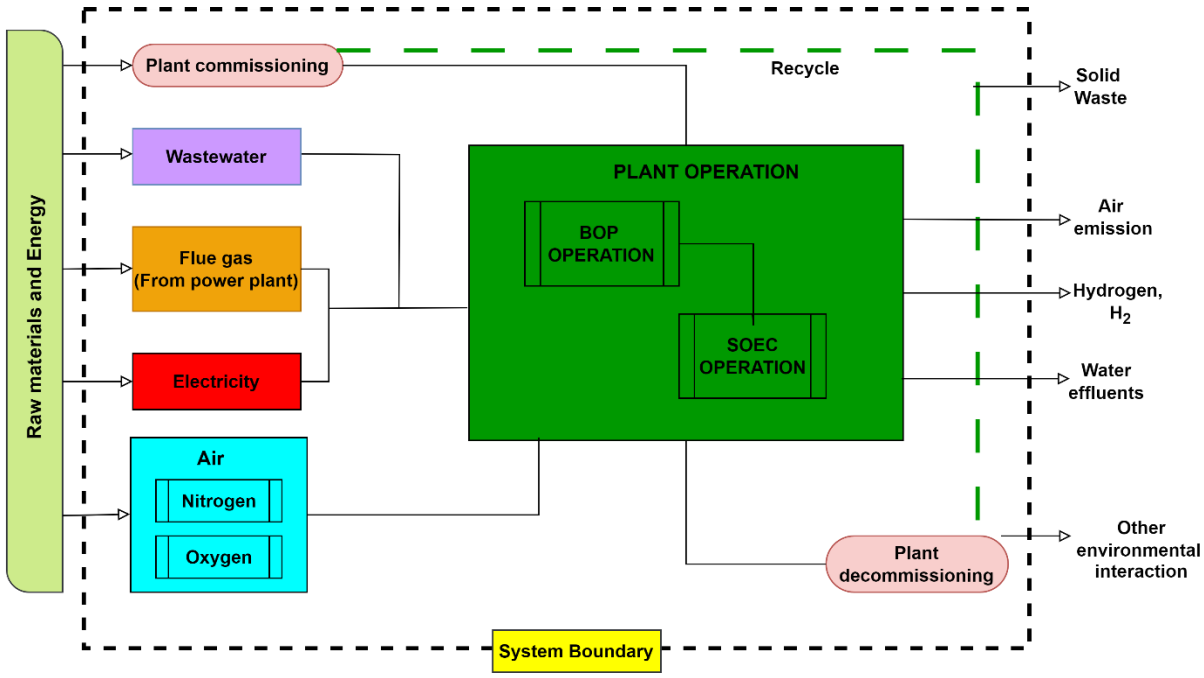

Fig. 5.2: Generic LCA illustration of the water-energy nexus hydrogen production

.

5.4.2.1 Manufacturing of the SOEC stack

The smallest units of SOEC (i.e, single cells) can either be planar or tubular configuration. However, Hino et al. [239] investigated the electrochemical characteristics of these two different configurations and found that the planar SOEC configuration is superior and outperformed its sister tubular design. And this has been traced to more uniform gas distribution coupled with ease of production of the planar cells. For this reason, planar configuration (Fig. 5.3) has been adopted in the design of the cells that make up the stack in the manufacturing process. In manufacturing the SOEC stack for our work, two production techniques are adopted, considering the elemental technique, the quantity of elements, and compounds that form the whole stack. The material technique whereby a completely built component is assembled and analyzed. The 200 MW stack comprises 10000 cell units of 20kW with interconnects arranged to intertwine with the cells to provide electrical connections to the adjacent cells, the electrodes, electrolytes, and the frames. The production process of the stack is diagrammatically represented by the flow chart in Fig. 5.4.

The two electrodes are heterogeneously manufactured, the strontium-doped lanthanum-based perovskites are commonly used as air electrodes, and lanthanum strontium cobalt ferrite (LSCF)

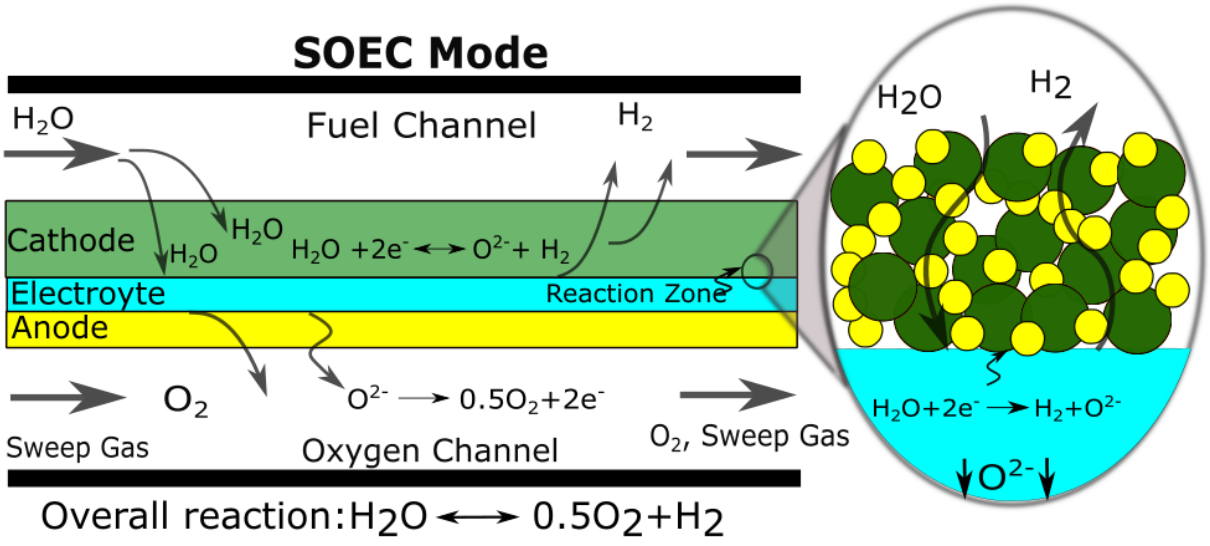

Fig. 5.3: The SOEC cell planar configuration [240]

is used due to its excellent structural stability and high electrochemical activity for Oxygen reduction reaction (ORR) coupled with it high mixed ionic and electronic conducting properties [241]. The hydrogen electrode is a composite of nickel and zirconia and possesses high catalytic activity for hydrogen oxidation, high electronic and ionic conductivity, and stability [242]. In its fabrication, a mixture of NiO and Yttria-stabilized zirconia (YSZ) powders is sintered in air at an extremely high temperature of over 1300℃. The powdered mix of NiO/YSZ is applied in a slurry form on a layer, fired, and sintered to become dense. However, hydrogen is passed over the layer at temperatures above 800℃, reducing NiO to nickel and forming Ni/YSZ [243]. Nickel is the dominating material with 90% weight composition, and for sensitivity and elemental analysis, 100% nickel is also assumed in the manufacture of this electrode. Yttria-stabilized zirconia (YSZ) is used as the electrolyte due to its pure O^{2-} conductivity, high chemical stability, and superior performance [244]. The manufacture of YSZ is on a nanoscale to enhance ionic conductivity, which goes higher to 0.6 S/cm at an operating temperature of 800℃. To manufacture a very thin YSZ, the maximum power of atomic layer deposition must be increased by 150%, producing the thinnest YSZ layer of 1nm [244].

The interconnect is typically made up of chromium steel, as Jeffrey [245] has shown chromium to be an important interconnect component to minimize oxidation in regenerative solid oxide cell operations and avoid reduced efficiency due to ohmic losses. The interconnects are typically

coated with a Co-rich material to prevent corrosion and to shield the air electrode from chromium which has the potential to block the reaction sites. The alumina-based coating is used for the frame to enhance adherence to the steel. All these parts are rigidly joined with silicone and assembled into the stack.

For the analysis, three production scenarios are considered for their impact; the first considered the constituent elements for the materials, and the second considered similar materials with the same properties and activities. The last scenario considers a case of dominant element or materials when you have two mixed elements or compounds, and the composition of one of them is far greater than the other, most especially considering the ease of making them, as shown in Table 5.4.

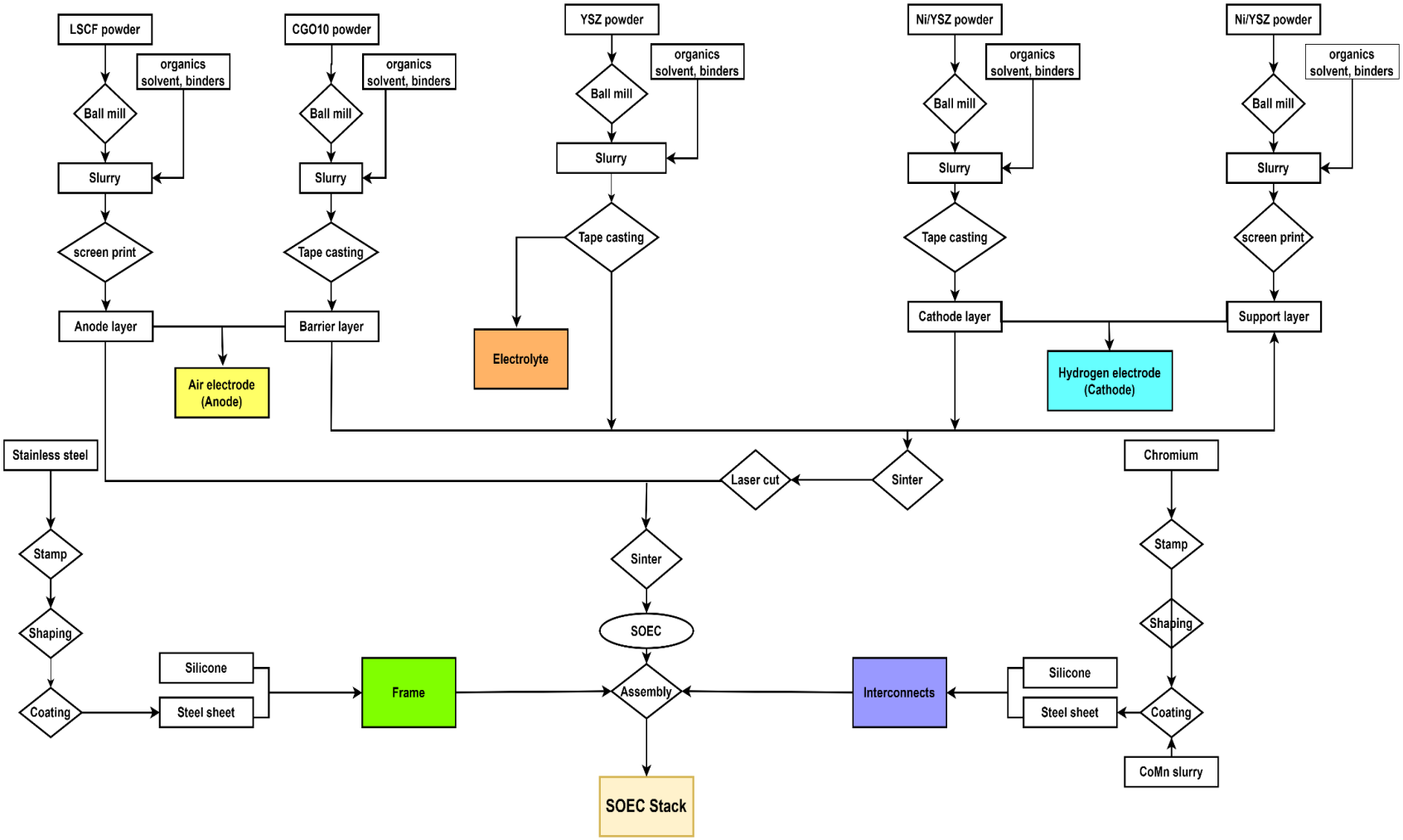

Fig. 5.4: The SOEC stack production process [238]

Table 5.4: A 200MW SOEC manufacturing materials for 10100kg/hr H_2 production (lifetime/FU 15000 hrs/100kg)

	Constituent elements, kg		**Similar compound, kg**		**Dominant compound, kg**
Electrolyte		SOEC R		SOEC T	
YSZ	1192.36		1192.36		
Zirconia, 92%	1096.97	Zirconium oxide	1096.97		
yttrium	95.39	Samarium	95.39		
Cathode					
LSCF	106.61	PrNi	106.61	LSCF	
Lanthanum	60.77	Praseodymium	95.95	Praseodymium	106.61
Cobalt	1.07	Nickel	10.66		
Strontium	40.51				
Iron	2.99				
Oxygen	1.28				
Anode					
Ni/YSZ				Ni/YSZ	
Ni	878.14	Ni	878.14	Ni	878.14
NiO	1444.86			NiO	1444.86
Ni	1437.64	Nickel	1437.64	Ni	1444.86
Oxygen	7.22	Oxygen	7.22		
Interconnects					

Chromium steel	57.69	Chromium steel	57.69	Chromium steel	57.69
YDC	735.06	YDC	735.06	YDC	735.06
Cerium	29.40	Cerium oxide, 90%	661.55	Cerium oxide, 90%	735.06
yttrium	698.30	Samarium, 10%	73.51		
Oxygen	7.35				
Nickel	507.81	Nickel, pure	507.81	Nickel	507.81
LSM	11.22	LSM	11.22	LSM	11.22
Lanthanum	4.49	Lanthanium oxide	5.61	Lanthunum	5.61
Manganese	4.49	Manganese	4.49	Manganese	5.61
Strontium	2.24	Calcium	1.12		
	Constituent elements	Silicone	165.53		

5.4.2.2 Balance of plant (BOP)

The BOP components, which comprise pumps, gas separators, evaporators, coolers, heaters and mixers have easily formed processes that are mostly available in the ecoinvent database except for the separator which is modeled in a separate process in the system using steel metal sheets. The model description of each component is detailed in Chapter 4 of this dissertation. The contribution of each element of the BOP is shown in Fig. 5. The figure shows the environmental contribution of each component to the manufacture of 1 kg of BOP. That is, if all the components are to be put together to form singular BOP of 1 kg. The line thickness indicates the level of impact contributed by a component towards the final product which is the BOP in this case. The separating cylinder has the thickest line and contributes 74.7% of the environmental impact towards the BoP. Followed

by the absorption chiller with 17.3% contribution, then the compressor, heat exchanger and the connecting pipes in the listed order.

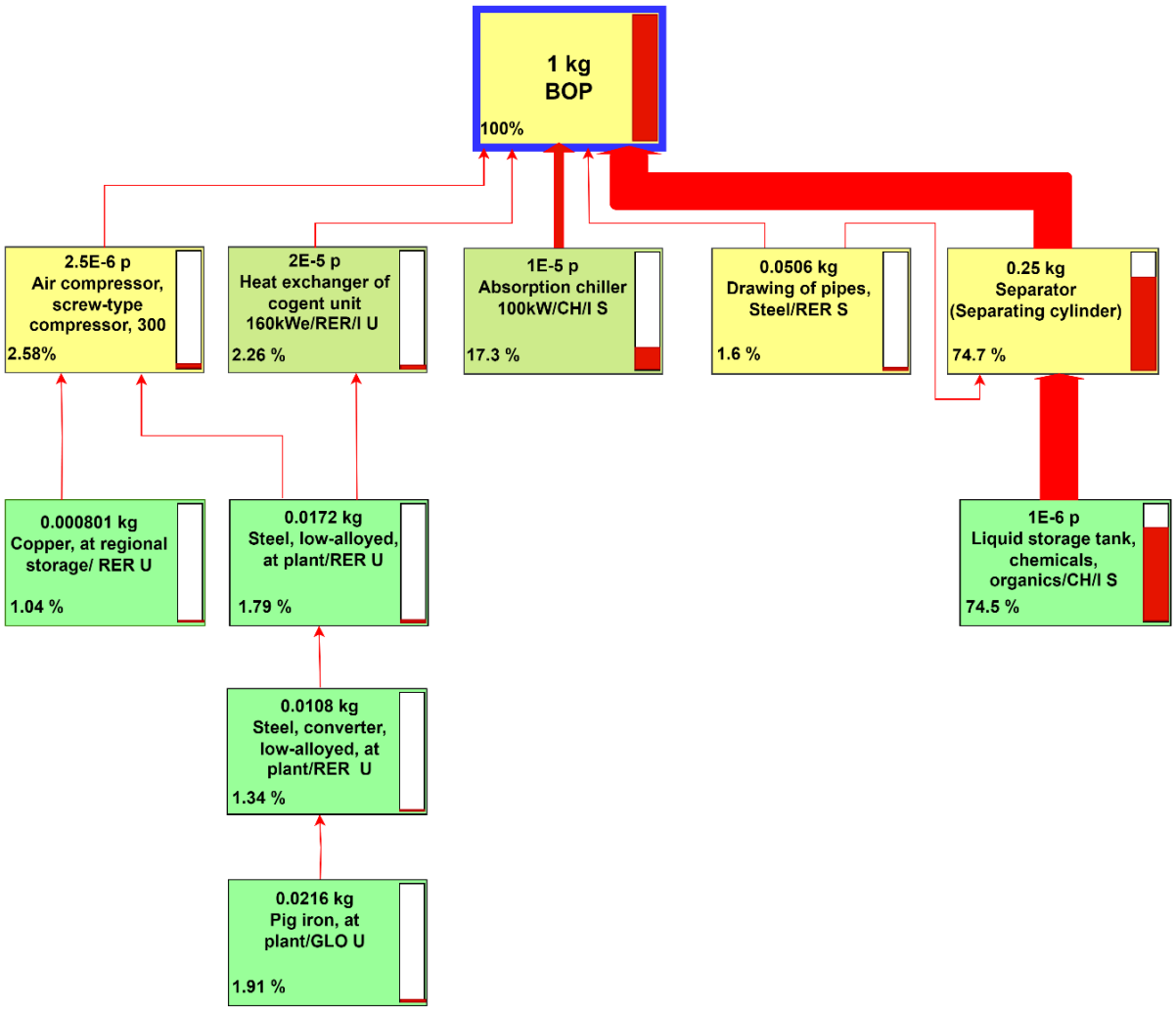

Fig. 5.5: BOP component contribution in the integrated SOEC system

5.4.3 Goal and scope definition

This work aims to evaluate the potential environmental impact of an energy-integrated SOEC system for hydrogen production considered as the base technology. This is then compared with PCEC integrated system to guide government and private agencies on investment decisions and the populace in adopting these technologies. The scope of this work begins with raw materials for the manufacturing of the SOEC and the BOP, and the LCA contains cradle-to-gate as such waste, and material disposal is not discussed, and the decommissioning of the plant is beyond the scope

of this work. Thus, the LCA boundary to this work is limited to the infrastructure for hydrogen production with raw materials and their transport and the hydrogen storage system.

5.4.3.1 Modeling approach

The process-based, attributional LCA modeling method based on ISO standards 14040 is adopted here with 100 kg of dry H_2 functional unit exiting the plant gate in one hour at the atmospheric pressure. The system boundary is restricted to the cradle-to-gate, as demarcated in Fig. 5.1, with the exemption of the plant commissioning and decommissioning. The cradle-to-gate gives and simplify the assessment of the production process from raw material to the finished product (hydrogen) and its use. It accounts for the carbon footprint of the production operation unlike cradle-to-grave that account for the environmental of the whole plant with the equipment. The SimaPro model for the LCA of hydrogen production is based on the modeled facilities in Aspen HYSYS with a 242400kg of hydrogen per day. The SimaPro model replicate the Aspen HYSYS model for the LCA. The LCA here includes the production of the raw materials and manufacturing of the electrolyzer and the BoP, steam generation, and finally, the hydrogen production for 15000 hours.

5.4.4 Lifecycle inventory

The supposed production plant has two internal units- the steam generation unit, which constitutes the BOP, and the hydrogen production unit which houses the SOEC, and an external one which supplies the electricity used in the plant. The steam generating unit supplies 5011 kmol/hr of steam mixed with hydrogen into the SOEC stack which works at full capacity with a 100% conversion thereby producing the same amount of hydrogen as modelled in Aspen HYSYS. The quantities of materials for the manufacturing of the SOEC stack are obtained from literature that relied on industrial partners for their supply [246]. Also, the values of materials for the BOP and the flue gas supply are from Aspen Plus and Aspen HYSYS in the work by Asadi and Kazempoor [165]. The Ecoinvent database is relied on for the emission from the manufacturing process for secondary data and for some processes their data are not easily accessible in the literature like the SOEC. Table 5.4 shows the chemical constituents of each component and equipment. For solar PV, local data in the United States was used from the SimaPro database.

5.4.4.1 Limitations

In the manufacturing of the BoP and the steam generations, some of the chosen ecoinvent data have the disposal of the materials included, which may reflect a slight difference in the natural value as expected. The actual lifetime of the BoP components is more than the reference standard of 15000 hours in this work. The distances for the collation of the SOEC stack components are limited to 100 km. More so, some components not available in the SimaPro database are formulated based on industrial aggregation like the water separator, which might not include some internal resources if produced on an industrial scale.

This dissertation did not discuss the cost of production of SOEC and PCEC even though, their reverse technologies, SOFC and PCFC have been reported to be highly competitive to deliver the same amount of energy. This is because the power density of two SOFCs is almost equivalent to that of three PCFCs. Though, the estimated manufacturing costs for PCFC stacks are evaluated to be approximately 27-37% lower than those of SOFCs [136] of similar size. The analysis of production costs indicates that employing more affordable raw materials in the fabrication of PCFC helps offset anticipated increased costs linked to lower power density and a greater number of cells needed to generate an equivalent amount of power compared to an SOFC stack [136].

However, with the recent improvement in PCFC and PCEC material design with high power density[247], there is a need for manufacturing cost re-evaluation.

5.4.5 Lifecycle impact assessment (LCIA) method

There are several standard impact assessment methods in SimaPro. While each technique has several impact categories ranging from 10 to 20, a more comprehensive one that permits the aggregation of values into a single score is preferred. Also, it is very critical to pay attention to the important elements- classification and characterization- in LCA based on ISO 14040/44, which are the minimum requirements. This study employs the ReCiPe Endpoint (H) as the life cycle impact assessment (LCIA) method and adopts the Europe ReCiPe H/A as the normalization setting. The ReCiPe method is the most recent and updated LCIA approach available for practitioners, it yields a harmonized implementation of cause-effect trajectories for the estimation of both midpoint and endpoint characterization factors [248]. The hierarchist social perspective (H) is adopted due to its common policy principle concerning the period. It is considered the consensus model since it fits most with scientific models and is politically embraced [249, 250].

This method has 17 different impact categories for the classification and characterization, and most of them have been chosen for an in-depth analysis to serve as a reference for subsequent works on LCA. Table 5.5 summarizes these impact parameters and their elemental or substance equivalents.

5.5 Facility overview

For large-scale hydrogen production for public and industrial consumption, the following constraints are set for the hypothetically modeled facilities; the hydrogen production and the steam generation site are not more than 5 km away from an existing coal power plant where they source their feedstock (flue gas) and wastewater reservoir for the same purpose. A huge area of land that serves as the solar farm that houses the photovoltaic technology. It is assumed not more than 20 km from the plant and close to the industrial center where operation and construction can be supported with infrastructure. The United States and North America are perfect match for these set conditions.

Table 5.5: The selected impact parameters and their elemental equivalents [251]

Impact category	**Indicator**	**Unit**	**Characterization factor**	**Abbr.**	**Equivalent Unit**
Climate change	Infra-red radiative forcing increase	$W \times yr/m^2$	global warming potential	GWP	kg CO_2-eq[a] to air
Ozone depletion	stratospheric ozone decrease	ppt×yr	ozone depletion potential	ODP	kg CFC-11-eq to air
Human toxicity	risk increase of cancer disease incidence	-	human toxicity potential	HTP	kg 1,4-DCB[b]-eq to urban air
Photochemical oxidant formation	tropospheric ozone increase (AOT40)	ppb.yr	Photochemical oxidant formation potential	EOFP	kg NO_x-eq to air
Particulate matter	$PM_{2.5}$ population intake increase	kg	particulate matter formation potential	PMFP	kg $PM_{2.5}$-eq to air

Ionizing radiation	absorbed dose increase	man×Sv	ionizing radiation potential	IRP	kBq[c] Co-60-eq to air
Terrestrial acidification	proton increase in natural soils	yr×m^2 ×mo l/l	terrestrial acidification potential	TAP	kg SO_2-eq to air
Freshwater eutrophication	phosphorus increase in fresh water	yr×m^3	freshwater eutrophication potential	FEP	kg P-eq to fresh water
Terrestrial ecotoxicity	hazard-weighted increase in natural soils	yr×m^2	terrestrial ecotoxicity potential	TETP	kg 1,4-DCB-eq to industrial soil
Freshwater ecotoxicity	hazard-weighted increase in fresh waters	yr×m^3	freshwater ecotoxicity potential	FETP	kg 1,4-DCB-eq to fresh water
Marine ecotoxicity	hazard-weighted increase in marine water	yr×m^3	marine ecotoxicity potential	METP	kg 1,4-DCB-eq to marine water
Agricultural land occupation	occupation and time-integrated transformation	yr×m^2	agricultural land occupation potential	LOP	m^2 × yr annual crop land
Urban land occupation	occupation	yr×m^2	urban land occupation potential	ULO	m^2 × yr annual urban land
Natural land transform	transformation	m^2	natural land transformation potential	NLT	m^2 natural land
Metal depletion	ore grade decrease	kg	surplus ore potential	SOP	kg Cu-eq

Fossil depletion	upper heating value	MJ	fossil fuel potential	FFP	kg oil-eq

a eq is equivalents, CO_2 mass equivalent of the emission in kg

b 1,4-DCB is 1,4-dichlorobenzene

c kBq is kilo Bq and the unit Becquerel (Bq) is the number of atom nuclei that decay per second.

5.5.1 Facility description

The assumed production facility is made up of three sites- the energy source site- which is the power plant, an alternative solar farm, and a hydrogen production site. This site is very close to the power plant, which consists of the steam generation plant, the SOEC plant, the compressor, heater, and hydrogen storage tank, as shown in Fig. 5.2. The solar farm is close to the power plant with the plan of a possible integration or merger between the two energy sources, though hypothetically occupying a large area. The distance is not more than 20km, as previously stated, and no sensitivity study on it as this work focused on comparing the extent of damage and impact of the two energy sources. All values and data for the two sources are picked from the ecoinvent, and the United States data is specified. Included processes on the solar farm from ecoinvent: Production mix of photovoltaic electricity in the US. Annual output, Roof-Top: 1390, Annual output, Facade: 839 kWh/kWp. Amount of solar energy transformed to electricity. Waste heat emission due to losses of electricity in the system. Annual output of grid-connected PV power plants differentiated for Roof-Top and Facade plants. Literature data for optimum installation from SimaPro database and not a real performance in the US have been corrected with a factor of 92% according to experiences in Switzerland for average production. The mix of PV plants is based on worldwide average and own assumptions. A lifetime of 30 years is taken into account for the installed PV. And the technology is such that the electricity production with grid-connected photovoltaic power plants is on buildings.

5.5.2 SOEC and balance of plant

a) SOEC- The planar SOEC configuration is adopted as it is superior and outperformed its sister tubular configuration, as investigated by Hino et al. [239]. This has been traced to more uniform gas distribution coupled with ease of production of the planar cells. It also offers the benefit of power (volumetric) densities and low cost of production [252]. This aims to increase the uniform distribution of gas and enhance mass and heat transport in the SOEC [39, 253]. The manufacturing

is detailed in the section below, while the energy requirements are based on the work by Hafele et al. [246].

b) Water Supply: the water here is of two kinds- steam and liquid water used as the stack feedstock for hydrogen production and cleaning, respectively. The water feedstock utilized in the SOEC does not need to be pure owing to its elevated temperature, this makes it easy to use the vapor component in the flue gas from the powerplant as the water source. The extraction of the steam from the flue gas has been detailed in the system description. For the cleaning, which is expected to be used in cleaning the panels, this is incorporated in the data in the ecoinvent from the US data.

c) Pipe System: The pipe is modeled to transport wastewater, flue gas, and steam into the SOEC. Another pipe network is modeled to accumulate the hydrogen and air (oxygen and nitrogen) and transport them for storage and place of use, respectively. The diameters of the pipe are based on the flow volume and heuristic recommendations of economically optimal velocities of various fluids [254, 255]. In our case, the steel alloys are chosen as the piping materials due to some of their distinguishing mechanical properties like strength, durability, and versatility which are factors for determining the longevity of their operation [256, 257]. This selected for implementation dataset describes the energy consumption and the emissions linked to the transport of 10 tkm average natural gas in Europe.

d) Electricity Transmission System: The dataset used in simaPro represents the construction of the infrastructure (poles, cables, transforming substations, etc.) of the electricity high voltage transmission network in Quebec. This dataset is based on the study on the production, transport, and distribution of electricity in Quebec in the 2008-2013 period. It represents the total of all the infrastructures that belong to Hydro-Quebec, which is the only transporter and distributor of electricity in the region. The inventory is based on all the transport lines and substations of the company. In 2012, the network, which includes the high voltage, counted 33911km of lines and 516 transforming substations divided into four classes: two transforming from very high voltage (735 kV-315kV) and two transforming to medium voltage (315 kV- 25kV). Lifetime is assumed to be between 75 and 50 years depending on the infrastructure and the material (50 years for transforming substations and 75 years for poles). However, for this work, the transmitting distance has been limited to 20 km, as previously stated.

e) Compressor and Storage: To aid the electrolysis reaction, the ambient air is compressed and transported to the SOEC, and likewise the compressed hydrogen product is stored in site-specific pressure vessels. A piston compressor model is assumed due to its prevalence of use, availability, and optimum design to reduce friction loss [258], nevertheless, screw-type compressors can also serve the same purpose as adopted in simaPro. The electricity consumption of the compression depends mainly on the respective pressure stage. The pressure stages 7 bar, 10 bar, and 14 bar, which are usual, are modeled, but the 7 bar is adopted due to low pressure operation. The power consumption values are based on average industrial data verified with literature data as used directly from ecoinvent. The storage tank is made up of 304 stainless steel resistant to hydrogen degradation or reaction at ambient temperature [259]. Since the size of the pressure tank is not critical to LCA, the geometry in the work by Graham et al [235] is used.

5.6 Source of energy

The energy source baseline scenario for the modeling is thermal to hydrogen, however, the system is designed such that it can work with varying energy sources, most especially renewable sources, including solar and wind, which is projected to grow by 50% in the next 30 years [260]. The integrated model works with energy from a bituminous coal power plant where it sources its water feedstock as this approach is cost-saving. Likewise, a hypothetical solar farm that houses a photovoltaic system is designed close to the power plant, where it serves as an alternative energy source. In designing the energy sources for analysis, the ecoinvent database is heavily used to account for the required parameters in SimaPro. The degree of damage using these sources is compared, more to be discussed in the result sections.

5.7 Comparison between the SOEC and PCEC

The SOEC is considered the base technology and used for the previous analysis. For balance comparison between the SOEC and PCEC technologies, the PCEC is used in place of the SOEC for the same integrated system. So that a step-by-step comparison is carried out from manufacturing to operation. Similar method used in the manufacturing of SOEC stack mentioned in section 5.3.2.1 is also adopted for PCEC of the same weight with different membrane electrode assembly (MEA) compositions. The MEA component for the PCEC is highlighted in Table 5.6. The PCEC stack is subjected to the same analysis as the SOEC stack as previously explained. The PCEC operates at far lower temperatures compared to the SOEC and as such its BoP components

require moderate temperature resistant materials which reduces their cost. There is no head-to-head comparison of the BoP components for both technologies as it is obvious the PCEC BoP components accrue more benefits for the system both economically and environmentally. Because the carbon footprint of manufactured special materials most especially those that can withstand high temperatures is higher compared to lower-temperature materials. Thus, the comparison focus for the two technologies in this dissertation is on their manufacturing and operations.

Table 5.6: PCEC stack manufacturing components and their constituents [136]

Component	Constituents
Anode (Ni-BYZ20)	Zirconium oxide
	Nickel
	Barite
	Oxygen
	Lanthanum oxide
Electrolyte (BYZ20)	Zirconium oxide
	Barite
	Oxygen
	Lanthanum oxide
Cathode (BCFZY0.1)	Zirconium oxide
	Barite
	oxygen
	Lanthanum oxide
	Iron sulfate
	Cobalt

5.8 Results

5.8.1 Net energy analysis

For higher system efficiency, there is a need for energy optimization and integration. Aspen Energy Analyzer (AEA) is used to estimate the potential energy savings that can be accrued from

this system model design, and this amounts to a total energy savings of 28.61% for the SOEC system, this is well depicted in Fig. 5.6. The real utility energy in the built model in Aspen HYSYS is termed actual as can be seen in the Fig. 5.6 for the heating and cooling utilizes. The AEA sum up all the heating utilities and does the same for the cooling utilities. After heat integration and recovery estimation by the AEA, it gives the optimum potential target values that will reduce energy use among equipment. The AEA uses the insight and energy-saving approach provided by pinch technology. There is a potential of saving 19% and 58% amount of used energy for the heating and cooling utilities respectively. Another significant advantage of this energy maximization other than lower cost is the negative carbon emission that can be achieved, which accrues to 28.61% as shown in Fig. 5.6. All the values are detailed in Table 5.7. The actual energy values in the figure and table indicate the real operational value in the simulated model and the target shows the minimum obtainable value for the system model if heat integration or energy optimization is carried out.

Table 5.7: System model potential energy savings

Property	**Actual**	**Target**	**Available Savings**	**% of Actual**
Total Utilities (GJ/h)	2156	1538	617.4	28.61
Heating Utilities (GJ/h)	1621	1312	309	19.03
Cooling Utilities (GJ/h)	534.7	226.3	308.4	57.67
Carbon Emissions (kg/h)	120500	86000	34470	28.61

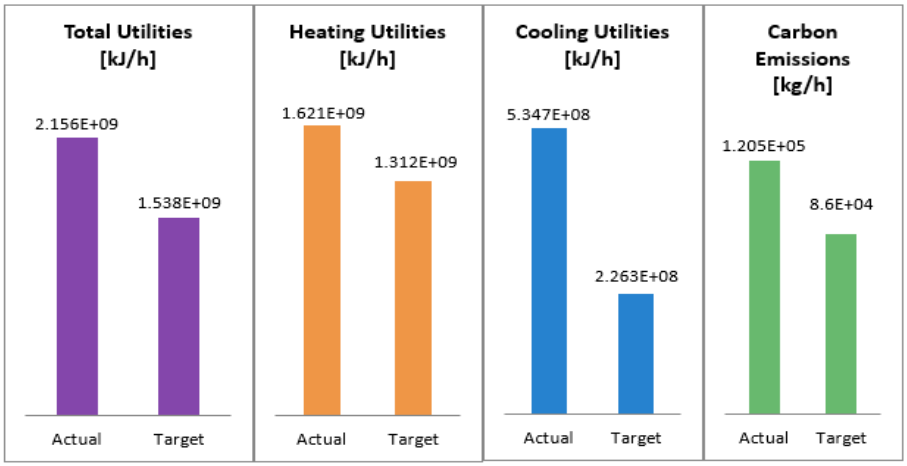

Fig. 5.6: System energy savings potential

There are several energy sources provided by the US DOE in the H2Analysis tool for for the cost analysis. The thermal energy source is chosen as the base source in this work, most especially to fulfill the BOP components energy demand for steam generation. Consequently, the thermal energy base is to estimate the system performance and given as,

Thermal Efficiency of SOEC system

$$= \frac{\text{Lower Heating value (LHV) of the produced hydrogen}}{\text{Total energy input into the system}} * 100 \quad (5.5)$$

On a base-case condition, the thermal-to-hydrogen (TTH) efficiency is 56% using equation 5.5. The annual energy balance for the steam generation and hydrogen production in the facility is shown in Fig. 5.7.

The system can generate an equivalent energy of 0.34 GW continuously for a span of a year, estimated from its energy content of the produced hydrogen of 10.62 PJ. The power consumed by the process for the mass-produced hydrogen is lower compared to what is obtainable in work by Graham et al. [235] for the same amount of hydrogen; this shows the opportunity and the prospect of this technology. Other than the SOEC operation, which is the largest energy consumer with 10.9 PJ annually, the condenser is the second highest single energy user with an annual usage of 4.68 PJ for condensing the flue gas from the power plant. This energy use can be reduced by almost 800% if a cheap technology is used to separate the water vapor content from the flue gas from the plant or even completely avoided and directly used in the system. The heaters also required a significant amount of energy (3.23PJ per year), while other facilities required low energy for their continuous operation. On an hour base condition, the heating and cooling utilities for the operations (steam generation and hydrogen production) are 1.621 TJ and 0.535 TJ, respectively, giving total utilities of 2.156 TJ, equivalent to the emission of 120500 kg of CO_2. However, with energy management and heat integration, a 19% reduction in the heating utilities and a 58% reduction in the cooling requirement is achievable. This reduces the carbon emission to 86000 kg and 28% savings on the total utilities and CO_2 emission, as shown in Fig. 5.8. However, comparing the energy usage during operations in both technologies, PCEC operates at 500℃ and SOEC at 850℃. Fig 5.9 shows a head-to-head comparison of energy usage and carbon emissions in Fig 5.10. It can be seen from Fig. 5.10 that using PCEC for the same operation reduces carbon emissions by 33.7% which is highly valuable for the process.

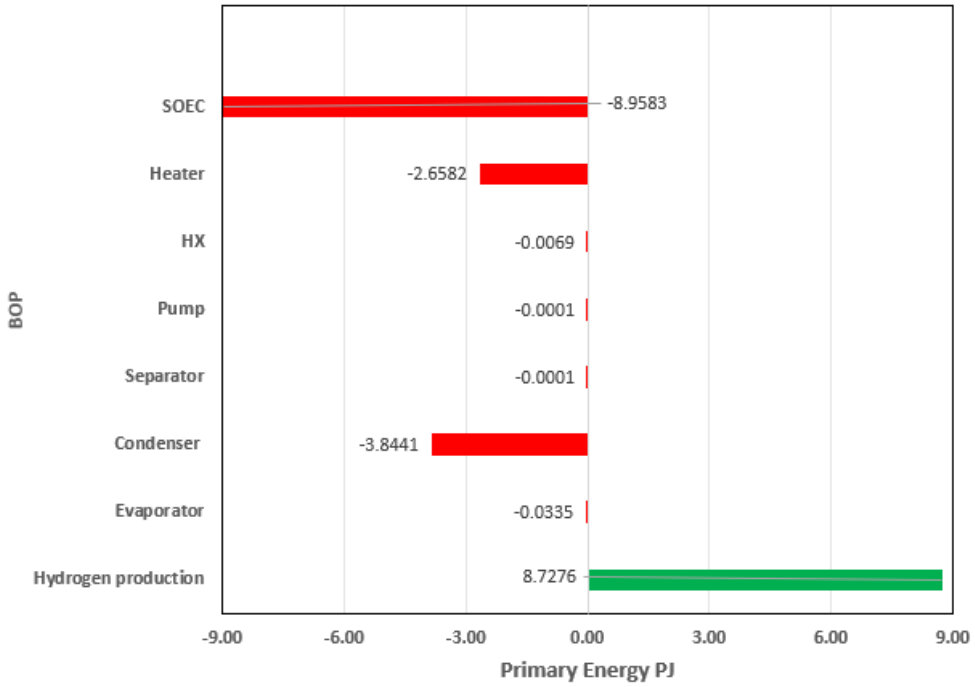

Fig. 5.7: Annual energy balance for hydrogen production. The red bars show the consumed energy by the BoP components and the green bar is the energy content of the produced hydrogen

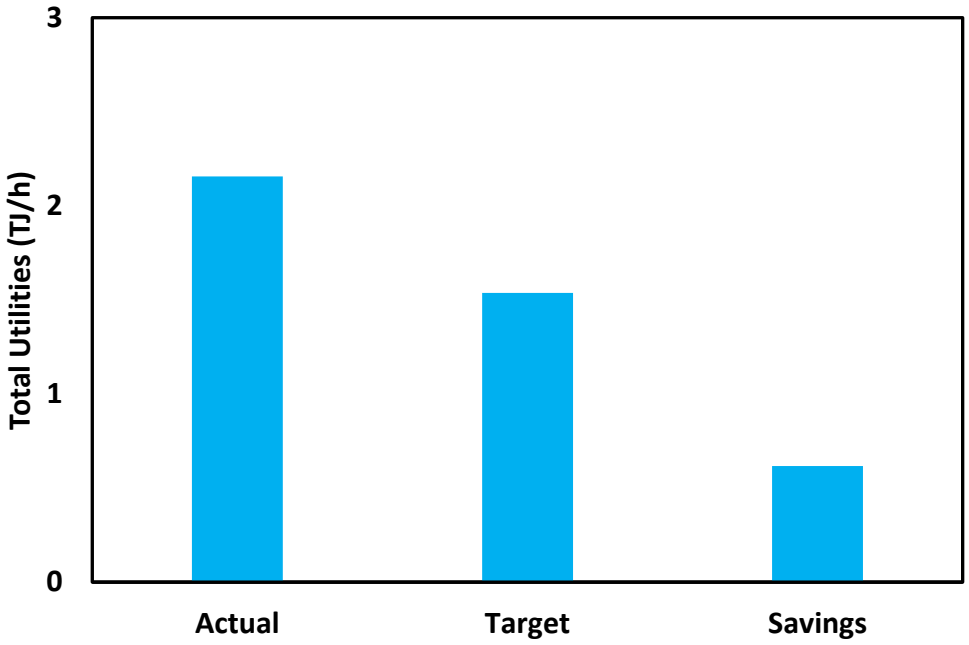

Fig. 5.8: The energy and emission savings potential of the system

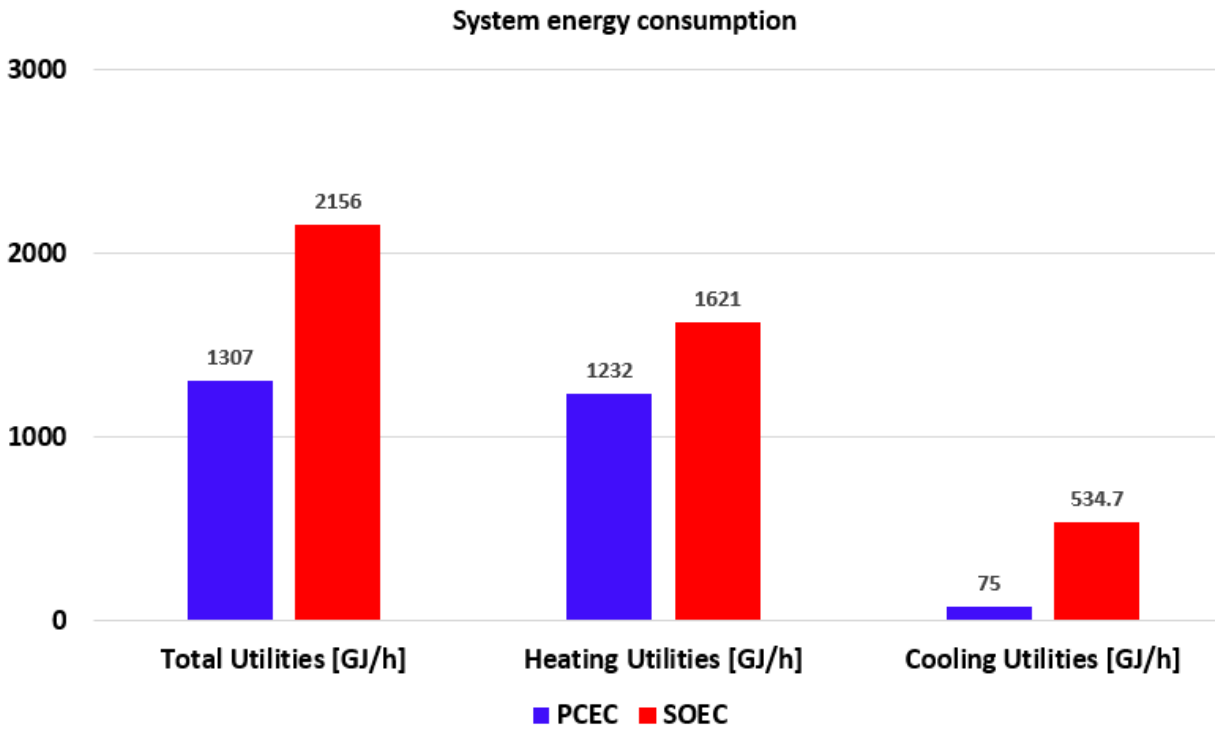

Fig. 5.9: Integrated system energy consumption with PCEC (purple) and SOEC (red)

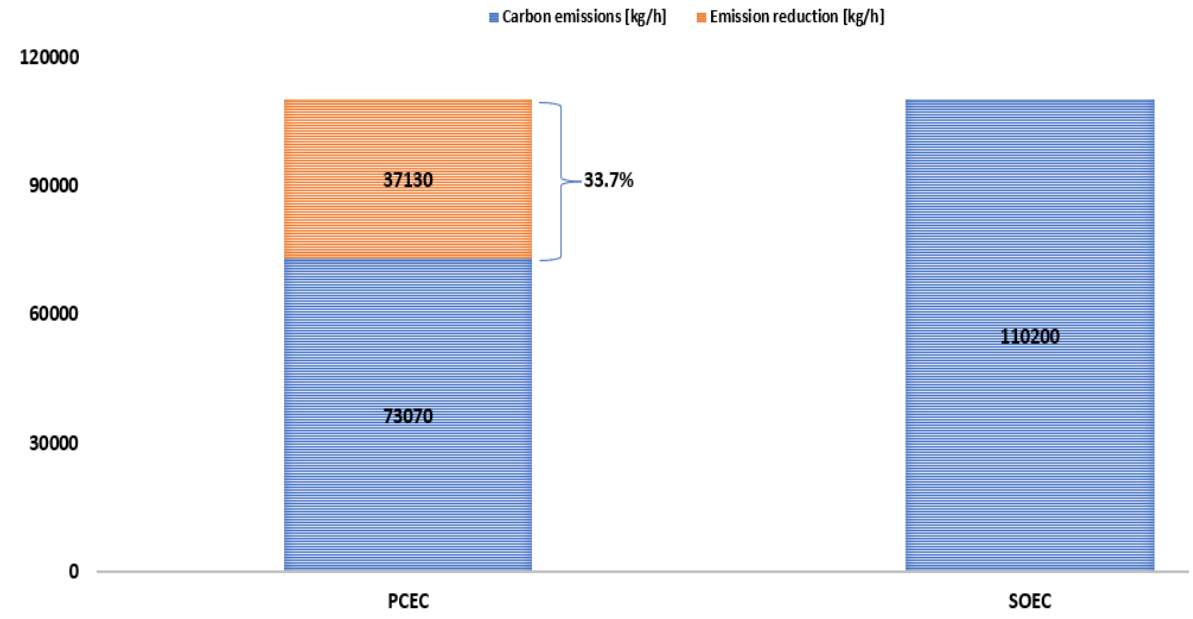

Fig. 5.10: Carbon emissions during operations by PCEC and SOEC

5.8.2 Economic analysis

5.8.2.1 Cost analysis

The levelized cost of hydrogen production (LCOH) involves assessing both capital and operating costs in the hydrogen production process per unit quantity of the produce hydrogen. It varies across different types of hydrogen, and it is important to note that LCOH does not encompass costs related to hydrogen storage and transportation. The LCOH is a metric denoting the cost of producing one kilogram of hydrogen (usually green hydrogen). Explicit cost outlines for the system considered in this work are given in section 5.1. Thereby, the DOE H_2 analysis tool and Aspen HYSYS-built Excel sheet are used to estimate the levelized cost of hydrogen for this system which gives \$3.13 and \$3.16 per kg of the produced hydrogen using the SOEC and \$2.88 and \$2.9 per kg H_2 with PCEC. Fig. 5.11a and b illustrate the result and the expenditure contribution. However, if the cost of energy for the photovoltaic technologies is met at the DOE target of less than 3cents/kWh [261], this leads to a significant drop in LCOH to about \$2.9/kg H_2 and \$2.5/kg H_2 for both SOEC and PCEC respectively. The operating temperature of the SOEC stack is 850 °C and 500°C for PCEC stack. The SOEC and PCEC operating cell potentials are 1.247 V and 1.191V respectively, and their current density is 0.3A/m^2 in all cases**.** The cost of carbon sequestration is not included in our estimates, but comparing our results to a lot of recent works [201, 232, 262] on hydrogen production, the LCOH here is cheaper, which shows this production pathway seems to be more promising and viable. It is worth noting that the effect of the different electricity feedstock on the final LCOH is because of the cost of varying electricity sources.

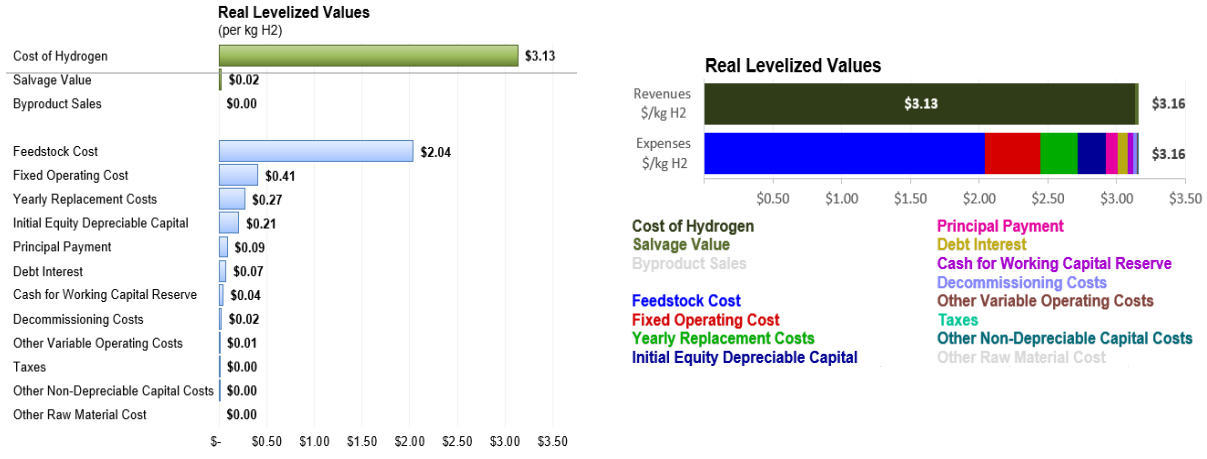

(a)

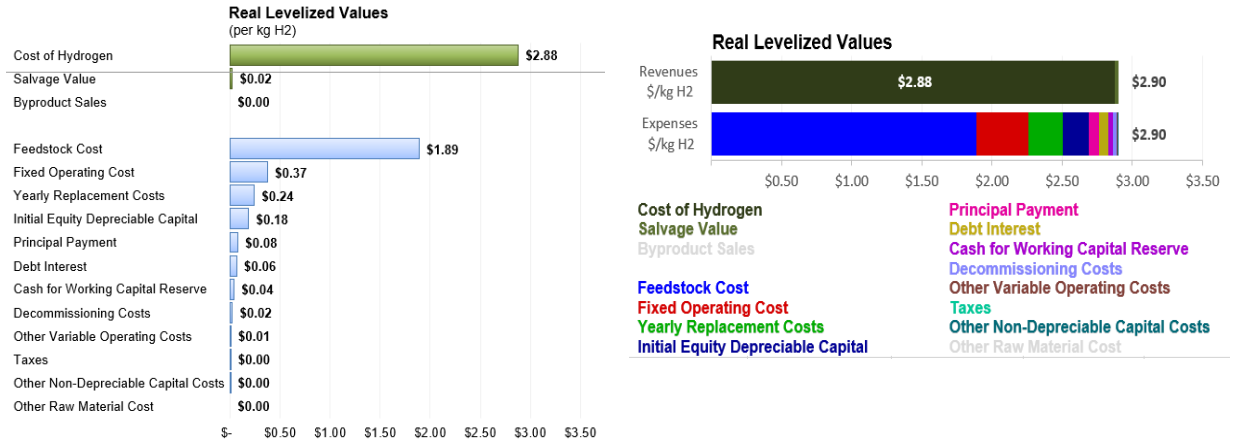

(b)

Fig. 5.11: Levelized cost of hydrogen analysis (a) SOEC (b) PCEC

To better understand the effects of various operating parameters on the cost of hydrogen, a parametric study is carried out using only SOEC at the same operating conditions considered in the technical analysis sections. Since SOEC is the base case and there are lots of similarities in their operation, so similar trend is expected.

5.8.2.2 Sensitivity analysis

Sensitivity analysis in this section discusses the effect of some parameters and their influence on the levelized cost of hydrogen. To actualize this, all other parameters are kept constant save for the one understudy. However, it is assumed that in the base case, energy is from the 334 MW coal power plant where the flue gas is sourced and a thermal utility which is used for the heat systems. The power plant provides the electricity used. Detailed explanations on each parameter are the following. For the parametric studies, SOEC is chosen as the reference case as it is expected that the LCOH will show similar response for both SOEC and PCEC, but the degree of responsiveness to the parameters might differs.

5.8.2.3 Effect of current density on LCOH

Fig. 5.12 shows the relationship between the current density and the cell potential in the V-I characteristics curve and the hydrogen production rate with current density. The linear relationship between the current density and hydrogen production rate shows that the higher the current density,

the higher the H_2 production, as shown in Fig 5.12b. This implies a notably higher electrolyzer-specific cost at a lower current density [263]. For investment decisions, an optimized current density should be applied to achieve a minimized cost of production. A balance needs to be reached between low capital expenditure and high efficiency.

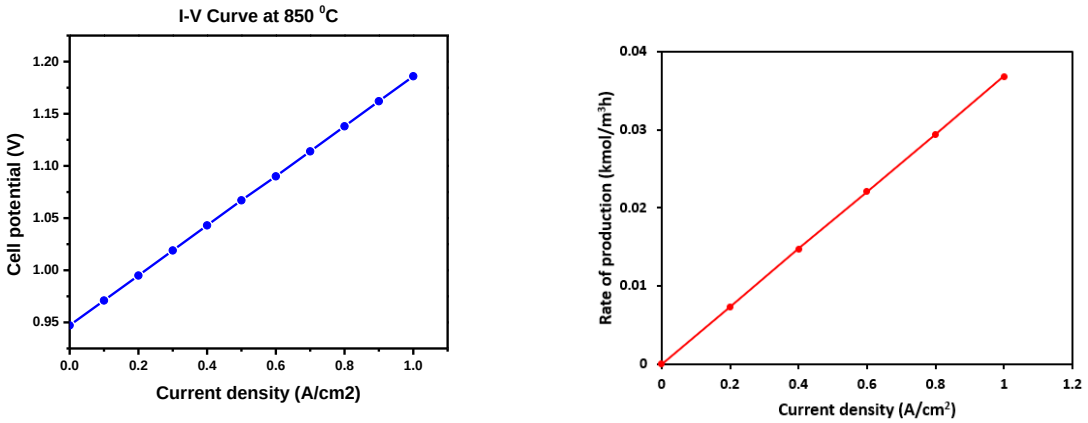

(a) (b)

Fig. 5.12: (a) Polarization curve for the HT SOEC system (b) Effect of current density on the hydrogen production rate

5.8.2.4 Effect of operating temperature

The effect of temperature on the LCOH is not significant, as portrayed in Fig. 5.13a. As expected, if there is an increase in temperature, there is an increase in the thermal energy demand of the system, which causes an increase in the capital and O&M cost. From the performance analysis, a temperature of 800-850°C seems to be the best operating condition for this system. While the higher temperature might increase the module efficiency, it increases the system degradation and shortens its longevity. The optimum temperature in this case is to minimize the cost of hydrogen production, high efficiency, and long service life.

5.8.2.5 Effect of operating pressure

The effect of pressure on the rate of hydrogen production is shown in Fig. 5.13b. This is an indirect assessment of the impact of pressure on LCOH. The rate of production increases with an increase in pressure, with the pressure limit for this system being 7MPa. However, an optimum balance

needs to be reached between higher production rate and cost as higher pressure will increase the capital cost to withstand its effect.

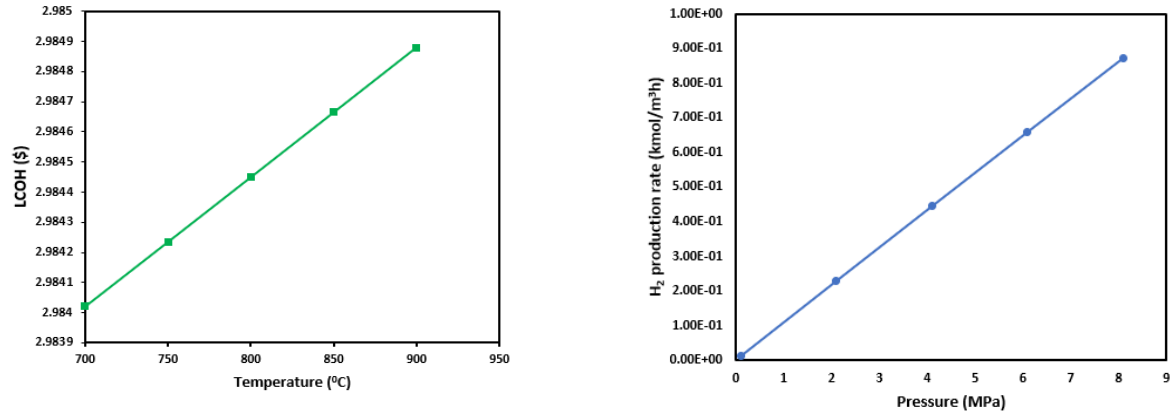

(a) (b)

Fig. 5.13: Effect of a) temperature on LCOH and b) pressure on the hydrogen production rate

The impacts of using several renewable energy sources on the economic performance of the system are evaluated in the sensitivity analysis.

5.8.2.6 Effects of feedstock

This system energy demand is shown in Fig. 5.14. The feedstock cost is currently the highest contributing cost factor to the LCOH, which is almost 41% of the base case cost.

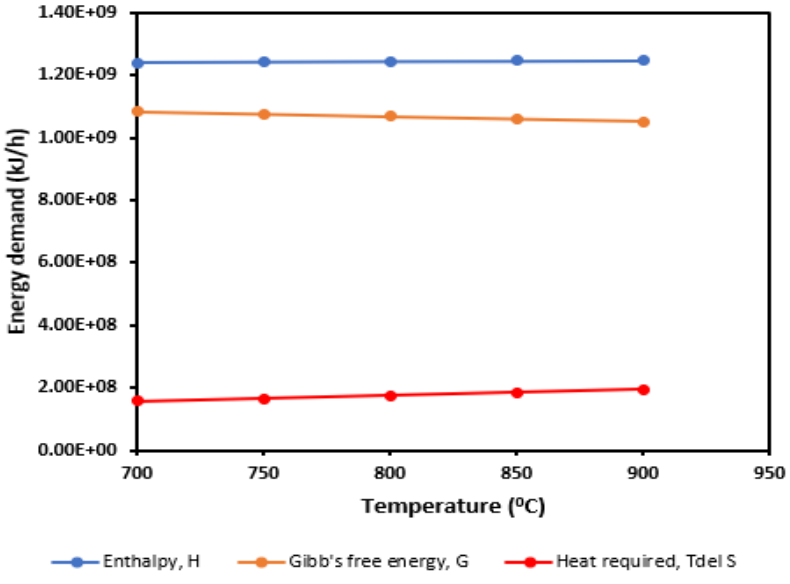

Fig. 5.14: H_2 production energy requirement during water electrolysis

There are two energy systems used in this work, the heat and electricity systems. The heat supplied is 37% of the total required energy, and the electricity made up the balance. The total energy required for the system is 53.7 kWh/kg H_2. Having the thermal utility as a base case for 20 kWh/kg H2, Fig. 5.15a shows the LCOH from different electricity feedstock. In this analysis, different feedstock from the DOE H_2 tool, which could be considered as an alternative, are used, and solar PV. As there are some other feedstocks that are totally off the target and are not worth the consideration, as depicted in Fig. 5.15b. From the chart in Fig. 5.15a, solar PV seems to be giving the lowest LCOH of \$2.99/kg H_2 based on the DOE target of LCOE of 3 cents/kWh for solar PV by 2020 and beyond [264]. It is important to note that this system is designed to fit in for the cheapest source of energy, and with the advancement in renewable energy, there are more renewable sources and a drop in their price, which is very promising for this type of system. Thermal utilities, TU, also shows a better LCOH of \$3.13 per kg Hydrogen, which is the second most admirable in the list and is the base case cost. It is noteworthy that the reduction in the cost of feedstocks is key to the competitiveness of a SOEC system and a similar case is observed by Reytier et al [265] in their work when they compare the LCOH of the SOEC system to PEMEC and AEC systems.

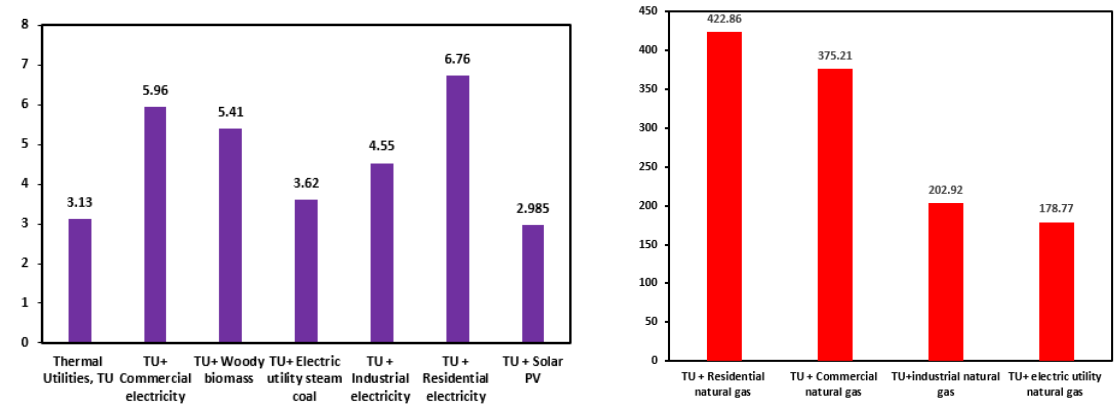

(a) (b)

Fig. 5.15: a) LCOH (in \$) from different feedstock b) LCOH Off-target feedstocks

5.8.2.7 Effect of compressor efficiency and BoP cost

The efficiency of the compressor has a significant influence on its cost, which is invariably the BoP cost. The BoP cost has been combined in this section because it has similar effects as the efficiency of the compressor. It can literally be said that the cost of the BoP is what is causing that

effect, as shown in Fig. 5.16. In Fig. 5.16a the efficiency of the compressor is varied with the LCOH and shows it is directly proportional, and the optimum efficiency is shown to be around 80%. Fig. 5.16b shows the influence of the SOEC module cost, which seems to be very significant. The high cost of the module increased the capital cost, which translates to an increase in the LCOH. If the capital cost is reduced, a proportional decrease in the O&M cost and higher electricity efficiency is observed. To achieve this, there is SOEC component development is required, which will also improve the performance level of hydrogen production.

5.8.3 LCA result interpretation and discussion

As mentioned earlier the SOEC stack technology is the base case for the analysis in this chapter of the dissertation, it is also adopted in this section. Since it has been established in section 5.7.1 that using PCEC reduces carbon emissions when compared to SOEC which is mostly attributed to the energy requirements. Thus, it is rational to deal with SOEC knowing well that PCEC gives a positive and greener outcome. The baseline scenario for greenhouse gas (GHG) emissions from the BoP components operations is shown in Fig. 5.17.

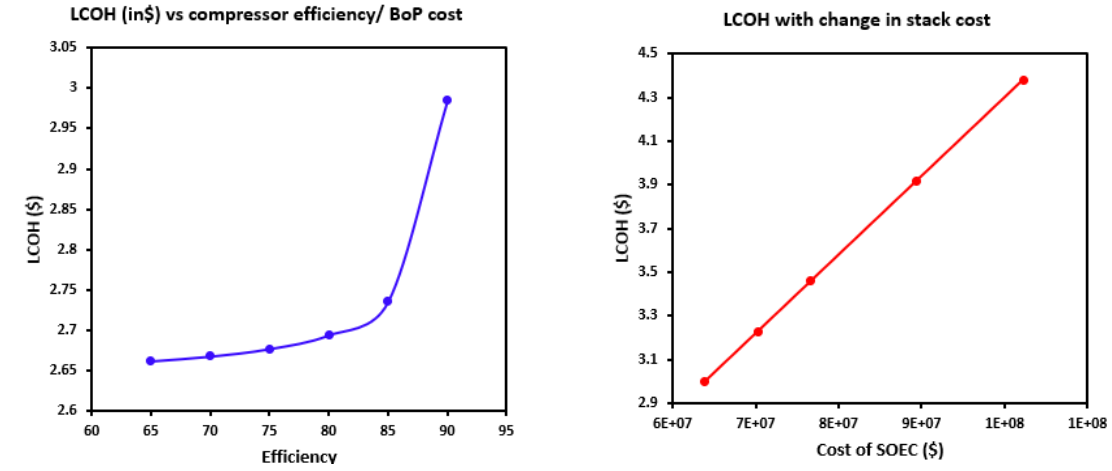

(a) (b)

Fig. 5.16: Effects of a) compressor efficiency/ BoP cost and b) SOEC cost on LCOH

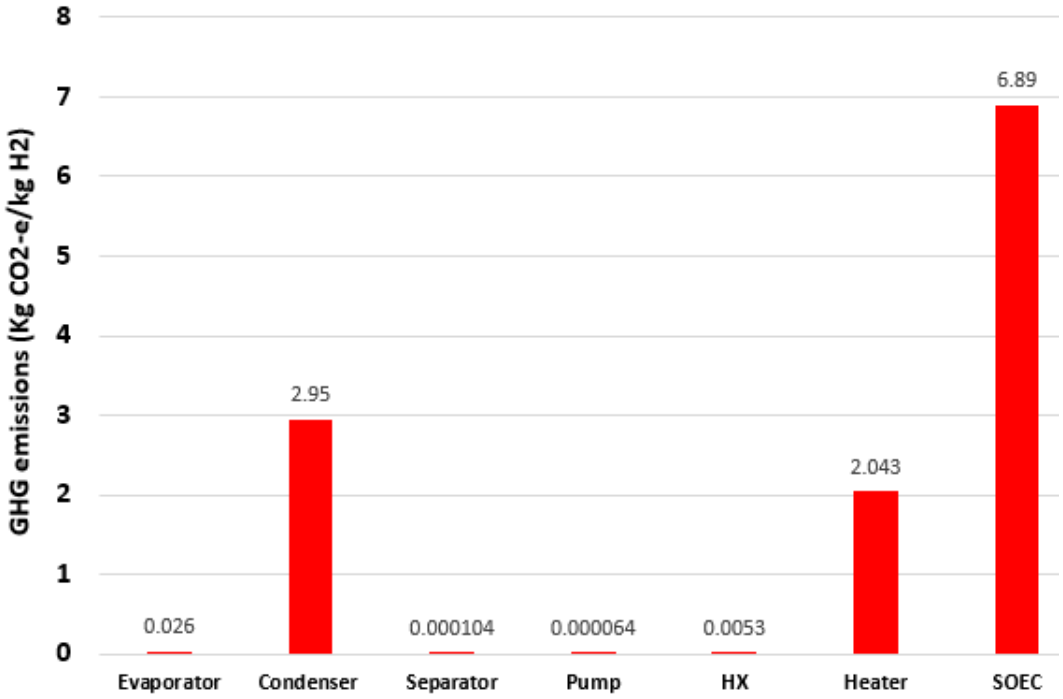

Fig. 5.17: GHG emissions for the thermal-to-hydrogen scenario

The explanation of 17 life cycle impact assessment (LCIA) parameters for the steam electrolysis for hydrogen production is presented in Table 5.5. The ReCiPe 2016 (H) LCIA method is used for this study. The characterization results for hydrogen production from the SOEC integrated system using both photovoltaic and coal power plant electricity sources are shown in Fig. 5.18a and 10 b.

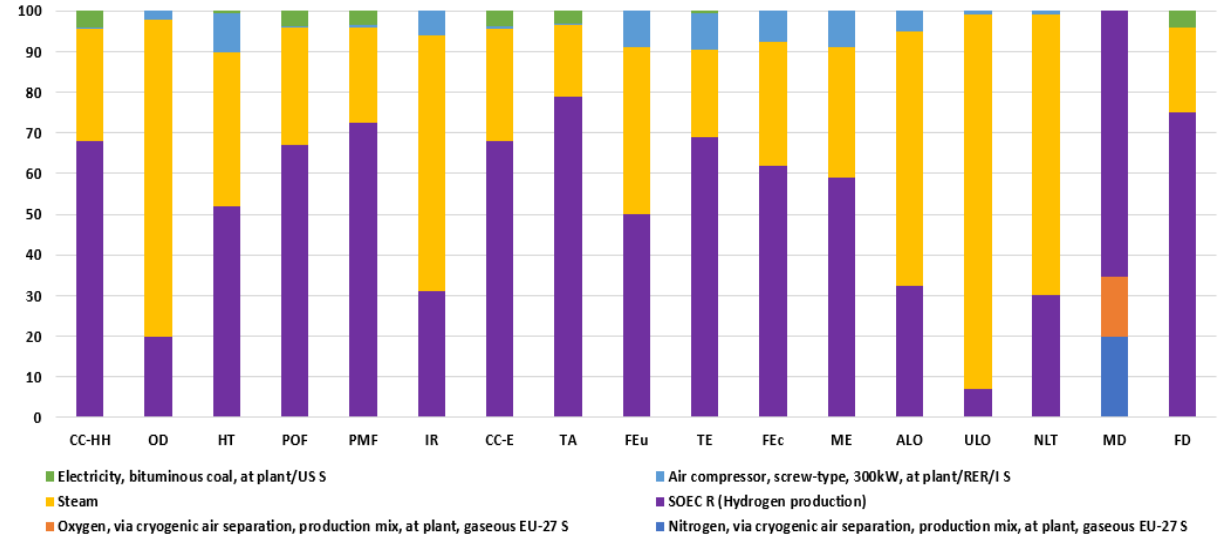

(a)

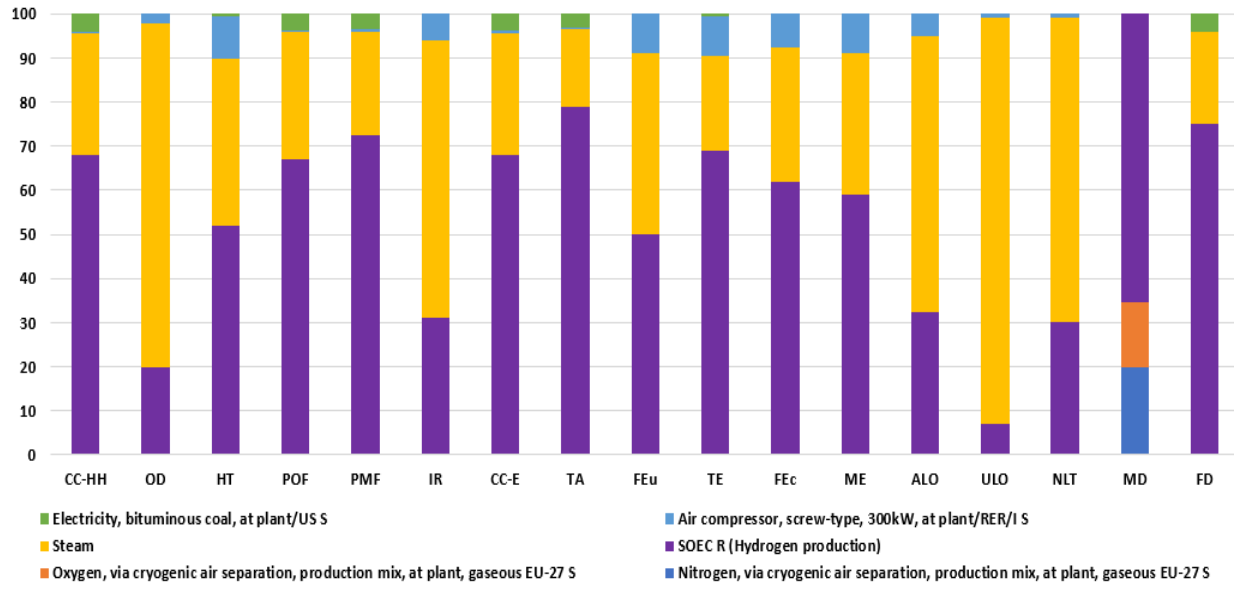

(b)

Fig. 5.18: Characterization result for hydrogen production with different energy sources a) photovoltaic b) bituminous coal power plant

For the two scenarios in Fig. 5.18a and 5.18b, it is obvious that the steam generation and the manufacturing of the SOEC have a very high environmental impact potential on the system. The bulk of the impact of the SOEC arose from the harmful manufacturing materials needed to withstand the high operating temperatures, with a similar trend observed by Schmidt et al. [266] and the electricity consumption for the manufacturing process. Of more significant concern is using fossil fuel in powering the system as the impact is greatly pronounced in all sections of the system compared to using a renewable energy source like the photovoltaic system in this work. This effect can be observed in the manufacture of the SOEC, as shown in the analysis presented in Fig. 5.19, and the same is observed in Fig. 5.18 when comparing the two scenarios. While a lot of LCA studies have excluded the BoP components from their work, it has been included here with extra components due to its being a new technology. The manufacture of the BoP components poses a great environmental impact, most especially on the metal depletion level due to the large amount of steel required to manufacture the separator.

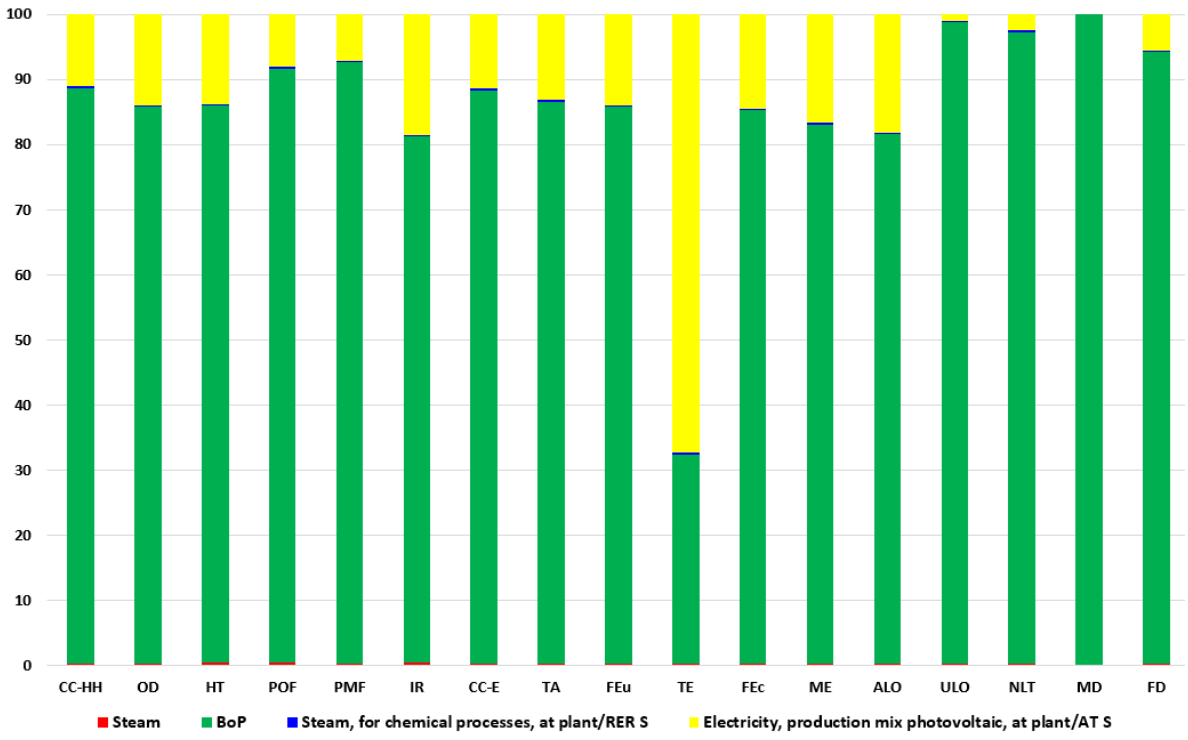

Fig. 5.19: Effect of BoP manufacturing on steam generation

A head-to-head comparison of the impact of the electricity used for the electrolysis reaction is shown in Fig. 5.20. The endpoint parameters that allow for the final damage estimate to human health, ecosystem, and resources are used to compare the impact of the two sources. The damaging impact of the coal power plant is over 400% of using photovoltaic in each case but more than 700% on average.

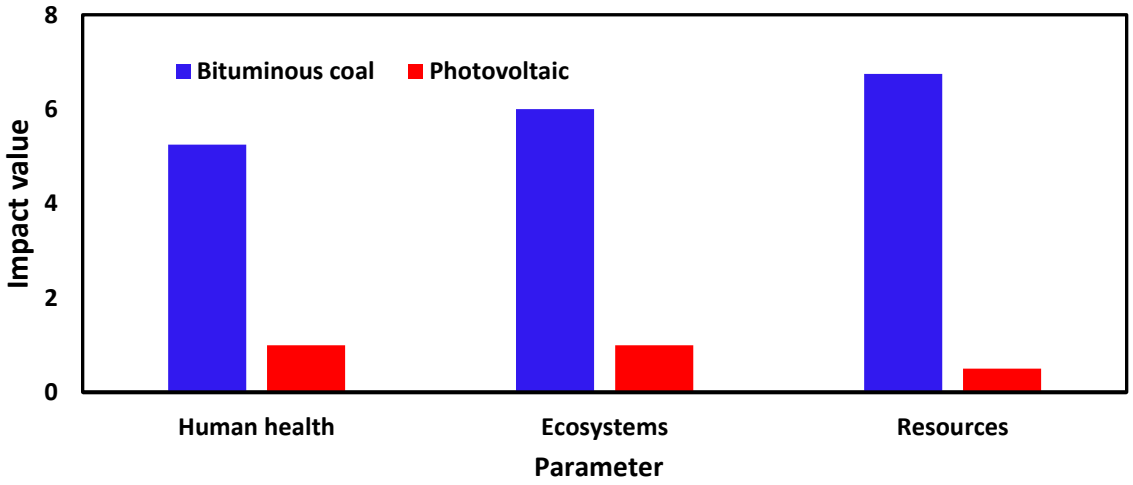

Fig. 5.20: Comparing the Electricity Damage Impact

The ReCiPe endpoint is also applied in analyzing the impact of the energy sources on the SOEC manufacturing process; this allows to expression of the total damage assessment by grouping the impact factors in terms of human health (having the unit Disability Adjusted Life Year (DALY)), ecosystem measured by loss of species within a year (unit is species. yr) and resource scarcity (in US Dollars (USD)). Fig. 5.21a-c shows the graphical representation for all three cases and the energy sources for the SOEC manufacturing process.

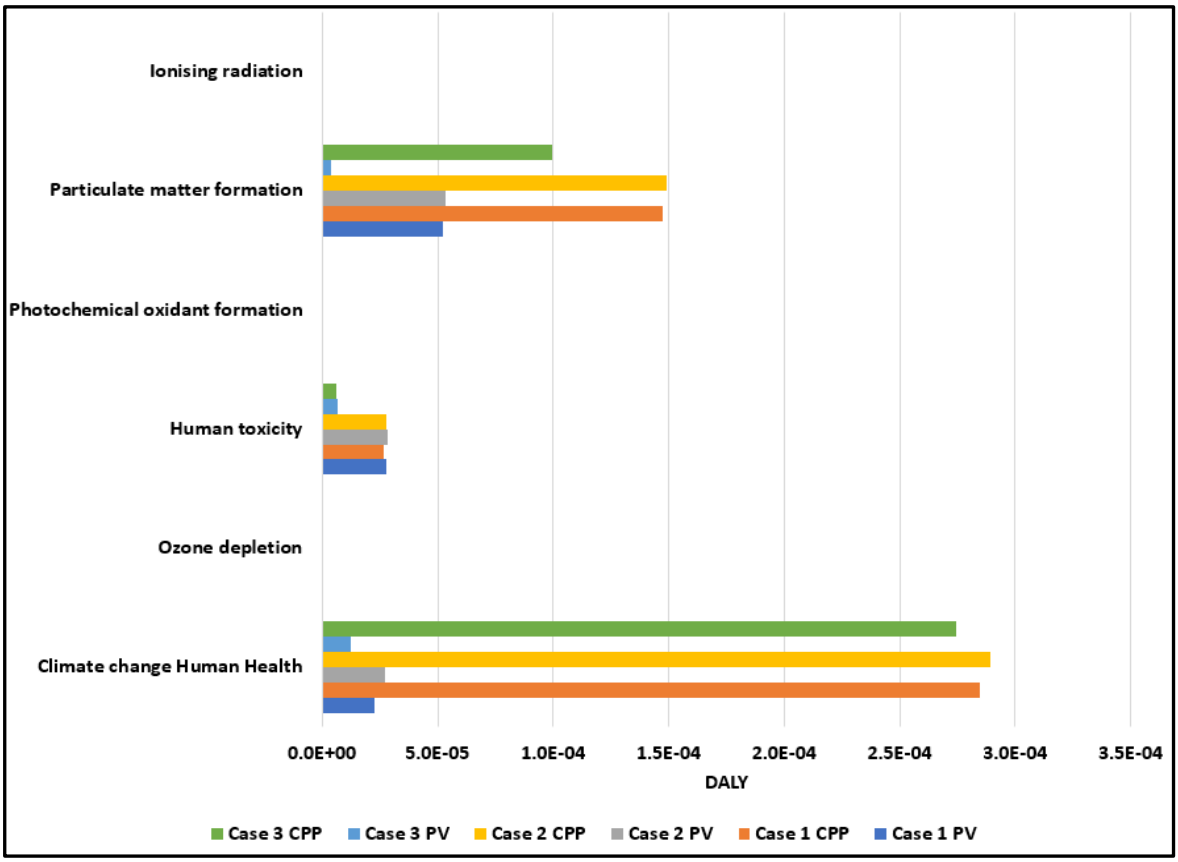

a) Human health

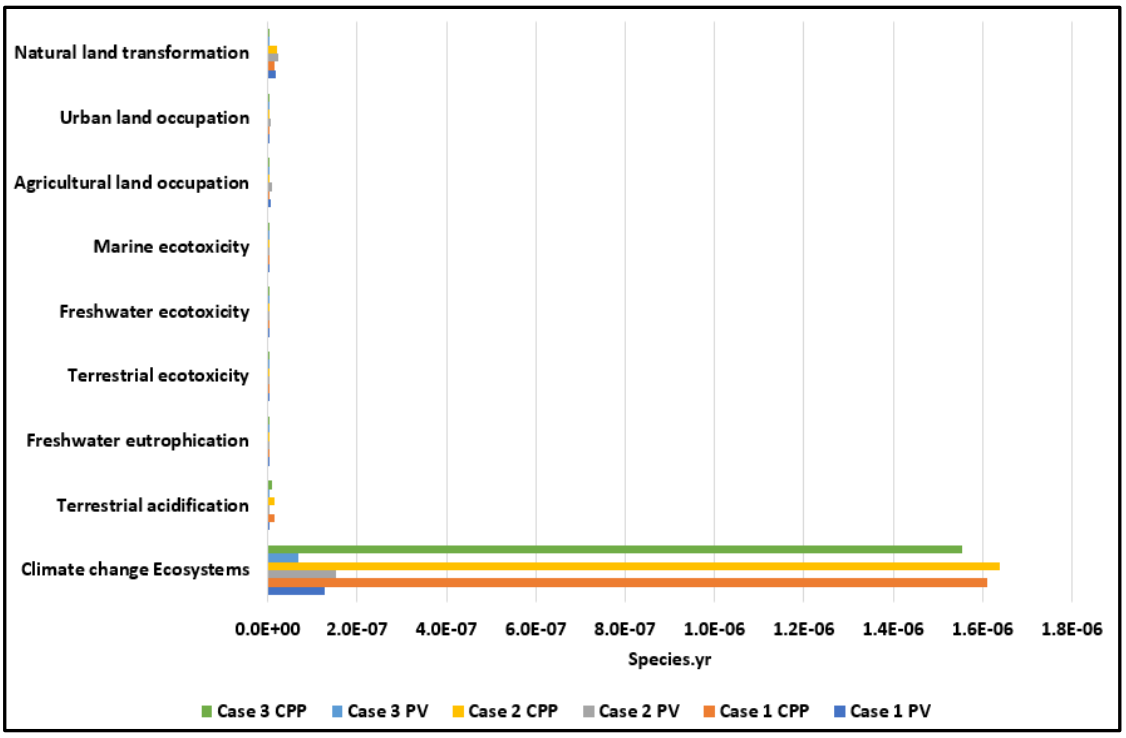

b) Ecosystem

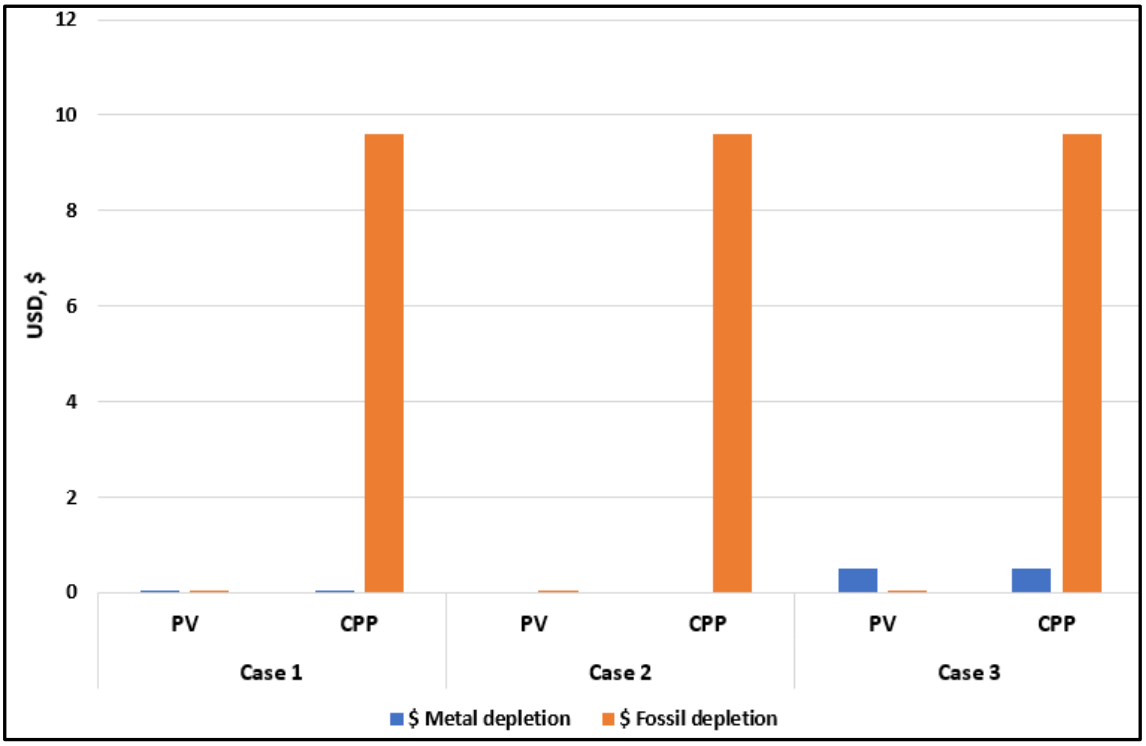

c) Resources

Fig. 5.21: Analysis of all three cases and the energy sources for the SOEC manufacturing process. Case 1: constituent elements Case 2: similar compounds Case 3: Dominant elements

As expected, the bituminous coal power plant has the greatest impact in all three cases. However, for the three endpoint cases, human health is the most impacted by climate change causing the greatest effect on human health in the category shown in Fig. 5.21a. A comprehensive look into Fig. 5.21a shows that no value was recorded for the ionizing radiation in all three cases, which is expected as no dose of radioactive materials was used, and none was absorbed. Similar observations are noticed for both photochemical oxidant formation and ozone depletion; this clearly depicts that these three impact categories have no impact on human health for all the defined cases. However, the other three impact categories- particulate matter formation, human toxicity, and climate change human health (CC-HH)- have a significant influence on human health, with the latter showing the highest degree. For climate change human health, the use of coal power plants (CPP) caused the greatest damage to human health for all three cases, with relatively little differences among them and case two being the highest. The particulate matter formation category which is almost half as impactful as the CC-HH follows the same trend as CC-HH while using the CPP. Though using PV seems to cause more particulate matter on human health than CPP for cases 1 and 2 with the same impact. Human toxicity levels for cases 1 and two are almost the same for both PV and CPP.

In Fig. 5.21b, terrestrial acidification, natural land transformation, and climate change ecosystem (CC-E) are the most significant impact categories on the ecosystem in their increasing order. It is worthy of note that CC-E impact is more than seventy (70) fold of the other two categories, making it more pronounced in its damage to the ecosystem diversity. Fig. 5.21c shows that using the CPP seriously impacts the depletion of fossil resources, with a price increase of almost $10/kg of the fossil materials for all three cases. When this is estimated in terms of the total extraction for running the plant to keep running the system, a huge number of losses would have accumulated compared to when the PV is used. Metal depletion for both PV and CPP usage is almost the same and accounts for less than 50 cents per kg just for case 3.

Considering all the scenarios, case two in the manufacture of the SOEC with powerplant seems to be causing the most significant environmental damage, followed by the first and the third case. This work shows that the extent of the damage by the coal power plant to the PV is in 6, 11, and 57 times greater in the human health, ecosystem, and resource scarcity, respectively. A similar

trend is observed for the balance of plant as shown in the supplementary information. Overall, these results are consistent with expectations as demonstrated by [234, 267-269] but unique in their values and analysis approach as the technological concept is novel.

5.8.3.1 Carbon footprint analysis

Analyzing and comparing the operation of the SOEC and PCEC, Fig. 5.22 shows the carbon footprint analysis of their operations for the production of an equivalent amount of hydrogen, 10100kg/h. It is obvious from the figure that during the system operation using the PCEC that there is a 33.7% reduction in CO_2 emissions compared to the SOEC. This is as expected because more energy is required to raise the steam temperature of 500℃ used in PCEC to 850℃ used in SOEC and additional energy is required to maintain this operating temperature. For further evaluation of the benefit and superiority of PCEC over the SOEC environmentally. The analysis is carried out on the manufacturing of 5000 kg weight of both the SOEC and PCEC.

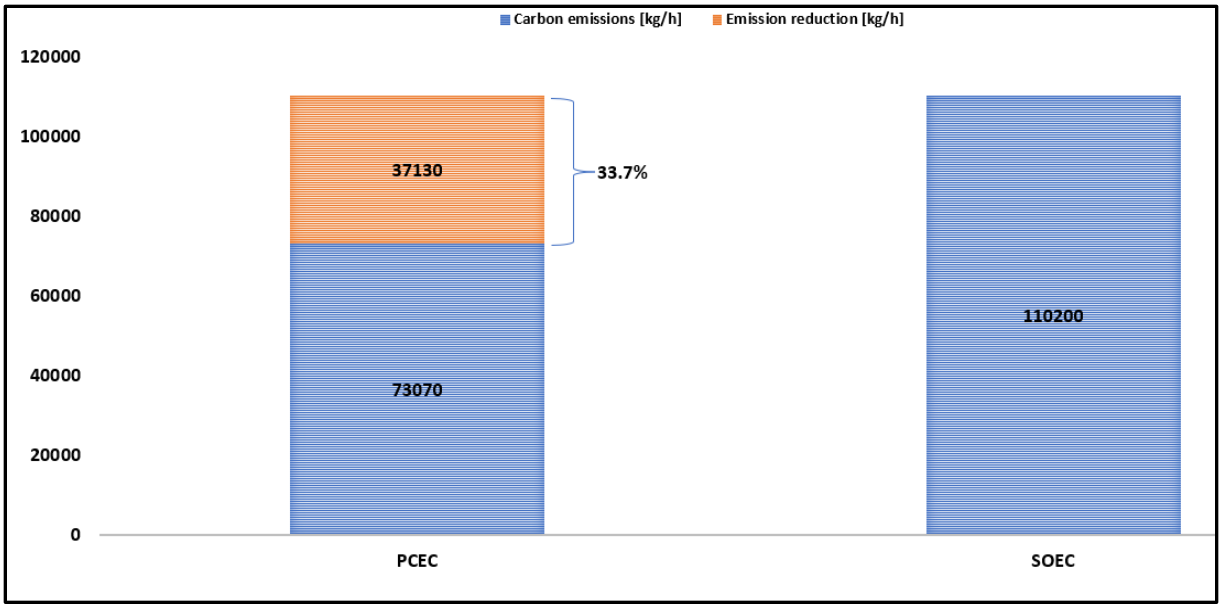

Fig. 5.22: Carbon Footprint Analysis during the Operation of PCEC and SOEC

Fig. 5.23 shows the global warming potential (GWP) for the manufacturing of both technologies. There is a reduction in the amount of CO_2 emitted during PCEC manufacturing when compared to the manufacturing of SOEC, rounding off the GWP reduction to about 37%.

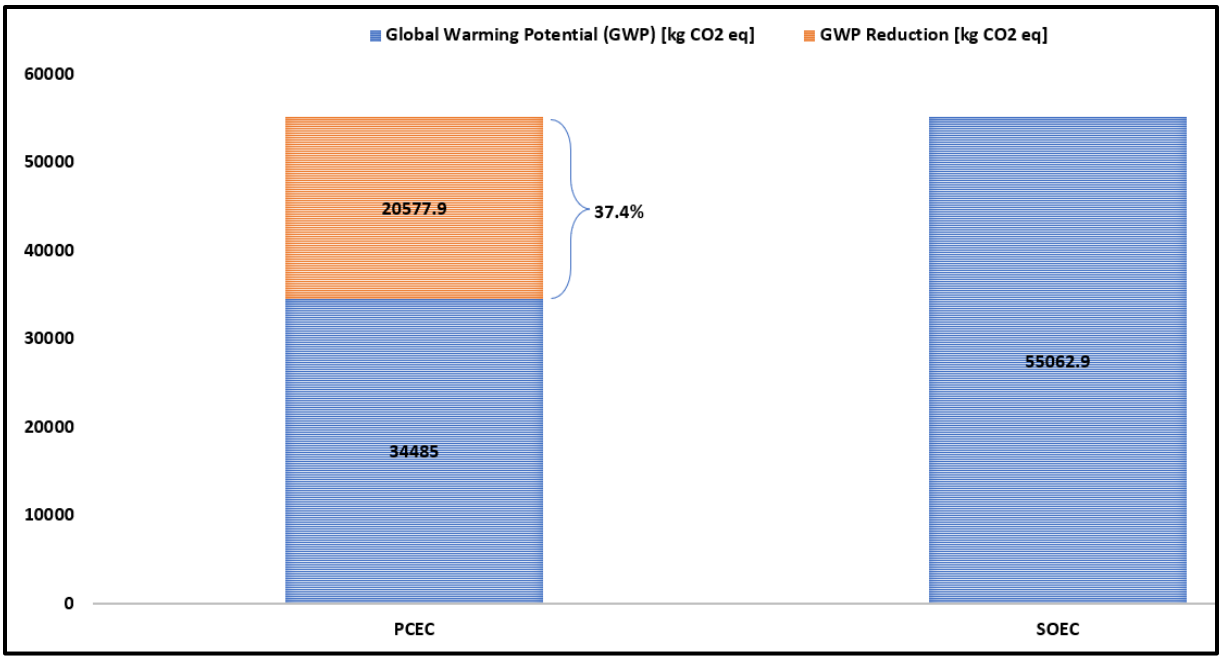

Fig. 5.23: Global warming potential (GWP) for stack manufacturing of PCEC and SOEC

5.9 Conclusion

Novel hydrogen production from high-temperature SOEC and PCEC integrated with fossil and energy resources is investigated in this work. A detailed analysis of this integration and discussion on the system operation and performance is studied. From the analysis, results show the possibility of the levelized cost of hydrogen lower than $3 per kg of hydrogen using SOEC and PCEC. This process is unique and efficient in the green hydrogen production realm and highly competitive with their counterparts and conventional technologies. To demonstrate this, Aspen HYSYS and the DOE H_2 analysis tool are used to assess its economic viability and prospects.

The techno-economic analysis is performed for the system; it shows one of the lowest levelized costs of green hydrogen that has been reported. This competitive with fossil fuel produced hydrogen with LCOH range of $1.3-4.5 per kg H_2 [270]. The thermal utilities, which is the assumed basis for this system give a LCOH of $3.13 and $2.88 per kg H_2 and solar PV gives the lowest LCOH of $2.9 and of $2.5 per kg H_2 for SOEC and PCEC respectively. There are major improvements that can be made to the system to reduce the LCOH in the range $2.5-5.96 per kg H_2 with different energy feedstocks. Solar PV is an excellent renewable source with the lowest

LCOH, and the system is up-and-coming and can meet the US DOE target if meticulously explored.

Moreover, other than the rational use of energy by the system during flue gas condensation, the system helps conserve a considerable amount of water that would have been used as SOEC feedstock. Opportunities abound in this water-energy nexus for government, researchers, and industries to annex for sustainable economic and environment and hydrogen as a futuristic medium for energy storage.

It is established that using PCEC for hydrogen production is more eco-friendly than using SOEC in the integrated system. The LCA studies show that solar PV is a good energy source for SOEC operations. With improved BoP design, the environmental impact of large-scale hydrogen production can meet the global standard for sustainability and a green economy.

CHAPTER 6 METHANE PRODUCTION THROUGH CO-ELECTROLYSIS OF CO_2 AND H_2O USING REPCEC SYSTEM: LIFECYCLE ANALYSIS (LCA), TECHNO-ECONOMIC ANALYSIS (LCA) AND PARAMETRIC STUDIES

? **Research Question, RQ5**: What are the impacts of renewables on the carbon footprint of the system and the types of uncertainties attached to the net energy usage and designing of energy storage systems?

➢ **Objective 5**: Estimation of integrated RePCEC system operation carbon footprint

✓ **New knowledge**: A comprehensive lifecycle analysis (LCA) of large-scale RePCEC operation and the balance of plant components for the integrated system to determine their global warming potential. Damage impact of coal-fired powerplant on human, environment and resource compared to solar photovoltaic.

6.1 Co-electrolysis RePCEC system lifecycle analysis (LCA)

It has been established in the previous chapter, that the degree of harm and impact of fossil fuels on humans, resources, and the environment when compared with solar photovoltaic sources is very high, the solar source is shown to be more environmentally friendly. Therefore, a solar farm is used to run the RePCEC in its co-electrolysis operation as shown in Fig. 61. Following the general lifecycle analysis (LCA) depicted in Fig. 6.2 which is similar to that in the previous chapter, a detailed LCA is carried out to assess the impact of this technology and its application on human, resources and environment. In this work, attention is paid to some critical parameters like the global warming potential, human toxicity potential, and ozone depletion potential. The LCA for the system shown in Fig. 6.1 is considered only from cradle-to-gate analysis and grave scenarios is not analyzed. Here, the approach for the LCA of hydrogen production using the SOEC in the previous chapter is typically followed. For all LCA, the framework is the same even if the approach of analysis differs.

6.2 Lifecycle analysis (LCA) frameworks

The LCA process entails four fundamental frameworks, namely

5. Goal and scope definition (system description and objectives)
6. Inventory analysis (data collation-knowing and quantifying the energy and materials in and out of the system)
7. Impact assessment (measuring the environmental effects of the system)
8. Interpretation (understanding and evaluation of result)

These frameworks are discussed in the following sections

6.2.1 Goal and scope definition

The RePCEC system has been well described in chapter 4. Base case having the carbon capture system integrated is considered. The integrated RePCEC system is powered by a solar farm housing an advanced solar photovoltaic (PV) system. The goal of this LCA is to evaluate the global warming potential of this technology for the production of methane from a co-electrolysis operation. The system boundary is as shown in Fig. 6.2. The scope of this work begins with raw materials for the manufacturing of the PCEC and the BOP components and the utilities as indicated in Fig. 6.2. As mentioned in the introduction, a cradle-to-gate analysis is carried out, and the plant decommissioning is not considered. The cradle-to-gate gives and simplify the assessment of the production process from raw material to the desired product (methane) and its use. It accounts for the carbon footprint of the continuous operation of the process unlike cradle-to-grave that account for the environmental of the whole plant with the equipment.

6.2.2 Lifecycle inventory

The proposed plant embodied three separate units integrated with a combined cycled powerplant namely, the two-stage membrane-based carbon capture system, the steam generating unit that comprises other BoP components, and co-electrolysis unit that houses the RePCEC. The material components for the manufacturing of PCEC and their quantities are obtained from the work by Dubois et al [136]. The number of BoP components and the energy demand in each unit is as modeled in Aspen HYSYS and the throughput and products are results from the Aspen HYSYS simulation. The Ecoinvent database is relied on for the emission from the manufacturing process for secondary data and for some processes their data are not easily accessible from literature and Aspen HYSYS. Solar farm which houses several solar PVs is used to supply power to the plant. For solar PV, local data in the United States was used from the SimaPro database.

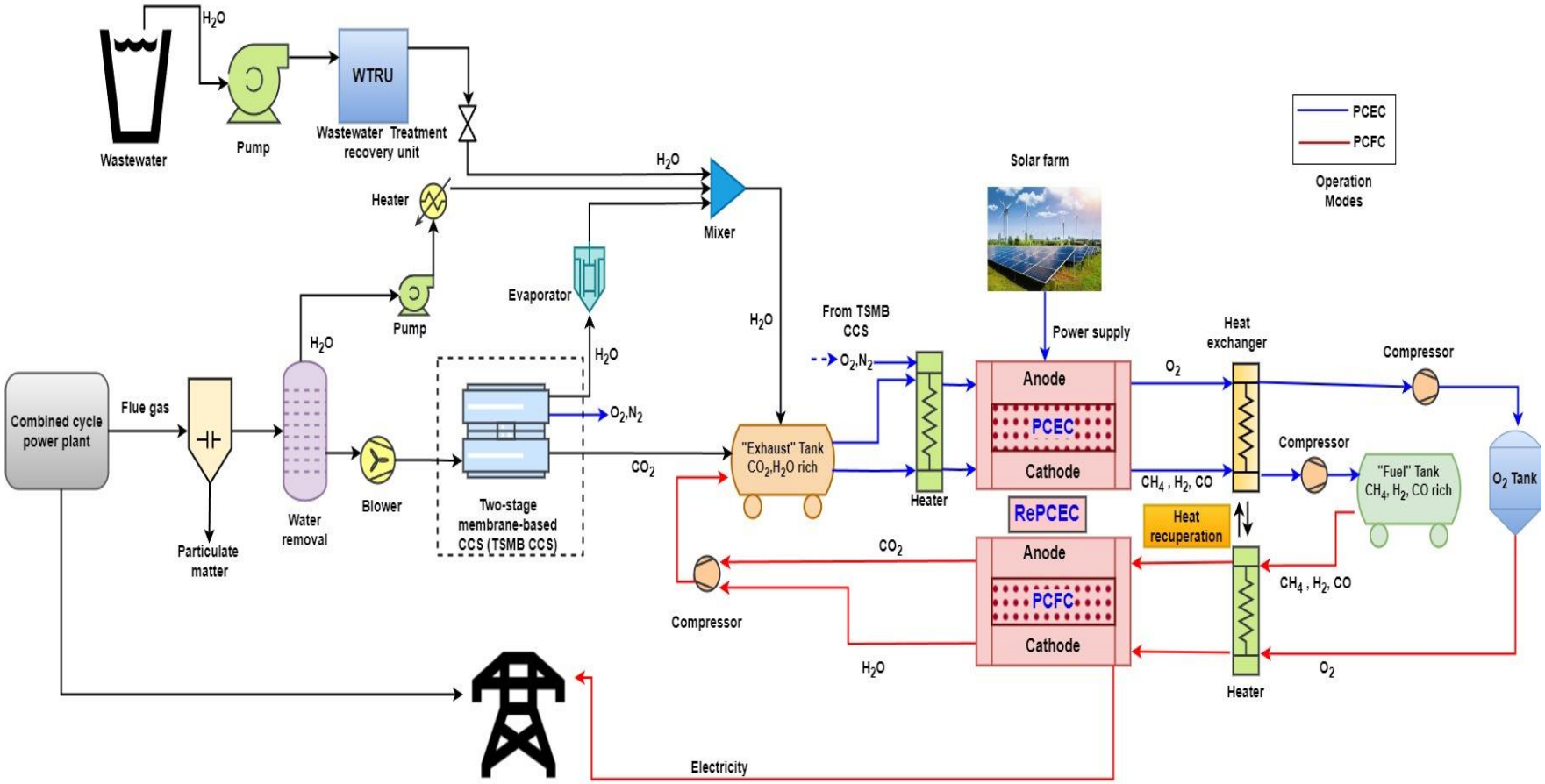

Fig. 6.1: Reversible protonic ceramic electrochemical cell (RePCEC) for co-electrolysis of H_2O and CO_2 powered by solar energy

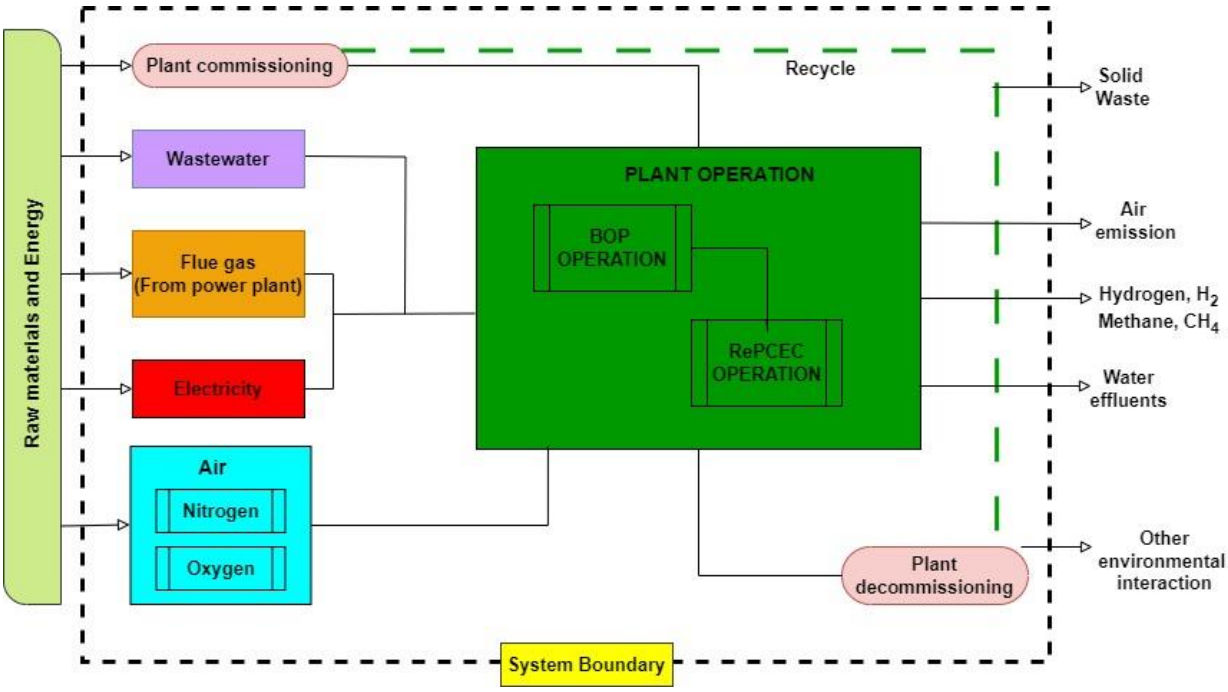

Fig. 6.2: RePCEC LCA system boundary for Co-electrolysis of CO_2 and H_2O

6.2.3 Lifecycle impact assessment (LCIA) method

SimaPro offers various standard methods for impact assessment, each encompassing 10 to 20 impact categories. However, a preferred approach is a more comprehensive method that enables the aggregation of values into a unified score. Additionally, a crucial aspect is to focus on the vital elements, classification, and characterization, as outlined in ISO 14040/44, which constitute the minimum requirements in Life Cycle Assessment (LCA). This study employs TRACI 2.1 with version 1.03 as the life cycle impact assessment (LCIA) method and adopts the US 2008 as the normalization and weighting set. The United States and North America are potential targets for this work so its criteria are a perfect match for their set of conditions. Tool for the Reduction and Assessment of Chemical and Other Environmental Impacts (TRACI) is a midpoint-oriented LCIA methodology developed by the U.S. Environmental Protection Agency specifically for the US using input parameters consistent with US locations. TRACI is an environmental impact assessment tool that provides characterization factors for Life Cycle Impact Assessment (LCIA), industrial ecology, and sustainability metrics. Characterization factors quantify the potential impacts that inputs and releases have on specific impact categories in common equivalence units [271]. Its impact categories include:

a) Ozone depletion,

b) Climate change,

c) Acidification,

d) Eutrophication,

e) Smog formation,

f) Human health impacts, and

g) Ecotoxicity.

Characterization Factors are available for the media listed for each impact category in Table 6.1.

Table 6.1: Available characterization factor and media [271]

Impact Category	**Media**
Ozone depletion	Air
Global Climate	Air
Acidification	Air, Water
Eutrophication	Air, Water
Smog formation	Air
Human Health Particulate	Air
Human Health Cancer	Urban Air, Nonurban Air, Freshwater, Seawater, Natural Soil, Agricultural Soil
Human Health Noncancer	Urban Air, Nonurban Air, Freshwater, Seawater, Natural Soil, Agricultural Soil
Ecotoxicity	Urban Air, Nonurban Air, Freshwater, Seawater, Natural Soil, Agricultural Soil

The facility overview and their descriptions are similar to what is used in chapter 5.

6.2.4 Results and interpretation

The co-electrolysis of H_2O and CO_2 from flue gas of a 600MW combined cycle power plant is carried out using an integrated RePCEC system comprising of the RePCEC stack and BoP components. The BoP components consist of the exhaust tank, compressor, heater evaporator,

blower, heat exchanger, mixer, electrostatic precipitator, pump, and the two-stage membrane-based carbon capture system as shown in Fig 6.2. The environmental impact of all the components is analyzed using the TRACI 2.1 LCIA method. Fig. 6.3 shows the characterization network of all the BoP components. The thickness of the arrow indicates the contribution of a component towards the product (BOP). Selection of the right equipment from database, accurate weight allocation and well-defined boundary are critical to reliable LCA. From the figure, the pipeline that transports the natural gas is having the highest impact contribution to the environmental decadence. It has the greatest global warming contribution followed by the storage tanks. Intuitively, this seems not correct as other bigger equipment is expected to have higher environmental contribution. The initially selected pipe for the process has a weighted average lifetime of 45 years made up of steel and concrete with a length of 100km, this far beyond the system boundary. This greatly contribute to the output in Fig. 6.3. To correct this anomaly, the appropriate pipe with weighted average lifetime of 40 years made up similar materials as the previous one and length 3km is used. this, there is a need to reduce the transport distance to reach the storage tank. Another alternative to minimize the environmental challenge by equipment is to use more environmentally friendly materials in its manufacturing. The BoP components are a major contributor to the global warming potential of many production plants and are often avoided in LCA [213]. Analyzing the BoP with the appropriate newly selected pipe with right specification gives the result in Fig. 6.4. From the new analysis outcome, making the storage tanks have the highest environmental impact. In fact, the pipe now has very low global warming potential compared to other equipment in the cut-off mode. The cut-off mode is the minimum weight criteria set by SimaPro to show participating equipment in the network. The cut-off in field in SimaPro also takes user input values. Components with insignificant impact contribution are not shown by the software but can be viewed in the global database. The characterization bar chart for all the components of the process also shows that the tank storage causes the most damage for most parameter categories except for ozone depletion where the water treatment takes the lead as shown in Fig. 6.5. The impact categories and their abbreviations are given in Table 6.2

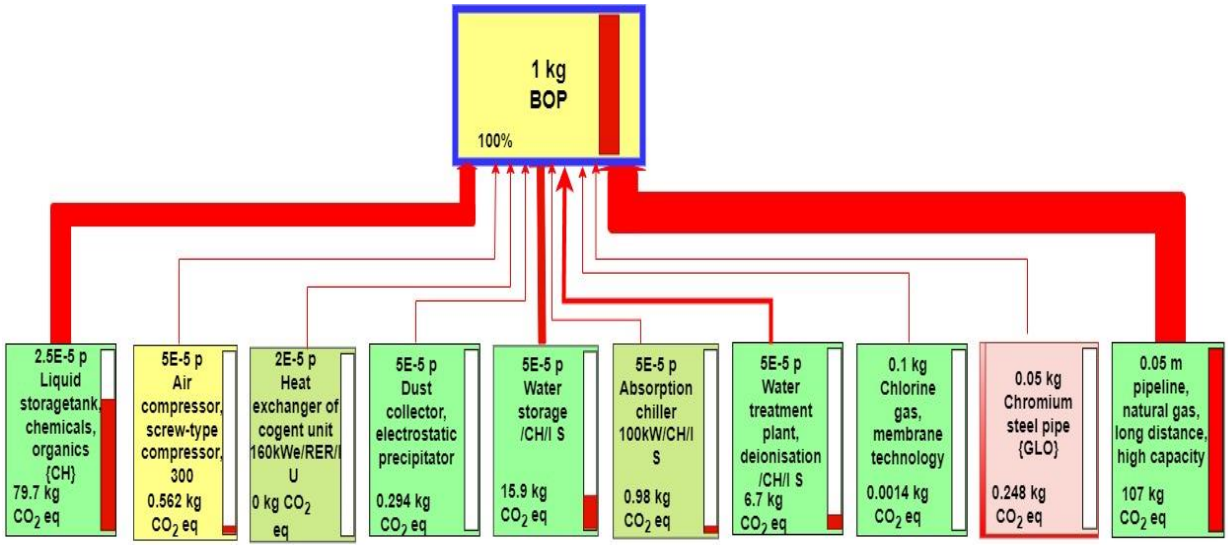

Fig. 6.3: Characterization network of BoP component for co-electrolysis

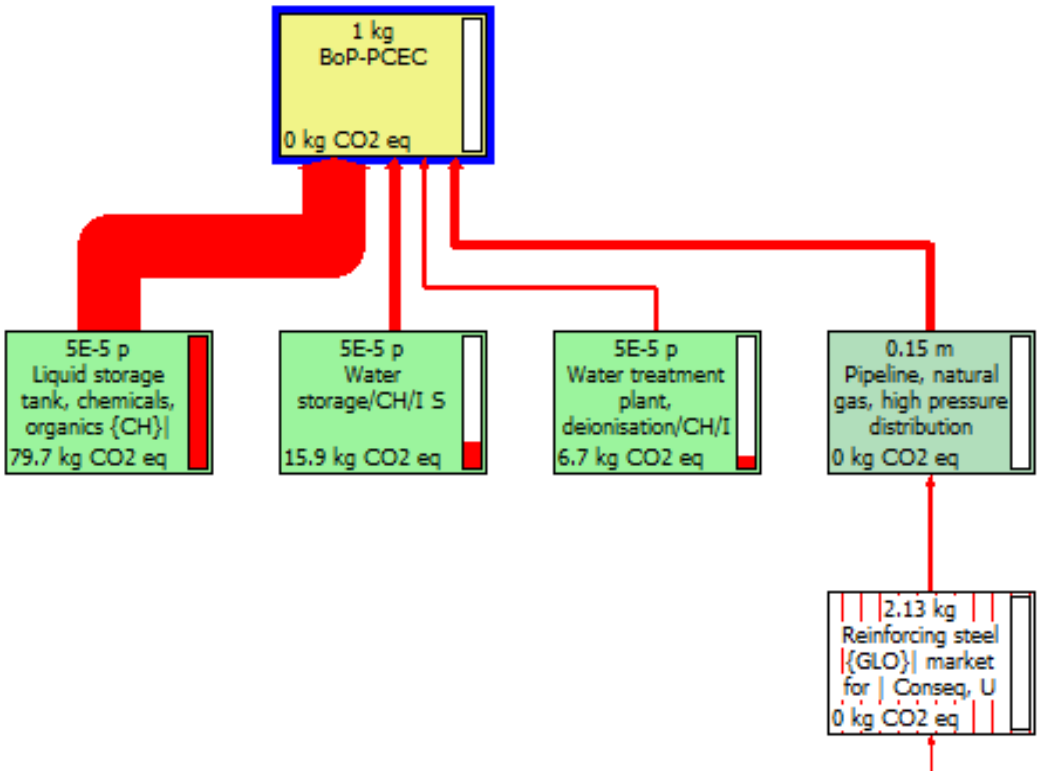

Fig. 6.4: Characterization network of BoP component for co-electrolysis with right pipeline specification.

Table 6.2: Impact categories and abbreviation as used in the charts

Impact category	**Abbreviation**
Ozone depletion	OD
Non carcinogenics	NC
Carcinogenics	Cg
Fossil fuel depletion	FFD
Respiratory effects	RE
Eutrophication	Eu
Acidification	Ac
Smog	Smog
Global warming	GWP
Ecotoxicity	Ec

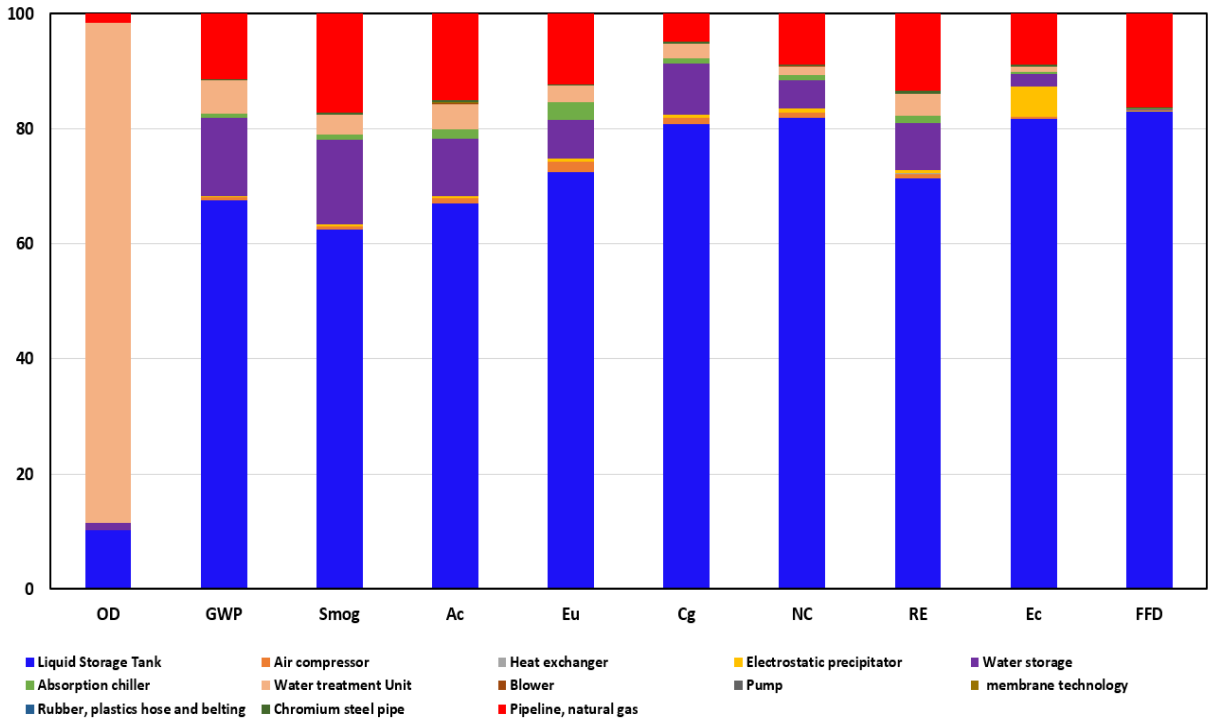

Fig. 6.5: Characterization chart for BoP components for co-electrolysis

Based on the selected life cycle impact assessment (LCIA) method, the potential environmental impact of the RePCEC stack manufacturing is carried out to identify the impact intensity of each parameter. The characterization is highlighted in Table 6.3 and the details about the units can be found in Ref [271]. The global warming potential (GWP) of the stack manufacturing process is 3.63 kg CO_2 eq.

Analyzing the stack component wise, Fig 6.6 shows the contribution network of each of the stack components (most especially, the electrodes and electrolyte) during its part assembly. This figure reveals that the anode materials have the highest global warming potential which is evident from the thickness of the arrow. A deeper dive into the figure shows that nickel is the greatest polluter from the anode materials. The GWP for the actual co-electrolysis operation for the production of methane and hydrogen is 3.83 3.63 kg CO_2 eq which is lower compared to 9.35 kg CO_2 eq emission during steam methane reforming for hydrogen production [272]. Comparing the GWP for methane production via RePCEC route with power-to-gas using the energy mix EU-27 countries with 13.8 kg CO_2 eq [272], shows the RePCEC to be more eco-friendly.

Table 6.3: RePCEC stack manufacturing characterization

Impact category	Value	Unit
Ozone depletion	0.00000049	kg CFC-11 eq
Non carcinogenics	1.18E-06	CTUh
Carcinogenics	0.00000114	CTUh
Fossil fuel depletion	1.17	MJ surplus
Respiratory effects	0.0242	kg $PM_{2.5}$eq
Eutrophication	0.0687	kg N eq
Acidification	0.307	kg SO_2 eq
Smog	0.448	kg O_3 eq
Global warming	3.63	kg CO_2 eq
Ecotoxicity	32.6	CTUe

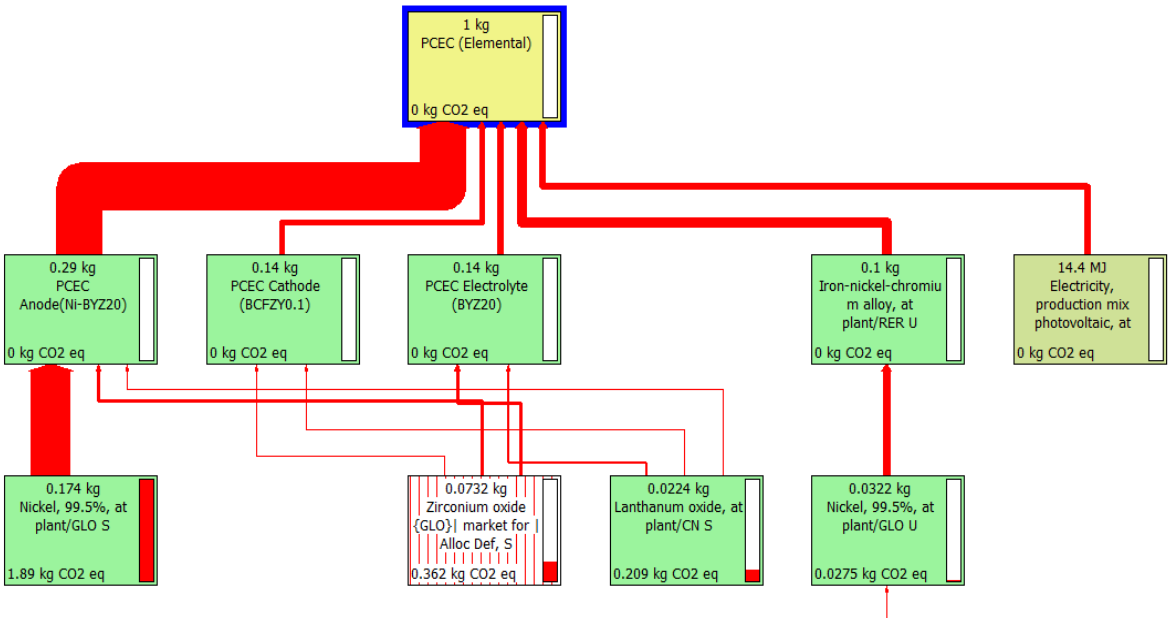

Fig. 6.6: PCEC stack component analysis network

Fig. 6.7 shows the contribution of each operational process, it is obvious from the graph that energy consumption during the process caused more damage. During the methane production CO_2 is removed from the atmosphere, this is shown as the green bars in Fig. 6.7 which is a negative carbon footprint. The savings on each impact category is shown in green. The red bars denote the environmental impact by the energy consumed during the methanation process. Ranging the energy for steam production which takes the larger share of the process and the actual co-electrolysis reaction initialization. The effect of the electrical energy consumed cut across all impact categories.

Fig. 6.8 shows the overall LCA of the plant and processes, it can be seen that the bar chart is almost a single color for the BoP, unlike previous bar chart with multiple colors. The color dominance indicates that the balance of plant is one of the biggest greenhouse gas emitters in an industrial process during a plant scale lifecycle analysis. The effect of other processes for the methanation process exhibit less than 1% GWP compared to the BOP. Sensitivity analysis is carried out on the methane leakage after production. This would make the methane production and the leakage limit that is environmentally friendly known. Table 6.4 highlight the environmental impact of methane leakage at 1%, 10% and 20%. In all cases it shows the RePCEC route is still ecofriendly when

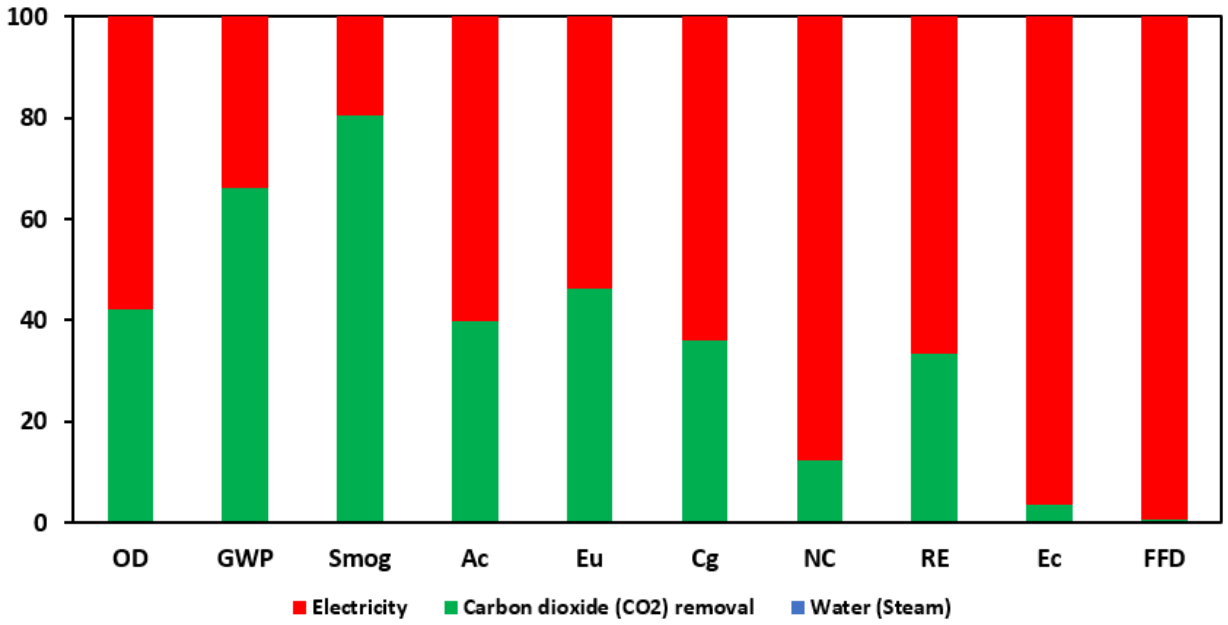

Fig. 6.7: Characterization of the methane production process

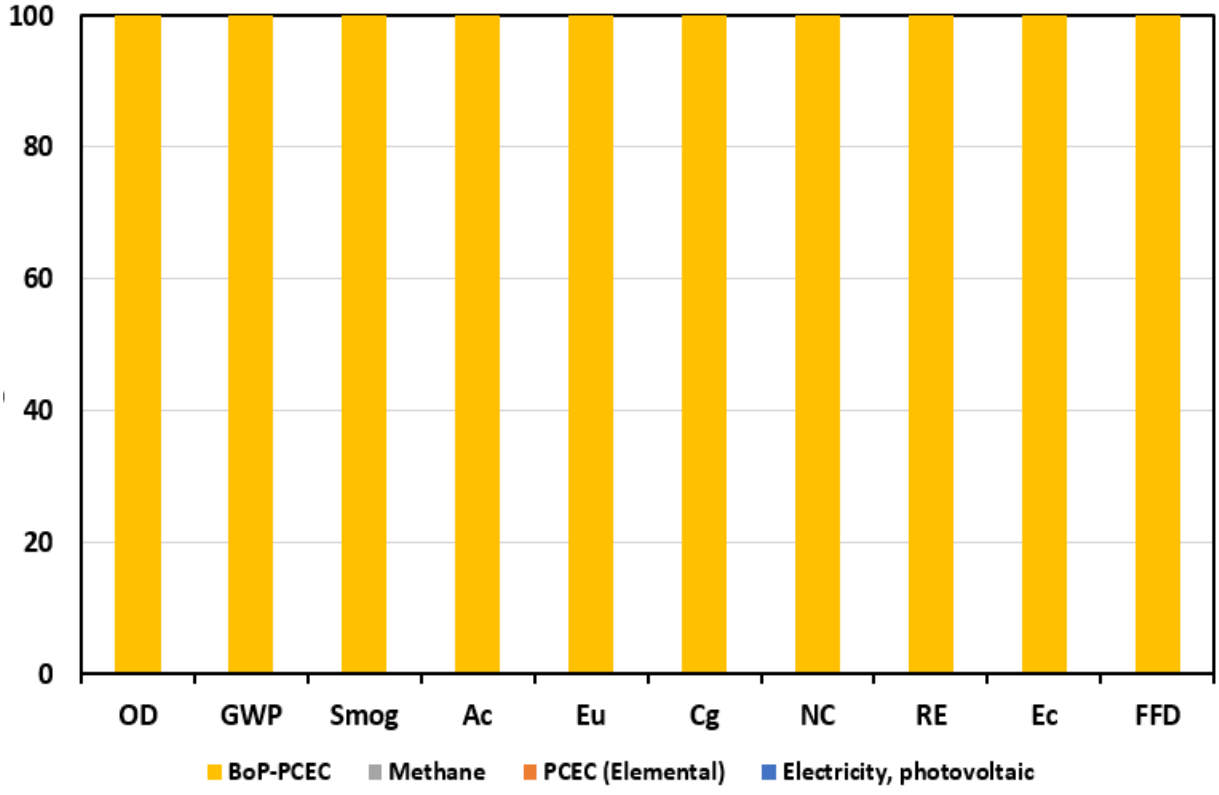

Fig. 6.8: Overall lifecycle analysis for methane production in RePCEC system

compared to the CO_2 consumed for the process. However, Fig. 6.9 shows the two prominent of the impact categories, global warming potential and ecotoxicity. The ecotoxicity impact indicate that 20% methane leakage is the upper threshold for the eco-friendliness of the RePCEC production route.

Table 6.4: Methane leakage analysis

Impact category	Unit	Carbon dioxide consumed, kg	Methane leakage, kg		
			1%	10%	20%
Ozone depletion	kg CFC-11 eq	$9.11*10^{-6}$	$3.53*10^{-8}$	$3.53*10^{-7}$	$7.06*10^{-7}$
Global warming	kg CO2 eq	115.1	0.644	6.44	12.9
Smog	kg O3 eq	15.1	0.0184	0.184	0.368
Acidification	kg SO2 eq	0.273	0.00242	0.0242	0.0483
Eutrophication	kg N eq	0.341	0.004956	0.0496	0.0991
Carcinogenics	CTUh	$4.93*10^{-6}$	$2.31*10^{-8}$	$2.31*10^{-7}$	$4.61*10^{-7}$
Non carcinogenics	CTUh	$6.20*10^{-6}$	$1.43*10^{-7}$	1.43E-06	$2.87*10^{-6}$
Respiratory effects	kg PM2.5 eq	0.031106	0.000348	0.00348	0.00695
Ecotoxicity	CTUe	106	5.09	50.9	102

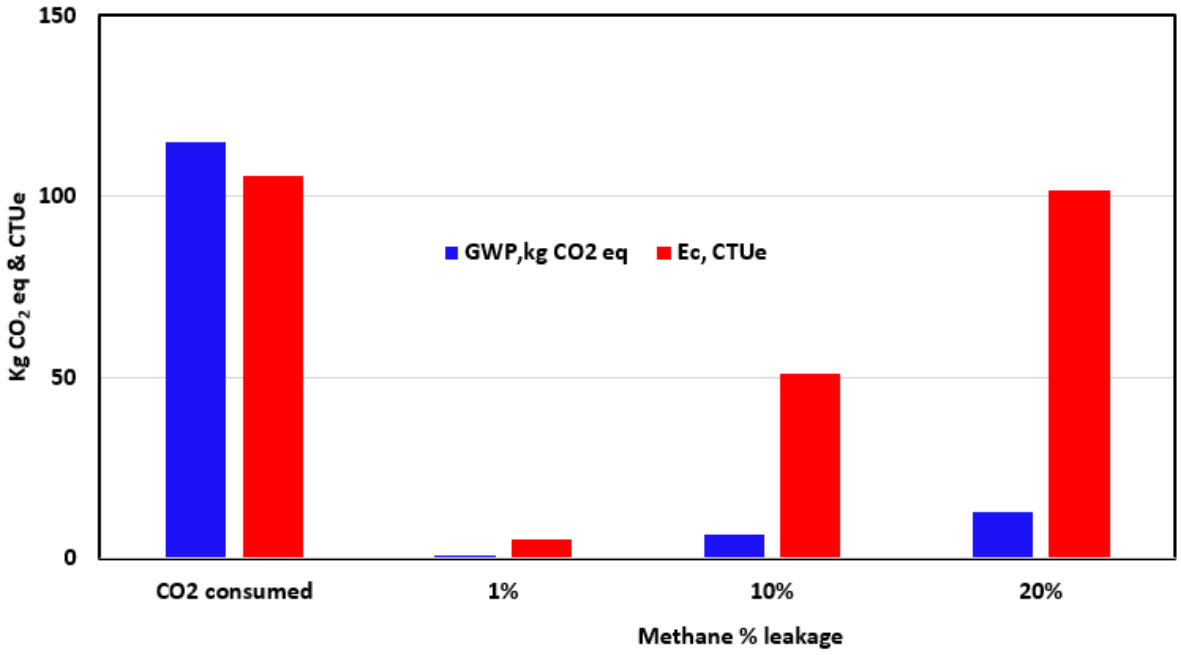

Fig. 6.9: Methane leakage analysis

6.3 Co-electrolysis RePCEC system economic analysis (EA)

The economic viability of using the RePCEC for the production of methane (natural gas) through co-electrolysis of CO_2 and H_2O is evaluated. The base case with a carbon capture system shown in Fig. 6.1 is used for this study. The main feedstock flow rates into the system are 4582 kmol/hr and 20000 kmol/hr for CO_2 and H_2O respectively. This yielded an output flow rate with 4046.6 kmol/hr of methane and 3783.2 kmol/hr of hydrogen. The equipment cost models used in section 5.1 are adopted which generate the equipment costs as shown in Table 6.5 with the equipment energy demand. The effect of scaling the equipment is detailed in the parametric studies in section 6.3. The cost of electricity from solar photovoltaic has been considered to be at $0.03 per kilowatt-hour following the projection of the US Department of Energy (DOE) for less expensive options. The total capital cost and total operation and maintenance cost are highlighted in Table 6.6. The estimation method for other variables after obtaining the equipment costs is detailed in Refs [165, 233, 273]

Table 6.5: Equipment cost models for co-electrolysis in 200MW RePCEC system

PCEC BoP	**Cost, $**	**Energy, GJ/hr**
Exhaust Tank	62000	--------
Compressor	201675	1729
Mixer	1040	---------
Heater	104871	147.5
Evaporator	1036830	468.9
Blower	25000	0.0425
Electrostatic precipitator	15000	0.04832
Separator (water) - (cooler)	23500	2862
Two-stage membrane-based CCS	2258000	950.652
Pump	24508	0.048400
WTRU	544547	468.9
REPCEC		4173.3

Table 6.6: The total capital cost and total operation and maintenance cost [165]

S/N	Expenses	Cost, $
1	**Direct expenses**	
a	Equipment F.o.b cost	71190913
b	Installation materials	8542909.56
c	Labor (installation)	170858.191
2	**Indirect Expenses**	
a	Freight, insurance and tax	2397140.42
b	Construction overhead	1598093.62
c	Engineering expenses	7990468.08
3	**Contingency and fee**	
A	contigency	5593327.65
B	contractor fee	3995234.04
C	Legal fee	7990468.08
4	**Auxiliary facilities**	
A	Site development	3995234.04
B	Auxiliary buildings	2397140.42
C	Off-sites and untilities	1198570.21
	Operating costs	
	Fixed	1198570.21
	Variable and others	75909446.7
	Maintenance Cost	9588561.69

Using an extract from the DOE cost analysis tool, a new techno-economic analysis tool is built using the Excel spreadsheet linked with the Aspen HYSYS system model for the estimation of the level cost of methane. The product output from Aspen HYSYS for the case under study, methane

heating value, and its conversions is shown in Table 6.7. Considering the levelized cost of hydrogen to be $2.5/kg of H_2 as evaluated in the previous chapter, the levelized cost of methane (LCOM) is $2.23/MMBtu exempting the separation cost of the two gases. The $/MMBtu is the conventional unit used for the levelized cost of natural gas and the unit conversion to the metric system is highlighted in Table 6.7. Comparing this value with the Henry Hub daily spot price for natural gas (NG) which ranges between $3.46/MMBtu and $9.85/MMBtu as reported by the US Energy Information Administration (EIA) [274], indicates an economic potential. The LCOM is highly responsive to the LCOH since both have a unified cost being produced from the same process which must be split. Since the LCOH has been established in a separate standalone process, the LCOM becomes the dependent variable of the two costs. Also, the LCOM depends greatly on the cost of RePCEC stack being the most expensive of the equipment, and on the cost of other balance of plant components as shown in the parametric study section in section 6.3. Estimating the LCOM at various conditions gives insight into reasonable cost ranges, this gives the upper and lower limits of the LCOM obtainable from the RePCEC system. Figures 6.10 and 6.11 compare the lower and the upper bands of the LCOM with the US annual NG price and the global NG price respectively.

Table 6.7: System output products and property

Product	**Flow rates**	
	kg/hr	kmol/hr
Methane flow rate	64967	4046.6
Hydrogen flow rate	7627	3783.2
Property	**Value**	
Heat value, MJ/kg	42-55	
Average HV, MJ/kg	48.5	
Average HV, GJ/kg	0.0485	
1MMBtu =	1.055 GJ	

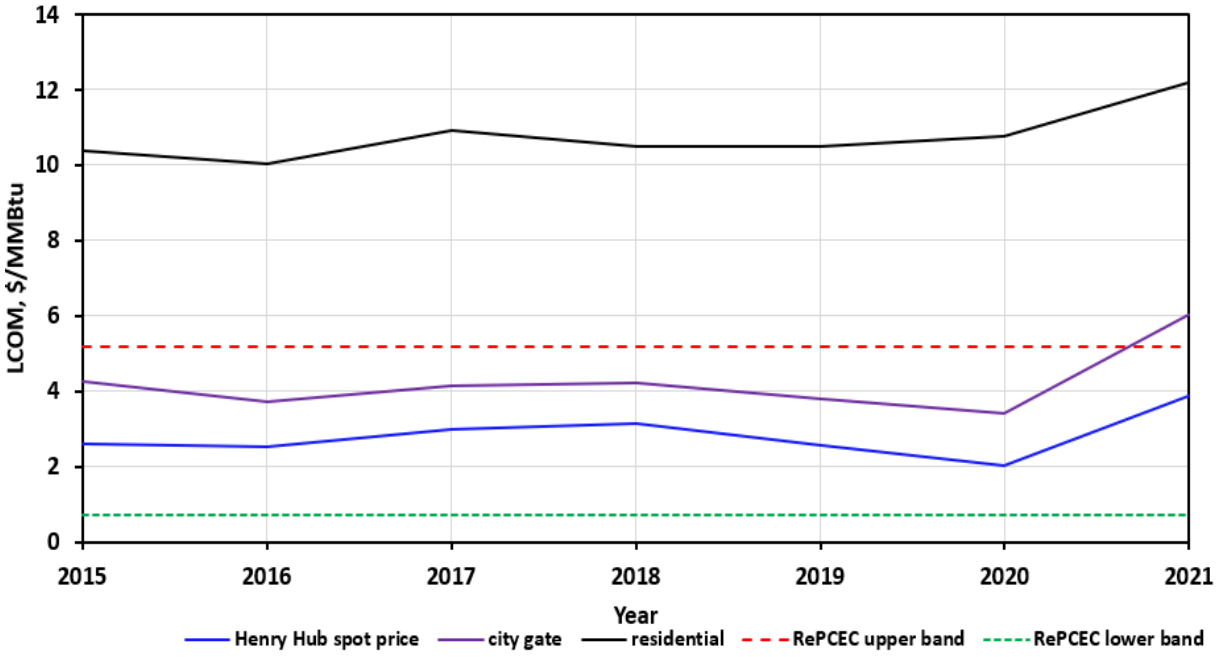

Fig. 6.10: LCOM from RePCEC system compared to the US average annual prices of natural gas [274]. Red dash line- highly inflated capital and operational costs for RePCEC system. Blue dash line-reduced capital and operational costs for RePCEC system.

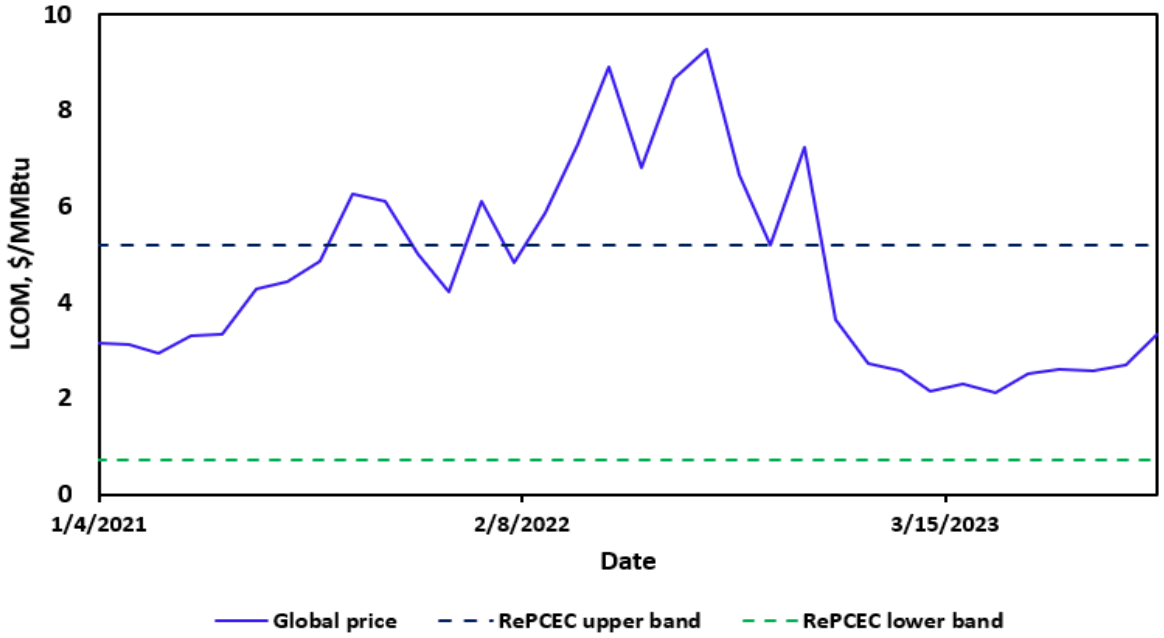

Fig. 6.11:LCOM from RePCEC system compared to the US average monthly prices of natural gas from 2021-2023[275]

It can be seen from Figs. 6.10 and 6.11 that adopting the RePCEC production route for methane competes relatively strongly with other routes even in extreme cases as its upper band LCOM depicted. What is obvious from the reports is that all other feasible production routes have been considered, thus operating the RePCEC at relatively optimum conditions as recommended in chapter 4, with progress in driving the cost of the technology down will drastically reduce the LCOM. This can probably lead to a paradigm shift in the methane production and markets. If this technology is implemented for this purpose and the potential profitability is confirmed, it enhances the investors' interest.

6.3.1 Effect of levelized cost of hydrogen on LCOM

Fig. 6.12 depicts how the cost of hydrogen produced from PCEC influences the cost of methane from the base case with CCS scenario. Since both hydrogen and methane are co-produced from the same unit process it is expected that their cost relates tightly well. Since out of plant levelized cost of the two products is constant for any selected system, an increase in the price of one of the two gases brings about a declining response in the cost of the other. The price of one product will determine the price of the other. Hydrogen can be produced separately in an electrolytic system using the PCEC, thus its cost is the independent variable. Therefore, an increase in the cost of

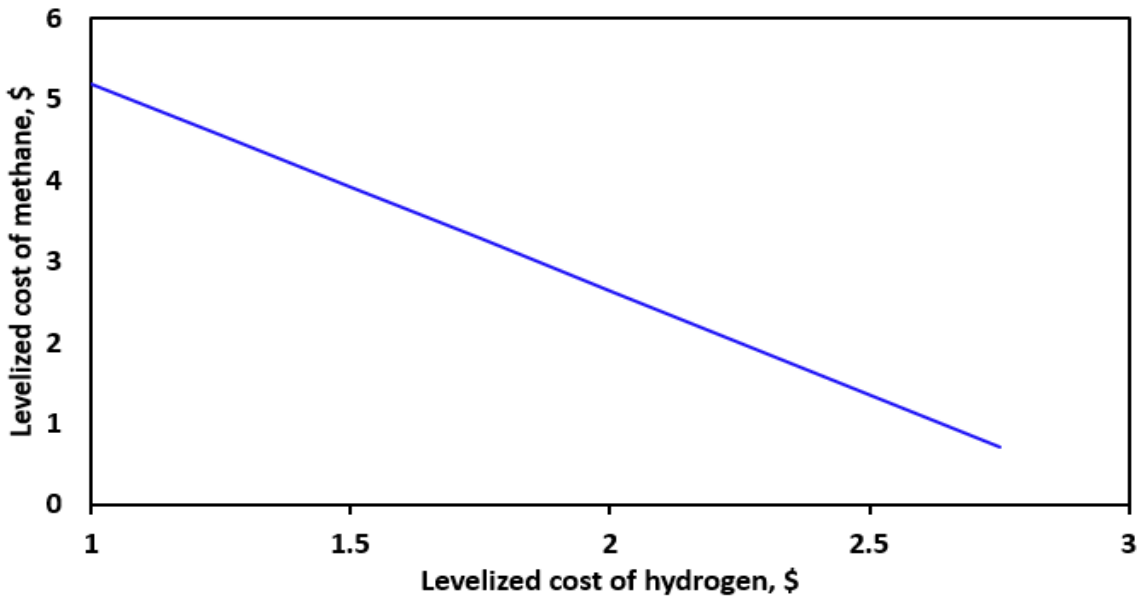

Fig. 6.12: Effect of LCOH on LCOM

producing hydrogen using PCEC for whatsoever reason brings down the levelized cost of methane as shown in Fig. 6.12.

6.3.2 Effects of operating temperature on LCOM

The influence of temperature on the direction and rate of reaction is well pronounced in reaction kinetics. For an endothermic reaction that needs heat, it is favored by increase in temperature while an exothermic reaction is favored by temperature decrease. The increase in temperature increases the production of hydrogen and reduces the production of methane as shown in Table 6.8. As previously mentioned in chapters 3 and 4, methane production is favored at a lower temperature, and an increase in temperature enhances steam electrolysis which results in higher hydrogen production. Correspondingly, Fig. 6.13 shows the non-linear relationship in the influence of temperatures on the LCOM at a fixed DOE target hydrogen price of \$1/kg of H_2 in 2030 [39].

Table 6.8: Product flow rate with changing temperatures

Temperature °C	Molar flow rate of CH_4	Mass flow rate of CH_4	Molar flow rate of H_2	Mass flow rate of H_2
C	kmole/h	kg/h	kmole/h	kg/h
400	4050	64970	3783	7627
450	3634	58300	5384	10850
500	3101	49740	7338	14790
550	2436	39070	9580	19310

This non-linearity seems reasonable as the temperature typically causes changes in two variables, i.e. the rate of production of the two gases. As shown in the Fig. 6.13, the LCOM decreases as the operating temperature increases. While high temperature can significantly impact other factors such as maintenance, performance of equipment, it can also enhance the production of hydrogen in the system, so there is a trade-off.

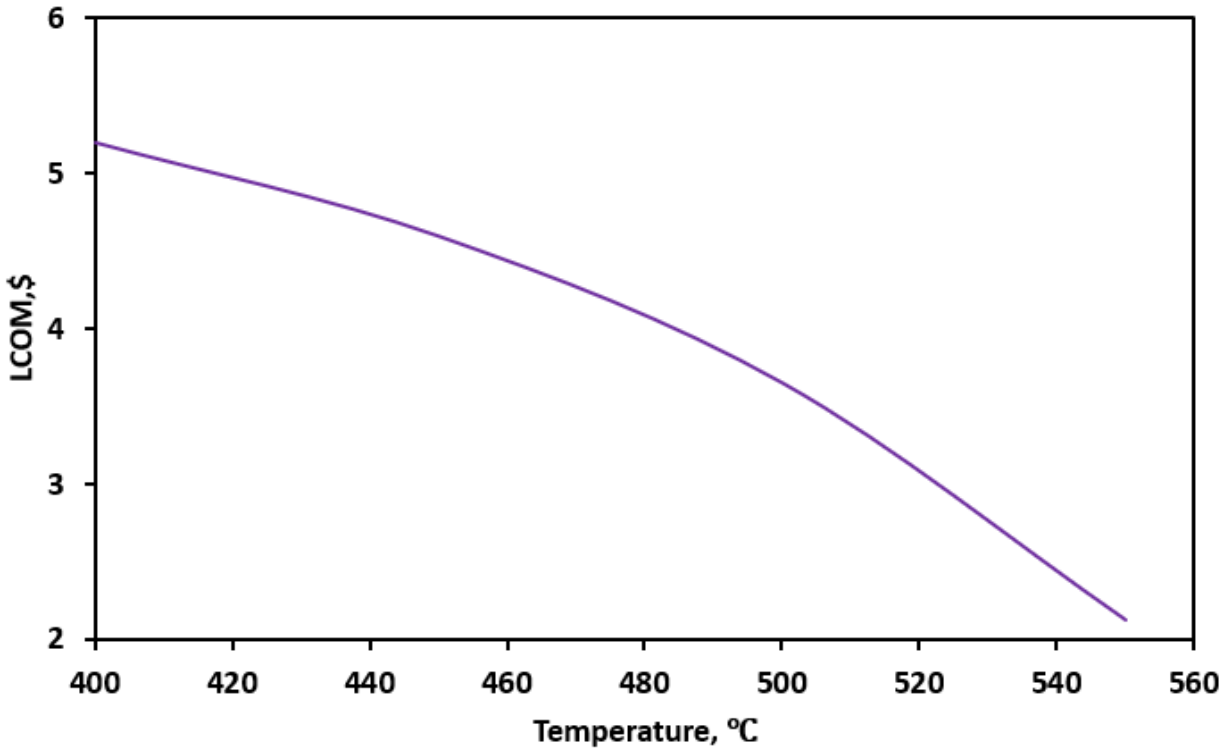

Fig. 6.13: Effect of operating temperatures on LCOM

6.3.3 Effects of RePCEC stack cost and BoP cost on LCOM

The cost of equipment is one of the most significant cost factors that influence the most merchandising businesses and production. Evaluating the cost of BoP cost and RePCEC stack cost on the LCOM, Fig. 6.14 shows the linear increase in LCOM for both cases as their cost increases. An increase in any of the equipment increases the capital investment which directly always increases the cost per unit of production. Fig. 6.14 shows there is a higher response to the RePCEC stack cost than the overall BoP component cost, this is due to the wide variance between the two costs. The stack cost takes over 50% of the total capital cost (TCC) unlike the BoP cost which is about 5% of the TCC. This has greatly contributed to the gap and how they both influence the LCOM. Overall, a lower equipment cost favors and reduce the LCOM which makes it good for business. Driving down the cost of the stack enhances the market friendliness of producing methane via this route.

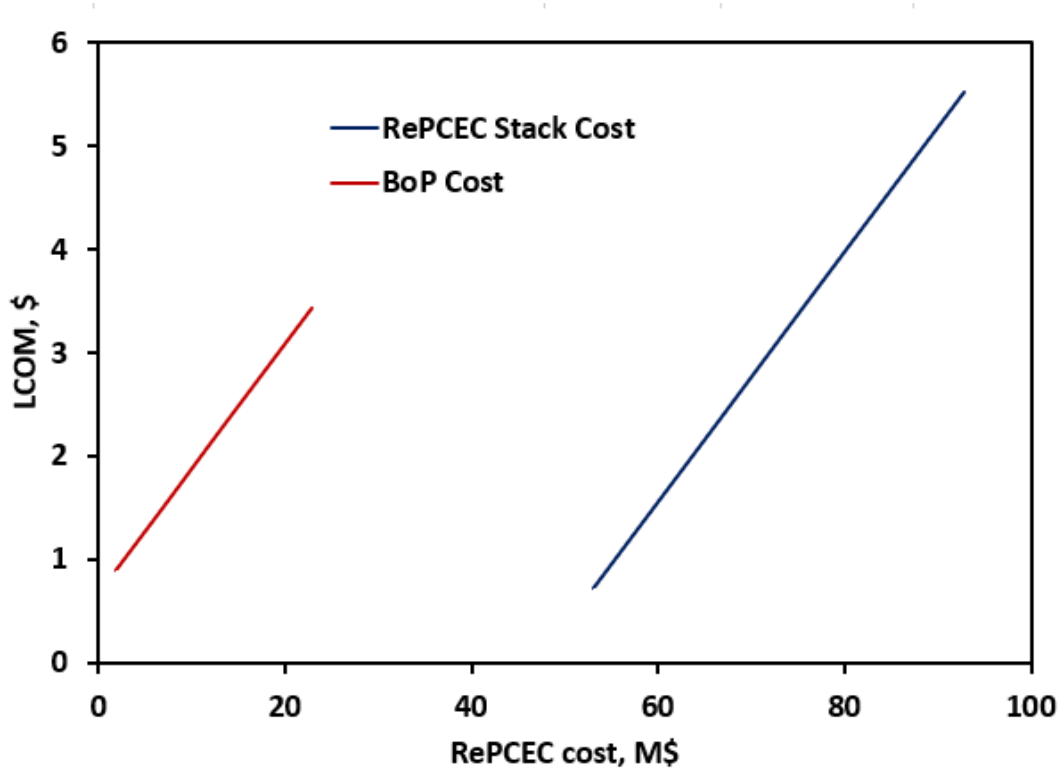

Fig. 6.14: Effect of equipment cost on LCOM

6.4 Conclusion

The economic and lifecycle analysis of base case with CCS configuration of integrated RePCEC system is studied. As posited by previous works that the manufacturing of balance of plant (BOP) components is one of the highest greenhouse gas emitters, this study shows that the same is applicable for co-electrolysis reaction in an integrated RePCEC system. However, the global warming potential (GWP) for this operational route for the production of methane and hydrogen is 3.83 3.63 kg CO_2 eq which is lower compared to 9.35 kg CO_2 eq emission during steam methane reforming for hydrogen production. Cost analysis of the system and operation revealed that $2.23/MMBtu levelized cost of methane (LCOM) is obtainable which makes it competitive with the conventional production routes with monthly average range between $3.46/MMBtu and $9.85/MMBtu. Overall, integrating reversible protonic ceramic electrochemical cells into fossil fuel assets while using renewables has high potential as energy storage system and revolutionizing natural gas production and market.

CHAPTER 7 CONCLUSION AND FUTURE WORK

7.1 Conclusions

The surge in renewables installation and the desire for increased penetration of renewable energy in the energy matrix brings about additional challenges. Energy storage and management systems are essential to address the time-varying nature of renewable energy supply and electrical energy demand by the populace. As renewable energy penetration increases, electrical energy becomes the predominant driving force. The gradual transition from chemical energy to electrical energy as the primary driving force implies the need to establish alternative synthesis routes for the production of vital industrial chemicals, currently sourced from fossil fuels. These challenges can be addressed with reversible protonic ceramic electrochemical cells (RePCEC). Its bifunctional operation ability makes it well-suited for energy storage and management, producing valuable chemicals in the PCEC mode with renewables. Additionally, generating electricity from valuable chemical fuels in the PCFC mode. However, as a new and standalone technology, several challenges accompanying its operation ranging from its reaction, the charge defect transport, and scale-up. Thus, there is a need to address these complexities and comprehensively answer the PCEC integration requirements with fossil fuel power plants, performance requirements, and technical and non-technical gaps for it to be used as large-scale energy storage and eventual implementation at the system level.

The goal of this dissertation is to address some of these challenges associated with the design, operation, and integration of RePCEC into fossil power plants and renewable energy sources for methane production. And to demonstrate the suitability of the integrated RePCEC system as a highly Efficient Energy Storage (EES) system. To solve these challenges, the following research questions are proposed after a comprehensive review of the literature in Chapter 2 and the identification of gaps.

- **RQ1**: What are the current status, challenges, and progress of PCFC, PCEC, and RePCEC technologies?
- **RQ2**: How is the complexity of the reactions and ion-defects transport addressed at the cellular and stack level to capture the PCEC activities?
- **RQ3**: Can the PCEC stack be integrated with fossil fuel power plants and

renewables and be used as energy storage?

- **RQ4**: What are the optimum conditions and their influence on designing a cost-effective integrated energy storage system?
- **RQ5**: What are the impacts of renewables on the carbon footprint of the system and the types of uncertainties attached to the net energy usage and designing of energy storage systems?

Answers to these questions led to significant contributions in the field and generation of new knowledge as summarized in Table 7.1. The summary of this dissertation is sectionalized by chapter in the following paragraphs. Starting from Chapter 2, each chapter answers a research question and the approaches employed to address it.

The introductory chapter described the surge in renewable energy installation and development. The deployment is expected to have an unprecedented rise in 2024 by over 500% of its 2050 projection in 2006. Being aware of the intermittence of common renewable energy like wind and solar, it elaborated the need for efficient energy storage systems to harvest the renewables at times of low demand. It further compared different energy storage technologies including electrochemical cells. The chapter addressed why electrochemical cells are essentially prospective energy storage systems and why PCEC is a potential candidate from pools of electrochemical cells. It gave an introduction to PCECs and their distinguishing features and potential as large-scale energy storage systems.

The second chapter addresses the first research question (RQ1). It thoroughly reviewed extant literature on PCFC, PCEC, and RePCEC and briefly on their materials, proton conducting oxides (PCOs). This review starts from the history and origin of all major electrochemical cells (fuel cells and electrolyzers) from alkaline electrochemical cells (AECs) to proton electrolyte membrane (PEM) electrochemical cells and finally to solid oxide cells (SOC) from which PCECs sprung up. Focusing on the PCEC, started from its material, proton conducting oxides, $LaAlO_3$ in the early 1960s from which subsequent ones were referenced. The PCEC material has been delved into since then till a breakthrough in material sintering in the early 2000s. This further developed their application into PCFC and later its reverse operation in PCEC and finally in a combined operation standalone cell, RePCEC. The progress among these standalone cells was discussed and individually reviewed. Overall, researchers and scientists have focused on the design of materials

for each of the cells to suit individual operation, electricity generation for PCFC, and electrolysis for PCEC. While the primary emphasis of material design has centered on water electrolysis reaction for the generation of hydrogen, several other reactions are yet to be explored. Thus, many gaps and challenges were identified and mentioned for each of the cells ranging from methane production from co-electrolysis of CO_2 and H_2O in PCEC and generating high power density electricity from PCFC when run with methane. In between is the design of efficient material that serves dual functions and is bidirectional in RePCEC operation. Integration of these cells to other systems is virtually non-existent on a small scale. Thus, large-scale integration most especially with the grid is not in the literature. The techno-economic analysis (TEA) and the lifecycle analysis (LCA) are areas with these technologies that are untouched and thereby need adequate attention for advancement.

The third chapter answers the second research question (RQ2). It starts by taking the lead in addressing one of the gaps mentioned in Chapter 2 and that is the production of other valuable chemicals other than hydrogen with PCEC. It specifically considers methane production. Since the end goal is for large-scale production and integration, the bottom-top approach is used. A comprehensive examination of the thermodynamics of an integrated RePCEC system is required, and a model needs to be developed to evaluate and predict its theoretical roundtrip performance at defined conditions. Operating conditions to be considered include temperature, current density, reactant composition, and utilization. This study is crucial for comprehending the performance implications of stack operating conditions on RePCEC energy storage systems. To achieve the objectives, technical modeling of the RePCEC unit cell for co-electolysis of CO_2 and H_2O using an engineering equation solver (EES). This model detailed the reactive porous-media transport, elementary catalytic chemistry, electrochemistry, and the high proton and oxygen vacancy transport at intermediate temperatures within unit cells. The cell electrochemical model is calibrated and validated with experimental results from our collaborators and national laboratories. The model is further simplified to a reduce-order model that can be used for fundamental analysis of the proposed concept. The cell characteristic curve shows lower voltage output as the operating temperature increases and predicts the cell potentials at lower operating current densities. The model presents the rate of methane production at different temperatures and reveals that efficient

PCEC for co-electrolysis of CO_2 and H_2O is operated in the temperature range of 420-470℃ and the optimum being 450℃ at the rate of 0.0391 $moldm^{-3}min^{-1}$.

The fourth chapter answers the third research question (RQ3). This chapter stands at the core of this dissertation, addressing research questions one to three and bridging significant gaps in the utilization of RePCEC as an energy storage system for large-scale grid applications. It described the stack model and highlighted the balance of the stack as this is consequential in its integration into larger systems. Some performance metrics like faradaic and roundtrip efficiencies, thermoneutral voltage, and fuel utilization peculiar to stack and system-level operations were explained. Furthering to the stack-level model, the unit cell electrochemical model is employed in a channel-level RePCEC model, using conservation equations. The stack model is calibrated and validated. This gives details of the effects of reactant composition on the PCFC and PCEC modes of operation. The cell-stack model is utilized to assess the performance implications of different cell operating parameters such as oxidant and reactant compositions and current density. This analysis is used to measure crucial system design and operation parameters like thermal characteristics and roundtrip efficiency.

Moving to the system model, the validated RePCEC stack is integrated with a 600 MW combined cycle powerplant, and solar farm (made up solar photovoltaic system) which serves as the renewable source and thermodynamic balance of plant models. This integrated RePCEC system model is developed in Aspen HYSYS for simulating the steady-state roundtrip operation of energy storage purposes. A detailed analysis of this innovative system's performance is given. The system-level model is explored to analyze different plant configurations and identify the best configuration for a large-scale energy storage system. In doing this, cleaning equipment like the two-stage membrane-based capture system is introduced at the system upstream to increase the CO_2 concentration entering the stack. The idea of recycling the PCEC exit products or purging them before storage for the reverse operation is also explored. Operating conditions of the system, including current density, tank storage volume, and fuel utilization are also investigated.

The goal of this chapter is to identify the best system configuration and operating conditions that enhance the usage of RePCEC as an energy storage system. Seven configurations were considered, four major ones, and the other three were used to evaluate the impact of recycle streams and excess

steam on the former. The base case required passing the flue gas directly into the stack after particulate matter removal. This configuration cropped up to be less efficient and energy-intensive due to the volume of non-reactive reactants. Then two-stage membrane-based carbon capture system (CCS) was introduced to remove the inert and increase the CO_2 concentration going to the stack. This shows better results with stack and system roundtrip efficiencies of 72% and 51.4% respectively compared to 65% and 42.8% in the former configuration. Adding recycle streams to these two configurations did not give a significant change in the stack and system performance. However, recycling unconverted CO_2 alone from the exit gases gave a better outcome. Adding purge streams to the base case with CCS to remove hydrogen and oxygen from the exit gases improves the stack and system efficiencies to 74% and 55.9% respectively. Likewise, adding a CO_2 tank to this system also improves the efficiencies. The base case with CCS and purge has the best performance on average compared to others. Some parametric studies were conducted on the base case with CCS, which revealed that working at 525℃ and current density in the range of 0.4-0.8 A/cm^2 is good for excellent performance.

The fifth chapter deals with the fourth and part of the fifth research question (RQ4 and RQ5). It discussed the economic analysis and carbon footprint of PCEC and compared it with SOEC for hydrogen production through water electrolysis. Using the same system for the PCEC and SOEC stacks, the levelized cost of hydrogen (LCOH) is $2.88 and 3.13 per kg H_2 respectively. This is expected as the energy demand benefits from the intermediate temperatures of PCEC compared to the high temperatures in SOEC. There is also about 34% CO_2 emission reduction with PCEC. A closer look into the LCA of manufacturing the two technologies shows that 37.4% global warming reduction with producing PCEC compared to SOEC. The SOEC system is used to compare the degree of damage using coal-fired power plants as an energy source and solar photovoltaic (PV). The LCA studies demonstrate that the power plant causes the damage of about 700% to human, the environment, and resources compared to solar PV.

The sixth chapter addressed the fifth research question (RQ5). It delved into the economic analysis (EA) and LCAs of RePCEC for methane production through a co-electrolysis reaction. The EA revealed that the $2.24/MMBtu levelized cost of methane (LCOM) is feasible and discussed the competitiveness of this production route to all the conventional ones. The LCA shows low global warming potential with this production route compared to methane steam reforming. This chapter

concludes with a parametric study for the LCOM, emphasizing the energy and stack cost reduction for lower LCOM.

Table 7.1: Summary of contributions and new knowledge in each chapter

Chapter 2	Overview of recent progress, advancement and highlight of gaps with PCEC technology.
Chapter 3	Standardized and satisficing design of PCEC unit cell for the production of methane, hydrogen, and other chemicals.
Chapter 4	Development of stack model and optimal design of integrated RePCEC systems for improved net energy usage and large-scale energy storage using water-energy nexus framework.
Chapter 5	A comprehensive techno-economic analysis (TEA) of large-scale RePCEC operation can predict the levelized cost of hydrogen and methane with the influencing factors. The first levelized cost of methane through co-electrolysis of CO_2 and H_2O in PCEC technology.
Chapter 6	A comprehensive lifecycle analysis (LCA) of large-scale RePCEC operation and the balance of plant components for the integrated system to determine their global warming potential. Damage impact of coal-fired power plant on humans, environment, and resources compared to solar photovoltaic.

Conclusions drawn from the individual modeling studies and analysis presented in chapters 3-5 are provided after that respective chapter. The results and conclusions are summarized in this section, and then broader conclusions are drawn based on the compilation of these results. The findings in this dissertation indicate that integrated RePCEC energy storage systems hold promise as a viable solution for future energy storage requirements. However, substantial further work is necessary before these systems can reach the technological readiness level for development and practical implementation.

7.2 Recommendations for future work

The PCEC technology under study is in its infancy. This dissertation showcases the first work in the co-electrolysis and early contributions to the RePCEC system field. This is intended to initiate new paths and research directions in industries and academia. While addressing specific questions,

it also aims to spark additional research inquiries. A succinct delineation of prospective research directions that build upon this work and related studies is presented below. Addressing these recommendations improves the technological readiness level (TRL) of PCEC technology and hasten its implementation as an efficient energy storage system to enhance sustainability.

1. The model in this work is in steady state, only the steady state operation of the stack, and the system is considered, unsteady state is not considered. Furthermore, while energy storage typically involves some sort of disturbance and dynamism in its operation like start-up, shutdown, mode switching, and load as a result dynamic operation of the cell, stack, and system is recommended to inform holistic decision-making about the technology and enhance system control.
2. Cell and stack models of electrochemical cells are usually material and reaction-centric; this has resulted in several models for the same technology. Future research should integrate machine learning to help with materials and reaction models that can be incorporated into cell and stack models. In that case, a single model can serve many functions, it will only require varying the material and reaction factors.
3. Model calibration and validation with pilot scale design of the PCEC technology is essential to guide on scalability for large-scale implementation.
4. The stack roundtrip efficiency of electrochemical cells is limited by the stack performance, usually pivoted on the operating temperature. High and intermediate-temperature cells are highly susceptible to degradation, future research should include cell and stack degradation in the model. This enhances the accurate economic value of technology.
5. There are myriad of configurations that can be considered for the system level operation, like including several cleaning equipment at the stack head and tail ends, and recycle for the PCFC operation. Other carbon capture technologies can be considered.
6. The circular economy has been adopted using different technologies. The methane produced can be used in the same PCEC operation to produce some other valuable hydrocarbons. Future research should investigate this for environmental and economic benefits.
7. This work focused on integration with a combined cycle power plant with a defined flue gas composition. Future work can integrate with other fossil fuel assets. Also, the oil and gas industries can integrate the technology into their assets.

8. Wastewater after primary treatment is considered as water backup, other sources of non-traditional water use can be considered in future work. Using waste steam is another alternative that is likely to improve overall system efficiency.

9. It was mentioned in the work for PCFC and SOFC benchmarking over five years ago that the cost of PCFC is not that competitive with SOFC as three PCFCs is required to generate the same power density as two SOFCs of the same size. As novel materials with higher power density for PCFC and PCEC are being designed, there is a need to re-evaluate the unit cost of PCEC technology and compare it with SOEC.

10. Lastly, the research on the carbon footprint of PCFC, PCEC, and other solid oxide electrochemical cells is very minimal. Consequently, there is not enough data in the LCA tool to account for the technology inventory. Researchers in industry and academia should start looking into this to build a good database for accurate analysis. Financial institutions can also support it as it might turn out to be millions of dollars in business in the later future.

Book chapter, journal and conference publications

1. **Lateef A. Jolaoso**, Abu Yousuf, Fan Liu, Chuancheng Duan, Pejman Kazempoor, "Analyzing Methane Production via Protonic Ceramic Electrochemical Cells for Efficient Energy Storage Design" Under review.
2. **Lateef A. Jolaoso**, Idris T. Bello, Opeyemi A. Ojelade, Abu Yousuf, Chuancheng Duan, Pejman Kazempoor, "Operational and scaling-up barriers of SOEC and mitigation strategies to boost H_2 production- a comprehensive review" International Journal of Hydrogen.
3. **Lateef A. Jolaoso**, Chuancheng Duan, Pejman Kazempoor, "Life cycle analysis of a hydrogen production system based on solid oxide electrolysis cells integrated with different energy and wastewater sources" International Journal of Hydrogen.
4. **Lateef A. Jolaoso,** Javad Asadi, Chuancheng Duan, Pejman Kazempoor, "A Novel Hydrogen Economy based on Electrochemical Cells Using Water-Energy Nexus Framework", Energy conversion and management.
5. **Lateef A Jolaoso**, Javad Asadi, Pejman Kazempoor, "A Novel Hydrogen Economy Based on Electrochemical Cells Integrated with Fossil Fuel Assets and Wastewater Resources"- Extended abstract -23rd World Hydrogen Energy Conference 2022.
6. **Lateef A Jolaoso,** Javad Asadi, Pejman Kazempoor. "A Novel Hydrogen Economy Based on Electrochemical Cells Integrated with Fossil Fuel Assets and Wastewater Resources"- Proceedings of the ASME 2022 16th International Conference on Energy Sustainability ES 2022.
7. Javad Asadi**, Lateef A Jolaoso,** Pejman Kazempoor, "Efficiency and Flexibility Improvement of an Amine-Based Post Combustion CO_2 Capturing System (CCS) in Full and Partial Loads", Proceedings of the ASME 2022 16th International Conference on Energy Sustainability ES 2022.
8. Opeyemi A. Ojelade, **Lateef A. Jolaoso**, "Electrodialysis and membrane capacitive deionization" Elsevier, Book Chapter, 2024.
9. **Lateef A. Jolaoso**, Oluwadare Badejo, Abu Yousuf, Pejman Kazempoor **"**Kinetics and performance of fuel cells - Solid oxide fuel cell (SOFC)**"** Book chapter-Under review.

REFERENCES

[1] A. G. Olabi, C. Onumaegbu, T. Wilberforce, M. Ramadan, M. A. Abdelkareem, and A. H. Al – Alami, "Critical review of energy storage systems," Energy, vol. 214, p. 118987, 2021/01/01/ 2021, doi: https://doi.org/10.1016/j.energy.2020.118987.

[2] X. Luo, J. Wang, M. Dooner, and J. Clarke, "Overview of current development in electrical energy storage technologies and the application potential in power system operation," Applied Energy, vol. 137, pp. 511-536, 2015/01/01/ 2015, doi: https://doi.org/10.1016/j.apenergy.2014.09.081.

[3] B. V. Mathiesen, H. Lund, D. Connolly, H. Wenzel, P. A. Østergaard, B. Möller, S. Nielsen, I. Ridjan, P. Karnøe, K. Sperling, and F. K. Hvelplund, "Smart Energy Systems for coherent 100% renewable energy and transport solutions," Applied Energy, vol. 145, pp. 139-154, 2015/05/01/ 2015, doi: https://doi.org/10.1016/j.apenergy.2015.01.075.

[4] A. G. Olabi, M. A. Abdelkareem, T. Wilberforce, and E. T. Sayed, "Application of graphene in energy storage device – A review," Renewable and Sustainable Energy Reviews, vol. 135, p. 110026, 2021/01/01/ 2021, doi: https://doi.org/10.1016/j.rser.2020.110026.

[5] T. Kousksou, P. Bruel, A. Jamil, T. El Rhafiki, and Y. Zeraouli, "Energy storage: Applications and challenges," Solar Energy Materials and Solar Cells, vol. 120, pp. 59-80, 2014/01/01/ 2014, doi: https://doi.org/10.1016/j.solmat.2013.08.015.

[6] Z. Zhang, T. Ding, Q. Zhou, Y. Sun, M. Qu, Z. Zeng, Y. Ju, L. Li, K. Wang, and F. Chi, "A review of technologies and applications on versatile energy storage systems," Renewable and Sustainable Energy Reviews, vol. 148, p. 111263, 2021/09/01/ 2021, doi: https://doi.org/10.1016/j.rser.2021.111263.

[7] M. Steilen and L. Jörissen, "Chapter 10 - Hydrogen Conversion into Electricity and Thermal Energy by Fuel Cells: Use of H2-Systems and Batteries," in Electrochemical Energy Storage for Renewable Sources and Grid Balancing, P. T. Moseley and J. Garche Eds. Amsterdam: Elsevier, 2015, pp. 143-158.

[8] K. Hemmes, J. M. Guerrero, and T. Zhelev, "Highly efficient distributed generation and high-capacity energy storage," Chemical Engineering and Processing: Process Intensification, vol. 51, pp. 18-31, 2012.

[9] P. Kazempoor and R. Braun, "Model validation and performance analysis of regenerative solid oxide cells: Electrolytic operation," International Journal of Hydrogen Energy, vol. 39, no. 6, pp. 2669-2684, 2014.

[10] H. Ritchie, P. Rosado, and M. Roser. Energy Production and Consumption [Online] Available: https://ourworldindata.org/energy-production-consumption

[11] B. Petroleum, "Statistical Review of World Energy 2021," ed: The BP London, UK, 2021.

[12] P. Malanima, "World Energy Consumption a Database 1820-2018," Harvard University. https://histecon. fas. harvard. edu/energyhistory/DATABASE% 20World% 20Energy% 20Consumption. pdf, 2020.

[13] IEA. "Renewables." https://www.iea.org/fuels-and-technologies/renewables (accessed 01-13-2023.

[14] I. E. Agency, Energy storage. OECD Publishing, 2014.

[15] U. D. o. Energy, "Energy Storage Grand Challenge: Energy Storage Market Report," NREL/TP-5400-78461; DOE/GO-102020-5497, 2020.

[16] K. C. Divya and J. Østergaard, "Battery energy storage technology for power systems—An overview," Electric Power Systems Research, vol. 79, no. 4, pp. 511-520, 2009/04/01/ 2009, doi: https://doi.org/10.1016/j.epsr.2008.09.017.

[17] A. G. Olabi and M. A. Abdelkareem, "Energy storage systems towards 2050," Energy, vol. 219, p. 119634, 2021/03/15/ 2021, doi: https://doi.org/10.1016/j.energy.2020.119634.

[18] P. Breeze, "Chapter 3 - Compressed Air Energy Storage," in Power System Energy Storage Technologies, P. Breeze Ed.: Academic Press, 2018, pp. 23-31.

[19] S. D. Garvey and A. Pimm, "6 - Compressed air energy storage (CAES)," in Storing Energy (Second Edition), T. M. Letcher Ed.: Elsevier, 2022, pp. 117-140.

[20] M. Read, R. Smith, and K. Pullen, "Optimisation of flywheel energy storage systems with geared transmission for hybrid vehicles," Mechanism and Machine Theory, vol. 87, pp. 191-209, 2015.

[21] K. T. Møller, T. R. Jensen, E. Akiba, and H.-w. Li, "Hydrogen - A sustainable energy carrier," Progress in Natural Science: Materials International, vol. 27, no. 1, pp. 34-40, 2017/02/01/ 2017, doi: https://doi.org/10.1016/j.pnsc.2016.12.014.

[22] E. S. G. C. Roadmap, "US Department of Energy (DOE), 2020," National Hydrogen Energy Roadmap.(Washington, DC, 2002).

[23] R. J. Remick and D. Wheeler, "Reversible Fuel Cells Workshop Summary Report," Energy USDo, editor, 2011.

[24] F. Bauer, S. Denneler, and M. Willert-Porada, "Influence of temperature and humidity on the mechanical properties of Nafion® 117 polymer electrolyte membrane," Journal of Polymer Science Part B: Polymer Physics, vol. 43, no. 7, pp. 786-795, 2005, doi: https://doi.org/10.1002/polb.20367.

[25] Y.-L. Ma, J. Wainright, M. Litt, and R. Savinell, "Conductivity of PBI membranes for high-temperature polymer electrolyte fuel cells," Journal of the Electrochemical Society, vol. 151, no. 1, p. A8, 2003.

[26] T. Lochner, R. M. Kluge, J. Fichtner, H. A. El-Sayed, B. Garlyyev, and A. S. Bandarenka, "Temperature Effects in Polymer Electrolyte Membrane Fuel Cells," ChemElectroChem, vol. 7, no. 17, pp. 3545-3568, 2020, doi: https://doi.org/10.1002/celc.202000588.

[27] P. Kazempoor and R. J. Braun, "Model validation and performance analysis of regenerative solid oxide cells for energy storage applications: Reversible operation," International Journal of Hydrogen Energy, vol. 39, no. 11, pp. 5955-5971, 2014/04/04/ 2014, doi: https://doi.org/10.1016/j.ijhydene.2014.01.186.

[28] C. H. Wendel, Design and analysis of reversible solid oxide cell systems for electrical energy storage. Colorado School of Mines, 2015.

[29] C. Duan, R. Kee, H. Zhu, N. Sullivan, L. Zhu, L. Bian, D. Jennings, and R. O'Hayre, "Highly efficient reversible protonic ceramic electrochemical cells for power generation and fuel production," Nature Energy, vol. 4, no. 3, pp. 230-240, 2019/03/01 2019, doi: 10.1038/s41560-019-0333-2.

[30] C. Duan, J. Huang, N. Sullivan, and R. O'Hayre, "Proton-conducting oxides for energy conversion and storage," Applied Physics Reviews, vol. 7, no. 1, 2020, doi: 10.1063/1.5135319.

[31] H. Zhu, S. Ricote, C. Duan, R. P. O'Hayre, and R. J. Kee, "Defect Chemistry and Transport within Dense $BaCe_{0.7}Zr_{0.1}Y_{0.1}Yb_{0.1}O_{3-\delta}$ (BCZYYb) Proton-Conducting Membranes," Journal of The Electrochemical Society, vol. 165, no. 10, p. F845, 2018/07/25 2018, doi: 10.1149/2.1091810jes.

[32] H. Zhu and R. J. Kee, "Membrane polarization in mixed-conducting ceramic fuel cells and electrolyzers," International Journal of Hydrogen Energy, vol. 41, no. 4, pp. 2931-2943, 2016.

[33] M. Marrony, Proton-conducting ceramics: from fundamentals to applied research. CRC Press, 2015.

[34] L. Q. Le, C. H. Hernandez, M. H. Rodriguez, L. Zhu, C. Duan, H. Ding, R. P. O'Hayre, and N. P. Sullivan, "Proton-conducting ceramic fuel cells: Scale up and stack integration," Journal of Power Sources, vol. 482, p. 228868, 2021/01/15/ 2021, doi: https://doi.org/10.1016/j.jpowsour.2020.228868.

[35] K. Katahira, Y. Kohchi, T. Shimura, and H. Iwahara, "Protonic conduction in Zr-substituted BaCeO3," Solid State Ionics, vol. 138, no. 1-2, pp. 91-98, 2000.

[36] L. Lei, J. Zhang, Z. Yuan, J. Liu, M. Ni, and F. Chen, "Progress report on proton conducting solid oxide electrolysis cells," Advanced Functional Materials, vol. 29, no. 37, p. 1903805, 2019.

[37] F. He, S. Liu, T. Wu, M. Yang, W. Li, G. Yang, F. Zhu, H. Zhang, K. Pei, Y. Chen, W. Zhou, and Z. Shao, "Catalytic Self-Assembled Air Electrode for Highly Active and Durable Reversible Protonic Ceramic Electrochemical Cells," Advanced Functional Materials, vol. 32, no. 48, p. 2206756, 2022, doi: https://doi.org/10.1002/adfm.202206756.

[38] K. Pei, Y. Zhou, K. Xu, H. Zhang, Y. Ding, B. Zhao, W. Yuan, K. Sasaki, Y. Choi, Y. Chen, and M. Liu, "Surface restructuring of a perovskite-type air electrode for reversible protonic ceramic electrochemical cells," Nature Communications, vol. 13, no. 1, p. 2207, 2022/04/22 2022, doi: 10.1038/s41467-022-29866-5.

[39] L. A. Jolaoso, I. T. Bello, O. A. Ojelade, A. Yousuf, C. Duan, and P. Kazempoor, "Operational and scaling-up barriers of SOEC and mitigation strategies to boost H2 production- a comprehensive review," International Journal of Hydrogen Energy, 2023/05/26/ 2023, doi: https://doi.org/10.1016/j.ijhydene.2023.05.077.

[40] F. C. Handbook, "US Department of Energy, Office of Fossil Energy, National Energy Technology Laboratory," Morgantown, USA, 2004.

[41] R. Hino, K. Haga, H. Aita, and K. Sekita, "38. R&D on hydrogen production by high-temperature electrolysis of steam," Nuclear Engineering and Design, vol. 233, no. 1-3, pp. 363-375, 2004.

[42] C. Vogt, M. Monai, G. J. Kramer, and B. M. Weckhuysen, "The renaissance of the Sabatier reaction and its applications on Earth and in space," Nature Catalysis, vol. 2, no. 3, pp. 188-197, 2019/03/01 2019, doi: 10.1038/s41929-019-0244-4.

[43] J. T. S. Irvine, D. Neagu, M. C. Verbraeken, C. Chatzichristodoulou, C. Graves, and M. B. Mogensen, "Evolution of the electrochemical interface in high-temperature fuel cells and electrolysers," Nature Energy, vol. 1, no. 1, p. 15014, 2016/01/11 2016, doi: 10.1038/nenergy.2015.14.

[44] S. Choi, T. C. Davenport, and S. M. Haile, "Protonic ceramic electrochemical cells for hydrogen production and electricity generation: exceptional reversibility, stability, and demonstrated faradaic efficiency," Energy & Environmental Science, 10.1039/C8EE02865F vol. 12, no. 1, pp. 206-215, 2019, doi: 10.1039/C8EE02865F.

[45] T. M. Gür, "Review of electrical energy storage technologies, materials and systems: challenges and prospects for large-scale grid storage," Energy & environmental science, vol. 11, no. 1, pp. 2696-2767, 2018, doi: 10.1039/c8ee01419a.

[46] C. Duan, J. Huang, N. Sullivan, and R. O'Hayre, "Proton-conducting oxides for energy conversion and storage," Applied Physics Reviews, vol. 7, no. 1, p. 011314, 2020/03/01 2020, doi: 10.1063/1.5135319.

[47] P. Babilo and S. M. Haile, "Enhanced Sintering of Yttrium-Doped Barium Zirconate by Addition of ZnO," Journal of the American Ceramic Society, vol. 88, no. 9, pp. 2362-2368, 2005, doi: https://doi.org/10.1111/j.1551-2916.2005.00449.x.

[48] J. Tong, D. Clark, M. Hoban, and R. O'Hayre, "Cost-effective solid-state reactive sintering method for high conductivity proton conducting yttrium-doped barium zirconium ceramics," Solid State Ionics, vol. 181, no. 11, pp. 496-503, 2010/04/29/ 2010, doi: https://doi.org/10.1016/j.ssi.2010.02.008.

[49] S. Nikodemski, J. Tong, and R. O'Hayre, "Solid-state reactive sintering mechanism for proton conducting ceramics," Solid State Ionics, vol. 253, pp. 201-210, 2013.

[50] J. Tong, D. Clark, L. Bernau, M. Sanders, and R. O'Hayre, "Solid-state reactive sintering mechanism for large-grained yttrium-doped barium zirconate proton conducting ceramics," Journal of Materials Chemistry, vol. 20, no. 30, pp. 6333-6341, 2010.

[51] H. Ding, W. Wu, C. Jiang, Y. Ding, W. Bian, B. Hu, P. Singh, C. J. Orme, L. Wang, Y. Zhang, and D. Ding, "Self-sustainable protonic ceramic electrochemical cells using a triple conducting electrode for hydrogen and power production," Nature Communications, vol. 11, no. 1, p. 1907, 2020/04/20 2020, doi: 10.1038/s41467-020-15677-z.

[52] M. Sterner, "Bioenergy and renewable power methane in integrated 100% renewable energy systems," kassel university press, 2009.

[53] U. Eberle, B. Müller, and R. von Helmolt, "Fuel cell electric vehicles and hydrogen infrastructure: status 2012," Energy & Environmental Science, 10.1039/C2EE22596D vol. 5, no. 10, pp. 8780-8798, 2012, doi: 10.1039/C2EE22596D.

[54] R. M. Navarro, R. Guil, and J. L. G. Fierro, "2 - Introduction to hydrogen production," in Compendium of Hydrogen Energy, V. Subramani, A. Basile, and T. N. Veziroğlu Eds. Oxford: Woodhead Publishing, 2015, pp. 21-61.

[55] M. Carmo, D. L. Fritz, J. Mergel, and D. Stolten, "A comprehensive review on PEM water electrolysis," International Journal of Hydrogen Energy, vol. 38, no. 12, pp. 4901-4934, 2013/04/22/ 2013, doi: https://doi.org/10.1016/j.ijhydene.2013.01.151.

[56] M. Lehner, R. Tichler, H. Steinmüller, and M. Koppe, Power-to-gas: technology and business models. Springer, 2014.

[57] C. Graves, S. D. Ebbesen, S. H. Jensen, S. B. Simonsen, and M. B. Mogensen, "Eliminating degradation in solid oxide electrochemical cells by reversible operation," Nature Materials, vol. 14, no. 2, pp. 239-244, 2015/02/01 2015, doi: 10.1038/nmat4165.

[58] A. Yilanci, I. Dincer, and H. K. Ozturk, "A review on solar-hydrogen/fuel cell hybrid energy systems for stationary applications," Progress in Energy and Combustion Science, vol. 35, no. 3, pp. 231-244, 2009/06/01/ 2009, doi: https://doi.org/10.1016/j.pecs.2008.07.004.

[59] A. Hauch, S. D. Ebbesen, S. H. Jensen, and M. Mogensen, "Highly efficient high temperature electrolysis," Journal of Materials Chemistry, 10.1039/B718822F vol. 18, no. 20, pp. 2331-2340, 2008, doi: 10.1039/B718822F.

[60] S. Gopalan, G. Ye, and U. B. Pal, "Regenerative, coal-based solid oxide fuel cell-electrolyzers," Journal of Power Sources, vol. 162, no. 1, pp. 74-80, 2006/11/08/ 2006, doi: https://doi.org/10.1016/j.jpowsour.2006.07.001.

[61] C. H. Wendel, P. Kazempoor, and R. J. Braun, "Novel electrical energy storage system based on reversible solid oxide cells: System design and operating conditions," Journal of Power Sources, vol. 276, pp. 133-144, 2015/02/15/ 2015, doi: https://doi.org/10.1016/j.jpowsour.2014.10.205.

[62] S. Dangwal, R. Liu, and S.-J. Kim, "High-temperature ethane dehydrogenation in microporous zeolite membrane reactor: Effect of operating conditions," Chemical Engineering Journal, vol. 328, pp. 862-872, 2017/11/15/ 2017, doi: https://doi.org/10.1016/j.cej.2017.07.108.

[63] Z. Li, Q. He, C. Wang, Q. Xu, M. Guo, I. T. Bello, and M. Ni, "Ethylene and power cogeneration from proton ceramic fuel cells (PCFC): A thermo-electrochemical modelling study," Journal of Power Sources, vol. 536, p. 231503, 2022/07/15/ 2022, doi: https://doi.org/10.1016/j.jpowsour.2022.231503.

[64] C. Chen and G. Ma, "Proton conduction in BaCe1− xGdxO3− α at intermediate temperature and its application to synthesis of ammonia at atmospheric pressure," Journal of Alloys and Compounds, vol. 485, no. 1-2, pp. 69-72, 2009.

[65] L. Zhu, C. Cadigan, C. Duan, J. Huang, L. Bian, L. Le, C. H. Hernandez, V. Avance, R. O'Hayre, and N. P. Sullivan, "Ammonia-fed reversible protonic ceramic fuel cells with Ru-based catalyst," Communications Chemistry, vol. 4, no. 1, p. 121, 2021/08/17 2021, doi: 10.1038/s42004-021-00559-2.

[66] N. Danilov, A. Tarutin, J. Lyagaeva, G. Vdovin, and D. Medvedev, "CO 2-promoted hydrogen production in a protonic ceramic electrolysis cell," Journal of Materials Chemistry A, vol. 6, no. 34, pp. 16341-16346, 2018.

[67] K. Ferguson, A. Dubois, K. Albrecht, and R. J. Braun, "High performance protonic ceramic fuel cell systems for distributed power generation," Energy Conversion and Management, vol. 248, p. 114763, 2021/11/15/ 2021, doi: https://doi.org/10.1016/j.enconman.2021.114763.

[68] F. Liu, D. Ding, and C. Duan, "Protonic Ceramic Electrochemical Cells for Synthesizing Sustainable Chemicals and Fuels," Advanced Science, vol. n/a, no. n/a, p. 2206478, doi: https://doi.org/10.1002/advs.202206478.

[69] V. Kyriakou, I. Garagounis, A. Vourros, E. Vasileiou, and M. Stoukides, "An Electrochemical Haber-Bosch Process," Joule, vol. 4, no. 1, pp. 142-158, 2020/01/15/ 2020, doi: https://doi.org/10.1016/j.joule.2019.10.006.

[70] F. He, Y. Zhou, T. Hu, Y. Xu, M. Hou, F. Zhu, D. Liu, H. Zhang, K. Xu, M. Liu, and Y. Chen, "An Efficient High-Entropy Perovskite-Type Air Electrode for Reversible Oxygen Reduction and Water Splitting in Protonic Ceramic Cells," Advanced Materials, vol. 35, no. 16, p. 2209469, 2023, doi: https://doi.org/10.1002/adma.202209469.

[71] K. Xu, H. Zhang, Y. Xu, F. He, Y. Zhou, Y. Pan, J. Ma, B. Zhao, W. Yuan, Y. Chen, and M. Liu, "An Efficient Steam-Induced Heterostructured Air Electrode for Protonic Ceramic Electrochemical Cells," Advanced Functional Materials, vol. 32, no. 23, p. 2110998, 2022, doi: https://doi.org/10.1002/adfm.202110998.

[72] S. H. Morejudo, R. Zanón, S. Escolástico, I. Yuste-Tirados, H. Malerød-Fjeld, P. K. Vestre, W. G. Coors, A. Martínez, T. Norby, and J. M. Serra, "Direct conversion of methane to

aromatics in a catalytic co-ionic membrane reactor," Science, vol. 353, no. 6299, pp. 563-566, 2016.

[73] R. De Levie, "The electrolysis of water," Journal of Electroanalytical Chemistry, vol. 476, no. 1, pp. 92-93, 1999.

[74] G. Chisholm and L. Cronin, "Chapter 16 - Hydrogen From Water Electrolysis," in Storing Energy, T. M. Letcher Ed. Oxford: Elsevier, 2016, pp. 315-343.

[75] T. Smolinka, H. Bergmann, J. Garche, and M. Kusnezoff, "Chapter 4 - The history of water electrolysis from its beginnings to the present," in Electrochemical Power Sources: Fundamentals, Systems, and Applications, T. Smolinka and J. Garche Eds.: Elsevier, 2022, pp. 83-164.

[76] G. Hoogers, "Fuel Cell Technology Handbook," CRC Press, vol. Technology & Engineering p. 360 pages, 2002.

[77] J. Zhang, L. Zhang, H. Liu, A. Sun, and R.-S. Liu, Electrochemical Technologies for Energy Storage and Conversion, 2 Volume Set. John Wiley & Sons, 2011.

[78] W. Kreuter and H. Hofmann, "Electrolysis: the important energy transformer in a world of sustainable energy," International Journal of Hydrogen Energy, vol. 23, no. 8, pp. 661-666, 1998.

[79] M.-C. Pera, D. Hissel, H. Gualous, and C. Turpin, Electrochemical components. John Wiley & Sons, 2013.

[80] A. H. Abdol Rahim, A. S. Tijani, S. K. Kamarudin, and S. Hanapi, "An overview of polymer electrolyte membrane electrolyzer for hydrogen production: Modeling and mass transport," Journal of Power Sources, vol. 309, pp. 56-65, 2016/03/31/ 2016, doi: https://doi.org/10.1016/j.jpowsour.2016.01.012.

[81] W. Dönitz and E. Erdle, "High-temperature electrolysis of water vapor—status of development and perspectives for application," International Journal of Hydrogen Energy, vol. 10, no. 5, pp. 291-295, 1985.

[82] R. J. Ortiz, "Oil-Fueled Accumulation in Late Capitalism: Energy, Uneven Development, and Climate Crisis," Critical Historical Studies, vol. 7, no. 2, pp. 205-240, 2020.

[83] A. M. Oliveira, R. R. Beswick, and Y. Yan, "A green hydrogen economy for a renewable energy society," Current Opinion in Chemical Engineering, vol. 33, p. 100701, 2021/09/01/ 2021, doi: https://doi.org/10.1016/j.coche.2021.100701.

[84] J. Haldane, "Daedalus or science and the future," Kegan, Paul, Trench, Trubner and Company Ltd., , London,, 1924.

[85] C. H. Wendel, "DESIGN AND ANALYSIS OF REVERSIBLE SOLID OXIDE CELL SYSTEMS FOR ELECTRICAL ENERGY STORAGE," 2015, doi: https://www.mines.edu/aes/wp-content/uploads/sites/320/2020/01/Wendel_PhD-Thesis-2015.pdf.

[86] C. Wulf, J. Linssen, and P. Zapp, "Chapter 9 - Power-to-Gas—Concepts, Demonstration, and Prospects," in Hydrogen Supply Chains, C. Azzaro-Pantel Ed.: Academic Press, 2018, pp. 309-345.

[87] M. Schalenbach, G. Tjarks, M. Carmo, W. Lueke, M. Mueller, and D. Stolten, "Acidic or Alkaline? Towards a New Perspective on the Efficiency of Water Electrolysis," Journal of The Electrochemical Society, vol. 163, no. 11, pp. F3197-F3208, 2016, doi: 10.1149/2.0271611jes.

[88] F. Forrat, M. Christen, G. Dauge, G. Danner, and P. Trevoux, "Electrolyte solide a base de aila03. application aux piles a combustible," Comptes rendus hebdomadaires des seances de l academie des sciences, vol. 259, no. 17, pp. 2813-&, 1964.

[89] H. Iwahara, H. Uchida, and S. Tanaka, "High temperature type proton conductor based on SrCeO3 and its application to solid electrolyte fuel cells," Solid State Ionics, vol. 9-10, pp. 1021-1025, 1983/12/01/ 1983, doi: https://doi.org/10.1016/0167-2738(83)90125-X.

[90] H. Iwahara, H. Uchida, and S. Tanaka, "High temperature-type proton conductive solid oxide fuel cells using various fuels," Journal of Applied Electrochemistry, vol. 16, no. 5, pp. 663-668, 1986/09/01 1986, doi: 10.1007/BF01006916.

[91] S. Stotz and C. Wagner, "Die löslichkeit von wasserdampf und wasserstoff in festen oxiden," Berichte der Bunsengesellschaft für physikalische Chemie, vol. 70, no. 8, pp. 781-788, 1966.

[92] H. Iwahara, H. Uchida, and S. Tanaka, "High temperature type proton conductor based on SrCeO3 and its application to solid electrolyte fuel cells," Solid State Ionics, vol. 9, pp. 1021-1025, 1983.

[93] S. H. Morejudo, R. Zanón, S. Escolástico, I. Yuste-Tirados, H. Malerød-Fjeld, P. K. Vestre, W. G. Coors, A. Martínez, T. Norby, J. M. Serra, and C. Kjølseth, "Direct conversion of methane to aromatics in a catalytic co-ionic membrane reactor," Science, vol. 353, no. 6299, pp. 563-566, 2016, doi: doi:10.1126/science.aag0274.

[94] Z. Pan, C. Duan, T. Pritchard, A. Thatte, E. White, R. Braun, R. O'Hayre, and N. P. Sullivan, "High-yield electrochemical upgrading of CO2 into CH4 using large-area protonic ceramic electrolysis cells," Applied Catalysis B: Environmental, vol. 307, p. 121196, 2022/06/15/ 2022, doi: https://doi.org/10.1016/j.apcatb.2022.121196.

[95] F. Liu, H. Deng, D. Diercks, P. Kumar, M. H. A. Jabbar, C. Gumeci, Y. Furuya, N. Dale, T. Oku, M. Usuda, P. Kazempoor, L. Fang, D. Chen, B. Liu, and C. Duan, "Lowering the operating temperature of protonic ceramic electrochemical cells to <450 °C," Nature Energy, 2023/09/07 2023, doi: 10.1038/s41560-023-01350-4.

[96] J. C. Ruiz-Morales, D. Marrero-López, J. Canales-Vázquez, and J. T. Irvine, "Symmetric and reversible solid oxide fuel cells," Rsc Advances, vol. 1, no. 8, pp. 1403-1414, 2011.

[97] L. Yang, S. Wang, K. Blinn, M. Liu, Z. Liu, Z. Cheng, and M. Liu, "Enhanced sulfur and coking tolerance of a mixed ion conductor for SOFCs: BaZr0. 1Ce0. 7Y0. 2–x Yb x O3–δ," Science, vol. 326, no. 5949, pp. 126-129, 2009.

[98] C. Duan, J. Tong, M. Shang, S. Nikodemski, M. Sanders, S. Ricote, A. Almansoori, and R. O'Hayre, "Readily processed protonic ceramic fuel cells with high performance at low temperatures," Science, vol. 349, no. 6254, pp. 1321-1326, 2015, doi: doi:10.1126/science.aab3987.

[99] Y. Zheng, J. Wang, B. Yu, W. Zhang, J. Chen, J. Qiao, and J. Zhang, "A review of high temperature co-electrolysis of H 2 O and CO 2 to produce sustainable fuels using solid oxide electrolysis cells (SOECs): advanced materials and technology," Chemical Society Reviews, vol. 46, no. 5, pp. 1427-1463, 2017.

[100] S. Liu, Q. Liu, X.-Z. Fu, and J.-L. Luo, "Cogeneration of ethylene and energy in protonic fuel cell with an efficient and stable anode anchored with in-situ exsolved functional metal nanoparticles," Applied Catalysis B: Environmental, vol. 220, pp. 283-289, 2018.

[101] H. Zhu, S. Ricote, C. Duan, R. P. O'Hayre, and R. J. Kee, "Defect chemistry and transport within dense BaCe0. 7Zr0. 1Y0. 1Yb0. 1O3− δ (BCZYYb) proton-conducting membranes," Journal of The Electrochemical Society, vol. 165, no. 10, p. F845, 2018.

[102] L. Lei, Z. Tao, X. Wang, J. P. Lemmon, and F. Chen, "Intermediate-temperature solid oxide electrolysis cells with thin proton-conducting electrolyte and a robust air electrode," Journal of Materials Chemistry A, vol. 5, no. 44, pp. 22945-22951, 2017.

[103] I. T. Bello, S. Zhai, S. Zhao, Z. Li, N. Yu, and M. Ni, "Scientometric review of proton-conducting solid oxide fuel cells," International Journal of Hydrogen Energy, vol. 46, no. 75, pp. 37406-37428, 2021.

[104] H. Zhu, S. Ricote, W. G. Coors, and R. J. Kee, "Interpreting equilibrium-conductivity and conductivity-relaxation measurements to establish thermodynamic and transport properties for multiple charged defect conducting ceramics," Faraday discussions, vol. 182, pp. 49-74, 2015.

[105] D. Medvedev, A. Murashkina, E. Pikalova, A. Demin, A. Podias, and P. Tsiakaras, "BaCeO3: Materials development, properties and application," Progress in materials science, vol. 60, pp. 72-129, 2014.

[106] K. Katahira, Y. Kohchi, T. Shimura, and H. Iwahara, "Protonic conduction in Zr-substituted BaCeO3," Solid State Ionics, vol. 138, no. 1, pp. 91-98, 2000/12/01/ 2000, doi: https://doi.org/10.1016/S0167-2738(00)00777-3.

[107] C. Duan, R. J. Kee, H. Zhu, C. Karakaya, Y. Chen, S. Ricote, A. Jarry, E. J. Crumlin, D. Hook, R. Braun, N. P. Sullivan, and R. O'Hayre, "Highly durable, coking and sulfur tolerant, fuel-flexible protonic ceramic fuel cells," Nature, vol. 557, no. 7704, pp. 217-222, 2018/05/01 2018, doi: 10.1038/s41586-018-0082-6.

[108] N. Kochetova, I. Animitsa, D. Medvedev, A. Demin, and P. Tsiakaras, "Recent activity in the development of proton-conducting oxides for high-temperature applications," Rsc Advances, vol. 6, no. 77, pp. 73222-73268, 2016.

[109] H. Zhu, S. Ricote, and R. J. Kee, "Thermodynamics, transport, and electrochemistry in protonic ceramic electrolysis cells," in High-Temperature Electrolysis: From fundamentals to applications: IOP Publishing, 2023.

[110] E. Vøllestad, R. Strandbakke, M. Tarach, D. Catalán-Martínez, M.-L. Fontaine, D. Beeaff, D. R. Clark, J. M. Serra, and T. Norby, "Mixed proton and electron conducting double perovskite anodes for stable and efficient tubular proton ceramic electrolysers," Nature Materials, vol. 18, no. 7, pp. 752-759, 2019/07/01 2019, doi: 10.1038/s41563-019-0388-2.

[111] S. Choi, C. J. Kucharczyk, Y. Liang, X. Zhang, I. Takeuchi, H.-I. Ji, and S. M. Haile, "Exceptional power density and stability at intermediate temperatures in protonic ceramic fuel cells," Nature Energy, vol. 3, no. 3, pp. 202-210, 2018/03/01 2018, doi: 10.1038/s41560-017-0085-9.

[112] H. An, H.-W. Lee, B.-K. Kim, J.-W. Son, K. J. Yoon, H. Kim, D. Shin, H.-I. Ji, and J.-H. Lee, "A 5×5 cm2 protonic ceramic fuel cell with a power density of 1.3 W cm–2 at 600 °C," Nature Energy, vol. 3, no. 10, pp. 870-875, 2018/10/01 2018, doi: 10.1038/s41560-018-0230-0.

[113] C. Duan, Ceramic electrochemical cells for power generation and fuel production. Colorado School of Mines, 2018.

[114] J. Kim, S. Sengodan, S. Kim, O. Kwon, Y. Bu, and G. Kim, "Proton conducting oxides: A review of materials and applications for renewable energy conversion and storage," Renewable and Sustainable Energy Reviews, vol. 109, pp. 606-618, 2019/07/01/ 2019, doi: https://doi.org/10.1016/j.rser.2019.04.042.

[115] W. Zhang and Y. H. Hu, "Progress in proton-conducting oxides as electrolytes for low-temperature solid oxide fuel cells: From materials to devices," Energy Science & Engineering, vol. 9, no. 7, pp. 984-1011, 2021, doi: https://doi.org/10.1002/ese3.886.

[116] B. Wang, X. Liu, L. Bi, and X. Zhao, "Fabrication of high-performance proton-conducting electrolytes from microwave prepared ultrafine powders for solid oxide fuel cells," Journal of Power Sources, vol. 412, pp. 664-669, 2019.

[117] J. H. Shim, "Ceramics breakthrough," Nature Energy, vol. 3, no. 3, pp. 168-169, 2018/03/01 2018, doi: 10.1038/s41560-018-0110-7.

[118] K. Bae, D. H. Kim, H. J. Choi, J.-W. Son, and J. H. Shim, "High-Performance Protonic Ceramic Fuel Cells with 1 μm Thick Y:Ba(Ce, Zr)O3 Electrolytes," Advanced Energy Materials, vol. 8, no. 25, p. 1801315, 2018, doi: https://doi.org/10.1002/aenm.201801315.

[119] Y. Xu, F. Hu, Y. Guo, J. Zhang, Y. Huang, W. Zhou, J. Sun, B. He, and L. Zhao, "Probing oxygen reduction and water uptake kinetics of BaCo0.4Fe0.4Zr0.1Y0.1-xZnxO3-δ cathodes for protonic ceramic fuel cells," Separation and Purification Technology, vol. 297, p. 121482, 2022/09/15/ 2022, doi: https://doi.org/10.1016/j.seppur.2022.121482.

[120] S. Im, J.-H. Lee, and H.-I. Ji, "PrBa0.5Sr0.5Co1.5Fe0.5O5+δ composite cathode in protonic ceramic fuel cells," Journal of the Korean Ceramic Society, vol. 58, no. 3, pp. 351-358, 2021/05/01 2021, doi: 10.1007/s43207-021-00109-5.

[121] E. Shin, M. Shin, H. Lee, and J.-S. Park, "Catalysts for composite cathodes of protonic ceramic fuel cells," Ceramics International, vol. 44, no. 7, pp. 8423-8426, 2018/05/01/ 2018, doi: https://doi.org/10.1016/j.ceramint.2018.02.036.

[122] N. Wang, C. Tang, L. Du, R. Zhu, L. Xing, Z. Song, B. Yuan, L. Zhao, Y. Aoki, and S. Ye, "Advanced Cathode Materials for Protonic Ceramic Fuel Cells: Recent Progress and

Future Perspectives," Advanced Energy Materials, vol. 12, no. 34, p. 2201882, 2022, doi: https://doi.org/10.1002/aenm.202201882.

[123] H. Matsuo, K. Nakane, Y. Matsuzaki, and J. Otomo, "Effect of lanthanum tungstate hole-blocking layer for improvement of energy efficiency in anode-supported protonic ceramic fuel cells," Journal of the Ceramic Society of Japan, vol. 129, no. 3, pp. 147-153, 2021, doi: 10.2109/jcersj2.20204.

[124] H. Shimada, T. Yamaguchi, H. Sumi, Y. Yamaguchi, K. Nomura, Y. Mizutani, and Y. Fujishiro, "A Key for Achieving Higher Open-Circuit Voltage in Protonic Ceramic Fuel Cells: Lowering Interfacial Electrode Polarization," ACS Applied Energy Materials, vol. 2, no. 1, pp. 587-597, 2019/01/28 2019, doi: 10.1021/acsaem.8b01617.

[125] H. J. Jeong, W. Chang, B. G. Seo, Y. S. Choi, K. H. Kim, D. H. Kim, and J. H. Shim, "High-Performance Ammonia Protonic Ceramic Fuel Cells Using a Pd Inter-Catalyst," Small, vol. 19, no. 22, p. 2208149, 2023, doi: https://doi.org/10.1002/smll.202208149.

[126] Y. Pan, H. Zhang, K. Xu, Y. Zhou, B. Zhao, W. Yuan, K. Sasaki, Y. Choi, Y. Chen, and M. Liu, "A high-performance and durable direct NH3 tubular protonic ceramic fuel cell integrated with an internal catalyst layer," Applied Catalysis B: Environmental, vol. 306, p. 121071, 2022/06/05/ 2022, doi: https://doi.org/10.1016/j.apcatb.2022.121071.

[127] W. G. Coors, "Protonic ceramic fuel cells for high-efficiency operation with methane," Journal of Power Sources, vol. 118, no. 1-2, pp. 150-156, 2003.

[128] J.-S. Park and N. H. Hao, "Direct ethanol-fueled protonic ceramic fuel cell with reforming layer operating at low temperature," International Journal of Hydrogen Energy, vol. 48, no. 50, pp. 19207-19216, 2023.

[129] A. Dhanasekaran, Y. Subramanian, L. A. Omeiza, V. Raj, H. P. H. M. Yassin, M. A. Sa, and A. K. Azad, "Computational fluid dynamics for protonic ceramic fuel cell stack modeling: a brief review," Energies, vol. 16, no. 1, p. 208, 2022.

[130] K. Li, T. Araki, T. Kawamura, A. Ota, and Y. Okuyama, "Numerical analysis of current efficiency distributions in a protonic ceramic fuel cell using Nernst-Planck-Poisson model," International Journal of Hydrogen Energy, vol. 45, no. 58, pp. 34139-34149, 2020/11/27/ 2020, doi: https://doi.org/10.1016/j.ijhydene.2020.09.143.

[131] H. Sumi, H. Shimada, Y. Yamaguchi, Y. Mizutani, Y. Okuyama, and K. Amezawa, "Comparison of electrochemical impedance spectra for electrolyte-supported solid oxide fuel cells (SOFCs) and protonic ceramic fuel cells (PCFCs)," Scientific Reports, vol. 11, no. 1, p. 10622, 2021/05/19 2021, doi: 10.1038/s41598-021-90211-9.

[132] K.-Y. Park, Y.-D. Kim, J.-I. Lee, M. Saqib, J.-S. Shin, Y. Seo, J. H. Kim, H.-T. Lim, and J.-Y. Park, "Operation Protocols To Improve Durability of Protonic Ceramic Fuel Cells," ACS Applied Materials & Interfaces, vol. 11, no. 1, pp. 457-468, 2019/01/09 2019, doi: 10.1021/acsami.8b04748.

[133] M. Hou, Y. Pan, and Y. Chen, "Enhanced electrochemical activity and durability of a direct ammonia protonic ceramic fuel cell enabled by an internal catalyst layer," Separation and Purification Technology, vol. 297, p. 121483, 2022/09/15/ 2022, doi: https://doi.org/10.1016/j.seppur.2022.121483.

[134] I. Zvonareva, X.-Z. Fu, D. Medvedev, and Z. Shao, "Electrochemistry and energy conversion features of protonic ceramic cells with mixed ionic-electronic electrolytes," Energy & Environmental Science, 10.1039/D1EE03109K vol. 15, no. 2, pp. 439-465, 2022, doi: 10.1039/D1EE03109K.

[135] A. Tarutin, J. Lyagaeva, A. Farlenkov, S. Plaksin, G. Vdovin, A. Demin, and D. Medvedev, "A reversible protonic ceramic cell with symmetrically designed Pr2NiO4+ δ-based electrodes: fabrication and electrochemical features," Materials, vol. 12, no. 1, p. 118, 2018.

[136] A. Dubois, S. Ricote, and R. J. Braun, "Benchmarking the expected stack manufacturing cost of next generation, intermediate-temperature protonic ceramic fuel cells with solid oxide fuel cell technology," Journal of Power Sources, vol. 369, pp. 65-77, 2017/11/30/ 2017, doi: https://doi.org/10.1016/j.jpowsour.2017.09.024.

[137] K. J. Albrecht, A. Dubois, K. Ferguson, C. Duan, R. P. O'Hayre, and R. J. Braun, "Steady-State and Dynamic Modeling of Intermediate-Temperature Protonic Ceramic Fuel Cells," Journal of The Electrochemical Society, vol. 166, no. 10, p. F687, 2019/06/28 2019, doi: 10.1149/2.0651910jes.

[138] M. Choi, J. Paik, D. Kim, D. Woo, J. Lee, S. J. Kim, J. Lee, and W. Lee, "Exceptionally high performance of protonic ceramic fuel cells with stoichiometric electrolytes," Energy & Environmental Science, 10.1039/D1EE01497H vol. 14, no. 12, pp. 6476-6483, 2021, doi: 10.1039/D1EE01497H.

[139] D. Zou, Y. Yi, Y. Song, D. Guan, M. Xu, R. Ran, W. Wang, W. Zhou, and Z. Shao, "The BaCe0.16Y0.04Fe0.8O3−δ nanocomposite: a new high-performance cobalt-free triple-conducting cathode for protonic ceramic fuel cells operating at reduced temperatures," Journal of Materials Chemistry A, 10.1039/D1TA10652J vol. 10, no. 10, pp. 5381-5390, 2022, doi: 10.1039/D1TA10652J.

[140] K. M. Nowicki, G. Carins, J. Bayne, C. Tupberg, G. J. Irvine, and J. T. S. Irvine, "Characterisation of direct ammonia proton conducting tubular ceramic fuel cells for

maritime applications," Journal of Materials Chemistry A, 10.1039/D2TA07310B vol. 11, no. 1, pp. 352-363, 2023, doi: 10.1039/D2TA07310B.

[141] M. Liang, Y. Zhu, Y. Song, D. Guan, Z. Luo, G. Yang, S. P. Jiang, W. Zhou, R. Ran, and Z. Shao, "A New Durable Surface Nanoparticles-Modified Perovskite Cathode for Protonic Ceramic Fuel Cells from Selective Cation Exsolution under Oxidizing Atmosphere," Advanced Materials, vol. 34, no. 10, p. 2106379, 2022, doi: https://doi.org/10.1002/adma.202106379.

[142] L. Zhu, R. O'Hayre, and N. P. Sullivan, "High performance tubular protonic ceramic fuel cells via highly-scalable extrusion process," International Journal of Hydrogen Energy, vol. 46, no. 54, pp. 27784-27792, 2021/08/05/ 2021, doi: https://doi.org/10.1016/j.ijhydene.2021.06.018.

[143] C. Duan, D. Hook, Y. Chen, J. Tong, and R. O'Hayre, "Zr and Y co-doped perovskite as a stable, high performance cathode for solid oxide fuel cells operating below 500 °C," Energy & Environmental Science, 10.1039/C6EE01915C vol. 10, no. 1, pp. 176-182, 2017, doi: 10.1039/C6EE01915C.

[144] H. Ding, W. Wu, C. Jiang, Y. Ding, W. Bian, B. Hu, P. Singh, C. J. Orme, L. Wang, Y. Zhang, and D. Ding, "Self-sustainable protonic ceramic electrochemical cells using a triple conducting electrode for hydrogen and power production," (in eng), Nat Commun, vol. 11, no. 1, p. 1907, Apr 20 2020, doi: 10.1038/s41467-020-15677-z.

[145] Y. Huang, J. Yu, N. Tian, Y. Qu, W. Tan, Y. Luo, C. Wang, R. Zheng, and J. Zheng, "Performance study of proton conducting electrolytes based on BaZr1− xYxO3-δ for solid oxide electrolysis cell," International Journal of Electrochemical Science, vol. 18, no. 3, p. 100033, 2023.

[146] Y. Patcharavorachot, W. Chalee, D. Saebea, and A. Arpornwichanop, "Performance improvement of the proton-conducting solid oxide electrolysis cell coupled with dry methane reforming," International Journal of Hydrogen Energy, vol. 48, no. 18, pp. 6705-6721, 2023.

[147] F. Liu, D. Ding, and C. Duan, "Protonic ceramic electrochemical cells for synthesizing sustainable chemicals and fuels," Advanced Science, vol. 10, no. 8, p. 2206478, 2023.

[148] L. Jolaoso and S. F. Zaman, "Catalytic ammonia decomposition for hydrogen production: utilization of ammonia in a fuel cell," Sustainable Ammonia Production, pp. 81-105, 2020.

[149] C. Wang, Z. Li, S. Zhao, L. Xia, M. Zhu, M. Han, and M. Ni, "Modelling of an integrated protonic ceramic electrolyzer cell (PCEC) for methanol synthesis," Journal of Power Sources, vol. 559, p. 232667, 2023/03/01/ 2023, doi: https://doi.org/10.1016/j.jpowsour.2023.232667.

[150] Y. Zhou, W. Zhang, N. Kane, Z. Luo, K. Pei, K. Sasaki, Y. Choi, Y. Chen, D. Ding, and M. Liu, "An Efficient Bifunctional Air Electrode for Reversible Protonic Ceramic Electrochemical Cells," Advanced Functional Materials, vol. 31, no. 40, p. 2105386, 2021, doi: https://doi.org/10.1002/adfm.202105386.

[151] F. Zhu, F. He, D. Liu, H. Zhang, Y. Xu, K. Xu, and Y. Chen, "A surface reconfiguration of a perovskite air electrode enables an active and durable reversible protonic ceramic electrochemical cell," Energy Storage Materials, vol. 53, pp. 754-762, 2022/12/01/ 2022, doi: https://doi.org/10.1016/j.ensm.2022.10.009.

[152] G. Li, Y. Gou, R. Ren, C. Xu, J. Qiao, W. Sun, Z. Wang, and K. Sun, "Fluorinated Pr2NiO4+δ as high-performance air electrode for tubular reversible protonic ceramic

cells," Journal of Power Sources, vol. 508, p. 230343, 2021/10/01/ 2021, doi: https://doi.org/10.1016/j.jpowsour.2021.230343.

[153] K. Pei, S. Luo, F. He, J. Arbiol, Y. Xu, F. Zhu, Y. Wang, and Y. Chen, "Constructing an active and stable oxygen electrode surface for reversible protonic ceramic electrochemical cells," Applied Catalysis B: Environmental, vol. 330, p. 122601, 2023/08/05/ 2023, doi: https://doi.org/10.1016/j.apcatb.2023.122601.

[154] Y. Zhou, E. Liu, Y. Chen, Y. Liu, L. Zhang, W. Zhang, Z. Luo, N. Kane, B. Zhao, L. Soule, Y. Niu, Y. Ding, H. Ding, D. Ding, and M. Liu, "An Active and Robust Air Electrode for Reversible Protonic Ceramic Electrochemical Cells," ACS Energy Letters, vol. 6, no. 4, pp. 1511-1520, 2021/04/09 2021, doi: 10.1021/acsenergylett.1c00432.

[155] Y. Niu, Y. Zhou, W. Zhang, Y. Zhang, C. Evans, Z. Luo, N. Kane, Y. Ding, Y. Chen, X. Guo, W. Lv, and M. Liu, "Highly Active and Durable Air Electrodes for Reversible Protonic Ceramic Electrochemical Cells Enabled by an Efficient Bifunctional Catalyst," Advanced Energy Materials, vol. 12, no. 12, p. 2103783, 2022, doi: https://doi.org/10.1002/aenm.202103783.

[156] M. Liang, Y. Song, D. Liu, L. Xu, M. Xu, G. Yang, W. Wang, W. Zhou, R. Ran, and Z. Shao, "Magnesium tuned triple conductivity and bifunctionality of BaCo0.4Fe0.4Zr0.1Y0.1O3-δ perovskite towards reversible protonic ceramic electrochemical cells," Applied Catalysis B: Environmental, vol. 318, p. 121868, 2022/12/05/ 2022, doi: https://doi.org/10.1016/j.apcatb.2022.121868.

[157] C. Lee, S. S. Shin, J. Kim, J. Choi, M. Choi, and H. H. Shin, "Tailoring an Interface Microstructure for High-Performance Reversible Protonic Ceramic Electrochemical Cells

via Soft Lithography," ACS Applied Materials & Interfaces, vol. 14, no. 28, pp. 32124-32133, 2022/07/20 2022, doi: 10.1021/acsami.2c08918.

[158] Z. Liu, Z. Tang, Y. Song, G. Yang, W. Qian, M. Yang, Y. Zhu, R. Ran, W. Wang, W. Zhou, and Z. Shao, "High-Entropy Perovskite Oxide: A New Opportunity for Developing Highly Active and Durable Air Electrode for Reversible Protonic Ceramic Electrochemical Cells," Nano-Micro Letters, vol. 14, no. 1, p. 217, 2022/11/09 2022, doi: 10.1007/s40820-022-00967-6.

[159] R. Braun, A. Dubois, K. Ferguson, C. Duan, C. Karakaya, R. Kee, H. Zhu, N. Sullivan, E. Tang, M. Pastula, A. Wood, T. Joia, and R. O'Hayre, "Development of kW-Scale Protonic Ceramic Fuel Cells and Systems," ECS Transactions, vol. 91, pp. 997-1008, 07/10 2019, doi: 10.1149/09101.0997ecst.

[160] S. P. Shafi, L. Bi, S. Boulfrad, and E. Traversa, "Y and Ni Co-Doped BaZrO3as a Proton-Conducting Solid Oxide Fuel Cell Electrolyte Exhibiting Superior Power Performance," Journal of The Electrochemical Society, vol. 162, no. 14, pp. F1498-F1503, 2015, doi: 10.1149/2.0701514jes.

[161] C. Duan, J. Tong, M. Shang, S. Nikodemski, M. Sanders, S. Ricote, A. Almansoori, and R. O'Hayre, "Readily processed protonic ceramic fuel cells with high performance at low temperatures," (in eng), Science, vol. 349, no. 6254, pp. 1321-6, Sep 18 2015, doi: 10.1126/science.aab3987.

[162] H. Zhu, R. J. Braun, and R. J. Kee, "Thermodynamic Analysis of Energy Efficiency and Fuel Utilization in Protonic-Ceramic Fuel Cells with Planar Co-Flow Configurations," Journal of The Electrochemical Society, vol. 165, no. 11, pp. F942-F950, 2018, doi: 10.1149/2.0401811jes.

[163] K. J. Albrecht, A. Dubois, K. Ferguson, C. Duan, R. P. O'Hayre, and R. J. Braun, "Steady-State and Dynamic Modeling of Intermediate-Temperature Protonic Ceramic Fuel Cells," Journal of The Electrochemical Society, vol. 166, no. 10, pp. F687-F700, 2019, doi: 10.1149/2.0651910jes.

[164] K. Motylinski, J. Kupecki, B. Numan, Y. S. Hajimolana, and V. Venkataraman, "Dynamic modelling of reversible solid oxide cells for grid stabilization applications," Energy Conversion and Management, vol. 228, p. 113674, 2021/01/15/ 2021, doi: https://doi.org/10.1016/j.enconman.2020.113674.

[165] L. A. Jolaoso, J. Asadi, C. Duan, and P. Kazempoor, "A novel green hydrogen production using water-energy nexus framework," Energy Conversion and Management, vol. 276, p. 116344, 2023/01/15/ 2023, doi: https://doi.org/10.1016/j.enconman.2022.116344.

[166] E. D. Wachsman, "(Invited) Mixed Protonic-Electronic Membrane Reactors; Converting Hydrocarbon Resources and CO2 to Fuels," ECS Meeting Abstracts, vol. MA2019-02, no. 40, p. 1861, 2019/09/01 2019, doi: 10.1149/MA2019-02/40/1861.

[167] R. Ren, J. Sun, G. Wang, C. Xu, J. Qiao, W. Sun, Z. Wang, and K. Sun, "Rational design of Sr2Fe1.5Mo0.4Y0.1O6-δ oxygen electrode with triple conduction for hydrogen production in protonic ceramic electrolysis cell," Separation and Purification Technology, vol. 299, p. 121780, 2022/10/15/ 2022, doi: https://doi.org/10.1016/j.seppur.2022.121780.

[168] H. Tian, W. Li, L. Ma, T. Yang, B. Guan, W. Shi, T. L. Kalapos, and X. Liu, "Deconvolution of Water-Splitting on the Triple-Conducting Ruddlesden–Popper-Phase Anode for Protonic Ceramic Electrolysis Cells," ACS Applied Materials & Interfaces, vol. 12, no. 44, pp. 49574-49585, 2020/11/04 2020, doi: 10.1021/acsami.0c12987.

[169] P. Kazempoor and R. J. Braun, "Model validation and performance analysis of regenerative solid oxide cells: Electrolytic operation," International Journal of Hydrogen Energy, vol. 39, no. 6, pp. 2669-2684, 2014/02/14/ 2014, doi: https://doi.org/10.1016/j.ijhydene.2013.12.010.

[170] H. Zhu and R. J. Kee, "Modeling Protonic-Ceramic Fuel Cells with Porous Composite Electrodes in a Button-Cell Configuration," Journal of The Electrochemical Society, vol. 164, no. 13, p. F1400, 2017/10/07 2017, doi: 10.1149/2.0591713jes.

[171] S. Nitopi, E. Bertheussen, S. B. Scott, X. Liu, A. K. Engstfeld, S. Horch, B. Seger, I. E. L. Stephens, K. Chan, C. Hahn, J. K. Nørskov, T. F. Jaramillo, and I. Chorkendorff, "Progress and Perspectives of Electrochemical CO2 Reduction on Copper in Aqueous Electrolyte," Chemical Reviews, vol. 119, no. 12, pp. 7610-7672, 2019/06/26 2019, doi: 10.1021/acs.chemrev.8b00705.

[172] S. J. Davis, N. S. Lewis, M. Shaner, S. Aggarwal, D. Arent, I. L. Azevedo, S. M. Benson, T. Bradley, J. Brouwer, and Y.-M. Chiang, "Net-zero emissions energy systems," Science, vol. 360, no. 6396, p. eaas9793, 2018.

[173] L. A. Jolaoso, J. Asadi, C. Duan, and P. Kazempoor, "A Novel Hydrogen Economy Based on Electrochemical Cells Fully Integrated With Fossil Fuel Assets and Wastewater Resources," in Energy Sustainability, 2022, vol. 85772: American Society of Mechanical Engineers, p. V001T10A001.

[174] D. T. Whipple and P. J. Kenis, "Prospects of CO2 utilization via direct heterogeneous electrochemical reduction," The Journal of Physical Chemistry Letters, vol. 1, no. 24, pp. 3451-3458, 2010.

[175] E. V. Kondratenko, G. Mul, J. Baltrusaitis, G. O. Larrazábal, and J. Pérez-Ramírez, "Status and perspectives of CO 2 conversion into fuels and chemicals by catalytic, photocatalytic and electrocatalytic processes," Energy & environmental science, vol. 6, no. 11, pp. 3112-3135, 2013.

[176] M. Gattrell, N. Gupta, and A. Co, "A review of the aqueous electrochemical reduction of CO2 to hydrocarbons at copper," Journal of electroanalytical Chemistry, vol. 594, no. 1, pp. 1-19, 2006.

[177] P. Błaszczak, M. Zając, A. Ducka, K. Matlak, B. Wolanin, S.-F. Wang, A. Mandziak, B. Bochentyn, and P. Jasiński, "High-temperature Co-electrolysis of CO2/H2O and direct methanation over Co-impregnated SOEC. Bimetallic synergy between Co and Ni," International Journal of Hydrogen Energy, vol. 47, no. 82, pp. 35017-35037, 2022/09/30/ 2022, doi: https://doi.org/10.1016/j.ijhydene.2022.08.057.

[178] A. D. N. Kamkeng and M. Wang, "Long-term performance prediction of solid oxide electrolysis cell (SOEC) for CO2/H2O co-electrolysis considering structural degradation through modelling and simulation," Chemical Engineering Journal, vol. 429, p. 132158, 2022/02/01/ 2022, doi: https://doi.org/10.1016/j.cej.2021.132158.

[179] H. Xu, B. Chen, J. Irvine, and M. Ni, "Modeling of CH4-assisted SOEC for H2O/CO2 co-electrolysis," International Journal of Hydrogen Energy, vol. 41, no. 47, pp. 21839-21849, 2016/12/21/ 2016, doi: https://doi.org/10.1016/j.ijhydene.2016.10.026.

[180] A. Mahmood, S. Bano, J. H. Yu, and K.-H. Lee, "Performance evaluation of SOEC for CO2/H2O co-electrolysis: Considering the effect of cathode thickness," Journal of CO2 Utilization, vol. 33, pp. 114-120, 2019/10/01/ 2019, doi: https://doi.org/10.1016/j.jcou.2019.05.014.

[181] R. J. Kee, H. Zhu, B. W. Hildenbrand, E. Vøllestad, M. D. Sanders, and R. P. O'Hayre, "Modeling the Steady-State and Transient Response of Polarized and Non-Polarized Proton-Conducting Doped-Perovskite Membranes," Journal of The Electrochemical Society, vol. 160, no. 3, p. F290, 2013/01/23 2013, doi: 10.1149/2.016304jes.

[182] P. Kazempoor, V. Dorer, and F. Ommi, "Modelling and Performance Evaluation of Solid Oxide Fuel Cell for Building Integrated Co-and Polygeneration," Fuel Cells, vol. 10, no. 6, pp. 1074-1094, 2010.

[183] A. J. Bard, L. R. Faulkner, and H. S. White, Electrochemical methods: fundamentals and applications. John Wiley & Sons, 2022.

[184] Q. Wang, L. Li, and C. Wang, "Numerical study of thermoelectric characteristics of a planar solid oxide fuel cell with direct internal reforming of methane," Journal of Power Sources, vol. 186, no. 2, pp. 399-407, 2009.

[185] M. Ni, "2D thermal modeling of a solid oxide electrolyzer cell (SOEC) for syngas production by H2O/CO2 co-electrolysis," International journal of hydrogen energy, vol. 37, no. 8, pp. 6389-6399, 2012.

[186] T. M. Koehler, D. B. Jarrell, and L. J. Bond, "High Temperture Ceramic Fuel Cell Measurement and Diagnostics for Application to Solid Oxide Fuel Cell Systems," Pacific Northwest National Lab.(PNNL), Richland, WA (United States), 2001.

[187] W. Li, H. Wang, Y. Shi, and N. Cai, "Performance and methane production characteristics of H2O–CO2 co-electrolysis in solid oxide electrolysis cells," International journal of hydrogen energy, vol. 38, no. 25, pp. 11104-11109, 2013.

[188] Y. Luo, W. Li, Y. Shi, T. Cao, X. Ye, S. Wang, and N. Cai, "Experimental characterization and theoretical modeling of methane production by H2O/CO2 co-electrolysis in a tubular

solid oxide electrolysis cell," Journal of The Electrochemical Society, vol. 162, no. 10, p. F1129, 2015.

[189] K. Xie, Y. Zhang, G. Meng, and J. T. Irvine, "Direct synthesis of methane from CO 2/H2O in an oxygen-ion conducting solid oxide electrolyser," Energy & Environmental Science, vol. 4, no. 6, pp. 2218-2222, 2011.

[190] IEA. "Renewable power on course to shatter more records as countries around the world speed up deployment." https://www.iea.org/news/renewable-power-on-course-to-shatter-more-records-as-countries-around-the-world-speed-up-deployment (accessed 09/20/2023, 2023).

[191] D. Arvizu, "Meeting the renewable energy challenge: what will it take to reach solar PV's ultimate potential," National Renewable Energy Lab.(NREL), Golden, CO (United States), 2006.

[192] P. Kazempoor and R. Braun, "Model validation and performance analysis of regenerative solid oxide cells for energy storage applications: Reversible operation," international journal of hydrogen energy, vol. 39, no. 11, pp. 5955-5971, 2014.

[193] S. Becker, B. A. Frew, G. B. Andresen, T. Zeyer, S. Schramm, M. Greiner, and M. Z. Jacobson, "Features of a fully renewable US electricity system: Optimized mixes of wind and solar PV and transmission grid extensions," Energy, vol. 72, pp. 443-458, 2014/08/01/ 2014, doi: https://doi.org/10.1016/j.energy.2014.05.067.

[194] D. Castelvecchi. "How Big a Battery Would It Take to Power All of the U.S.?" SPRINGER NATURE AMERICA. https://www.scientificamerican.com/article/castelvecchi-how-big-battery-would-it-take-power-usa/ (accessed.

[195] J. Bai, S. Xin, J. Liu, and K. Zheng, "Roadmap of realizing the high penetration renewable energy in China," Proceedings of the CSEE, vol. 35, no. 14, pp. 3699-3705, 2015.

[196] S. H. Jensen, C. Graves, M. Mogensen, C. Wendel, R. Braun, G. Hughes, Z. Gao, and S. A. Barnett, "Large-scale electricity storage utilizing reversible solid oxide cells combined with underground storage of CO2 and CH4," Energy & Environmental Science, 10.1039/C5EE01485A vol. 8, no. 8, pp. 2471-2479, 2015, doi: 10.1039/C5EE01485A.

[197] C. H. Wendel, Z. Gao, S. A. Barnett, and R. J. Braun, "Modeling and experimental performance of an intermediate temperature reversible solid oxide cell for high-efficiency, distributed-scale electrical energy storage," Journal of Power Sources, vol. 283, pp. 329-342, 2015/06/01/ 2015, doi: https://doi.org/10.1016/j.jpowsour.2015.02.113.

[198] T. F. Fuller and J. N. Harb, Electrochemical engineering. John Wiley & Sons, 2018.

[199] A. Engelbrecht, C. Uhlig, O. Stark, M. Hämmerle, G. Schmid, E. Magori, K. Wiesner-Fleischer, M. Fleischer, and R. Moos, "On the electrochemical CO2 reduction at copper sheet electrodes with enhanced long-term stability by pulsed electrolysis," Journal of The Electrochemical Society, vol. 165, no. 15, p. J3059, 2018.

[200] J. O'Brien, "Thermodynamic considerations for thermal water splitting processes and high temperature electrolysis," in ASME International Mechanical Engineering Congress and Exposition, 2008, vol. 48692, pp. 639-651.

[201] K. Motazedi, Y. K. Salkuyeh, I. J. Laurenzi, H. L. MacLean, and J. A. Bergerson, "Economic and environmental competitiveness of high temperature electrolysis for hydrogen production," International Journal of Hydrogen Energy, vol. 46, no. 41, pp. 21274-21288, 2021/06/15/ 2021, doi: https://doi.org/10.1016/j.ijhydene.2021.03.226.

[202] Z. Li, H. Zhang, H. Xu, and J. Xuan, "Advancing the multiscale understanding on solid oxide electrolysis cells via modelling approaches: A review," Renewable and Sustainable Energy Reviews, vol. 141, p. 110863, 2021/05/01/ 2021, doi: https://doi.org/10.1016/j.rser.2021.110863.

[203] J. Stempien, "FUNDAMENTAL ASPECTS OF SOLID OXIDE ELECTROLYZER CELL MODELLING AND THE APPLICATION FOR THE SYSTEM LEVEL ANALYSIS," 2014.

[204] J. M. Kay and R. M. Nedderman, Fluid mechanics and transfer processes. CUP Archive, 1985.

[205] R. G. Hunter, J. W. Day, A. R. Wiegman, and R. R. Lane, "Municipal wastewater treatment costs with an emphasis on assimilation wetlands in the Louisiana coastal zone," Ecological Engineering, vol. 137, pp. 21-25, 2019/10/01/ 2019, doi: https://doi.org/10.1016/j.ecoleng.2018.09.020.

[206] F. G. Russell, S. Adler, L. R. Albaugh, and G. J. Aldana, "GPSA engineering data book," Gas Process. Suppliers Assoc, vol. 821, 2004.

[207] T. Uki, S. T. Sarda, and T. Mathew, "Design of gas-liquid separator for complete degasing," International Journal of Chemical Engineering and Applications, vol. 3, no. 6, pp. 477-480, 2012.

[208] C. H. Wendel, "Design and analysis of reversible solid oxide cell systems for electrical energy storage," Ph.D., Colorado School of Mines, United States -- Colorado, 3703686, 2015. [Online].

[209] W. Doenitz, R. Schmidberger, E. Steinheil, and R. Streicher, "Hydrogen production by high temperature electrolysis of water vapour," International Journal of Hydrogen Energy,

vol. 5, no. 1, pp. 55-63, 1980/01/01/ 1980, doi: https://doi.org/10.1016/0360-3199(80)90114-7.

[210] S. Dutta, "Technology assessment of advanced electrolytic hydrogen production," International Journal of Hydrogen Energy, vol. 15, no. 6, pp. 379-386, 1990/01/01/ 1990, doi: https://doi.org/10.1016/0360-3199(90)90194-4.

[211] J. Asadi and P. Kazempoor, "Techno-economic analysis of membrane-based processes for flexible CO2 capturing from power plants," Energy Conversion and Management, vol. 246, p. 114633, 2021/10/15/ 2021, doi: https://doi.org/10.1016/j.enconman.2021.114633.

[212] A. Mey. Utility-scale batteries and pumped storage return about 80% of the electricity they store [Online] Available: https://www.eia.gov/todayinenergy/detail.php?id=46756

[213] L. A. Jolaoso, C. Duan, and P. Kazempoor, "Life cycle analysis of a hydrogen production system based on solid oxide electrolysis cells integrated with different energy and wastewater sources," International Journal of Hydrogen Energy, 2023.

[214] F. Safari and I. Dincer, "A review and comparative evaluation of thermochemical water splitting cycles for hydrogen production," Energy Conversion and Management, vol. 205, p. 112182, 2020/02/01/ 2020, doi: https://doi.org/10.1016/j.enconman.2019.112182.

[215] P. Moriarty and D. Honnery, "Intermittent renewable energy: The only future source of hydrogen?," International Journal of Hydrogen Energy, vol. 32, no. 12, pp. 1616-1624, 2007/08/01/ 2007, doi: https://doi.org/10.1016/j.ijhydene.2006.12.008.

[216] L. Jolaoso and S. F. Zaman, "Catalytic Ammonia Decomposition for Hydrogen Production: Utilization of Ammonia in a Fuel Cell," in Sustainable Ammonia Production, Inamuddin, R. Boddula, and A. M. Asiri Eds. Cham: Springer International Publishing, 2020, pp. 81-105.

[217] S. Cen, K. Li, Q. Liu, and Y. Jiang, "Solar energy-based hydrogen production and post-firing in a biomass fueled gas turbine for power generation enhancement and carbon dioxide emission reduction," Energy Conversion and Management, vol. 233, p. 113941, 2021/04/01/ 2021, doi: https://doi.org/10.1016/j.enconman.2021.113941.

[218] M. H. Nehrir and C. Wang, "6 - Fuel cells," in Electric Renewable Energy Systems, M. H. Rashid Ed. Boston: Academic Press, 2016, pp. 92-113.

[219] S. Şahin and H. M. Şahin, "Generation-IV reactors and nuclear hydrogen production," International Journal of Hydrogen Energy, 2021/01/14/ 2021, doi: https://doi.org/10.1016/j.ijhydene.2020.12.182.

[220] M. Mahmoud, M. Ramadan, S. Naher, K. Pullen, M. Ali Abdelkareem, and A.-G. Olabi, "A review of geothermal energy-driven hydrogen production systems," Thermal Science and Engineering Progress, vol. 22, p. 100854, 2021/05/01/ 2021, doi: https://doi.org/10.1016/j.tsep.2021.100854.

[221] H. Association, 2016. [Online]. Available: www.HydrogenAssociation.org.

[222] M. A. Qyyum, R. Dickson, S. F. Ali Shah, H. Niaz, A. Khan, J. J. Liu, and M. Lee, "Availability, versatility, and viability of feedstocks for hydrogen production: Product space perspective," Renewable and Sustainable Energy Reviews, vol. 145, p. 110843, 2021/07/01/ 2021, doi: https://doi.org/10.1016/j.rser.2021.110843.

[223] S. Shiva Kumar and V. Himabindu, "Hydrogen production by PEM water electrolysis – A review," Materials Science for Energy Technologies, vol. 2, no. 3, pp. 442-454, 2019/12/01/ 2019, doi: https://doi.org/10.1016/j.mset.2019.03.002.

[224] D. Bonaquist, "Analysis of CO2 emissions, reductions, and capture for large-scale hydrogen production plants," Praxair. Our-company/sustainable-

development/greentechnologies-and-climate-change/less-carbon-more-green. http://www. praxair. ca/praxair. nsf/0/6D73B5DA741457DA8525772900703E30/$ file/Praxair-CO2EmissionsReductionCapture-WhitePaper. pdf (Document consulté le 18 janvier 2013), 2010.

[225] P. E. Burk, "Techno-economic modeling for new technology development," Chemical Engineering Progress, vol. 114, 01/01 2018.

[226] M. Penev, G. Saur, C. Hunter, and J. Zuboy, "H2A: Hydrogen production model: Version 3.2018 user guide (draft)," in Tech. Rep.: National Renewable Energy Lab.(NREL), 2018.

[227] J. Hartvigsen, R. Petri, and G. Tao, "DOE Hydrogen and Fuel Cells Program Record."

[228] B. Shi, W. Xu, W. Wu, and P.-C. Kuo, "Techno-economic analysis of oxy-fuel IGCC power plants using integrated intermittent chemical looping air separation," Energy Conversion and Management, vol. 195, pp. 290-301, 2019/09/01/ 2019, doi: https://doi.org/10.1016/j.enconman.2019.05.006.

[229] G. Towler and R. Sinnott, Chemical engineering design: principles, practice and economics of plant and process design. Butterworth-Heinemann, 2021.

[230] W. Wu, F. Wen, and B. Shi, "Assessing the commercial potential of IGCC polygeneration/power plants integrated with chemical-looping processes," Journal of the Taiwan Institute of Chemical Engineers, vol. 112, pp. 296-305, 2020/07/01/ 2020, doi: https://doi.org/10.1016/j.jtice.2020.06.003.

[231] K. Gerdes, E. Grol, D. Keairns, and R. Newby, "Integrated gasification fuel cell performance and cost assessment," National Energy Technology Laboratory, US Department of Energy, pp. 1-26, 2009.

[232] K. Frick, D. Wendt, P. Talbot, C. Rabiti, and R. Boardman, "Technoeconomic assessment of hydrogen cogeneration via high temperature steam electrolysis with a light-water reactor," Applied Energy, vol. 306, p. 118044, 2022/01/15/ 2022, doi: https://doi.org/10.1016/j.apenergy.2021.118044.

[233] G. Towler and R. Sinnott, "Principles, practice and economics of plant and process design," Chemical Engineering Design: Butterworth-Heinemann (December 10, 2007), 2008.

[234] R. Bhandari, C. A. Trudewind, and P. Zapp, "Life cycle assessment of hydrogen production via electrolysis – a review," Journal of Cleaner Production, vol. 85, pp. 151-163, 2014/12/15/ 2014, doi: https://doi.org/10.1016/j.jclepro.2013.07.048.

[235] G. Palmer, A. Roberts, A. Hoadley, R. Dargaville, and D. Honnery, "Life-cycle greenhouse gas emissions and net energy assessment of large-scale hydrogen production via electrolysis and solar PV," Energy & Environmental Science, 10.1039/D1EE01288F 2021, doi: 10.1039/D1EE01288F.

[236] M. Finkbeiner, A. Inaba, R. Tan, K. Christiansen, and H.-J. Klüppel, "The New International Standards for Life Cycle Assessment: ISO 14040 and ISO 14044," The International Journal of Life Cycle Assessment, vol. 11, no. 2, pp. 80-85, 2006/03/01 2006, doi: 10.1065/lca2006.02.002.

[237] I. ISO, "ISO-14040 Environmental management–life cycle assessment–principles and framework: International Organization for Standardization," 2006.

[238] G. Zhao, M. R. Kraglund, H. L. Frandsen, A. C. Wulff, S. H. Jensen, M. Chen, and C. R. Graves, "Life cycle assessment of H2O electrolysis technologies," International Journal of Hydrogen Energy, vol. 45, no. 43, pp. 23765-23781, 2020/09/03/ 2020, doi: https://doi.org/10.1016/j.ijhydene.2020.05.282.

[239] R. Hino, K. Haga, H. Aita, and K. Sekita, "38. R&D on hydrogen production by high-temperature electrolysis of steam," Nuclear Engineering and Design, vol. 233, no. 1, pp. 363-375, 2004/10/01/ 2004, doi: https://doi.org/10.1016/j.nucengdes.2004.08.029.

[240] P. Kazempoor, C. Wendel, and R. J. Braun, "Pressurized Regenerative Solid Oxide Cells for Electrical Energy Storage," ECS Transactions, vol. 58, no. 37, pp. 45-54, 2014/04/08 2014, doi: 10.1149/05837.0045ecst.

[241] S. P. Jiang, "Development of lanthanum strontium cobalt ferrite perovskite electrodes of solid oxide fuel cells – A review," International Journal of Hydrogen Energy, vol. 44, no. 14, pp. 7448-7493, 2019/03/15/ 2019, doi: https://doi.org/10.1016/j.ijhydene.2019.01.212.

[242] B. Shri Prakash, S. Senthil Kumar, and S. T. Aruna, "Properties and development of Ni/YSZ as an anode material in solid oxide fuel cell: A review," Renewable and Sustainable Energy Reviews, vol. 36, pp. 149-179, 2014/08/01/ 2014, doi: https://doi.org/10.1016/j.rser.2014.04.043.

[243] R. J. Gorte and J. M. Vohs, "Nanostructured anodes for solid oxide fuel cells," Current Opinion in Colloid & Interface Science, vol. 14, no. 4, pp. 236-244, 2009/08/01/ 2009, doi: https://doi.org/10.1016/j.cocis.2009.04.006.

[244] V. Subotić and T. W. Napporn, "10 - Nanostructured metal oxides for high-performance solid oxide fuel cells (SOFCs)," in Metal Oxide-Based Nanostructured Electrocatalysts for Fuel Cells, Electrolyzers, and Metal-air Batteries, T. W. Napporn and Y. Holade Eds.: Elsevier, 2021, pp. 235-261.

[245] J. W. Fergus, "Metallic interconnects for solid oxide fuel cells," Materials Science and Engineering: A, vol. 397, no. 1, pp. 271-283, 2005/04/25/ 2005, doi: https://doi.org/10.1016/j.msea.2005.02.047.

[246] S. Häfele, M. Hauck, and J. Dailly, "Life cycle assessment of the manufacture and operation of solid oxide electrolyser components and stacks," International Journal of Hydrogen Energy, vol. 41, no. 31, pp. 13786-13796, 2016/08/17/ 2016, doi: https://doi.org/10.1016/j.ijhydene.2016.05.069.

[247] F. Liu, H. Deng, D. Diercks, P. Kumar, M. H. A. Jabbar, C. Gumeci, Y. Furuya, N. Dale, T. Oku, and M. Usuda, "Lowering the operating temperature of protonic ceramic electrochemical cells to< 450° C," Nature Energy, pp. 1-13, 2023.

[248] M. Goedkoop, R. Heijungs, M. Huijbregts, A. De Schryver, J. Struijs, and R. Van Zelm, "ReCiPe 2008," A life cycle impact assessment method which comprises harmonised category indicators at the midpoint and the endpoint level, vol. 1, pp. 1-126, 2009.

[249] SimaPro. "Perspectives and weighing approach in ReCiPe method." https://support.simapro.com/s/article/Perspectives-and-weighing-approach-in-ReCiPe-method (accessed 01-17-2023, 2023).

[250] PRe. "ReCiPe." https://pre-sustainability.com/articles/recipe/ (accessed 01-17-2023, 2023).

[251] M. A. Huijbregts, Z. J. Steinmann, P. M. Elshout, G. Stam, F. Verones, M. Vieira, M. Zijp, A. Hollander, and R. Van Zelm, "ReCiPe2016: a harmonised life cycle impact assessment method at midpoint and endpoint level," The International Journal of Life Cycle Assessment, vol. 22, pp. 138-147, 2017.

[252] F. C. Handbook, "7th EG&G Technical Services, Inc, U," S Department of Energy office of Fossil Energy National Energy Technology Laboratory.

[253] S. C. Singhal and K. Kendall, High-temperature solid oxide fuel cells: fundamentals, design and applications. Elsevier, 2003.

[254] S. Hall, Rules of thumb for chemical engineers. Butterworth-Heinemann, 2017.

[255] D. R. Woods, Rules of thumb in engineering practice. John Wiley & Sons, 2007.

[256] O. I. Balyts'kyi, I. V. Ripei, and K. A. Protsakh, "Reliability of steam pipelines of thermal power plants in the course of long-term operation," Materials Science, vol. 42, no. 4, pp. 461-465, 2006/07/01 2006, doi: 10.1007/s11003-006-0101-x.

[257] V. Lazić, D. Arsić, R. R. Nikolić, D. Rakić, S. Aleksandrović, M. Djordjević, and B. Hadzima, "Selection and Analysis of Material for Boiler Pipes in a Steam Plant," Procedia Engineering, vol. 149, pp. 216-223, 2016/01/01/ 2016, doi: https://doi.org/10.1016/j.proeng.2016.06.659.

[258] R. Li, L. Jing, X. Meng, Z. Liu, and R. Zhang, "Numerical analysis of vane–slot friction pair in a rolling piston compressor considering deformation and groove design," Tribology International, vol. 162, p. 107124, 2021/10/01/ 2021, doi: https://doi.org/10.1016/j.triboint.2021.107124.

[259] A. Züttel, "Materials for hydrogen storage," Materials Today, vol. 6, no. 9, pp. 24-33, 2003/09/01/ 2003, doi: https://doi.org/10.1016/S1369-7021(03)00922-2.

[260] R. Newell, D. Raimi, S. Villanueva, and B. Prest, "Global energy outlook 2021: pathways from Paris," Resources for the Future Report, pp. 11-21, 2021.

[261] NREL.gov. "Solar Levelized Cost of Energy Analysis." NREL. https://www.nrel.gov/solar/market-research-analysis/solar-levelized-cost.html (accessed.

[262] A. Mohammadi and M. Mehrpooya, "Techno-economic analysis of hydrogen production by solid oxide electrolyzer coupled with dish collector," Energy Conversion and Management, vol. 173, pp. 167-178, 2018/10/01/ 2018, doi: https://doi.org/10.1016/j.enconman.2018.07.073.

[263] P. Lettenmeier, "Efficiency-electrolysis (white paper)," ed: Siemens, 2019.

[264] M. Woodhouse, R. Jones-Albertus, D. Feldman, R. Fu, K. Horowitz, D. Chung, D. Jordan, and S. Kurtz, "The role of advancements in solar photovoltaic efficiency, reliability, and costs," NREL, p. 38, 2016.

[265] M. Reytier, S. Di Iorio, A. Chatroux, M. Petitjean, J. Cren, M. De Saint Jean, J. Aicart, and J. Mougin, "Stack performances in high temperature steam electrolysis and co-electrolysis," International Journal of Hydrogen Energy, vol. 40, no. 35, pp. 11370-11377, 2015/09/21/ 2015, doi: https://doi.org/10.1016/j.ijhydene.2015.04.085.

[266] O. Schmidt, A. Gambhir, I. Staffell, A. Hawkes, J. Nelson, and S. Few, "Future cost and performance of water electrolysis: An expert elicitation study," International Journal of Hydrogen Energy, vol. 42, no. 52, pp. 30470-30492, 2017/12/28/ 2017, doi: https://doi.org/10.1016/j.ijhydene.2017.10.045.

[267] R. Sathre, C. D. Scown, W. R. Morrow, J. C. Stevens, I. D. Sharp, J. W. Ager, K. Walczak, F. A. Houle, and J. B. Greenblatt, "Life-cycle net energy assessment of large-scale hydrogen production via photoelectrochemical water splitting," Energy & Environmental Science, 10.1039/C4EE01019A vol. 7, no. 10, pp. 3264-3278, 2014, doi: 10.1039/C4EE01019A.

[268] M. Bernardi, N. Ferralis, J. H. Wan, R. Villalon, and J. C. Grossman, "Solar energy generation in three dimensions," Energy & Environmental Science, 10.1039/C2EE21170J vol. 5, no. 5, pp. 6880-6884, 2012, doi: 10.1039/C2EE21170J.

[269] M. A. Pellow, C. J. M. Emmott, C. J. Barnhart, and S. M. Benson, "Hydrogen or batteries for grid storage? A net energy analysis," Energy & Environmental Science, 10.1039/C4EE04041D vol. 8, no. 7, pp. 1938-1952, 2015, doi: 10.1039/C4EE04041D.

[270] T. Ramsden, D. Steward, and J. Zuboy, "Analyzing the levelized cost of centralized and distributed hydrogen production using the H2A production model, version 2," National Renewable Energy Lab.(NREL), Golden, CO (United States), 2009.

[271] J. Bare, D. Young, S. Qam, M. Hopton, and S. Chief, "Tool for the Reduction and Assessment of Chemical and other Environmental Impacts (TRACI)," US Environmental Protection Agency: Washington, DC, USA, 2012.

[272] H. H. Cho, V. Strezov, and T. J. Evans, "Environmental impact assessment of hydrogen production via steam methane reforming based on emissions data," Energy Reports, vol. 8, pp. 13585-13595, 2022/11/01/ 2022, doi: https://doi.org/10.1016/j.egyr.2022.10.053.

[273] R. Turton, R. C. Bailie, W. B. Whiting, and J. A. Shaeiwitz, Analysis, synthesis and design of chemical processes. Pearson Education, 2008.

[274] K. Lawrence. Average cost of wholesale U.S. natural gas in 2022 highest since 2008 [Online] Available: https://www.eia.gov/todayinenergy/detail.php?id=55119

[275] Macrotrends. Natural Gas Prices - Historical Chart [Online] Available: https://www.macrotrends.net/2478/natural-gas-prices-historical-chart